

AN APPLICATION OF ANTI-OPTIMIZATION IN THE PROCESS OF VALIDATING AERODYNAMIC CODES

By

Juan R. Cruz

A DISSERTATION SUBMITTED TO THE FACULTY OF THE
VIRGINIA POLYTECHNIC INSTITUTE AND STATE UNIVERSITY
IN PARTIAL FULFILLMENT OF THE REQUIREMENTS FOR THE DEGREE OF
DOCTOR OF PHILOSOPHY
IN
AEROSPACE ENGINEERING

William H. Mason, Chairman

Raphael T. Haftka, Chairman

Bernard M. Grossman

Elaine P. Scott

Eric R. Johnson

April 4, 2003
Blacksburg, Virginia

Keywords: anti-optimization, analysis validation, design of experiments,
aerodynamics, wind tunnel testing, Mars airplanes

AN APPLICATION OF ANTI-OPTIMIZATION IN THE PROCESS OF VALIDATING AERODYNAMIC CODES

By

Juan R. Cruz

Committee Chairmen: William H. Mason and Raphael T. Haftka
Aerospace Engineering
(ABSTRACT)

An investigation was conducted to assess the usefulness of anti-optimization in the process of validating of aerodynamic codes. Anti-optimization is defined here as the intentional search for regions where the computational and experimental results disagree. Maximizing such disagreements can be a useful tool in uncovering errors and/or weaknesses in both analyses and experiments.

The codes chosen for this investigation were an airfoil code and a lifting line code used together as an analysis to predict three-dimensional wing aerodynamic coefficients. The parameter of interest was the maximum lift coefficient of the three-dimensional wing, $C_{L,max}$. The test domain encompassed Mach numbers from 0.3 to 0.8, and Reynolds numbers from 25,000 to 250,000.

A simple rectangular wing was designed for the experiment. A wind tunnel model of this wing was built and tested in the NASA Langley Transonic Dynamics Tunnel. Selection of the test conditions (i.e., Mach and Reynolds numbers) were made by applying the techniques of response surface methodology and considerations involving the predicted experimental uncertainty. The test was planned and executed in two phases. In the first phase runs were conducted at the pre-planned test conditions. Based on these results additional runs were conducted in areas where significant differences in $C_{L,max}$ were observed between the computational results and the experiment – in essence applying the concept of anti-optimization. These additional runs were used to verify the differences in $C_{L,max}$ and assess the extent of the region where these differences occurred.

The results of the experiment showed that the analysis was capable of predicting $C_{L,max}$ to within 0.05 over most of the test domain. The application of anti-optimization

succeeded in identifying a region where the computational and experimental values of $C_{L,max}$ differed by more than 0.05, demonstrating the usefulness of anti-optimization in process of validating aerodynamic codes. This region was centered at a Mach number of 0.55 and a Reynolds number of 34,000. Including considerations of the uncertainties in the computational and experimental results confirmed that the disagreement was real and not an artifact of the uncertainties.

Dedication

A mi tía Irma, con amor, cariño, y gratitud.

Acknowledgements

I would like to thank all the members of my dissertation committee for their help and advice. I am especially grateful for the opportunity to have worked with, and learned from, Dr. Haftka and Dr. Mason. Without their guidance and patience this dissertation would not have been possible.

Two individuals at NASA Langley were key in starting and completing this degree. James Starnes provided the key encouragement to start. Mark Saunders made it possible for me to complete it. To both of them I am extremely grateful.

Time is a most valuable asset in a project like this. I thank the following individuals at NASA for making it available to me: Glenn Taylor, Rob Calloway, Mary Kae Lockwood, Robert Braun, and James Corliss.

Numerous other individuals at NASA helped in one way or another with the research presented here. I am particularly grateful for the assistance rendered by Donald Keller, Mark Guynn, Richard Re, Richard Campbell, and Catherine McGinley. The engineering and technical staff at the NASA Langley Transonic Dynamics Tunnel were key to the success of the experiment. As with many other projects, the staff at the NASA Langley Technical Library were an invaluable resource. Terry Hertz at NASA Headquarters provided funding that made this research possible. Thanks to all of you.

The support of NASA is also gratefully acknowledged.

Without good friends to provide support and encouragement completing this dissertation would not have been possible. Thank you Debbie for providing the above as well as making “Camp Dissertation” available. Michael and Jenny: trials and tribulations of all sorts come through, and you have always been there to help me cope with them. Thanks for listening Dannie. Kate and Drew: thank you for being there through lift and sink. The preliminaries and qualifiers were a long time ago, but I still remember your help Dianne.

Table of Contents

Dedication	iv
Acknowledgements	v
Table of Contents	vi
List of Tables	ix
List of Figures	xii
Symbols	xvi
Acronyms	xxiv
Chapter 1: Introduction	1
1.1 Motivation	1
1.2 Objectives	2
1.3 Approach	2
1.4 Outline	5
Chapter 2: Literature Review	8
2.1 Response Surface Methodology	8
2.2 Design of Experiments	10
2.3 Experimental Optimization	11
2.4 Model Discrimination	12
2.5 <i>Verification and Validation</i> of Aerodynamic Codes	13
2.6 Concluding Remarks	17
Chapter 3: Aerodynamic Codes and Analysis	18
3.1 Two-Dimensional Airfoil Code	20
3.2 Lifting Line Theory Code.....	21
3.3 Convergence Studies	23
3.4 Sensitivity of C_{Lmax} to N_{crit}	25
3.5 Uncertainty in the Aerodynamic Analysis Results	25

Chapter 4: Experiment Design	40
4.1 Wing Design	40
4.2 Test Design Space	41
4.3 Precision Uncertainty Structure	42
4.3.1 Precision Uncertainty Structure of the Maximum Lift Coefficient...	43
4.3.2 Precision Uncertainty Structure of the Maximum Lift Force	44
4.4 Test Design Analyses and Procedure	44
4.4.1 Normalization of Dynamic Pressure and Lift	45
4.4.2 Estimation of P_{Lmax}	46
4.4.3 Response Surface Uncertainty Analysis	49
4.4.4 Test Design Procedure	51
4.5 Test Design and Planned Testing Sequence	54
4.6 A Note on the Bias Uncertainty	56
Chapter 5: Test Setup and Operations.....	67
5.1 Wind Tunnel Model	67
5.2 Wind Tunnel Balance	69
5.3 Wind Tunnel	70
5.4 Wind Tunnel Test Setup	71
5.5 Test Operations	72
5.6 Data Acquired	76
Chapter 6: Experimental Data Analyses	90
6.1 Wind Tunnel Operating Parameters	90
6.2 Forces, Moments, and Nondimensional Aerodynamic Coefficients	91
6.3 Maximum Lift Coefficients	93
6.4 Uncertainties in the Maximum Lift Coefficients	96
Chapter 7: Experimental Test Results, Analyses Results, and Comparisons	
Between the Two Sets	108
7.1 Experimental Test Results	108
7.2 Analyses Results	109
7.3 Comparison of the Experimental Test Results Against the Analyses	
Results	110
Chapter 8: Conclusions and Observations	122
References	127
Appendix A: Wind Tunnel Turbulence and N_{crit}	135

Appendix B: MASC1 Airfoil Nondimensional Coordinates	140
Appendix C: Wind Tunnel Model Drawings	143
Appendix D: Experimental Data and Analyses Results	147
Vita	199

List of Tables

3.1	Convergence studies points	27
3.2	Values of C_{Lmax} for $N_{crit} = 155$ and the range of C_{Lmax} at the convergence studies points for the MSES convergence study	27
3.3	Values of N_{crit} at the convergence studies points	28
3.4	Sensitivity of C_{Lmax} to N_{crit} at the convergence studies points	28
3.5	Comparison of the range of C_{Lmax} from the MSES convergence study and the N_{crit} sensitivity study at the convergence studies points	29
4.1	Values of constants used for fluid properties	57
4.2	Pre-test precision uncertainty estimates for NF , AF , α , p_0 , p , and T_0 at the one-sigma level.....	57
4.3	Pre-test aerodynamic analyses results	58
4.4	Evaluation of P_{Lmax} as a function of M and Re	59
4.5	Pre-selected test points	60
4.6	Minimum precision error test design	60
4.7	D-optimal test design	61
4.8	Final test design	61
4.9	Planned test conditions and run schedule	62
5.1	Key wind tunnel model parameters	77
5.2	Values of K_{NF} and K_{PM} for the forces/moment and pressures test setups	77
5.3	Planned test conditions and run schedule	78
5.4	Actual test conditions and run schedule	79
5.5	Data acquired during forces/moment testing	81
5.6	Data acquired during pressure testing	81
6.1	Pressure and forces/moment runs correspondence for base pressure correction	99
6.2	Lift curve type for forces/moment runs	100
6.3	Example choice of C_{Lmax} , tab point, M , Re , and α for a Type I lift curve (Run 15)	101
6.4	Example choice of C_{Lmax} , tab point, M , Re , and α for a Type II lift curve (Run 11)	101

6.5	Example choice of $C_{L_{max}}$, tab point, M , Re , and α for a Type III lift curve (Run 10).....	102
6.6	Coefficient values for the $C_{L_{max}}$ response surface in equation 6.23	102
6.7	$\overline{s_{NF}}$ for all tab points identified with $C_{L_{max}}$	103
6.8	Sample standard deviation of $C_{L_{max\ adj}}$, $s_{C_{L_{max}}}$, for nominal conditions with three or more runs	104
6.9	Estimates of the bias uncertainty for NF , AF , α , p_0 , p , c , and b at the $1 - \nu = 0.95$ (i.e., two-sigma) confidence level	104
7.1	Summary of experimental data	115
7.2	Summary of the uncertainty in the experimental data	116
7.3	Summary of aerodynamic analyses results	117
7.4	Comparison of experimental and analysis results for $C_{L_{max}}$	118
A.1	Turbulence intensity data and calculated values of N_{crit}	137
A.2	Values of the coefficients in the response surface for N_{crit}	137
A.3	Comparison of N_{crit} values	138
B.1	MASC1 airfoil nondimensional coordinates	140
D.1	Data from Run 10; nominal conditions $M = 0.800$, $Re = 70,000$	147
D.2	Data from Run 11; nominal conditions $M = 0.300$, $Re = 59,140$	148
D.3	Data from Run 12; nominal conditions $M = 0.300$, $Re = 59,140$	149
D.4	Data from Run 14; nominal conditions $M = 0.800$, $Re = 141,000$	150
D.5	Data from Run 15; nominal conditions $M = 0.407$, $Re = 250,712$	151
D.6	Data from Run 16; nominal conditions $M = 0.301$, $Re = 249,123$	152
D.7	Data from Run 20; nominal conditions $M = 0.700$, $Re = 27,680$	154
D.8	Data from Run 23; nominal conditions $M = 0.800$, $Re = 24,584$	155
D.9	Data from Run 24; nominal conditions $M = 0.700$, $Re = 27,680$	156
D.10	Data from Run 25; nominal conditions $M = 0.500$, $Re = 36,790$	157
D.11	Data from Run 26; nominal conditions $M = 0.500$, $Re = 36,790$	159
D.12	Data from Run 27; nominal conditions $M = 0.800$, $Re = 70,000$	161
D.13	Data from Run 28; nominal conditions $M = 0.700$, $Re = 27,680$	162
D.14	Data from Run 29; nominal conditions $M = 0.500$, $Re = 36,790$	163
D.15	Data from Run 30; nominal conditions $M = 0.651$, $Re = 92,327$	165
D.16	Data from Run 31; nominal conditions $M = 0.300$, $Re = 59,140$	166
D.17	Data from Run 32; nominal conditions $M = 0.300$, $Re = 59,140$	167
D.18	Data from Run 33; nominal conditions $M = 0.451$, $Re = 138,206$	168
D.19	Data from Run 35; nominal conditions $M = 0.300$, $Re = 59,140$	169
D.20	Data from Run 36; nominal conditions $M = 0.599$, $Re = 176,488$	170

D.21	Data from Run 37; nominal conditions $M = 0.300$, $Re = 160,000$	171
D.22	Data from Run 38; nominal conditions $M = 0.551$, $Re = 33,521$	172
D.23	Data from Run 39; nominal conditions $M = 0.500$, $Re = 36,790$	173
D.24	Data from Run 40; nominal conditions $M = 0.452$, $Re = 40,055$	174
D.25	Data from Run 41; nominal conditions $M = 0.501$, $Re = 69,870$	175
D.26	Data from Run 42; nominal conditions $M = 0.550$, $Re = 90,900$	176
D.27	Data from Run 43; nominal conditions $M = 0.450$, $Re = 92,088$	177
D.28	Data from Run 45; nominal conditions $M = 0.800$, $Re = 70,000$	178
D.29	Data from Run 46; nominal conditions $M = 0.800$, $Re = 141,000$	180
D.30	Data from Run 47; nominal conditions $M = 0.300$, $Re = 160,000$	181

List of Figures

1.1	Mars airplane concept of operations; graphics courtesy of the Ares Project, NASA Langley Research Center	7
3.1	c_l vs α curve for $M = 0.800$, $Re = 141,000$, generated by MSES showing interpolated region	30
3.2	Test design space and location of convergence studies points	30
3.3	C_L vs α curve for $M = 0.800$, $Re = 141,000$, showing the definition of the engineering value of C_{Lmax}	31
3.4	MSES convergence study results for $M = 0.300$, $Re = 250,000$	31
3.5	MSES convergence study results for $M = 0.300$, $Re = 59,140$	32
3.6	MSES convergence study results for $M = 0.407$, $Re = 250,000$	32
3.7	MSES convergence study results for $M = 0.550$, $Re = 137,500$	33
3.8	MSES convergence study results for $M = 0.600$, $Re = 177,160$	33
3.9	MSES convergence study results for $M = 0.600$, $Re = 31,410$	34
3.10	MSES convergence study results for $M = 0.800$, $Re = 141,000$	34
3.11	MSES convergence study results for $M = 0.800$, $Re = 25,000$	35
3.12	Lifting line code convergence study results for $M = 0.300$, $Re = 250,000$	35
3.13	Lifting line code convergence study results for $M = 0.300$, $Re = 59,140$	36
3.14	Lifting line code convergence study results for $M = 0.407$, $Re = 250,000$	36
3.15	Lifting line code convergence study results for $M = 0.550$, $Re = 137,500$	37
3.16	Lifting line code convergence study results for $M = 0.600$, $Re = 177,160$	37
3.17	Lifting line code convergence study results for $M = 0.600$, $Re = 31,410$	38
3.18	Lifting line code convergence study results for $M = 0.800$, $Re = 141,000$	38
3.19	Lifting line code convergence study results for $M = 0.800$, $Re = 25,000$	39
4.1	Mars airplane design (top view) showing wing planform. Adapted from figure 2 of reference 4.1.	63
4.2	Test design space	63
4.3	Conditions used for pre-test aerodynamic analyses	64

4.4	Aerodynamic analysis C_L vs α for $M = 0.800$, $Re = 25,000$	64
4.5	Minimum precision error test design. Predicted maximum precision error in $C_{L_{max}}$ at the 95% confidence level = 0.0098. D-efficiency = 2.7%.	65
4.6	D-optimal test design. Predicted maximum precision error in $C_{L_{max}}$ at the 95% confidence level = 0.0154. D-efficiency = 10.4%.	65
4.7	Final test design. Predicted maximum precision error in $C_{L_{max}}$ at the 95% confidence level = 0.0116. D-efficiency = 8.2%.	66
5.1	MASC1 airfoil with zero and finite trailing edge thickness; vertical axis exaggerated for clarity	82
5.2	Wing tunnel model assembly with key design dimensions noted	82
5.3a	Wing and balance block assembly, top view, disassembled	83
5.3b	Wing and balance block assembly, bottom view, disassembled	83
5.3c	Wing and balance block assembly, bottom view, assembled, including wind tunnel balance UT-61A and windshield	83
5.4	Model in wind tunnel showing attachment of windshield to sting	84
5.5	Wind tunnel model components	84
5.6	Drawing of NASA LaRC wind tunnel balance UT-61A	85
5.7	Photograph of NASA LaRC wind tunnel balance UT-61A	85
5.8	NASA LaRC Transonic Dynamics Tunnel (TDT) aerial view	86
5.9	TDT operating envelope in air; upper bound adapted from reference 5.4, figure 1(a)	86
5.10	TDT schematic drawing	87
5.11	TDT sting with the Mars airplane wing	87
5.12	Pumping time required to achieve low pressures in the TDT	88
5.13	Model installation, view from below	88
5.14	Model installation, side view	89
5.15	Actual test conditions; digit next to symbol indicates number of tests ...	89
6.1	Definition of x_{bar} and y_{bar} and sign convention for NF , AF , and PM_{bmc}	105
6.2	Lift curve Type (I, II, or III) as a function of M and Re	105
6.3	Example of a Type I lift curve (Run 15)	106
6.4	Example of a Type II lift curve (Run 11)	106
6.5	Example of a Type III lift curve (Run 10)	107
7.1	Contour plot of $ E $, a measure of the difference between the experimental and analysis values of $C_{L_{max}}$ over the test domain	119
7.2	C_L and C_M vs α ; nominal conditions $M = 0.800$, $Re = 24,584$	119
7.3	C_L and C_M vs α ; nominal conditions $M = 0.551$, $Re = 33,521$	120
7.4	C_L and C_M vs α ; nominal conditions $M = 0.800$, $Re = 70,000$	120

7.5	C_L and C_M vs α ; nominal conditions $M = 0.700$, $Re = 27,680$	121
7.6	Contour plot using $ E $ for all conditions with Type I and II C_L vs α curves and $ E_{alt} $ for all conditions with Type III C_L vs α curves: measures of the difference between the experimental and analysis values of C_{Lmax} over the test domain	121
A.1	Available turbulence data and test design space	139
C.1	Drawing 1158620, test wing assembly	143
C.2	Drawing 1158621, test wing	144
C.3	Drawing 1158622, balance block and balance roll pin	145
C.4	Drawing 1158623, sting adapter	146
D.1	C_L and C_M vs α ; nominal conditions $M = 0.301$, $Re = 249,123$	182
D.2	C_L vs C_D ; nominal conditions $M = 0.301$, $Re = 249,123$	182
D.3	C_L and C_M vs α ; nominal conditions $M = 0.300$, $Re = 160,000$	183
D.4	C_L vs C_D ; nominal conditions $M = 0.300$, $Re = 160,000$	183
D.5	C_L and C_M vs α ; nominal conditions $M = 0.300$, $Re = 59,140$	184
D.6	C_L vs C_D ; nominal conditions $M = 0.300$, $Re = 59,140$	184
D.7	C_L and C_M vs α ; nominal conditions $M = 0.407$, $Re = 250,712$	185
D.8	C_L vs C_D ; nominal conditions $M = 0.407$, $Re = 250,712$	185
D.9	C_L and C_M vs α ; nominal conditions $M = 0.451$, $Re = 138,206$	186
D.10	C_L vs C_D ; nominal conditions $M = 0.451$, $Re = 138,206$	186
D.11	C_L and C_M vs α ; nominal conditions $M = 0.450$, $Re = 92,088$	187
D.12	C_L vs C_D ; nominal conditions $M = 0.450$, $Re = 92,088$	187
D.13	C_L and C_M vs α ; nominal conditions $M = 0.452$, $Re = 40,055$	188
D.14	C_L vs C_D ; nominal conditions $M = 0.452$, $Re = 40,055$	188
D.15	C_L and C_M vs α ; nominal conditions $M = 0.501$, $Re = 69,870$	189
D.16	C_L vs C_D ; nominal conditions $M = 0.501$, $Re = 69,870$	189
D.17	C_L and C_M vs α ; nominal conditions $M = 0.500$, $Re = 36,790$	190
D.18	C_L vs C_D ; nominal conditions $M = 0.500$, $Re = 36,790$	190
D.19	C_L and C_M vs α ; nominal conditions $M = 0.550$, $Re = 90,900$	191
D.20	C_L vs C_D ; nominal conditions $M = 0.550$, $Re = 90,900$	191
D.21	C_L and C_M vs α ; nominal conditions $M = 0.551$, $Re = 33,521$	192
D.22	C_L vs C_D ; nominal conditions $M = 0.551$, $Re = 33,521$	192
D.23	C_L and C_M vs α ; nominal conditions $M = 0.599$, $Re = 176,488$	193
D.24	C_L vs C_D ; nominal conditions $M = 0.599$, $Re = 176,488$	193
D.25	C_L and C_M vs α ; nominal conditions $M = 0.651$, $Re = 92,327$	194
D.26	C_L vs C_D ; nominal conditions $M = 0.651$, $Re = 92,327$	194
D.27	C_L and C_M vs α ; nominal conditions $M = 0.700$, $Re = 27,680$	195

D.28	C_L vs C_D ; nominal conditions $M = 0.700$, $Re = 27,680$	195
D.29	C_L and C_M vs α ; nominal conditions $M = 0.800$, $Re = 141,000$	196
D.30	C_L vs C_D ; nominal conditions $M = 0.800$, $Re = 141,000$	196
D.31	C_L and C_M vs α ; nominal conditions $M = 0.800$, $Re = 70,000$	197
D.32	C_L vs C_D ; nominal conditions $M = 0.800$, $Re = 70,000$	197
D.33	C_L and C_M vs α ; nominal conditions $M = 0.800$, $Re = 24,584$	198
D.34	C_L vs C_D ; nominal conditions $M = 0.800$, $Re = 24,584$	198

Symbols

a	speed of sound
A_{base}	model base area
AF	axial force
AF_{corr}	axial force corrected for base pressures
AF_{norm}	normalized axial force
AR	wing aspect ratio
b	wing span
$b_0, b_M,$ $b_{Re}, b_{M Re},$ b_{Re^2}	coefficients in the response surface model for N_{crit}
$\bar{\mathbf{b}}$	vector of coefficients for the response surface model of $\hat{L}_{norm max}$
$B_{AF,1-\nu}$	bias uncertainty of AF at the $1 - \nu$ confidence level
$B_{b,1-\nu}$	bias uncertainty of b at the $1 - \nu$ confidence level
$B_{c,1-\nu}$	bias uncertainty of c at the $1 - \nu$ confidence level
$B_{NF,1-\nu}$	bias uncertainty of NF at the $1 - \nu$ confidence level
$B_{p,1-\nu}$	bias uncertainty of p at the $1 - \nu$ confidence level
$B_{p_0,1-\nu}$	bias uncertainty of p_0 at the $1 - \nu$ confidence level

$B_{\alpha,1-\nu}$	bias uncertainty of α at the $1 - \nu$ confidence level
$B_{C_{Lmax},1-\nu}$	bias uncertainty of C_{Lmax}
$\overline{B_{C_{Lmax},1-\nu}}$	bias uncertainty of $\overline{C_{Lmaxadj}}$ at the $1 - \nu$ confidence level
c	wing chord
c_d	airfoil section drag coefficient
c_l	airfoil section lift coefficient
c_{lmax}	airfoil section maximum lift coefficient
$c_{l\alpha}$	airfoil section lift curve slope
$c_{m\ c/4}$	airfoil section pitching moment coefficient about the quarter-chord
C_A	axial force coefficient
C_{base}	base pressure correction coefficient
C_D	wing drag coefficient
C_L	wing lift coefficient
C_{Lmax}	wing maximum lift coefficient
$C_{Lmaxadj}$	maximum lift coefficient adjusted to the nominal values of M and Re
$\overline{C_{Lmaxadj}}$	mean value of the maximum lift coefficient adjusted to the nominal values of M and Re
C_{LmaxRS}	maximum lift coefficient response surface as a function of M and Re
$C_{Lmax}^{Analysis}$	maximum lift coefficient from aerodynamic analysis
C_M	wing pitching moment coefficient about the quarter chord
C_N	normal force coefficient

D_{norm}	normalized drag force
E	difference between the experimental and analysis values of C_{Lmax}
$ E_{alt} $	alternate difference between the experimental and analysis values of C_{Lmax}
E_L	lower bound of the 95 percent confidence interval of E
E_p	percent difference between the experimental and analysis values of C_{Lmax}
E_U	upper bound of the 95 percent confidence interval of E
h	distance of the flow tangency point aft of the quarter chord
$k_0, k_M,$ $k_{Re}, k_{MRe},$ $k_{M^2}, k_{Re^2},$ k_{MRe^2}	coefficients in the response surface model for C_{Lmax} as a function of M and Re
K_{NF}	normal force angle of attack correction factor
K_{PM}	pitching moment angle of attack correction factor
K_q	normalizing factor for dynamic pressure, forces, and moments
L	lift force
L_{max}	maximum lift force
L_{norm}	normalized maximum lift force
$\hat{L}_{normmax}$	response surface model for the normalized maximum lift force as a function of M and Re
L/D	lift to drag ratio
M	Mach number
n	exponent for the determination of the coefficient of viscosity, 0.798803

n_e	number of elements in the vectors $\bar{\mathbf{x}}$ and $\bar{\mathbf{b}}$
n_{obs}	number of observations used in the creation of the response surface for $\hat{L}_{norm\ max}$
N_{crit}	boundary layer transition turbulence parameter
$N_{crit\ RS}$	N_{crit} response surface as a function of M and Re
NF	normal force
NF_{norm}	normalized normal force
N_{grid}	number of grid points on the airfoil surface used in the MSES calculations
N_{runs}	number of runs at a particular test condition
$N_{vortices}$	number of vortices for the lifting line analysis
p	static pressure
p_{base1} , p_{base2} , p_{base3}	base pressure at locations 1, 2, and 3, respectively
p_0	stagnation pressure
P_{AF}	precision uncertainty of the axial force
$P_{C_{L\ max}}$	precision uncertainty of $C_{L\ max}$
$\overline{P_{C_{L\ max}, 1-\nu}}$	precision uncertainty of the mean of $C_{L\ max}$ at the $1 - \nu$ confidence level
$P_{L_{max}}$	precision uncertainty of L_{max}
$P_{\hat{L}_{norm\ max}}$	precision uncertainty of the response surface model $\hat{L}_{norm\ max}$
$P_{L_{meas}}$	precision uncertainty of the measured lift force

PM_{bmc}	pitching moment about the balance moment center
$PM_{bmc\ corr}$	pitching moment about the balance moment center corrected for base pressures
$PM_{c/4}$	pitching moment about the airfoil quarter chord
$PM_{c/4\ norm}$	normalized pitching moment about the airfoil quarter chord
P_{NF}	precision uncertainty of the normal force
P_p	precision uncertainty of the static pressure
P_{p_0}	precision uncertainty of the stagnation pressure
P_q	precision uncertainty of the dynamic pressure
P_{T_0}	precision uncertainty of the stagnation temperature
P_α	precision uncertainty of the angle of attack
q	dynamic pressure
q_{norm}	normalized dynamic pressure
R	gas constant, 287.05 J/kg K
Re	Reynolds number
\mathfrak{R}^2	coefficient of multiple determination
\mathfrak{R}_{adj}^2	adjusted coefficient of multiple determination
$s_{C_{Lmax}}$	sample standard deviation of $C_{Lmax\ adj}$
$\overline{s_{NF}}$	normal force sample standard error of the mean
S	wing area
t	airfoil thickness or Student t-Distribution

T	static temperature
TI	wind tunnel turbulence intensity
T_{ref}	reference value of temperature for the calculation of the coefficient of viscosity, 300 K
T_0	stagnation temperature
$T_{0\ ref}$	reference stagnation temperature; 303.8 K for pre-test analyses, 296.1 K for post-test analyses
t/c_{max}	maximum airfoil thickness to chord ratio
$U_{C_{Lmax}, 1-\nu}^{Analysis}$	total uncertainty of $C_{Lmax}^{Analysis}$ at the $1 - \nu$ confidence level
$\overline{U_{C_{Lmax}, 1-\nu}}$	total uncertainty of the mean of $\overline{C_{Lmax\ adj}}$ at the $1 - \nu$ confidence level
$U_{E, 0.95}$	uncertainty of E at the 95 percent confidence level
V	true airspeed
x	airfoil coordinate along chordline
x_{bar}	x -component of distance from airfoil quarter chord to the wind tunnel balance moment center
$\bar{\mathbf{x}}$	vector of independent variables in the response surface model for $\hat{L}_{norm\ max}$
$\bar{\mathbf{x}}_0$	location vector of independent variables in the response surface model for $\hat{L}_{norm\ max}$
$\bar{\mathbf{X}}$	matrix of observation locations used in the creation of the response surface model for $\hat{L}_{norm\ max}$
y	airfoil coordinate perpendicular to chordline
y_{bar}	y -component of distance from airfoil chordline to the wind tunnel balance centerline

y_{base}	y-component offset from the base pressures center of pressure to the wind tunnel balance centerline
z	percentage point of the standard normal distribution
α	angle of attack
$\alpha_{C_{L,max}}$	model angle of attack at $C_{L,max}$
$\overline{\alpha_{C_{L,max}}}$	mean value of the model angle of attack at $C_{L,max}$
α_s	sting angle of attack
$\alpha_{C_{L,max}}^{Analysis}$	model angle of attack at $C_{L,max}^{Analysis}$ from aerodynamic analysis
$\beta_0, \beta_M,$ $\beta_{Re}, \beta_{MRe},$ $\beta_{M^2}, \beta_{M^2Re},$ β_{M^3}	coefficients for the response surface model of $\hat{L}_{norm,max}$
γ	ratio of specific heats, 1.399
$\Delta p_{base1},$ $\Delta p_{base2},$ Δp_{base3}	differential base pressures at locations 1, 2, and 3, respectively
Δp_{wing}	differential wing surface pressures
μ	coefficient of viscosity
μ_{ref}	reference value of the coefficient of viscosity, 1.846×10^{-5} N s/m ²
v	tail probability of the standard normal distribution
ρ	air density
σ	standard deviation of $L_{norm,max}$

$\hat{\sigma}$ estimated value of σ , the standard deviation of $L_{norm\ max}$

$\sigma_{C_{L,max}}$ standard deviation of $C_{L,max\ adj}$

Acronyms

AGARD	Advisory Group for Aerospace Research and Development
AIAA	American Institute of Aeronautics and Astronautics
ATI	Advanced Technologies Incorporated
CFD	Computational Fluid Dynamics
DAS	Data Acquisition System
ISES	two-dimensional airfoil code for single-element airfoils
LaRC	Langley Research Center
MASC1	Mars Airplane Super Critical #1
MSES	two-dimensional airfoil code used in the present investigation; similar to ISES but with multiple-element airfoil capability
NASA	National Aeronautics and Space Administration
NATO	North Atlantic Treaty Organization
RMS	Root-Mean-Square
RSM	Response Surface Methodology
TDT	Transonic Dynamics Tunnel
V&V	Verification and Validation

Chapter 1: Introduction

1.1 Motivation

Practitioners of design optimization have often observed that optimization algorithms seem to possess an uncanny ability to exploit weaknesses in the underlying analyses and constraints. Unger [1, pp. 51-53] presents an example of such behavior. During the optimization of a wing for a high-speed civil transport the optimization algorithm determined that there was an advantage in using a highly swept wing tip to reduce the drag due to lift. This behavior was deemed unrealistic and was eliminated as a possible outcome of the optimization procedure by adding a geometric constraint. In other cases such behavior identifies errors in the underlying analyses which, once isolated by the optimization algorithm, can then be corrected. Thus, this “ability” of optimization algorithms can sometimes yield useful information.

These observations led to the question: Why not use this behavior of optimization algorithms to assist in the process of validating codes and/or analyses¹ by helping to identify weaknesses and errors? This idea was proposed by Haftka and Kao [2], and others as discussed in the literature review. Pursuing the application and determining the usefulness of this idea to the process of validating aerodynamic analyses² is the subject matter of the present research. To differentiate this use of optimization from other applications (e.g., design optimization, optimal design of experiments), the use being pursued herein will be called anti-optimization - active search for the “worst” behavior.³ Besides identifying weaknesses in analyses, anti-optimization may have other qualities that are useful. It is often difficult to isolate problems with an analysis as compared to another analysis or experimental data if the differences are small; multiple sources

¹ In this work a code is considered to be a single computer program. An analysis is defined here as a single code or combination of codes used to yield the output parameter being investigated (e.g., maximum lift coefficient). In general the term code will be used here to refer to specific computer programs.

² Unless otherwise stated, in the present research validation is used in reference to the ability of an analysis to model physical reality. Verification, on the other hand, is used to describe the ability of a code to solve the intended governing equations correctly, regardless of the suitability of the governing equations to model physical reality. A complete discussion of this terminology is given in the literature review, chapter 2, section 2.5.

³ The term anti-optimization was coined by Elishakoff in reference to the search for the “least favorable response” [3, 4]. Various researchers have proposed the concept of validating analyses by maximizing differences. These works are discussed in the literature review (chapter 2).

(e.g., inadequacy of the physical model, convergence problems, coding errors) could be the reason for small discrepancies. By maximizing the differences, however, it may be easier to diagnose the reason for the weakness in the analysis. Anti-optimization can be used in the process of validating analyses by either comparing competing models (an area of study often known as model discrimination), or by seeking discrepancies between analyses and experiments. In the present investigation, the later approach is pursued.

1.2 Objectives

The primary objectives of the work performed for this dissertation are to develop an approach using anti-optimization in the process of validating aerodynamic analyses through experiments, and to evaluate the effectiveness of this approach. Consistent with the desire to apply optimization as a tool to achieve these objectives, methods from the optimal design of experiments literature will be utilized. In particular, tools developed for the statistical design of experiments and response surface methodology [5] will be used. The concept of anti-optimization will be applied to search for regions in which the analysis and experiment disagree, and to maximize these disagreements.

Since the present research is an applied study, a suitable aerodynamic analysis needing validation and an appropriate corresponding experiment were selected to serve as a testbed for the approach being developed. A combination of two aerodynamic codes integrated into an analysis to predict the maximum lift coefficient of a wing and a related wind tunnel experiment were chosen to exercise and evaluate the proposed approach. An interesting flight domain for the validation of this analysis is the combination of Mach and Reynolds numbers encountered by airplanes operating within the atmosphere of Mars. As detailed in the next section, Mars airplanes operate at unusual combinations of these parameters. The scarcity of data in this flight domain, the possibility of validating the analysis in an efficient manner through the approach proposed herein, and National Aeronautics and Space Administration (NASA) interest in these data for future Mars missions, made the experiment of interest in and of itself. Thus, secondary objectives of the dissertation were assist in the validation of an analysis in the flight regime used by airplanes designed to fly in the Martian atmosphere, and to generate an aerodynamics database in this flight regime.

1.3 Approach

Given the research objectives presented in the previous section, the following general approach is proposed to fulfill them:

- 1) *Selection of the analysis and output parameter to be validated.* In choosing an analysis and output parameter the capability to perform a suitable experiment should be kept in mind. For example, if an experiment yielding sufficiently

accurate results is not possible, the prospects of making meaningful comparisons between computational and experimental results is doubtful.

- 2) *Definition of the experiment.* The experiment should yield the required experimental data to compare against the results from the analysis. At this stage the possibility of performing a suitable experiment within the available resources should be evaluated.
- 3) *Generation of preliminary computational results.* These preliminary computational results will assist in the design of the experiment as described below. In addition, these preliminary computational results can be used to perform real-time comparisons against the experimental results while the experiment is being executed. Making these comparisons while the test is being conducted allows on-the-spot changes in the test design as required, especially since the goal is to search for regions where the correlation between the computational and experimental results is poor.
- 4) *Design of the experiment.* In this stage all the details of the experiment that can be specified before testing starts should be defined. Items that require definition include physical aspects (e.g., models, equipment, facilities) and other considerations such as selection of the experimental test conditions (which may be done, for example, by formal optimal design of experiments techniques).
- 5) *Execution of the experiment.* At this stage the experiment is conducted, guided by the pre-test planning, but making changes as necessary as experimental results are generated.
- 6) *Comparison of experimental and computational results.* In comparing these results, areas where the computational and experimental results do not agree are isolated. In an additional stage, not included in the present research, a search for the reasons why the computational and experimental results differ is conducted (i.e., diagnosing problems with the analysis and/or experiment).
- 7) *Generate conclusions.* Evaluate how well the general approach proposed herein, and the details of the particular implementation for the validation of experiments, satisfied the objectives of the present investigation.

In subsequent chapters of this dissertation points three through seven above are covered in detail. However, the choices made with regards to items one and two are discussed here. To understand the reasons for these choices, a brief description of the operation and challenges of operating airplanes in the atmosphere of Mars is required.

Over the last 25 years, NASA has investigated the possibility of conducting robotic missions on Mars using airplanes as the platform for the scientific instruments. One of

the earliest, and yet most thorough, studies was presented in reference 6. In this proposed design the airplane concept of operations, shown in figure 1.1, proceeds as follows:

- The airplane is packaged in a folded configuration inside an aeroshell.
- The aeroshell enters the Mars atmosphere and protects the airplane from the heat generated during entry.
- A parachute is deployed at supersonic speeds. This parachute slows the aeroshell to subsonic speeds.
- The heat shield is released, exposing the folded airplane to the airstream.
- The airplane is released from the backshell.
- The airplane unfolds, assembling itself in mid-air.
- The airplane performs a pullout maneuver from its initial steep dive, finally achieving level flight. Because of the thin Martian atmosphere this pullout requires several kilometers of altitude. During the pullout the airplane accelerates to transonic Mach numbers.

This Mars airplane concept of operations, although not the only possible option, has been investigated further by other researchers. In reference 7 a detailed entry/descent/flight analysis was conducted. This analysis included all phases listed above, from the time the aeroshell enters the atmosphere and concluding with the end of the pullout from the initial dive. Among the key observations made in this reference is that the maximum lift coefficient of the wing is critical to the success of the pullout maneuver. Airplanes with higher values of the maximum lift coefficient can accomplish the pullout maneuver with less altitude loss while experiencing a lower maximum Mach number – thus enhancing mission safety. Conversely, higher values of the maximum lift coefficient allow heavier airplanes to perform the pullout maneuver within given altitude loss and maximum Mach number constraints. This added pullout mass capability can be used to enhance mission value by allowing additional scientific instrumentation to be flown. Because of the low atmospheric density on Mars, the combination of Mach and Reynolds numbers during the pullout of Mars airplanes such as the one described in reference 7 is highly unusual: Mach numbers up to 0.8 and Reynolds numbers as low as 43,000. Thus, during pullout this proposed airplane operates in the Mach number regime usually associated with commercial transports and the Reynolds numbers regime usually associated with birds and model airplanes. This unusual combination of Mach and Reynolds numbers generated concerns regarding the capability of current aerodynamic analyses to accurately predict wing performance, in particular the maximum lift coefficient.

Validating the ability of an analysis to predict the maximum lift coefficient was an interesting and attractive option for the research proposed in this dissertation for a variety of reasons. The problem was naturally constrained to a clearly identifiable response parameter, namely the maximum lift coefficient that, for a given wing, is only a function of two independent variables – Mach and Reynolds number. Analyses exist for the prediction of the aerodynamic performance of wings at the required Mach and Reynolds numbers, although they had not been validated at the Mach and Reynolds number combinations required by Mars airplanes. A wind tunnel that can operate at the required test conditions exists at the NASA Langley Research Center (LaRC), namely the Transonic Dynamics Tunnel. Previous research efforts at NASA LaRC related to Mars airplanes (both computational and experimental) could be used as a starting point for the present investigation. Finally, continuing interest at NASA in Mars airplane missions made it possible to undertake the required experiment.

The aerodynamic codes chosen for the present investigation were an airfoil code to predict the two-dimensional airfoil properties, and a lifting line code to predict the three-dimensional wing aerodynamic parameters (in particular the maximum lift coefficient) based on the two-dimensional airfoil data. The relative simplicity and speed of execution of these codes made it possible for them to be used for the present investigation. The computational cost of more complex codes (i.e., three-dimensional Navier-Stokes) would be prohibitive. The design of the test wing was influenced by the analyses in reference 7, and previous unpublished experimental work performed at the TDT on the aerodynamics of Mars airplanes

1.4 Outline

This dissertation is organized as follows:

In chapter 2 a literature review is presented, focusing on the statistical design of experiments and the validation of aerodynamic codes through experiments.

In chapter 3 the aerodynamic codes used in the analysis used herein: a two-dimensional airfoil code and a lifting line code, are discussed. Together these two codes were used to predict the maximum lift coefficient of a three dimensional wing. In this chapter the results of convergence studies are presented. These convergence studies were conducted to determine appropriate values of discretization variables in the two-dimensional airfoil code and the lifting line code. The sensitivity of the computational results to the wind tunnel turbulence was also investigated. As closure to chapter 3, an assessment of the computational aerodynamic results uncertainty is presented. Knowledge of this uncertainty is important when comparing analysis vs experimental results.

In chapter 4 the experimental design, including the design of the wing, the definition of the experimental design space, and the selection of the test conditions based on design of experiments techniques and response surface methodology is presented and discussed.

In chapter 5, the wind tunnel test setup and its operation are discussed. Included in this discussion are detailed descriptions of the wind tunnel model and balance. Because of the unusual test conditions (i.e., high Mach number and low Reynolds numbers) used during the present research, the wind tunnel used and how it is operated is relevant to this discussion. Thus the wind tunnel, test setup, and test operations are also presented in detail. Finally the data to be acquired during testing is specified.

In chapter 6 the methodology used to analyze the experimental data is presented. Included are the determination of wind tunnel conditions, forces, moments, and nondimensional aerodynamic coefficients with emphasis on the maximum lift coefficient and its uncertainty.

In chapter 7 the experimental and computational test results, including their uncertainties, are presented and discussed. The experimental and computational results are compared, and areas of disagreement between experiments and computations found through the use of anti-optimization are isolated.

Finally in chapter 8 the conclusions reached at during the present research are summarized and discussed. Included in these conclusions is an evaluation of the suitability of the approach implemented to achieve the stated research objectives.

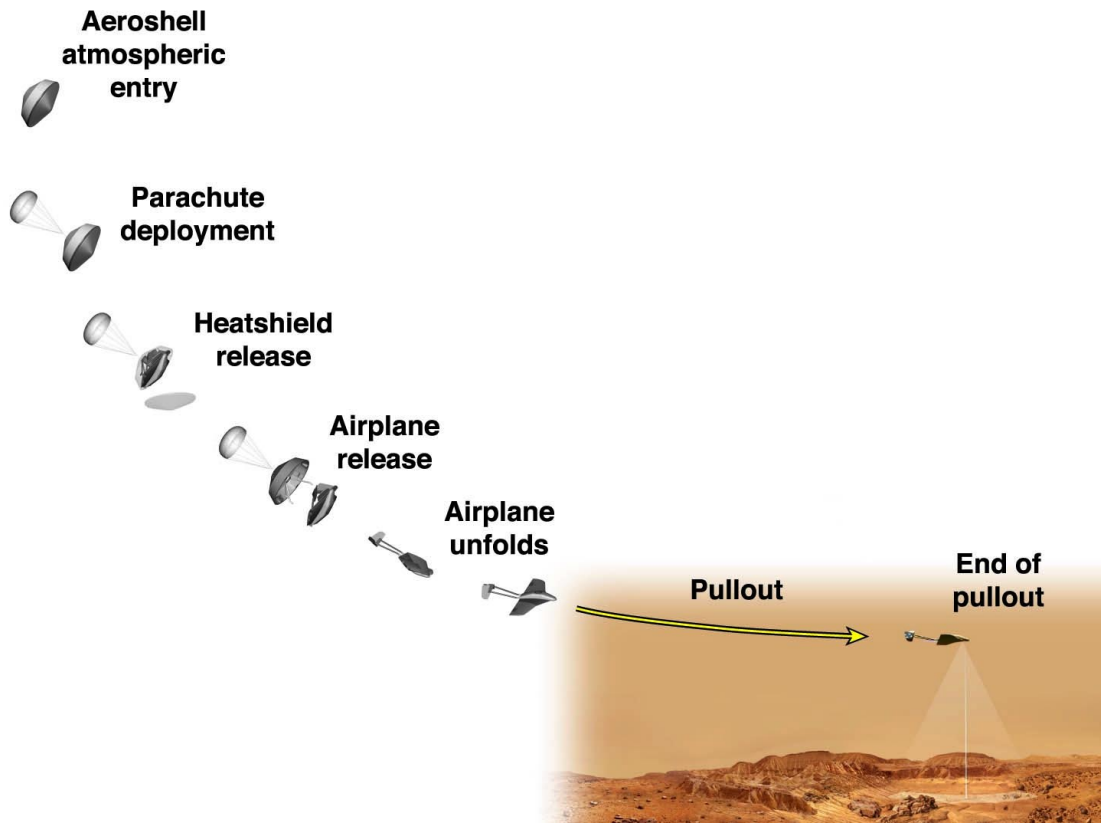


Figure 1.1 – Mars airplane concept of operations; graphics courtesy of the Ares Project, NASA Langley Research Center

Chapter 2: Literature Review

Literature relevant to the present investigation can be categorized into the following groups:

- Response Surface Methodology
- Design of Experiments
- Experimental Optimization
- Model Discrimination
- *Verification and Validation of Aerodynamic Codes*

Each of these areas will be discussed separately in this literature review. However, it should be noted that there is significant overlap among them; they should not be considered to be completely independent areas of study.

Haftka et al. [8] reviewed the relationship between optimization and experiments. In this review paper they divided the topic into four areas:

- Use of optimization for designing experiments
- Use of experiments to perform optimization
- Use of experimental optimization techniques in numerical optimization
- Importance of experimental validation of optimization

Of these four areas, the first two are relevant to the present investigation. This review paper will be used extensively to discuss the first four subjects in the present literature review.

2.1 Response Surface Methodology

Response surface methodology (RSM) concerns itself with the creation and analysis of functions to model how some particular quantity (known as the response) varies with respect to a set of relevant independent variables. Topics usually included within RSM include:

- Generation of response functions. Low-level polynomials are commonly, but not exclusively, used as response functions.

- Fitting experimental and computational data to response surface functions, usually through least-squares procedures.
- Estimation of the values of unknown coefficients in the response function.
- Analysis of uncertainty of both the response surface and the estimates of the parameters in the response function.
- Seeking maximum and minimum values of the fitted response surface.
- The design of optimal experiments where the experimental results are to be fitted with a particular response surface. A common example of this is the optimal design of an experiment to minimize the uncertainty in the response function parameters (e.g., D-optimal designs).

In their 1951 paper, Box and Wilson [9] discussed many of the important aspects of RSM. Their main goal was to identify the maximum (or minimum) of a response function generated on the basis of experimental data. They achieved this by sequential experimentation using previous results to guide the continuing experimental designs. The response surfaces they used were linear in the response variables (i.e., factors); least squares were used to determine the unknown coefficients. Box and Wilson also identified lack-of-fit (i.e., bias) in the assumed response function as an area of concern. By the mid 1960s, RSM had been sufficiently developed to warrant a literature review paper by Hill and Hunter [10]. This review paper discusses both the theoretical aspects of RSM, as well as practical applications in a variety of fields. Another, more comprehensive, review paper was published by Mead and Pike [11] in 1985. In addition to the usual topics such as response functions, this paper covers D-optimal experimental designs and experimental designs for model discrimination. More recently, RSM has been used to fit response functions to the results of computer analyses. This is not surprising, since computational results can exhibit two key similarities with physical experiments: they can be expensive to perform, and numerical noise can mimic experimental uncertainty.¹ By fitting a simple and computationally inexpensive response surface to selected computer analyses, and then using the response surface as a surrogate for the computer analyses, computational efficiencies can be achieved. This use of RSM is reviewed by Haftka et al. [8]. At the present time, RSM is an established tool to model both experimental and computational results, and the subject of recent textbooks and manuals [5, 12].

¹ Although computational results are the same every time a code is executed with identical inputs, converged solutions can yield slightly different results when certain parameters such as the computational grid are changed. It is these variations in the computational results that mimic experimental uncertainty and are referred to as numerical noise.

2.2 Design of Experiments

The term design of experiments, as commonly used, implies the selection of test conditions to achieve some specific goal. Among the goals usually sought in the design of experiments are maximization or minimization of the response (whether this is done via response surface functions or by other means), minimization of the uncertainty of the response function, minimization of the uncertainty of the parameters being identified, and model discrimination. The application of design of experiments to model discrimination is particularly relevant to the present investigation, and is discussed separately in a subsequent section. Regardless of the specific goals being sought, most design of experiments techniques have one thing in common: maximizing the quality of the data obtained while minimizing the number of experiments to be conducted.

In an early example, Fisher and MacKenzie [13] report the design, execution, and results of a planned experiment to determine the response of various potato varieties to manure. By carefully selection of the planting locations of different varieties, the manurial treatments, and the number of replicates this experiment was able to quantify the influence of these parameters with statistical confidence. Box and Wilson [9] suggested the use of two-level factorial, fractional factorial, and composite designs for seeking the maxima of a response surface. The properties and usefulness of these designs in RSM are discussed by Myers and Montgomery [5]. Taguchi methods [14] apply similar orthogonal designs for maximizing responses.

If the goal of the experimental design is identification of the parameters in the response surface, a set of optimality criteria based on the Fisher information matrix for the design of such experiments have been developed [8]. Numerous optimality criteria have been proposed (e.g., A-, C-, D-, E-, and L-optimality). These are reviewed by Walter and Pronzato [15], and Haftka et al. [8].

Although design of experiment techniques have been used for years in various fields (e.g., chemistry, biology), it is only recently that they have begun to be applied to aerospace wind tunnel testing. DeLoach [16, 17, and 18] has proposed the use of design of experiments and RSM techniques in wind tunnel experiments instead of the commonly used “one factor at a time” approach. He cites reductions in costs to achieve the desired objectives and improvements in precision accuracy as a significant reasons to apply the design of experiments approach to wind tunnel testing. In an experiment to quantify the deformation of a supersonic transport model as a function of angle of attack, Mach number, and Reynolds number, the designed experiment required 60 percent fewer wind-on minutes than the “one factor at a time” experiment for the same level of accuracy. Landman et al. [19] discuss the results of a designed wind tunnel experiment using RSM techniques to predict the performance of a racecar. The regression models identified interactions in the lift and lift to drag responses the authors state “would have been overlooked in a traditional OFAT (one factor at a time) approach to testing.”

2.3 Experimental Optimization

How experimental optimization can be conducted has already been discussed as it relates to the design of experiments and RSM. This section focuses on the reasons why experimental optimization is pursued. The discussion in this section follows that of Haftka et al. [8].

Experimental optimization, instead of analytical optimization, is undertaken for a variety of reasons. In the present investigation, experimental optimization is used to maximize the difference between analysis and experiment, since the goal is to validate the analysis and the experiment is considered to be the “ground truth.” However, there are other reasons for pursuing experimental optimization instead of analytical optimization. In some cases there are doubts on the reliability of computational models, or no computational model exists. Landman [20] optimized the position of the flap on a multi-element airfoil to yield the maximum lift coefficient. Among the reasons cited by Landman to perform this optimization experimentally was the accuracy limitations of current computational tools to predict the maximum lift coefficient of such airfoils.

In cases where the response and thus the optimum varies within supposedly identical systems, and/or within a given system with time, experimental optimization may be the preferred approach. Stuckman et al. [21] discuss the experimental optimization of the gains in the control system of a robot to minimize the cycle time to perform certain tasks. By conducting an experimental optimization procedure, Stuckman et al. were able to optimize the control system gains of a robot to reduce the cycle times for two specific tasks. They note that these optimizations could be conducted again at a later time to re-optimize the system, which would account for wear in the robot’s mechanism.

Experimental optimization is also an attractive option in situations where the experiments are inexpensive. Process control is an example of such an application. Semones and Lim [22] report on the optimization of the productivity of a yeast culture, where the control variables were the temperature and the dilution rate. The optimization algorithm was able to bring the productivity to an optimum steady state value, and recover from intentional and unintentional disturbances. If the experiment is inexpensive, can be easily performed one at a time, and the noise level is low, slope based methods from analytical optimization can be used in experimental optimization. In the multi-element airfoil study by Landman [20], all these conditions were met. Thus, he was able to optimize the flap position by using a steepest ascent algorithm. However, in many experimental optimization situations the noise level is not low, and alternate optimization algorithms must be used. Spendley et al. [23] proposed the sequential use of a simplex designs (an equilateral triangle in two dimensions) to seek the experimental optimum of a response. Based on three simple rules, this procedure would seek the maximum of an experimental response. The basic idea in two dimensions is the replacement of the vertex with the lowest response by moving away from it by rotating

the equilateral triangle about the other two vertices. Experimental noise is dealt with by periodically replacing previous measurements according to specified rules.

2.4 Model Discrimination

The concept of using designed experiments to differentiate between competing models is known in the literature as model discrimination. A key element of model discrimination is the maximizing of differences between the competing models. Thus, in principle it is similar to the concept of anti-optimization being used herein. This makes the model discrimination literature of interest to the present investigation. The discussion related to model discrimination in this section is adapted from the review by Haftka et al. [8] of which I am a co-author and main contributor to this section.

Optimization can be used to design experiments that will discriminate among competing models of physical phenomena. Hill [24] reviewed proposed experimental design procedures to discriminate among competing models. One of the earliest procedures reviewed by Hill is that of Hunter and Reiner [25]. The Hunter and Reiner experimental design procedure is intended to discriminate among two competing models. After an initial set of experiments is completed, the two competing models are fitted to the experimental data. Additional experimental points are placed at locations where the predictions of both models differ the most. Doing this intentionally places the models in jeopardy, so that one is shown to be more correct than the alternate. By its very nature this procedure is sequential and requires repeated experimentation. In the present investigation this sequential experimental procedure to maximize differences is named anti-optimization, and is conducted between a single analysis and a corresponding experiment. Froment [26] shows how the Hunter and Reiner procedure can be extended to more than two models.

The Hunter and Reiner procedure is intended to be applied to chemical reaction kinetics, and it is often cited in this literature. However, no references in the chemical literature were found of it being used with actual experimental data. A likely reason for this is the development of a more general procedure, discussed below, by Box and Hill [27]. Nevertheless, the Hunter and Reiner procedure is general and has been applied to other fields. Schmid-Hempel [28] presents an example of its use to discriminate among two models of nectar-collecting by honeybees. It has also been proposed for use in the study of water resources by Knopman and Voss [29] and for environmental field studies by Eberhardt and Thomas [30].

Box and Hill [27] proposed an alternate approach to model discrimination that addressed two criticisms of the Hunter and Reiner [25] procedure. First, their approach allows for the discrimination among multiple models, not just two. Second, their approach allows for consideration of the error of the estimated difference among models. As with the Hunter and Reiner procedure, that proposed by Box and Hill is sequential in

nature. Several applications of the Box and Hill approach appear in the chemistry literature [31, 32, and 33]. Atkinson [34] compared the Hunter and Reiner and the Box and Hill procedures for the case of two competing models. In the examples he considered, no significant differences were found between the two procedures.

Atkinson [35] proposed a procedure to test the adequacy of a particular model. The model under consideration is incremented with additional extension terms with unknown coefficients. Experimental designs such as D-optimal are then used to define experiments to determine the values of all unknown coefficients, including the extension coefficients. The suitability of the original model is assessed by testing the significance of the extension terms. Candas et al. [36] used a variant of Atkinson's procedure to discriminate among models for the distribution and metabolism of corticotropin-releasing factors in rats. The models consisted of sums of exponential terms with unknown parameters (coefficients and exponents). Two models were considered: a biexponential (i.e., two-term) model, and a triexponential (i.e., three-term) model. The biexponential model was contained within the triexponential model. Using a combined sampling set, they determined that the triexponential model produced the best fit to their data. A feature of this procedure for model discrimination is that, since it is not sequential, it is suited for experiment preferably performed in pre-determined batches.

In the aerospace field, Haftka and Kao [2] suggested the use of numerical optimization to sharpen the differences between competing models for composite laminate failure, and using these results to guide subsequent experiments. Wamelen et al. [37] followed through on this suggestion, undertaking the indicated optimization and performing a set of experiments that validated one of the two competing analyses.

2.5 *Verification and Validation of Aerodynamic Codes*

Although not all the codes used in the present investigation can be considered to be Computational Fluid Dynamics (CFD) codes, the substantial literature related to the *verification* and *validation* (V&V)² of CFD codes is directly applicable. Thus, the literature related to V&V of CFD codes is of interest to the present investigation and reviewed in this section.

During the late 1980s it became evident that there was a need for a more formalized approach to the *verification* and *validation* (V&V) of CFD codes. To satisfy that need, the North Atlantic Treaty Organization's (NATO) Advisory Group for Aerospace

² The terms *verification* and *validation* have not been used consistently in the literature. In the present investigation *verification* relates to the numerical correctness of codes, while *validation* refers to a code's ability to model the physical world. When *verification* and *validation* are used with these meanings they appear in italics within this chapter. The acronym V&V is always used with these meanings. In subsequent chapters they are always used with these meanings and appear in regular type. When *verification* and *validation* are used with other meanings by specific authors cited in this literature review they appear in regular type with the meaning given to them by the specific authors.

Research and Development (AGARD) organized a conference in 1988 to discuss V&V and survey the current thinking and state of the art in this area within the aerospace community. The proceedings of this conference were published in two volumes [38, 39], and evaluated by Sacher et al. in reference 40. Particularly important among the papers of this conference were those in Session I, “CFD Validation Concepts,” by Bradley [41], Marvin [42], and Boerstoeel [43] since they set the tone for the work in this area through the following decade. Bradley stressed the need for code validation to achieve “Mature Capability” or “Level V” in the five-step CFD development cycle he presents. He used the term validation in referring to both *verification* and *validation*. Marvin addresses the “role of experiment in the development of Computational Fluid Dynamics (CFD) for aerodynamic flow prediction,” with the key point being that “CFD verification is a concept that depends on closely coordinated planning between computational and experimental disciplines” [42, p. 2-1]. With respect to experiments he stresses the need for completeness and accuracy. Boerstoeel stresses the need to assess the numerical accuracy of the codes (by what he calls numerical experiments), independently of comparisons of physical data. These papers thus establish: 1) the need for CFD V&V (Bradley), 2) the importance of *verification* (Boerstoeel), and the role of experiments in *validation* (Marvin). Following this conference, significant work in this area was undertaken. By 1998 CFD code V&V was the subject of a special section in an issue of the American Institute of Aeronautics and Astronautics (AIAA) Journal [44], a book by Roache [45], and a set of guidelines by the AIAA [46]. Oberkampf et al. [47] recently reviewed the state of the art. At the present, a consensus in the terminology and methods has evolved, but much work remains to be done. This is stated in the AIAA guide as follows: “The document’s goal is to provide a foundation for the major issues and concepts in verification and validation. However, this document does not recommend standards in these areas because a number of important issues are not yet resolved.” [46, p. i].

As has been noted, the terms verification and validation have been used with different meanings and/or interchangeably in the literature. Oberkampf [48] reviewed the terms and definitions used by various authors, and concluded that the definitions for *verification* and *validation* proposed by Blottner [49] based on the work of Boehm [50, p. 728] captured the essence of the terms, and clearly separated them so that the activities they imply could be addressed. Blottner defined *verification* and *validation* as follows:

Verification: “Code verification (*solving governing equations right*) is the determination of the accuracy of the numerical solution of the chosen governing equations.”

Validation: “Code validation (*solving right governing equations*) is the evaluation of the accuracy of the governing equations that are being solved.”

(quotations from reference 49, page 113; italics in quotes by the original author.). These are essentially the definitions adopted by Roache [45] in his book, and by the AIAA in its

guide [46]. Thus, there is a consensus building around these definitions and they are adopted in the present investigation.

As pointed out by Roache [45] *verification* is a mathematical exercise and can be undertaken without experimentation. Aeschliman et al. [51] identified the issues pertinent to CFD code verification as falling into one of the following categories: discretization of the continuum equations, spatial and temporal discretization convergence, iterative convergence, programming errors, and round-off/truncation errors. Aeschliman and Oberkampf have proposed that comparison with “exact analytic solutions, computations from previously verified codes, and codes that address simplified, or specialized, cases” be used for code *verification* [52, p. 733]. Roache [53] proposed the Grid Convergence Index method for assessment of the convergence of a CFD code, without having to double the grid density. Once a code is *verified*, there are some assurances that the code will converge to a correct solution of the equations used as the grid density increases. However, even after a code is *verified*, Roache [53] has pointed out that its use for a particular calculation also needs to be *verified* to assess the accuracy for the particular calculation at the specified grid density. A good example of calculation *verification* is given in reference 54 by McWherther Walker and Oberkampf. In this study, designed specifically for code *verification* and *validation*, the force and moment coefficients of a hypersonic vehicle were studied as a function of the number of streamwise grid points, circumferential grid points and body to shock grid points. Richardson extrapolation was used to estimate the “‘exact’ solution as the number of grid points approaches infinity.” [54, p. 2012]. The convergence criteria used was a one percent difference between the actual solution and the extrapolated “exact” solution. Based on this criteria, particular values of the streamwise, circumferential, and shock grid points were selected for the computations. In order to proceed with *validation*, *verification* of the code and the particular calculation, is recommended. This sequential approach is advocated by several authors, including Melnik et al. [55, p. 3] and Roache [45, p. 29].

Roache [45, p. 24] has pointed out that the key difference between *verification* and *validation* is that *verification* lies in the realm of mathematics, where as *validation* is part of science and engineering. Thus, *validation* requires experimentation. In the earlier papers on this subject the required experimental data was obtained from previously published research [56], existing databases [57, 58], or databases explicitly collected for code validation [59, 60]. However, existing experimental data and/or data bases were often found to be inadequate for CFD code *validation*. Baltar and Tjonneland [61] noted that lack of documentation in the existing experimental data they used was of concern. Bertin et al. [62] noted that in their area of interest (sharp cones at hypersonic speeds) “the quality of the data available in the open literature is uneven and, in most cases, no attempt was made in the past to assess the relative or absolute uncertainty of the results” and they proposed the development of a database specifically for *validation*. Along these same lines Aeschliman et al. [51] noted that comparisons with existing experimental data generated for purposes other than *validation* was unsatisfactory. Thus they proposed, in a

comprehensive set of guidelines for CFD code *validation* experiments, that these experiments be designed specifically for *validation* purposes by those developing the CFD codes and experimentalists. In the design of experiments for CFD code *validation*, the importance of reducing and quantifying uncertainty has been noted by several authors. Bobbitt [63] presented a comprehensive list of uncertainty and error sources in wind tunnel testing. Marvin and Holst [64], Aeschliman et al. [51], Roache [45], and the AIAA guide for V&V [46] have stressed the importance of quantifying uncertainty. The methods to do so, both for precision (random) and bias (systematic) uncertainty are have been documented in an AGARD advisory report [65]. Roache [45, pp. 331-335] reports on a method devised by Coleman and Stern [66] for taking into consideration the uncertainties of both the CFD code calculations and the experimental results in comparing them for the purpose of *validation*. Although of some usefulness, Roache and the original authors point out this approach contains some paradoxes and pitfalls in interpretation that should be clearly understood. For example, increasing uncertainty in the CFD code results yields a higher probability that the comparison will yield a verdict of “*validated*.”

Two additional, and related, points regarding *validation* need to be discussed. First, as Roache [45] points out, *validation* can only be shown for a given calculation or range of calculations (e.g., geometry, Mach number, Reynolds number, etc.). However, most CFD codes are quite general, and calculations well beyond those which have been already *validated* can be carried out. For these later cases, the CFD code cannot be considered to be *validated*. This situation leads to the second point: CFD code *validation* is an ongoing process, with additional experimentation and required to extend the *validation* to additional calculations.

Of the numerous papers reporting *validation* of CFD codes, two are particularly relevant to the present investigation. Firmin and McDonald [67] reported on the design of a low aspect ratio wing for the validation of CFD codes. The interesting aspect of this research is that the wing was designed specifically to stress the ability of the CFD codes to predict the flow accurately. In particular, their goals were to design a wing that exhibited “extreme three-dimensionality within the boundary layer for at least part of the flow” and “incipient separation near to the trailing edge of the upper surface.” Using this approach to the design of the wing yielded an unconventional airfoil shape (i.e., thicker than usual and with an unusual camber) and twist distribution. Initial testing with a pilot model indicated that the design goals were met. Their approach to *validation* is similar to that being proposed herein, namely anti-optimization, since it pursues *validation* by intentionally stressing the computational models. The other relevant paper is that of Cutler et al. [68]. They report on an effort to validate a CFD code to design supersonic combustors. This work is of particular interest because it uses modern design of experiments techniques for the *validation* of a CFD code. By using design of experiments they were able to “reduce the quantity of data required to meet the goals of this work” and “minimize systematic errors” associated with uncontrolled variables. In the search for relevant literature for this review this was the only paper found in which

design of experiments was used in the service of a CFD code *validation*. The experiments performed by Cutler et al. did not agree with the pre-test CFD calculations. They conclude that improvements are needed in the modeling accuracy of chemical kinetics, turbulence-chemistry interactions, and turbulence mixing.

2.6 Concluding Remarks

Having reviewed the relevant literature, the present investigation can be placed in this larger context and the contributions identified. The present investigation falls within the field of *validation* of aerodynamic codes. This has been an active area of research for the past 15 years. Within this area it follows the approach of performing *validation* with an experiment specifically design for this purpose [51]. In pursuit of this validation, and in order to help in identifying possible problems with the codes, the concept of anti-optimization as proposed by Haftka and Kao [2] is applied. Although the concept of anti-optimization has been applied to structural problems [37], it has not been used for the *validation* of aerodynamic codes. Thus, the application of anti-optimization in the present investigation is a contribution to the field of aerodynamic codes *validation*. Although Haftka and Kao were the first to propose the use of anti-optimization in aerospace and came up with the concept independently, similar ideas had been proposed earlier under the name of model discrimination in the field of chemistry. Hunter and Reiner [25] had proposed the idea of conducting experiments to maximize the difference between models. Box and Hill [27] expanded the proposal of Hunter and Reiner by including considerations related to the uncertainties in the experimental data. The present investigation applies both of these ideas: planning experiments to maximize differences taking into account uncertainties in the experimental results. Consideration of uncertainties in both calculations and experiments is also stressed in the literature related to the *validation* of aerodynamic codes. The present investigation also applies these recommendations. Although response surface methods, design of experiments, and experimental optimization methods have a long development history and have been applied in numerous fields, their use in wind tunnel testing is fairly recent. Only one example of the application of these methods to the *validation* of aerodynamic codes was found in the literature [68].

Chapter 3: Aerodynamic Codes and Analysis

As detailed in the introduction (section 1.3) the maximum lift coefficient, $C_{L_{max}}$, is a critical parameter for the operation of an airplane intended for flight on Mars. The maximum lift coefficient of such an airplane affects the altitude lost during pullout, the maximum Mach number encountered during pullout, and the maximum mass the airplane can carry. Because of the low atmospheric density on Mars, high values of $C_{L_{max}}$ are needed at unusual combinations of Mach and Reynolds numbers: namely Mach numbers up to 0.8 and Reynolds numbers as low as 43,000. Aerodynamic codes that can predict $C_{L_{max}}$ have not been validated at these operating conditions mainly because of a lack of experimental data. This fact makes the validation undertaken in this work more interesting since it is conducted in a hitherto unexplored flight regime.

Predictions for the maximum lift coefficient were performed by combining the results of two codes. A two-dimensional airfoil code (using an Euler solver combined with an integral boundary layer formulation) was used to obtain the airfoil section lift characteristics. A lifting line code, which used the results of the two-dimensional airfoil code as input, was then used to predict the behavior of the three-dimensional wing. The ability of this combination of codes to predict $C_{L_{max}}$ was the example analysis to be validated in the present investigation.¹ Although it may seem unusual to validate an analysis arrived at by the use of two separate codes it should be realized that such combinations already typically exist within a single code. For example, the single two-dimensional airfoil code used in the present work (i.e., MSES) incorporates several physical models:

- an Euler analysis to calculate the inviscid portion of the flow,
- an integral boundary layer formulation,
- an algorithm to match the viscous and inviscid analyses,
- a transition prediction analysis to determine where the boundary layer transitions from laminar to turbulent,

¹ When reference is being made to either one of the computer programs in isolation, they will be referred to as “codes.” The term “analysis” is used to denote combined results of both codes to yield the three-dimensional wing parameters of interest, principally $C_{L_{max}}$.

- a boundary layer separation/re-attachment analysis.

Thus, the use of more than one code (i.e., computer program) does not conflict with the idea of validation.

There are other code options for predicting the maximum lift coefficient of a wing at the operating conditions investigated herein. These options fall mainly in two groups: three-dimensional Euler codes (without boundary layer models) and three-dimensional Navier-Stokes codes. Neither of these options was suitable for the present investigation for several reasons. First there are problems related to modeling effort and cost. Considering the number of analyses required to undertake the present work, both the modeling effort and computational cost of using either three-dimensional Euler or Navier-Stokes codes would have been prohibitive. The codes used in the present investigation involved negligible modeling effort and moderate computational cost. Another reason for not using these alternate code options was their suitability to accurately model the relevant physics at the conditions of interest. At the Reynolds numbers being considered here, the accurate modeling of the boundary layer (including separation and possible re-attachment) is critical for the determination of $C_{L,max}$. A three-dimensional Euler code without a boundary layer model is thus unsuitable since it does not include key relevant physics. Current three-dimensional Navier-Stokes are typically intended for use at much higher Reynolds numbers, and require advanced knowledge of boundary layer behavior such as transition or separation. Thus, they also seemed unsuitable for the present investigation. As discussed above and in the following section, the two-dimensional airfoil code used here is intended for use at low Reynolds numbers and includes physical models to deal with such conditions. Coupling two-dimensional airfoil data (whether its source be experiments or analyses) with a lifting line analysis to generate three-dimensional wing coefficients has been proven in the past to yield adequate results. Thus, although the codes chosen for validation are not perfect, they offered the possibility of modeling most of the flow physics of interest with reasonable accuracy, minimal modeling effort, and acceptable computational cost.

In this chapter the two-dimensional airfoil code and the lifting line code are described. It is assumed that both codes have been verified² and that only verification of the particular calculation needs to be performed to assess convergence and generate estimates of the analysis uncertainty. Results of convergence studies for both codes are presented in this chapter. The calculation of the two-dimensional airfoil performance depends on the boundary layer transition parameter N_{crit} (discussed in more detail later in this chapter). This parameter was derived from experimental measurements of freestream turbulence in the particular wind tunnel being used, and is thus subject to experimental uncertainty. To assess the effect of the uncertainty in N_{crit} on $C_{L,max}$, a sensitivity study was conducted. The results of this sensitivity study are discussed in this chapter. Finally, an estimate of the uncertainty in the analysis results are presented.

² Verification of the codes being used is outside the scope of the present investigation.

3.1 Two-Dimensional Airfoil Code

The code used to perform the two-dimensional airfoil analyses was MSES,³ as described in references 69 through 71. MSES is an airfoil design and analysis code intended to yield good results over a wide range of Mach, M , and Reynolds, Re , numbers. The inviscid flowfield is modeled by the steady Euler equations in integral form. An integral viscous formulation is used to model the boundary layers and wakes. The code is capable of modeling moderately separated flows, allowing calculation of airfoil performance beyond $C_{L,max}$. Boundary layer transition is modeled by the Orr-Sommerfeld spatial amplification theory using an $\exp(N_{crit})$ criterion. N_{crit} depends on the freestream turbulence as described in references 72 and 73 (appendix A discusses this dependency in more detail). MSES solves for the inviscid and viscous flowfields simultaneously through the Newton-Raphson method.

MSES has been used successfully to design and analyze airfoils at transonic Mach numbers and low Reynolds numbers. In reference 69 comparisons are presented between analysis and experiments for various airfoils (e.g., NACA 0012, RAE 2822, FX76-MP160, LNV109A) in the Mach numbers from 0.1 up to 0.8 and Reynolds numbers from 250,000 to 9×10^6 . The analysis/experiment correlation in all cases was fair to excellent. Reference 74 describes the use of MSES for the design of the airfoils for the MIT Daedalus prototype human-powered aircraft. These airfoils were designed to operate at subsonic Mach numbers and Reynolds numbers from 540,000 to 180,000. MSES has been applied to the design of transonic low-Reynolds number airfoils for ultra high-altitude aircraft [75, 76]. These airfoils were intended to operate at Mach numbers between 0.5 and 0.65 and Reynolds numbers from 100,000 to 700,000.

The ability of MSES to model transonic low-Reynolds number airfoils made it an ideal choice as the two-dimensional airfoil analysis code for the present investigation. In addition, the fact that MSES has not been checked against experimental data in an extensive portion of the Mach and Reynolds number range being considered in the present investigation makes the validation of the analysis more interesting.

In using MSES during the present investigation most of the default parameters for grid generation were used. The only parameter varied was the number of grid points on the airfoil surface, N_{grid} . For the preliminary analyses performed for the experimental design the default value of N_{grid} , 141, was used. This number of grid points on the airfoil surface yielded solutions that were essentially converged. Subsequently, a convergence study was conducted and N_{grid} was increased to 155 for the final set of analyses. This convergence study is discussed in section 3.3. The variable N_{crit} (used in the boundary layer transition model) is related to the freestream turbulence in the wind tunnel. In the Transonic Dynamics Tunnel, N_{crit} depends on the condition to be analyzed (i.e., M and

³ MSES is the multiple airfoil version of the ISES code. Except for the multiple airfoil capability of MSES, both codes are equivalent. The terms MSES and ISES are names with no specific meanings.

Re). Calculation of the appropriate value for N_{crit} for a given combination of M and Re is presented in appendix A. Computations for the airfoil section aerodynamic coefficients were typically initiated at zero angle of attack. To the greatest extent possible, the angle of attack was increased/decreased by 0.1° when calculating the airfoil section aerodynamic coefficients.

At the highest Mach number considered in this study, namely 0.8, MSES was unable to converge over the whole range of angles of attack. In particular, MSES was unable to converge at angles of attack around the two-dimensional airfoil maximum lift coefficient, c_{lmax} . An example of this occurrence is shown in figure 3.1. It may be that there is not a steady state solution in this range of angles of attack. In such a case MSES may be unable to converge since it is a steady-state code. This type of unsteady behavior has been observed before, both experimentally and by analysis, at transonic speeds [77, 78]. In order to proceed with the calculations, the aerodynamic coefficients have been interpolated in the range of angles of attack for which MSES is unable to converge. An example of such an interpolation is shown in figure 3.1 (note that this figure shows the two-dimensional airfoil lift coefficient, c_l , versus angle of attack, α , not the three-dimensional wing lift coefficient, C_L). If it is true that the inability of MSES to converge at these angles of attack is due to the inherently unsteady nature of the flow, the interpolation can be considered to be a time-averaged response.

3.2 Lifting Line Theory Code

The code used to generate three-dimensional wing results implements a lifting line theory. This code is a modified version of that described in reference 79, which in turn was an improvement on the code described in reference 80. This code is based on the method of Weissinger [81]. Mark Guynn of the NASA Langley Research Center modified the code to improve its convergence characteristics. The code is capable of modeling multiple lifting surfaces (e.g., wing, horizontal stabilizer). However, in the present investigation only a single surface needed to be modeled.

In the lifting line code, the wing is modeled by a series of horseshoe vortices along the quarter-chord of the wing. The strengths of these vortices are calculated from the solution of a linear system generated by specifying flow tangency points at each station (i.e. strip) along the wing. The chordwise location of these flow tangency points is determined from the two-dimensional airfoil lift curve slope data at the appropriate angle of attack provided as input to the code (in the present investigation this two-dimensional airfoil data was generated by MSES). At a particular station the relationship between the two-dimensional airfoil lift curve slope, $c_{l\alpha}$, and the distance of the flow tangency point aft of the quarter chord, h , is given by:

$$h = \frac{c}{2} \frac{c_{l\alpha}}{2\pi} \quad (3.1)$$

where c is the wing chord. Note that if c_{l_α} is equal to 2π , equation 3.1 yields the well known result that the flow tangency point is at the three-quarter chord point (i.e., $h = c/2$) for thin airfoils in incompressible flow. Although the system of equations that need to be solved for the strength of the vortices is linear, the typically nonlinear two-dimensional airfoil behavior requires a nonlinear solution algorithm to converge to a solution. Once the strength of the vortices is determined, wing performance parameters such as the lift, drag, and pitching moment coefficients (C_L , C_D , and C_M , respectively) are calculated based on the vortex strengths and the two-dimensional airfoil data (i.e., c_l , c_d , $c_m c/4$) at specific angles of attack. At each condition the angles of attack used ranged from the angle of attack for which $C_L = 0$ up to the highest angle of attack for which convergence could be attained but not exceeding 24° (the highest angle of attack for which experimental data was obtained). In general, calculations were performed with angle of attack increments of 0.1° through most of the angle of attack range, and by 0.01° increments near $C_{L_{max}}$. In the present investigation the lifting line code was used with the planar wake assumption and uniform spacing of the vortices. Although the option of using a semi-cosine distribution of vortices was available, comparisons of results with both options did not identify any advantage in using the semi-cosine distribution. For the preliminary analyses performed for the experimental design, a value of 100 was used for the number of spanwise vortices, $N_{vortices}$. This number of vortices yielded a nearly converged solution. Subsequently a convergence study was conducted and $N_{vortices}$ was increased to 300 for the final set of runs. This convergence study is discussed in section 3.3.

As shown in references 79 and 80, the lifting line code has been shown to provide good results for simple wing geometries when provided with adequate two-dimensional airfoil data. Good correlation between lifting line codes and experiments for simple wing geometries have been reported by other researchers using similar codes [82]. Given appropriate post-stall two-dimensional airfoil data, the lifting line code captures the maximum lift coefficient, although the post-stall behavior is not captured as accurately. Problems and concerns with the post-stall behavior and accuracy of lifting lines codes such as the one used in the present investigation have been reported by other researchers [82, 83]. The lifting line code used in this investigation extrapolates the two-dimensional airfoil data in an attempt to obtain post-stall behavior. Thus, the post-stall results should be considered qualitative. Nevertheless, the C_L vs α curves for cases where post-stall result were generated by the lifting line code were adequate to identify $C_{L_{max}}$. In a few cases, no value of $C_{L_{max}}$ could be clearly identified from the C_L vs α curve. This behavior was observed in both the analysis and experimental results. For these cases an engineering definition of $C_{L_{max}}$ was created and implemented. This definition and its implementation is described in detail in sections 3.3 (with regards to the aerodynamic analysis data) and 6.3 (with regards to the experimental data). For some cases the lifting line code was unstable in the post-stall region, and convergence to a post-stall solution was not possible. However, in these cases the lift coefficient at the wing centerline was equal to the maximum lift coefficient of the two-dimensional airfoil at the highest

converged angle of attack, indicating that C_{Lmax} had been reached at this angle of attack. Thus, in these cases C_{Lmax} was the value of C_L obtained at highest angle of attack for which convergence was achieved.

3.3 Convergence Studies

As mentioned in sections 3.1 and 3.2, the values of N_{grid} and $N_{vortices}$ used in the preliminary analyses performed for the experimental design were 141 and 100, respectively. Subsequently, convergence studies were performed to ascertain that these results were converged. These convergence studies confirmed that the preliminary analyses were close enough to being converged for the purpose of designing the experiment. However, the values of N_{grid} and $N_{vortices}$ were updated for the final set of calculations (i.e., for the analysis results used to compare against the experimental data) as a results of the convergence studies. The results of the convergence studies, and the final values of N_{grid} and $N_{vortices}$ are presented in this section.

The wing design and test design space are presented in sections 4.1, 4.2 and 5.1. However, some knowledge of these items is necessary at this point in order to understand the convergence studies. Thus, brief descriptions of the wing and test design space are given here. The airfoil used was the MASC1 (Mars Airplane Super Critical #1) with finite trailing edge thickness. The wing was rectangular, and approximates a quarter-scale model of a small Mars airplane. It was unswept with a chord of 0.08750 m (3.445 in) and a wing span of 0.43180 m (17.000 in), which yielded a wing area of 0.037784 m² (58.565 in²) and an aspect ratio of 4.934 (these dimensions and the aspect ratio are nominal values, the actual as-built values for the wind tunnel model are given in section 5.1). The test design space was as shown in figure 3.2. This design space was chosen so as to include regions in which MSES is thought to yield good results ($M = 0.300$, $Re = 250,000$), and regions of interest to the flight of Mars airplanes ($M = 0.800$, $Re = 25,000$) which could present a challenge to MSES. The curved portions of the test design space boundary are lines of constant dynamic pressure. On the upper (i.e., high Re) boundary, dynamic pressure was limited for reasons related to the maximum load capability of the wind tunnel balance. On the lower (i.e., low Re) boundary, dynamic pressure was limited for reasons related to the accuracy of the wind tunnel balance.

Figure 3.2 shows the test design space and the location of the points used for the convergence studies. The values of M and Re for the convergence studies points are given in table 3.1. Calculations were performed with MSES at these points for varying values of N_{grid} . For most points these calculations were performed at 11 values of N_{grid} from 141 to 285.⁴ However, for the cases in which $M = 0.800$, it became extremely difficult to generate airfoil performance data for $N_{grid} > 155$. Thus, for cases in which $M = 0.800$, calculations were performed with N_{grid} equal to 141 and 155 only. The two-dimensional airfoil data was used by the lifting line analysis (using $N_{vortices} = 300$) to

⁴ The values of N_{grid} used were 141, 155, 170, 185, 200, 215, 230, 245, 260, 275, and 285.

generate values of $C_{L\max}$. For $M = 0.800$ the calculated C_L vs α curve did not yield a mathematically defined value of $C_{L\max}$ as shown in figure 3.3. In these cases an engineering value of $C_{L\max}$ was used, defined as the value of C_L where $d^2C_L/d\alpha^2 = 0$ as obtained from a sixth order polynomial interpolation of the C_L vs α data. This engineering definition of $C_{L\max}$ is discussed further in chapters 4 and 6. The results of the N_{grid} convergence study are shown in figures 3.4 through 3.11 (all results are shown with the same vertical and horizontal scale size to facilitate comparisons between figures). From these figures it can be observed that for cases in which $M < 0.800$, solutions with $N_{grid} \geq 155$ were converged; there was no clear increase or decrease in $C_{L\max}$ as N_{grid} increased from 155 to 285. For cases in which $M = 0.800$ the maximum value of N_{grid} for which solutions could be generated was 155; there was little difference between these solutions and those obtained with $N_{grid} = 141$. These results imply that $N_{grid} = 155$ should be sufficient to consider the solution converged. The added time and difficulty of obtaining solutions for higher values of N_{grid} also argues for choosing the lowest value that will yield a sufficiently accurate solution.

The differences in the solution for the various values of N_{grid} can be attributed to numerical noise, which yields some level of uncertainty in the solution. A quantification of the magnitude of this uncertainty can be generated by calculating the range of $C_{L\max}$ obtained by solutions that are considered to be converged. Once such range can be defined as the maximum absolute value of the difference between $C_{L\max}$ obtained with $N_{grid} = 155$ (the value of N_{grid} used for the final calculations), and the $C_{L\max}$ obtained with $N_{grid} > 155$. The value of $C_{L\max}$ obtained with $N_{grid} = 155$, and the range as defined above at the available convergence studies points are shown in table 3.2 (note that no values are shown for the convergence studies points with $M = 0.800$ since no calculations were performed with $N_{grid} > 155$ for the reasons discussed above). Examining these data yields two observations. First, the range of $C_{L\max}$ is relatively small, never exceeding 0.0163 in absolute value, or 1.6 percent in relative value. Second, the range of $C_{L\max}$ has a tendency to decrease with Re , both in absolute and relative values. The data in table 3.2 are used, in conjunction with the data from the N_{crit} sensitivity analysis discussed in section 3.4, to generate an uncertainty bound of the analysis values of $C_{L\max}$ as discussed in section 3.5.

A convergence study was conducted for the lifting line code by varying the number of spanwise vortices, $N_{vortices}$, in eight steps from 50 to 300.⁵ Although the computing time required increased rapidly as the number of $N_{vortices}$ increased, the ability of the code to converge was not compromised. The convergence study was conducted at the conditions specified in figure 3.2 and table 3.1. The input two-dimensional airfoil data was generated by MSES with $N_{grid} = 141$. The results of this convergence study can be seen in figures 3.12 through 3.19. In these figures the $C_{L\max}$ is plotted vs $1/N_{vortices}$.⁶ From these figures the fully converged results can be estimated by extrapolating to $1/N_{vortices} = 0$ (i.e., $N_{vortices} = \infty$). As can be seen from these figures, solutions for all cases using

⁵ The values of $N_{vortices}$ used were 50, 75, 100, 125, 150, 200, 250, and 300.

⁶ For the cases in which $M = 0.800$, the engineering definition of $C_{L\max}$ as described in section 3.3 was used.

$N_{vortices} = 100$ ($1/N_{vortices} = 0.01$) are within 0.015 in C_{Lmax} of the extrapolated value for $N_{vortices} = \infty$ ($1/N_{vortices} = 0$); solutions using $N_{vortices} = 300$ ($1/N_{vortices} = 0.00333$) are within 0.001. These observations indicate that using $N_{vortices} = 100$ for the preliminary results used in the experimental design was adequate. For the final analyses (i.e., those undertaken to compare with the experimental results), 300 vortices were used. Although the solution time for 300 vortices is significantly greater than for 100 vortices, the limited number of runs required for the final analyses made these calculations possible in a reasonable amount of time.

3.4 Sensitivity of C_{Lmax} to N_{crit}

The values of N_{crit} used in the present investigation are based on a response surface fit to experimental measurements taken in the Transonic Dynamics Tunnel as described in appendix A. N_{crit} values derived from this response surface have an uncertainty associated with them. Table 3.3 shows the mean values of N_{crit} for the convergence studies points calculated from the response surface function, and the 95 percent confidence interval of the mean at these points. To assess the sensitivity of C_{Lmax} to N_{crit} , additional calculations of C_{Lmax} were performed for values of N_{crit} equal to the upper and lower values of the 95 percent confidence interval of the mean of N_{crit} as given in table 3.3. These calculations were performed with values of N_{grid} and $N_{vortices}$ equal to 141 and 300, respectively. The results of these calculations, and those performed for the mean value of N_{crit} , are shown in table 3.4. In addition to showing the calculated values of C_{Lmax} , the range of C_{Lmax} for each condition are also shown. This range is defined as the absolute value of the difference between the highest and lowest value of C_{Lmax} at a given condition for the three values of N_{crit} listed in table 3.3. These data indicate that C_{Lmax} is insensitive to N_{crit} . For all convergence studies points (other than the one for $M = 0.800$ and $Re = 25,000$), the range of C_{Lmax} is less than or equal to 0.0127 in absolute value or 1.2 percent in relative value. The convergence study point with $M = 0.8$ and $Re = 25,000$ is slightly more sensitive to N_{crit} ; its range of C_{Lmax} is 0.0190 in absolute value or 2.4 percent in relative value. Combined with the realization that these small ranges in C_{Lmax} due to N_{crit} also include numerical noise as discussed in section 3.3, it can be argued that a significant portion of the differences in C_{Lmax} observed for various values of N_{crit} are probably related to numerical noise.

3.5 Uncertainty in the Aerodynamic Analysis Results

To make comparisons between the analysis and experimental results, uncertainty bounds for both sets of results must be established. In table 3.5 the range of C_{Lmax} for both the MSES convergence study and the N_{crit} sensitivity study as presented and defined in sections 3.3 and 3.4 respectively, are shown side by side at the convergence studies points. From these data, and discussions in the previous sections, the following two observations can be made. First, for the first five convergence studies points, the sensitivity to N_{crit} is small as compared to the numerical noise as shown by the range of

$C_{L\ max}$ from the MSES convergence study. This is particularly evident when one takes into account that the range of $C_{L\ max}$ from the N_{crit} sensitivity study contains, in addition to N_{crit} related effects, a contribution from the numerical noise in the calculation. Second, for the convergence studies points $M = 0.600$, $Re = 31,410$ and $M = 0.800$, $Re = 25,000$, the range of $C_{L\ max}$ from the N_{crit} sensitivity study is the dominant contribution to the uncertainty in the calculation. This statement relies on the observation that the range of $C_{L\ max}$ from the MSES convergence study is generally smaller at the lower Reynolds numbers.

Creating a statistically rigorous uncertainty for the $C_{L\ max}$ analysis results as a function of Reynolds and Mach number is extremely time consuming and beyond the scope of the present investigation. Thus, a *single value estimate* for this uncertainty was decided upon based on the data in table 3.5 and the two observations above. The magnitude of this uncertainty was bounded by two considerations. First, it had to be large enough to encompass the largest uncertainty within the test design space. Second, it could not be set to an artificially large value since doing so get in the way of making meaningful comparisons between the experimental and analysis results. If an unrealistically large value of the analysis uncertainty is selected, it is easier for an experimental result to fall within these uncertainty bounds, even if the experimental results differ significantly from the analysis results (these considerations are discussed in reference 66). The value of the analysis uncertainty in $C_{L\ max}$, denoted as $U_{C_{L\ max}, 1-\nu}^{Analysis}$ (where $1 - \nu$ denotes the confidence level), was thus selected to be 0.02. It was set at this value based on the range of $C_{L\ max}$ from the N_{crit} sensitivity study at $M = 0.8$, $Re = 25,000$. Given that the N_{crit} sensitivity study was performed at values of N_{crit} at the 95 percent confidence level of the mean, and that $U_{C_{L\ max}, 1-\nu}^{Analysis} = 0.02$ is greater than expected over a significant portion of the test design space, it will be assumed that the confidence level of this value of $U_{C_{L\ max}, 1-\nu}^{Analysis}$ is at least 95 percent; in other words, $1 - \nu \geq 0.95$.

Table 3.1 – Convergence studies points

M	Re
0.300	250,000
0.300	59,140
0.407	250,000
0.550	137,500
0.600	177,160
0.600	31,410
0.800	141,000
0.800	25,000

Table 3.2 – Values of C_{Lmax} for $N_{crit} = 155$ and the range of C_{Lmax} at the convergence studies points for the MSES convergence study

M	Re	C_{Lmax} for $N_{grid} = 155$	Range of C_{Lmax}
0.300	250,000	1.0351	0.0128
0.300	59,140	0.9575	0.0053
0.407	250,000	1.0165	0.0163
0.550	137,500	0.9658	0.0014
0.600	177,160	0.9992	0.0117
0.600	31,410	0.8421	0.0039
0.800	141,000	0.8086	Not Available
0.800	25,000	0.9204	Not Available

Notes:

- 1) Range of C_{Lmax} defined as the maximum absolute value of the difference between C_{Lmax} obtained with $N_{grid} = 155$ and C_{Lmax} obtained with $N_{grid} > 155$ for the values of N_{grid} used (i.e., $N_{grid} = 170, 185, 200, 215, 230, 245, 260, 275, 285$).
- 2) No calculations were performed for $N_{grid} > 155$ at $M = 0.800$. Thus, values for the range of C_{Lmax} at $M = 0.800$ are not available (see text for details).

Table 3.3 – Values of N_{crit} at the convergence studies points

M	Re	Response Surface Mean Value of N_{crit}	95% Confidence Interval of the Mean for N_{crit}
0.300	250,000	6.315	(5.896, 6.734)
0.300	59,140	4.919	(4.760, 5.078)
0.407	250,000	5.932	(5.638, 6.225)
0.550	137,500	5.218	(5.042, 5.394)
0.600	177,160	5.253	(5.037, 5.468)
0.600	31,410	4.144	(3.890, 4.397)
0.800	141,000	4.641	(4.359, 4.922)
0.800	25,000	3.837	(3.404, 4.269)

Table 3.4 – Sensitivity of C_{Lmax} to N_{crit} at the convergence studies points

M	Re	C_{Lmax} for the Response Surface Mean Value of N_{crit}	C_{Lmax} for the Lower Mean 95% Confidence Interval Value of N_{crit}	C_{Lmax} for the Upper Mean 95% Confidence Interval Value of N_{crit}	Range of C_{Lmax}
0.300	250,000	1.0260	1.0314	1.0220	0.0094
0.300	59,140	0.9563	0.9622	0.9572	0.0059
0.407	250,000	1.0364	1.0348	1.0237	0.0127
0.550	137,500	0.9663	0.9668	0.9662	0.0006
0.600	177,160	1.0091	1.0108	1.0123	0.0032
0.600	31,410	0.8421	0.8384	0.8451	0.0067
0.800	141,000	0.9204	0.9144	0.9224	0.0080
0.800	25,000	0.8075	0.7974	0.8164	0.0190

Notes:

- 1) All calculations performed with $N_{grid} = 141$ and $N_{vortices} = 300$.
- 2) C_{Lmax} range is defined as the absolute value of the difference between the highest and lowest value of C_{Lmax} for a given condition.

Table 3.5 – Comparison of the range of $C_{L,max}$ from the MSES convergence study and the N_{crit} sensitivity study at the convergence studies points

M	Re	Range of $C_{L,max}$ from the MSES Convergence Study	Range of $C_{L,max}$ from the N_{crit} Sensitivity Study
0.300	250,000	0.0128	0.0094
0.300	59,140	0.0053	0.0059
0.407	250,000	0.0163	0.0127
0.550	137,500	0.0014	0.0006
0.600	177,160	0.0117	0.0032
0.600	31,410	0.0039	0.0067
0.800	141,000	Not Available	0.0080
0.800	25,000	Not Available	0.0190

Notes:

- 1) Range of $C_{L,max}$ from the MSES convergence study is defined as the maximum absolute value of the difference between $C_{L,max}$ obtained with $N_{grid} = 155$ and $C_{L,max}$ obtained with $N_{grid} > 155$ for the values of N_{grid} used (i.e., $N_{grid} = 170, 185, 200, 215, 230, 245, 260, 275, 285$).
- 2) In the MSES convergence study no calculations were performed for $N_{grid} > 155$ at $M = 0.800$. Thus, values for the range of $C_{L,max}$ from the MSES convergence study at $M = 0.800$ are not available (see text for details).
- 3) Range of $C_{L,max}$ from the N_{crit} sensitivity study is defined as the absolute value of the difference between the highest and lowest value of $C_{L,max}$ for a given condition.
- 4) All calculations for range of $C_{L,max}$ from N_{crit} sensitivity study performed with $N_{grid} = 141$ and $N_{vortices} = 300$.

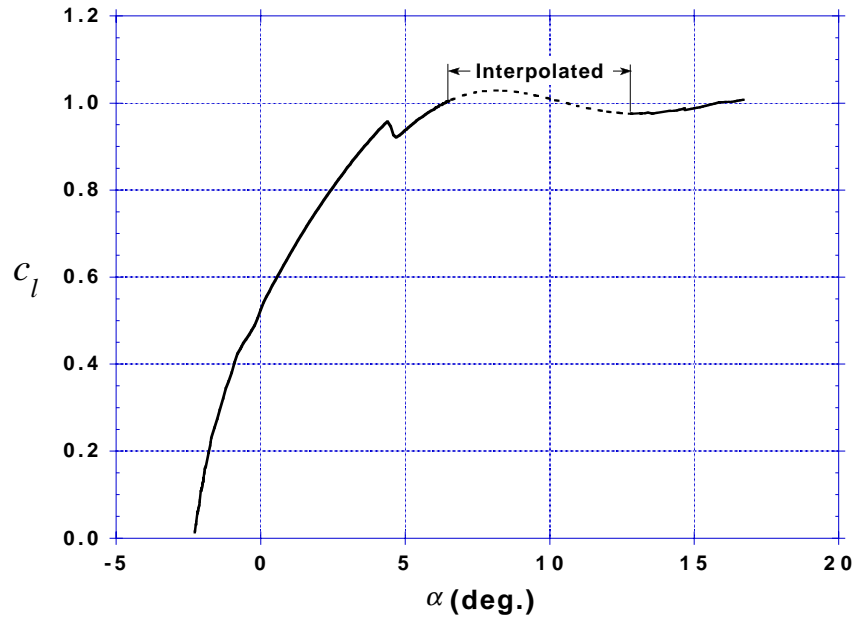


Figure 3.1 – c_l vs α curve for $M = 0.800$, $Re = 141,000$, generated by MSES showing interpolated region

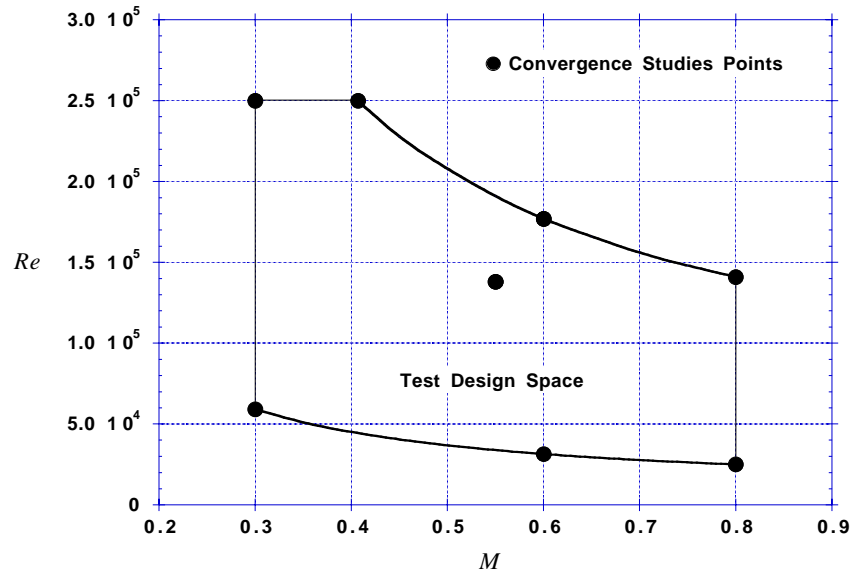


Figure 3.2 – Test design space and location of convergence studies points

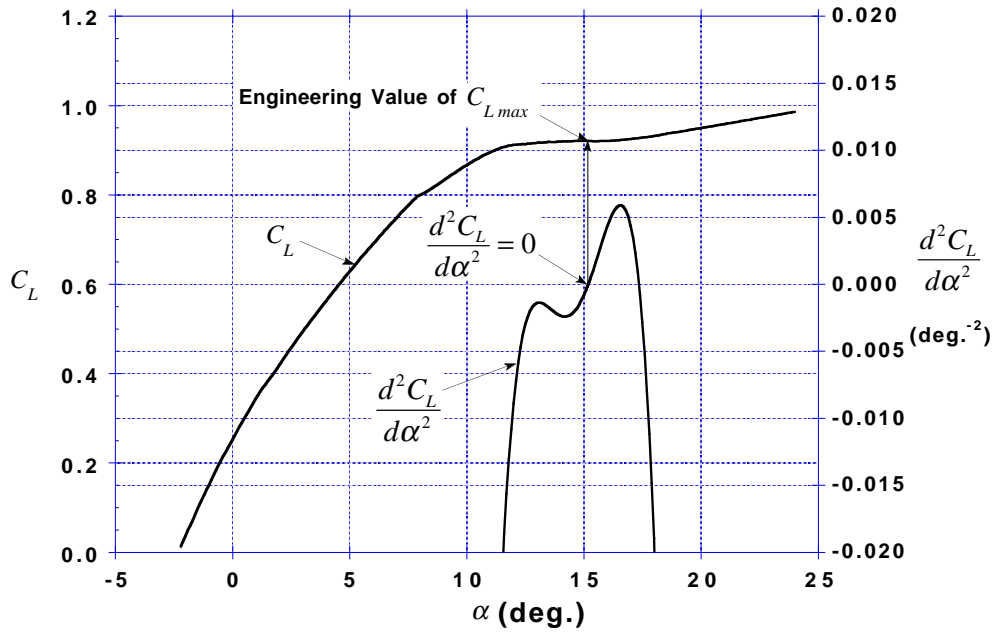


Figure 3.3 – C_L vs α curve for $M = 0.800$, $Re = 141,000$, showing the definition of the engineering value of C_{Lmax}

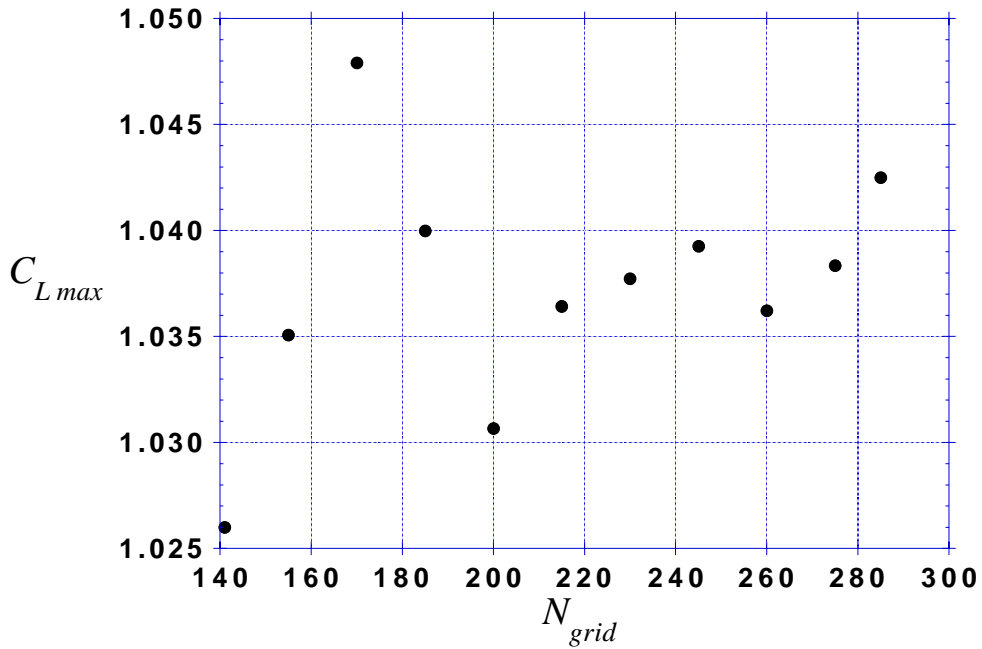


Figure 3.4 – MSES convergence study results for $M = 0.300$, $Re = 250,000$

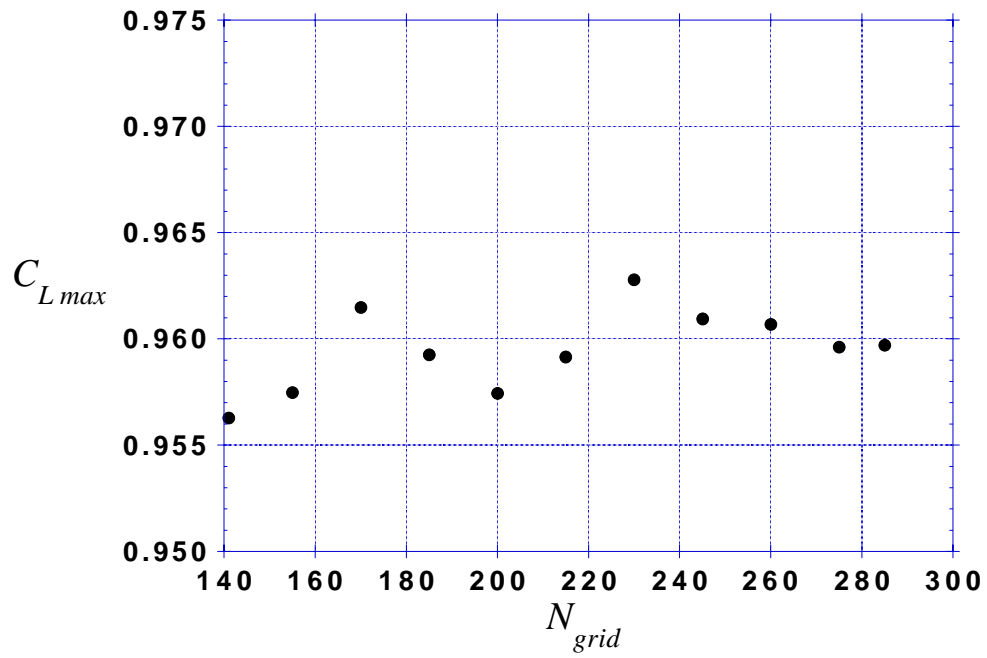


Figure 3.5 – MSES convergence study results for $M = 0.300$, $Re = 59,140$

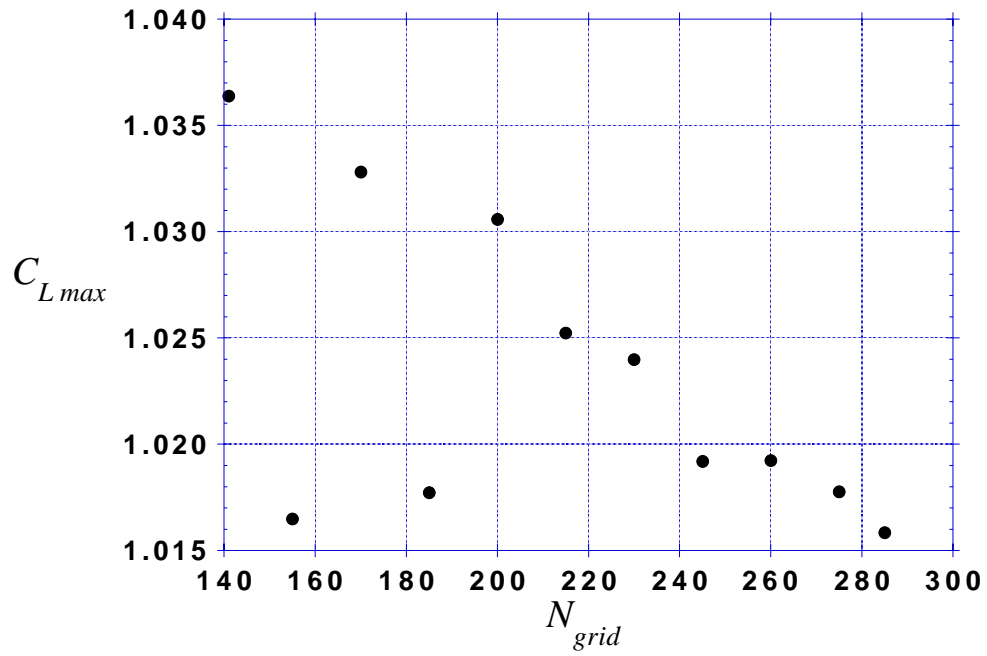
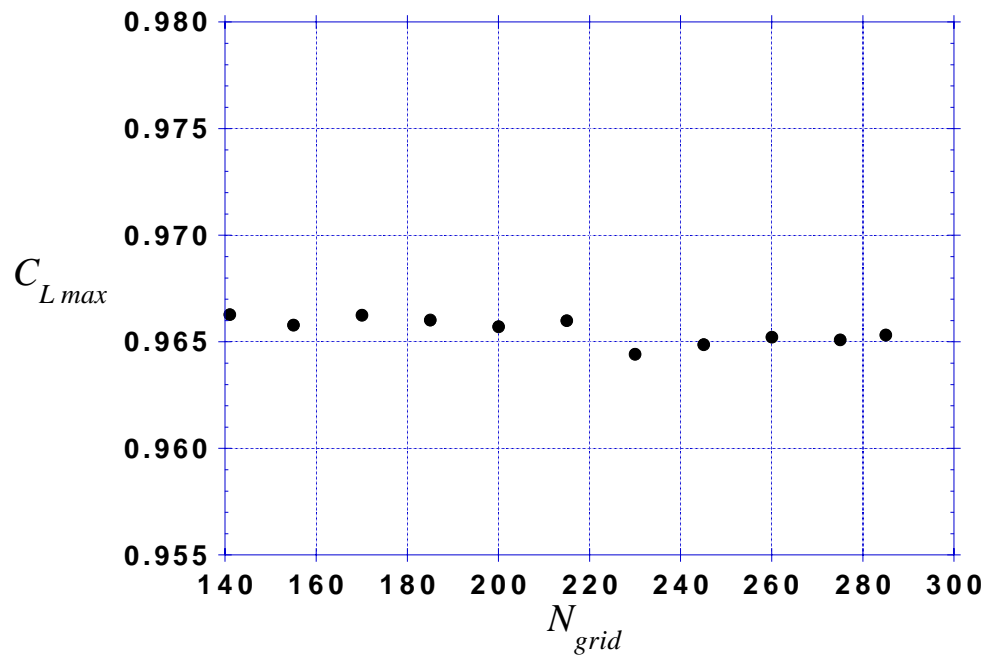
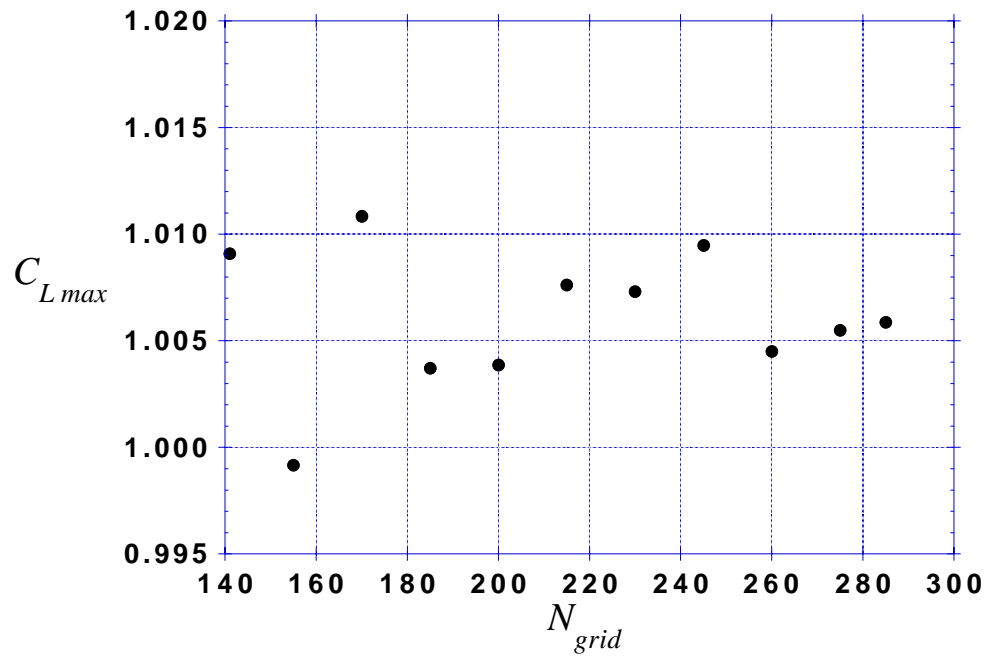
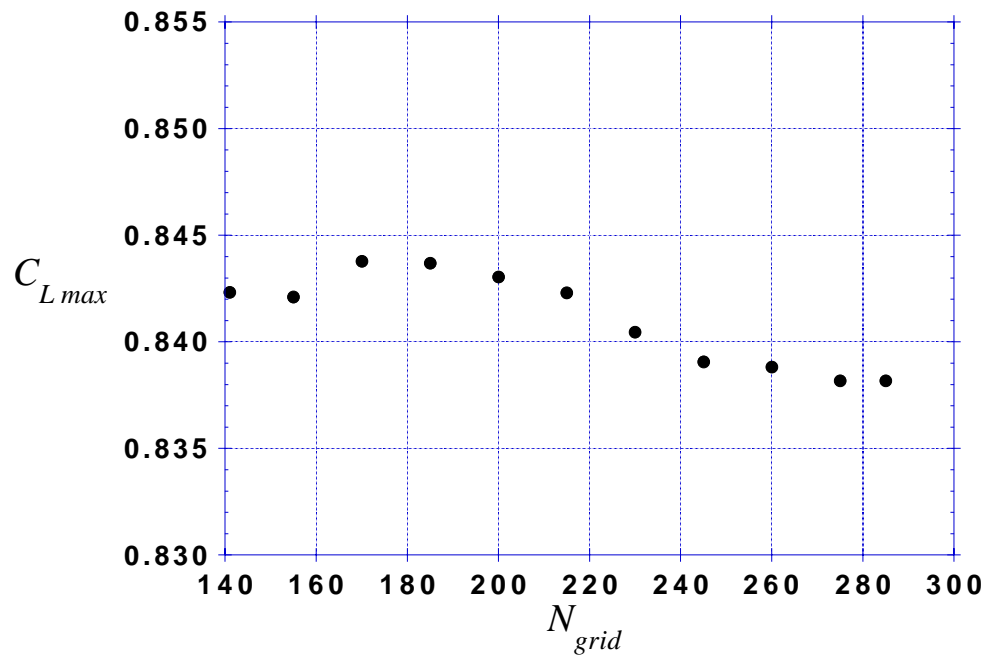
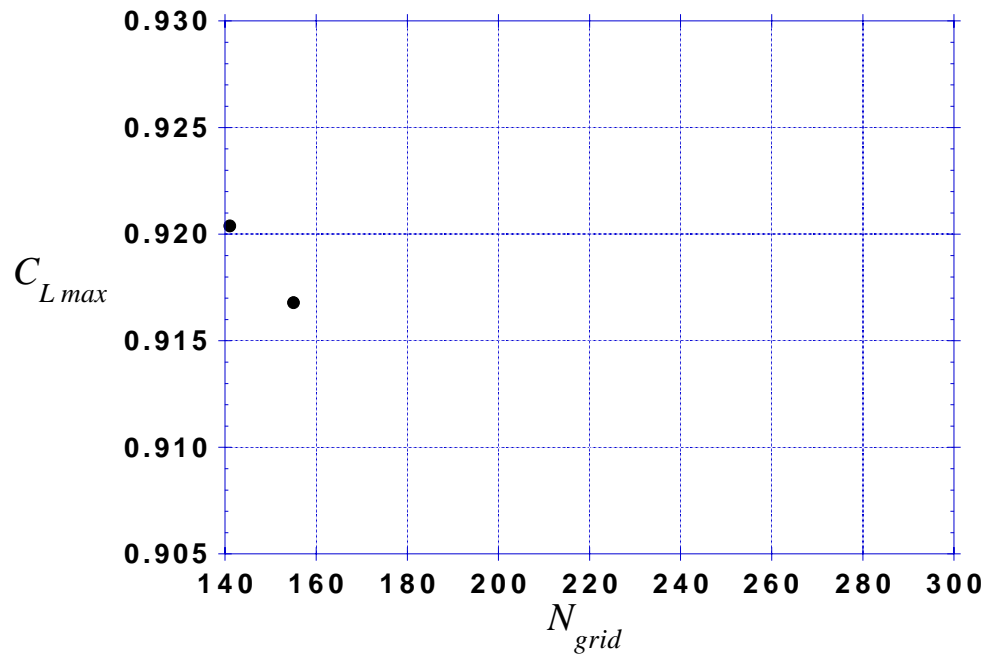
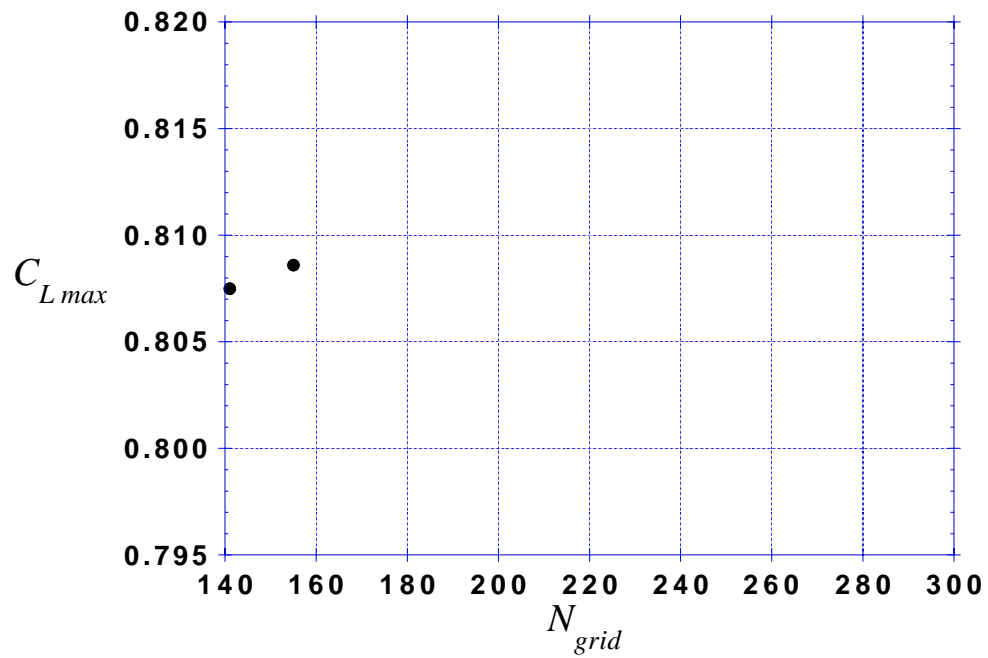
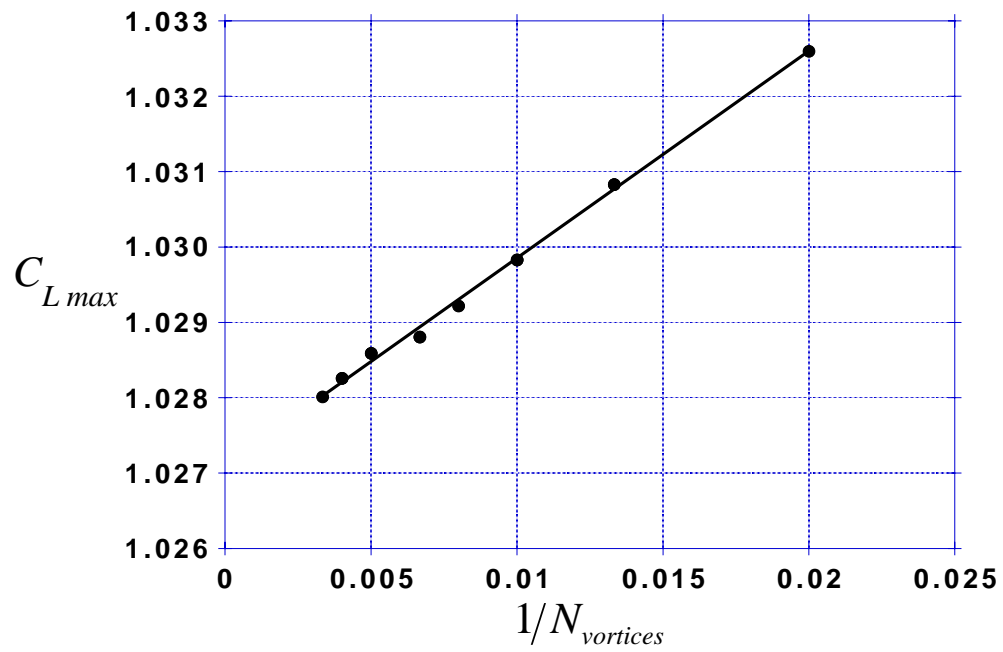
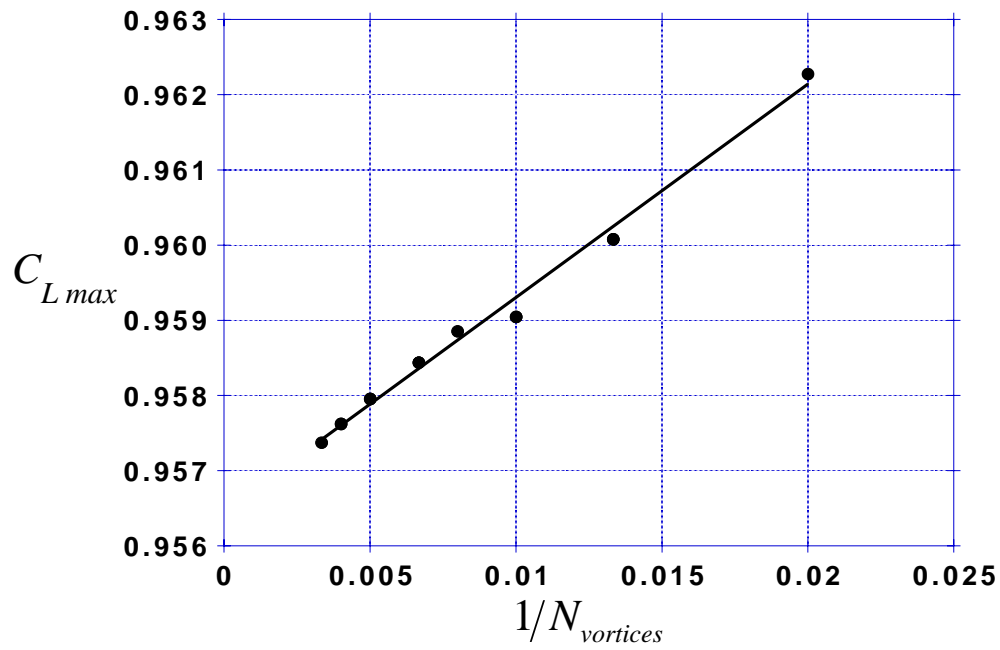
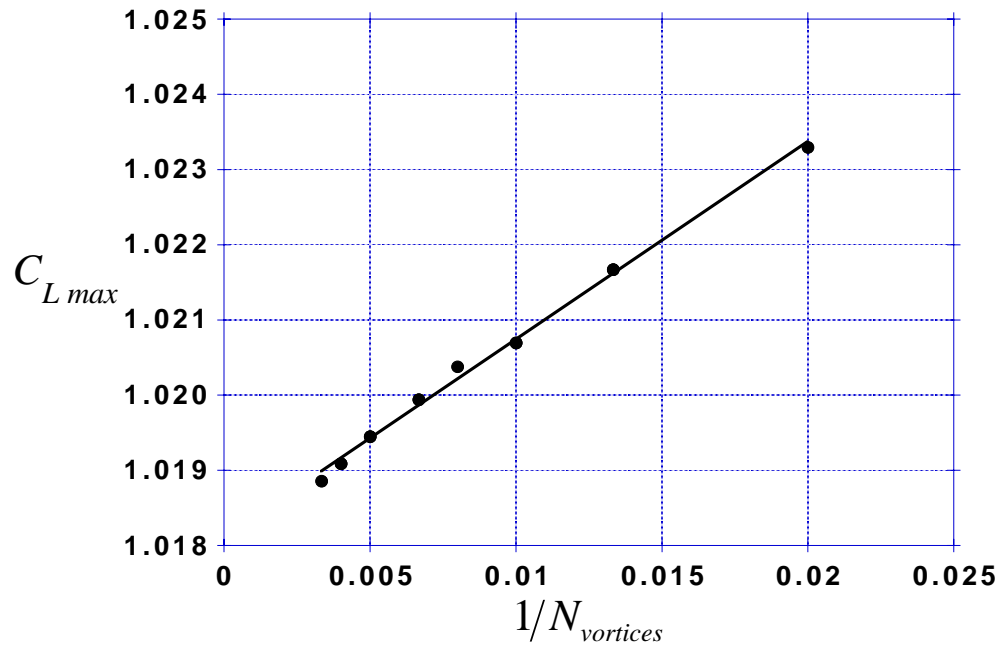


Figure 3.6 – MSES convergence study results for $M = 0.407$, $Re = 250,000$

Figure 3.7 – MSES convergence study results for $M = 0.550$, $Re = 137,500$ Figure 3.8 – MSES convergence study results for $M = 0.600$, $Re = 177,160$

Figure 3.9 – MSES convergence study results for $M = 0.600$, $Re = 31,410$ Figure 3.10 – MSES convergence study results for $M = 0.800$, $Re = 141,000$

Figure 3.11 – MSES convergence study results for $M = 0.800$, $Re = 25,000$ Figure 3.12 – Lifting line code convergence study results for $M = 0.300$, $Re = 250,000$

Figure 3.13 – Lifting line code convergence study results for $M = 0.300$, $Re = 59,140$ Figure 3.14 – Lifting line code convergence study results for $M = 0.407$, $Re = 250,000$

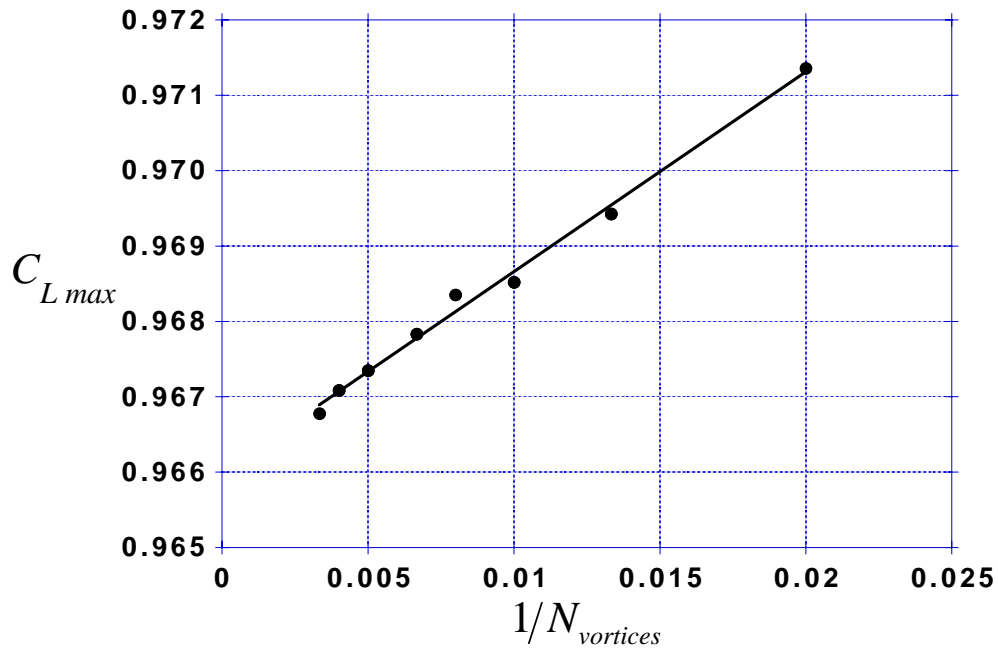


Figure 3.15 – Lifting line code convergence study results for $M = 0.550$, $Re = 137,500$

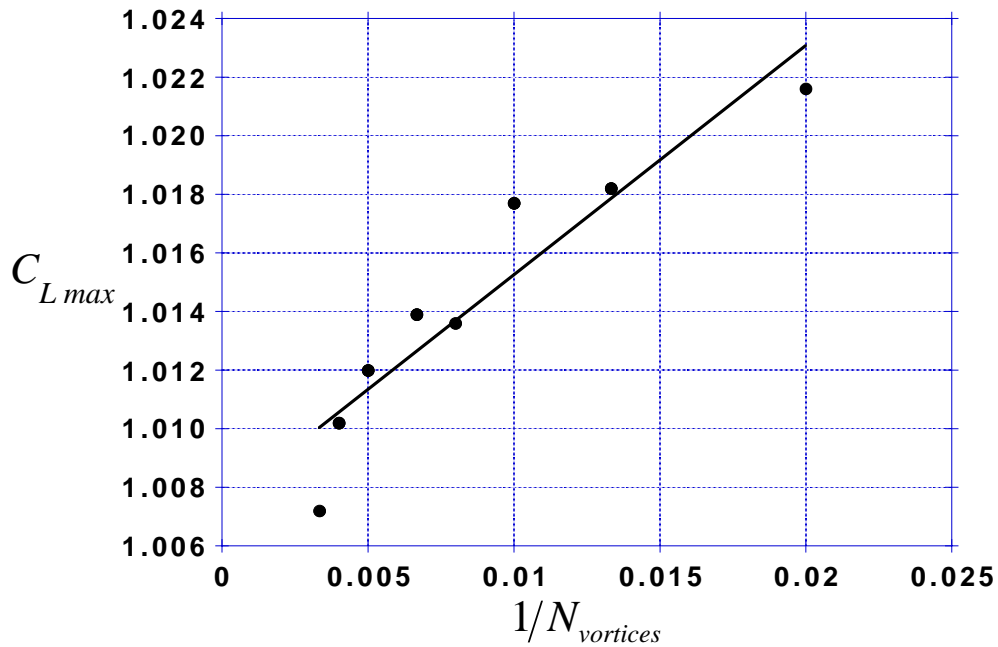


Figure 3.16 – Lifting line code convergence study results for $M = 0.600$, $Re = 177,160$

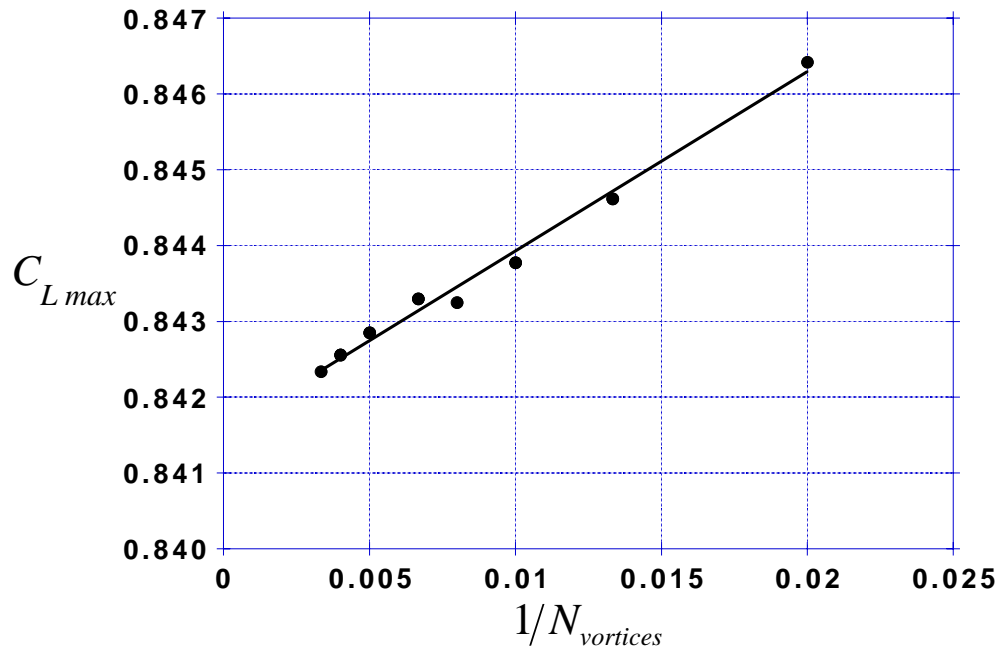


Figure 3.17 – Lifting line code convergence study results for $M = 0.600$, $Re = 31,410$

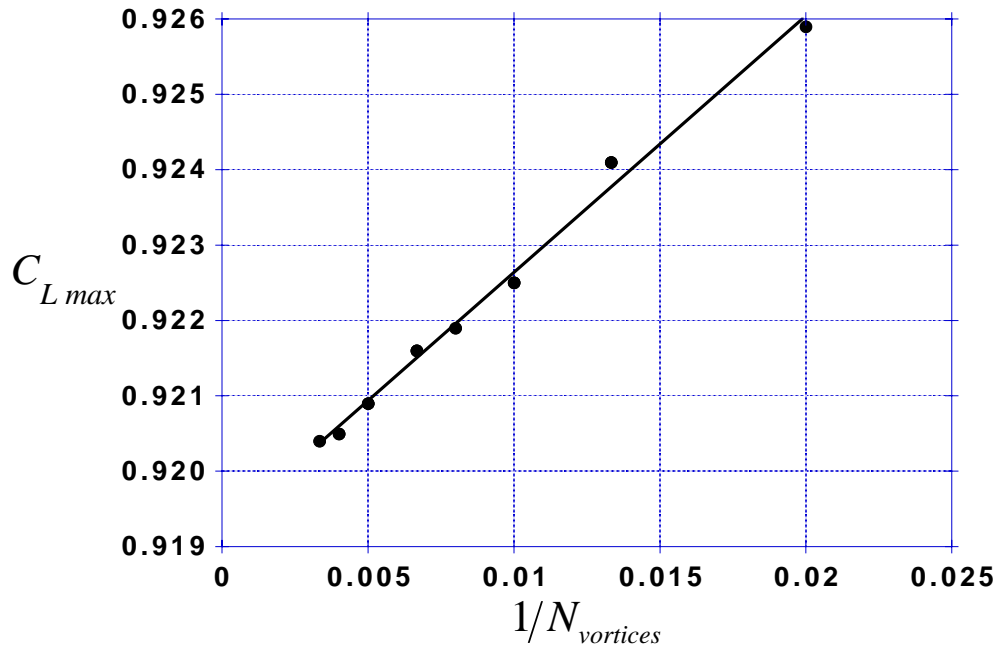


Figure 3.18 – Lifting Line Code Convergence Study results for $M = 0.800$, $Re = 141,000$

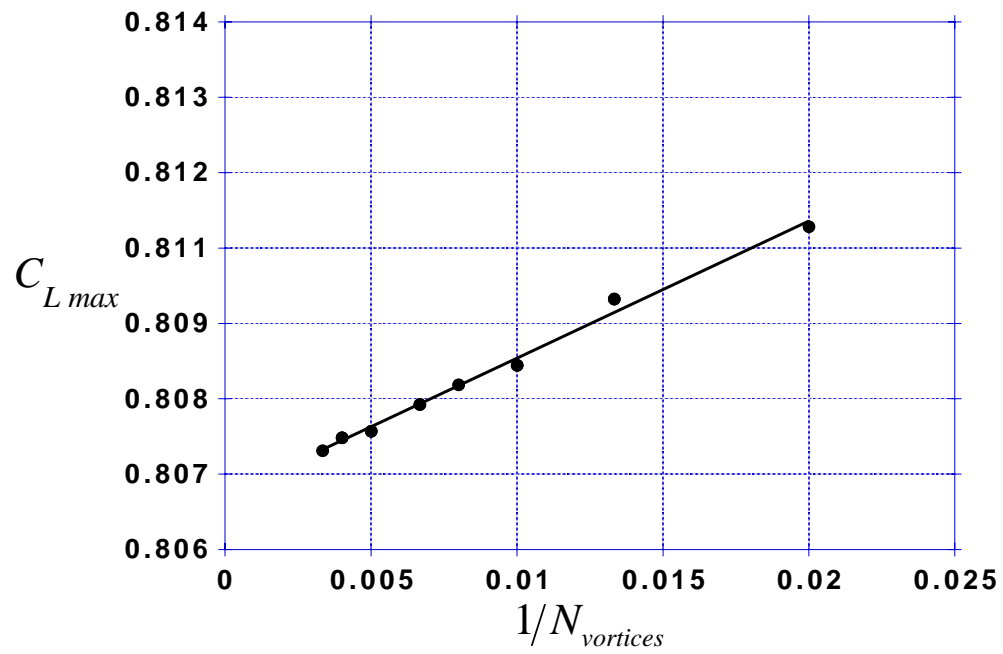


Figure 3.19 – Lifting line code convergence study results for $M = 0.800$, $Re = 25,000$

Chapter 4: Experimental Design

The main tasks involved in the experimental design are: design of the test wing, definition of the Mach/Reynolds test design space, and selection of test points within the test design space. All three of these tasks are discussed in this chapter. First, the design of the wing to be used for testing, and the selection of the Mach/Reynolds design space are discussed, noting how the choices made were influenced by the application to Mars airplanes as noted in the introduction. Next, a first-order analysis of the uncertainty structure of the maximum lift force and maximum lift coefficient is conducted to assist in the selection of the response variable used in the response surface analysis. The discussion then proceeds to the analysis of precision uncertainty in the design space. Next, the two test design procedures used to select the test points, minimum precision uncertainty and D-optimal, are presented together with their results and a discussion of how these results were used to generate the final test design and test sequence. Finally, some remarks on bias uncertainty in the experimental results are presented.

4.1 Wing Design

For this investigation, the test wing design used was a simplified version of that described in reference 7 for a small Mars airplane. The wing described in reference 7 had a wing span of 1.727 m (68.00 in),¹ and a constant chord in the outer portion of the wing panels of 0.35 m (13.78 in). However, as shown in Figure 4.1, this wing also included cutouts to allow this wing to fold into the aeroshell, and its center section had been modified to blend into the fuselage. For the present investigation, whose main purpose is to develop methods for the validation of analyses, this wing was simplified to have a rectangular planform with a full-scale wing span of 1.727 m (68.00 in) and a constant chord throughout the wing span of 0.3500 m (13.78 in), yielding a wing area of 0.6044 m² (937.0 in²) and an aspect ratio of 4.934. This test wing had no twist throughout its wing span. None of the cutouts and other shape changes required for an actual Mars airplane were incorporated into the test wing. By simplifying the wing in this way, a more appropriate comparison could be made between the aerodynamic analyses used in the present investigation (as described in chapter 3), and the experimental data. The airfoil used on the test wing was the MASC1 (Mars Airplane Super Critical #1) designed

¹ The dimension given in reference 7, figure 2(b), for the wing span is 1.06 m. A review of the original design showed that the wing span was actually 1.727 m.

by Dr. Richard L. Campbell of NASA LaRC (more details on the airfoil are given in section 5.1). The wind tunnel model of this test wing was built at quarter-scale for the reasons discussed in section 5.1. In order to accommodate the attachment of the wind tunnel balance, a small wind tunnel block was added to the bottom of the wing. Interference effects of this wind tunnel block were not accounted for in the aerodynamic analyses.

4.2 Test Design Space

The Mach and Reynolds number domain during pullout for the Mars airplane considered in the study of reference 7 can be approximately defined by the boundaries $0.6 \leq M \leq 0.8$ and $43,000 \leq Re \leq 140,000$. This a critical portion of the domain in which the aerodynamic analyses needed to be validated. However, it was desirable to expand this domain in two ways. First, by including Reynolds numbers as low as 25,000, other Mars airplane designs could be accommodated. Second, by including lower Mach numbers and higher Reynolds numbers, the accuracy of the aerodynamic analyses at less challenging conditions could be confirmed. In particular, it was of interest to confirm the analyses ability to predict $C_{L\ max}$ at Mach numbers where compressibility effects are negligible ($M \approx 0.3$), and at high enough Reynolds numbers where previous researchers had found MSES to yield good results ($Re \approx 250,000$). Using the these considerations, the boundaries of the test design space included the domain defined by $0.300 \leq M \leq 0.800$ and $25,000 \leq Re \leq 250,000$. However, limitations on the wind tunnel balance capabilities related to the maximum forces and moments it can sustain, and the minimum forces and moments it can measure accurately, placed additional constraints on the test design space. Assuming that the maximum lift coefficient is relatively invariant throughout the test design space,² the maximum lift force will be proportional to the dynamic pressure, q , since:

$$L_{max} = qSC_{L\ max} \quad (4.1)$$

where L_{max} is the maximum lift force and S is the wing area. An upper boundary for q was defined by the maximum pitching moment capability of the wind tunnel balance.³ The center of pressure of the wing was forward of the wind tunnel balance moment center placing a significant bending moment on the wind tunnel balance. Preliminary analyses indicated that the maximum pitching moment capability of the wind tunnel balance (including appropriate safety factors) would be reached at a dynamic pressure of 3,746 Pa (78.23 psf). A lower boundary for q was defined by the minimum value of L_{max} that could be resolved accurately by the wind tunnel balance.⁴ This minimum value of q

² Aerodynamic analysis and experimental data confirmed this assumption; $C_{L\ max}$ varies about 15% throughout the test design space.

³ Additional details on the wind tunnel balance and its selection can be found in chapter 5.

⁴ This lower bound is somewhat arbitrary; it was set sufficiently low to include the test point $M = 0.800$, $Re = 25,000$.

was set at 664 Pa (13.87 psf). It can be shown that the dynamic pressure can be expressed in terms of the Mach number and Reynolds number as:

$$q = \frac{1}{2} \frac{MRe}{c} \mu \sqrt{\gamma RT} \quad (4.2)$$

where c is the wing chord, μ is the coefficient of viscosity, γ is the ratio of specific heats, R is the gas constant, and T is the static temperature. Assuming a constant value of the stagnation temperature, T_0 , allows the calculation of μ and T as a function of Mach number. With this assumption, lines of constant q in the Mach-Reynolds number space can be defined. The Mach-Reynolds number domain $0.300 \leq M \leq 0.800$ and $25,000 \leq Re \leq 250,000$, constrained by the limits on the dynamic pressure, $664 \text{ Pa} \leq q \leq 3,746 \text{ Pa}$ ($13.87 \text{ psf} \leq q \leq 78.23 \text{ psf}$), thus defines the test design space as shown in Figure 4.2. Note that throughout this domain, the dynamic pressure varies by a factor of 5.6. This range of dynamic pressures had a significant effect on the uncertainty structure of $C_{L,max}$ and the test design procedure as discussed in the next two sections.

4.3 Precision Uncertainty Structure

As previously noted, the test design was to be conducted using the statistical tools of response surface methodology. In order to apply these tools, the underlying assumptions used in deriving them need to be confirmed for the particular application. Key among these assumptions is that the precision (i.e., random) uncertainty of the response variable is constant throughout the response surface domain. Two possible response variable choices were available for validating the maximum lift predictive capabilities of the aerodynamic analyses: the maximum lift coefficient and the maximum lift force. In this section the uncertainty structure of both of these response variable choices is examined. It is shown that, due to the large variation in dynamic pressure throughout the test design space, the precision uncertainty of the maximum lift coefficient was not constant throughout the experiment design space. Conversely, the precision uncertainty of the maximum lift force, was approximately constant throughout the experiment design space. Thus, the maximum lift force was the better response variable and was used in the minimum precision uncertainty RSM analyses.

In the following first-order uncertainty structure analyses the following assumptions were made:

- The precision uncertainty in the dynamic pressure, P_q , is approximately constant throughout the test design space. This conclusion follows from the assumption that the precision uncertainty in the total and static pressure measurements (p_0 and p) are constant regardless of the absolute value of the pressure being measured, and that the dynamic pressure is dominated by the difference in these two quantities.

- The precision uncertainty in the lift force measured by the wind tunnel balance, $P_{L_{meas}}$, is approximately constant within the measurement range of the wind tunnel balance.
- The precision uncertainty of the wing area is zero. This is consistent with using a single number for the wing area, S , to analyze all the experimental data. (The bias uncertainty of the wing area, however, is not zero. It was taken into account in the final experimental data analyses as discussed in chapter 6.)
- To within the accuracy needed for the following arguments, the maximum lift coefficient is constant. This assumption was verified by both the aerodynamic analyses and the experimental data; the maximum variation of $C_{L_{max}}$ within the test design space was approximately 15 percent.

4.3.1 Precision Uncertainty Structure of the Maximum Lift Coefficient

The calculated value of the maximum lift coefficient, $C_{L_{max}}$, derived from the wing area, S , and the experimentally measured values of the dynamic pressure, q , and the measured maximum lift force, L_{max} , from:

$$C_{L_{max}} = \frac{L_{max}}{qS} \quad (4.3)$$

The precision uncertainty in this calculated value of $C_{L_{max}}$, $P_{C_{L_{max}}}$, can be estimated from:

$$P_{C_{L_{max}}} = \sqrt{\left(\frac{\partial C_{L_{max}}}{\partial L_{max}}\right)^2 P_{L_{meas}}^2 + \left(\frac{\partial C_{L_{max}}}{\partial q}\right)^2 P_q^2} \quad (4.4)$$

where $P_{L_{meas}}$ and P_q need to be at the same level of confidence for equation 4.4 to be valid. Performing the indicated differentiations, and some substitutions allows equation 4.4 to be re-written as:

$$P_{C_{L_{max}}} = \sqrt{\left(\frac{1}{qS}\right)^2 P_{L_{meas}}^2 + \left(\frac{C_{L_{max}}}{q}\right)^2 P_q^2} \quad (4.5)$$

It is clear from examining equation 4.5 that $P_{C_{L_{max}}}$ is inversely dependent to the dynamic pressure, q . Thus, in the present application where the dynamic pressure was expected to vary by a factor of 5.6 (as discussed in section 4.2), the precision uncertainty of $C_{L_{max}}$ was not constant throughout the test design space. This behavior makes $C_{L_{max}}$ unsuitable

for the response variable in the minimum precision uncertainty RSM formulation and test design.

4.3.2 Precision Uncertainty Structure of the Maximum Lift Force

In the present discussion, the maximum lift force, L_{max} , can be considered to be measured and reported directly by the wind tunnel's data acquisition system.⁵ Given that the L_{max} is associated with a measured value of q , which has a precision uncertainty associated with it, P_q , the precision uncertainty of L_{max} , $P_{L_{max}}$, can be estimated from:

$$P_{L_{max}} = \sqrt{P_{L_{meas}}^2 + (SC_{L_{max}})^2 P_q^2} \quad (4.6)$$

where $P_{L_{meas}}$ and P_q need to be at the same level of confidence for equation 4.6 to be valid. The first term involving $P_{L_{meas}}$ is due to the uncertainty in the measurement from the wind tunnel balance. The second term involving P_q involves the uncertainty in the lift force due to the uncertainty in q . This term is equal to $(\partial L_{max} / \partial q)^2 P_q^2$ where $L_{max} = qSC_{L_{max}}$ (in this case L_{max} , q , S , and $C_{L_{max}}$ are assumed to be the true values). Considering the previously stated assumptions regarding $P_{L_{meas}}$ and P_q , it can be seen that $P_{L_{max}}$ is constant throughout the test design space at a given level of confidence.⁶ Thus, L_{max} was used as the response variable in the RSM formulation and test design. The details of the test design procedure are described in the next section.

4.4 Test Design Analyses and Procedures

The main purpose of the test design analyses was to generate a set of test points within the test design space suitable for accomplishing the stated goal, namely the identification of discrepancies between the values of $C_{L_{max}}$ as determined from the analyses and the experiment. Because of the limited wind tunnel time available this goal had to be accomplished with a relatively small number of runs. Doing so required an efficient test design. In order to create such a test design, in spite of the experimental noise, an analysis was needed that would predict the precision uncertainty. For this task, RSM techniques were used to create the test design.

⁵ The lift force was calculated from the normal and axial forces, NF and AF respectively, reported by the wind tunnel balance, and the angle of attack, α . In practice the normal force component dominates the calculation of the lift force, and the uncertainties in AF and α played a small role in the total uncertainty of the lift force. Thus, for the argument presented in this section, taking the lift force as measured to have a constant precision uncertainty was a good approximation.

⁶ As discussed in chapter 6, the assumption that $P_{L_{max}}$ was constant was rendered invalid during the experiment due to stall flutter at the maximum lift condition. Although the goal of the experiment was achieved (i.e., to identify regions of disagreement between the analytical and experimental results), an approach different from what is discussed here in the design of the experiment was used in the calculation of the uncertainty of the experimental results.

In this section the test design analyses and procedures are described. Because of the limited control of the stagnation temperature in the TDT, the dynamic pressure and the lift force must be normalized to a constant value of the stagnation temperature throughout the test design space. This normalization is discussed in sub-section 4.4.1. As discussed in sub-section 4.3.2, the maximum lift force, L_{max} , was shown to be a suitable response variable for the minimum precision uncertainty RSM analysis. In order to apply these analyses, an estimate of the precision uncertainty of the maximum lift, $P_{L_{max}}$, was needed. The calculation of this estimate is described in sub-section 4.4.2. Next, in sub-section 4.4.3, the application of the response surface analysis to the prediction of the maximum lift force and maximum lift coefficient uncertainties are discussed. Although the response surface used L_{max} as the response variable, the uncertainty in $C_{L_{max}}$ was calculated from the uncertainty in L_{max} . The test design was constrained by several factors, including the number of test runs that could be reasonably expected during the available wind tunnel time. These constraints, and the application of the uncertainty analyses in the test design procedure are discussed in sub-section 4.4.4.

4.4.1 Normalization of Dynamic Pressure and Lift

Before the estimation of $P_{L_{max}}$ could proceed, a normalized lift force had to be defined. As given by equation 4.2, the dynamic pressure varies through the Mach/Reynolds number test regime. In addition, the dynamic pressure is also a function of the static temperature, T , and the coefficient of viscosity, μ (which depends on the static temperature). The static temperature and coefficient of viscosity can be written in terms of the stagnation temperature, T_0 , the Mach number, and various constants as given by:

$$T = \frac{T_0}{1 + \frac{\gamma - 1}{2} M^2} \quad (4.7)$$

and

$$\mu = \mu_{ref} \left(\frac{T}{T_{ref}} \right)^n = \mu_{ref} \left(\frac{1}{T_{ref}} \frac{T_0}{1 + \frac{\gamma - 1}{2} M^2} \right)^n \quad (4.8)$$

Substituting equations 4.7 and 4.8 into equation 4.2 yields:⁷

⁷ The values of the constants R , γ , μ_{ref} , T_{ref} , and n used in the present investigation are given table 4.1 and in the symbols section of the front matter. The references used to obtain these quantities are listed in table 4.1.

$$q = \frac{1}{2} \frac{MRe}{c} \mu_{ref} \left(\frac{1}{T_{ref}} \frac{T_0}{1 + \frac{\gamma-1}{2} M^2} \right)^n \sqrt{\gamma \mathcal{R} \frac{T_0}{1 + \frac{\gamma-1}{2} M^2}} \quad (4.9)$$

From this equation it can be seen that the dynamic pressure for a given Mach and Reynolds number also depends on the stagnation temperature. As is discussed in chapter 5, there is a limited ability to control the stagnation temperature in the TDT. Thus, every test run will have a slightly different stagnation temperature. Since the lift force depends on the dynamic pressure, and it is to be used as the response variable vs Mach and Reynolds number, a normalized dynamic pressure, q_{norm} , and normalized lift force, L_{norm} , had to be generated. These quantities were to be normalized to a common stagnation temperature, $T_{0\ ref}$. This normalization can be accomplished by multiplying the measured values of the dynamic pressure and lift force by the normalization factor K_q :

$$q_{norm} = K_q q \quad (4.10)$$

$$L_{norm} = K_q L \quad (4.11)$$

Where q , L , and T_0 are the dynamic pressure, lift, and stagnation temperature measured during the test, and q_{norm} and L_{norm} are the normalized values of the dynamic pressure and the lift force.⁸ The normalizing factor K_q can be shown to be:

$$K_q = \left(\frac{T_{0\ ref}}{T_0} \right)^{n+0.5} \quad (4.12)$$

Based on previous test experience in the TDT, a pre-test value of 303.8 K was selected for $T_{0\ ref}$. Note that this normalization cancels out, as it should, when calculating the lift coefficient since both the lift force and the dynamic pressure is multiplied by the same normalizing factor.

4.4.2 Estimation of $P_{L\ max}$

In sub-section 4.3.2, a first-order analysis was used to demonstrate that $P_{L\ max}$ is approximately constant throughout the test design space being considered in this investigation. In this sub-section, a more detailed analysis is described to estimate the value of $P_{L\ max}$ at the one-sigma level of confidence (i.e., 68%). This analysis confirmed the conclusion presented in sub-section 4.3.2 regarding $P_{L\ max}$ and provided a numerical value to use in the subsequent response surface analysis.

⁸ Note that this normalizing factor also applies to the other aerodynamic forces and moments on the wing.

The normalized lift force, L_{norm} , is a function of the normal and axial forces measured by the wind tunnel balance, NF and AF , the angle of attack, α , the stagnation and static pressures, p_0 and p respectively (since they determine the dynamic pressure), and the stagnation temperature, T_0 (since it affects the normalizing factor, K_q). If we consider only the normalized lift force at maximum lift, $P_{L_{max}}$ can be estimated from:

$$P_{L_{max}} = \left[\left(\frac{\partial L_{norm}}{\partial NF} \right)^2 P_{NF}^2 + \left(\frac{\partial L_{norm}}{\partial AF} \right)^2 P_{AF}^2 + \left(\frac{\partial L_{norm}}{\partial \alpha} \right)^2 P_{\alpha}^2 + \left(\frac{\partial L_{norm}}{\partial T_0} \right)^2 P_{T_0}^2 + \left(\frac{\partial L_{norm}}{\partial p_0} \right)^2 P_{p_0}^2 + \left(\frac{\partial L_{norm}}{\partial p} \right)^2 P_p^2 \right]^{1/2} \quad (4.13)$$

where P_{NF} , P_{AF} , P_{α} , P_{p_0} , P_p , and P_{T_0} are the precision uncertainties of NF , AF , α , p_0 , p , and T_0 , respectively. The estimated values of these uncertainties at the one-sigma level are given in table 4.2. These estimates were generated from instrument manufacturers data sheets and discussions with various test engineers at NASA LaRC.

The first four partial derivatives of equation 4.13 are determined from:

$$L_{norm} = K_q (NF \cos \alpha - AF \sin \alpha) \quad (4.14)$$

where it can be recalled from the previous sub-section that the dependency on T_0 arises in the K_q term.⁹ These derivatives in can thus be written explicitly as:

$$\frac{\partial L_{norm}}{\partial NF} = K_q \cos \alpha \quad (4.15)$$

$$\frac{\partial L_{norm}}{\partial AF} = -K_q \sin \alpha \quad (4.16)$$

$$\frac{\partial L_{norm}}{\partial \alpha} = -K_q (NF \sin \alpha + AF \cos \alpha) \quad (4.17)$$

$$\frac{\partial L_{norm}}{\partial T_0} = -(n + 0.5) T_{0_{ref}}^{n+0.5} T_0^{-(n+1.5)} (NF \cos \alpha - AF \sin \alpha) \quad (4.18)$$

To evaluate these derivatives, the values of $T_{0_{ref}}$, T_0 , NF , AF , and α are required. As stated in the previous section, the pre-test value of $T_{0_{ref}}$ was set at 313.9 K. For the pre-test analyses T_0 was set to 313.9 K as well, making $K_q = 1$. Preliminary aerodynamic analyses were conducted to obtain the values of NF , AF , and α at $C_{L_{max}}$. These analyses

⁹ See chapter 6, figure 6.1, for the sign convention used by NF and AF .

were conducted at the 48 combinations of Mach and Reynolds numbers shown in table 4.3 and figure 4.3, and yielding the values of C_L , C_D , and α at $C_{L\max}$ listed in table 4.3. With the values of K_q and α at hand, the derivatives in equations 4.15 and 4.16 were calculated. From the values of C_L , C_D , and α , the corresponding values of the normal and axial force coefficients C_N and C_A , can be calculated from:

$$C_N = C_L \cos \alpha + C_D \sin \alpha \quad (4.19)$$

$$C_A = -C_L \sin \alpha + C_D \cos \alpha \quad (4.20)$$

The values of C_N and C_A are also given in table 4.3. Having calculated C_N and C_A , NF and AF were determined from:

$$NF = qSC_N \quad (4.21)$$

$$AF = qSC_A \quad (4.22)$$

using the dynamic pressure calculated from equation 4.9 and the wing area, S , whose pre-test estimate was 0.037784 m^2 (58.564 in^2).¹⁰ With this information the derivatives in equations 4.17 and 4.18 were evaluated.

The last two partial derivatives in equation 4.13 are associated with the uncertainty in the dynamic pressure arising from the uncertainties in p_0 and p . The dynamic pressure can be determined from the measured values of p_0 and p from:

$$q = \frac{\mathcal{P}}{\gamma - 1} \left[\left(\frac{p}{p_0} \right)^{1-\gamma/\gamma} - 1 \right] \quad (4.23)$$

L_{norm} at $C_{L\max}$ can be expressed as:

$$L_{norm} = K_q q S C_{L\max} = K_q \frac{\mathcal{P}}{\gamma - 1} \left[\left(\frac{p}{p_0} \right)^{1-\gamma/\gamma} - 1 \right] S C_{L\max} \quad (4.24)$$

From equation 4.24 the two partial derivatives of L_{norm} with respect to p_0 and p can be shown to be:

¹⁰ Because this analysis was performed before the model was built, only pre-test estimates of parameters such as wing area were available. Once the model was completed, as-built values for such parameters were determined. The pre-test and as-built dimensions of the wind tunnel model are discussed in chapter 5, and given in table 5.1. Both sets of values are very close.

$$\frac{\partial L_{norm}}{\partial p_0} = K_q \frac{\gamma}{\gamma-1} \left[\frac{\gamma-1}{\gamma} p^{2-\gamma/\gamma} p_0^{-1/\gamma} - p \right] SC_{L_{max}} \quad (4.25)$$

and

$$\frac{\partial L_{norm}}{\partial p} = K_q \frac{\gamma}{\gamma-1} \left[\frac{2-\gamma}{\gamma} p^{2(1-\gamma)/\gamma} p_0^{\gamma-1/\gamma} - 1 \right] SC_{L_{max}} \quad (4.26)$$

For particular values of M and Re , p and p_0 can be determined from:

$$p = \frac{Re}{Mc} \mu_{ref} \left(\frac{1}{T_{ref}} \frac{T_0}{1 + \frac{\gamma-1}{2} M^2} \right)^n \sqrt{\frac{RT_0}{\gamma \left(1 + \frac{\gamma-1}{2} M^2 \right)}} \quad (4.27)$$

and

$$p_0 = p \left(1 + \frac{\gamma-1}{2} M^2 \right)^{\gamma/\gamma-1} \quad (4.28)$$

Using the previously defined constants, the partial derivatives in equations 4.25 and 4.26 were evaluated for at the Mach/Reynolds number combinations given in table 4.3 by choosing the appropriate value of $C_{L_{max}}$.

With the partial derivatives evaluated, and the precision uncertainties in table 4.2, $P_{L_{max}}$ as given in equation 4.13 could be evaluated. The results of these calculations, for the various Mach and Reynolds numbers considered, are shown in table 4.4. As can be seen, $P_{L_{max}}$ varied little over the test domain; its range was from 0.19 N (0.043 lb) to 0.22 N (0.049 lb), with a mean of 0.21 N (0.047 lb).¹¹ Given these results, a constant value of 0.22 N (0.049 lb) was used for $P_{L_{max}}$ for the subsequent analyses of this chapter. Choosing the upper bound value was a conservative decision to avoid underestimating the uncertainty of the maximum lift force.

4.4.3 Response Surface Uncertainty Analysis

In this sub-section an uncertainty analysis based on a response surface using maximum lift as the response is outlined. The ultimate purpose is to derive a formula for the response surface precision uncertainty for the maximum lift coefficient that can be

¹¹ Note that these results validate the first-order analysis in sub-section 4.3.2.

used in the test design procedure described in the next sub-section. The analysis presented in this sub-section follows the approach presented in reference 5.

Using the pre-test aerodynamic analysis data presented in table 4.3, an appropriate¹² linear model for the normalized maximum lift force as a function of the Mach and Reynolds number was determined to have the form:

$$\hat{L}_{norm\ max}(M, Re) = \beta_0 + \beta_M M + \beta_{Re} Re + \beta_{M Re} M Re + \beta_{M^2} M^2 + \beta_{M^2 Re} M^2 Re + \beta_{M^3} M^3 \quad (4.29)$$

This linear model can be more compactly represented as:

$$\hat{L}_{norm\ max}(\bar{\mathbf{x}}) = \bar{\mathbf{x}}^T \bar{\mathbf{b}} \quad (4.30)$$

where,

$$\bar{\mathbf{x}}^T = \{1 \quad M \quad Re \quad M Re \quad M^2 \quad M^2 Re \quad M^3\} \quad (4.31)$$

and

$$\bar{\mathbf{b}}^T = \{\beta_0 \quad \beta_M \quad \beta_{Re} \quad \beta_{M Re} \quad \beta_{M^2} \quad \beta_{M^2 Re} \quad \beta_{M^3}\} \quad (4.32)$$

Note that the superscript **T** indicates the vector is transposed, and that the vectors $\bar{\mathbf{x}}$ and $\bar{\mathbf{b}}$ have (in this case) 7 elements (i.e., $n_e = 7$). Assuming that the linear model is created based on n_{obs} observations of L_{norm} at locations M_i, Re_i ($i = 1$ to n_{obs}), these observations can be organized in a matrix $\bar{\mathbf{X}}$:

$$\bar{\mathbf{X}} = \begin{bmatrix} 1 & M_1 & Re_1 & M_1 Re_1 & M_1^2 & M_1^2 Re_1 & M_1^3 \\ \vdots & \vdots & \vdots & \vdots & \vdots & \vdots & \vdots \\ 1 & M_{n_{obs}} & Re_{n_{obs}} & M_{n_{obs}} Re_{n_{obs}} & M_{n_{obs}}^2 & M_{n_{obs}}^2 Re_{n_{obs}} & M_{n_{obs}}^3 \end{bmatrix} \quad (4.33)$$

The precision uncertainty of the linear model's mean response at the $1 - \nu$ confidence level at a given location $\bar{\mathbf{x}}_0$ in the test design space, denoted as $P_{\hat{L}_{norm\ max}}(1 - \nu, \bar{\mathbf{x}}_0)$, is then given by:

$$P_{\hat{L}_{norm\ max}}(1 - \nu, \bar{\mathbf{x}}_0) = t(\nu/2, n_{obs} - n_e) \sqrt{\hat{\sigma}^2 \bar{\mathbf{x}}_0^T (\bar{\mathbf{X}}^T \bar{\mathbf{X}})^{-1} \bar{\mathbf{x}}_0} \quad (4.34)$$

¹² The coefficient of multiple determination, \mathfrak{R}^2 , and the adjusted coefficient of multiple determination, \mathfrak{R}_{adj}^2 , were determined to be 0.9987 and 0.9985, respectively for the response surface using the pre-test analysis data. Tests on the individual regression coefficients and other statistical tests also indicated this model was appropriate for these data.

where $t(v/2, n_{obs} - n_e)$ is the Student's t -Distribution evaluated with a tail probability of $v/2$ and $n_{obs} - n_e$ degrees of freedom. When equation 4.34 is generated from experimental data, $\hat{\sigma}$ is the estimated value of σ , the standard deviation of L_{norm} . For the test design analyses $P_{L_{max}}$, as calculated in the previous sub-section, was used as an approximation to $\hat{\sigma}$. Note that equation 4.34 is a continuous function of M and Re , and that $\bar{\mathbf{x}}_0$ does not necessarily have to be at the location of one of the observations used to generate the linear model. The goal of the uncertainty analysis derived in this sub-section is to estimate the precision uncertainty of $C_{L_{max}}$, $P_{C_{L_{max}}}$, for possible experimental designs. Since $P_{L_{norm\ max}}$ already contains the precision uncertainty contribution of all relevant quantities, $P_{C_{L_{max}}}(1 - v, \bar{\mathbf{x}}_0)$ can be calculated from:

$$P_{C_{L_{max}}}(1 - v, \bar{\mathbf{x}}_0) = \frac{P_{L_{norm\ max}}(1 - v, \bar{\mathbf{x}}_0)}{q_{norm} S} \quad (4.35)$$

4.4.4 Test Design Procedure

The objective of the test design was to select the test conditions (i.e., Mach and Reynolds numbers) where the initial set of tests would be conducted to identify discrepancies between the aerodynamic analyses and the experimental results. Two test design procedures were used to identify suitable test points. The first procedure minimized the maximum precision error in $C_{L_{max}}$ over the experimental test design space. This procedure used the response surface uncertainty analysis described in the previous sub-section. The second procedure generated a D-optimal design in the Mach/Reynolds number design space. Neither of these test design procedures generated suitable test designs by themselves. The final test design was a combination of the results from the two test design procedures. In this sub-section both test design procedures are discussed, preceded by a description of the constraints applied to both of them. The test designs generated by these procedures, and the final test design generated by combining their results are presented in the next section.

In searching for a suitable test design, the following constraints and requirements were placed on both test design procedures:

- The test designs could not include more than 18 tests (including replicates). This constraint was based on the number of test days available, and the number of test that could be completed in a given day. Four days were available for testing. The first two days were allocated to the pre-planned test points (as defined by the test procedures described in this section). The third test day was allocated to pursuing additional testing in areas where the data from the first two days of testing indicated poor correlation between analysis and experiment. The fourth day was allocated to pressure testing, which would not yield maximum lift coefficient information (see chapter 5 for a description of the pressure tests). From previous

experience at the TDT, it was expected that nine tests could be conducted each day. Thus, since two days were allocated to the pre-planned portion of the test, the test design was limited to 18 test points.

- At least ten of the test points had to be unique (i.e., different combinations of M and Re). This would be a sufficient number of unique points to fit the seven-term polynomial in the normalized force used in equation 4.29, and the complete cubic polynomial in C_{Lmax} used for the D-optimal designs.
- The implementation of the test design procedures needed to allow for pre-selected test points. This was done to allow for the selection of key test points along the boundary. In the final test designs, four points were prescribed. These points are listed in table 4.5.
- The test points were to be selected from a fixed list of 47 test conditions. This was done to simplify the software implementation of the test design procedures. The list of available test conditions was the same as that used to conduct the pre-test aerodynamic analyses shown in table 4.3 and figure 4.3 with one exception; the condition at $M = 0.800$, $Re = 25,000$ was eliminated from consideration. The reason for deleting this condition was that it required an extreme application of the use of the engineering definition of C_{Lmax} (as described in chapter 3). The C_L vs α curve for this point is shown in figure 4.4.

The first test design procedure attempted to select a set of test points that would minimize $P_{C_{Lmax}}$ in the test domain as given by equation 4.35 ($1 - v$ was set to 0.95 for these calculations). The numerical implementation of this design procedure involved a random number generator to generate initial designs, and a simple point replacement strategy to improve them. This test design algorithm worked as follows, while satisfying the requirements specified above:

- 1) Generate an initial design.
- 2) Calculate the precision uncertainty at all possible test conditions using equation 4.35.
- 3) Add a test point at the test condition with maximum precision uncertainty.
- 4) Remove the test point at the test condition with minimum precision uncertainty.
- 5) Return to step 2. The maximum number of iterations was set at 20.

Approximately 50,000 initial random designs (within the constraints specified above) were used. From most of these initial random designs the algorithm converged to very

similar designs with nearly identical maximum values of $P_{C_{L,max}}$. One of these designs was chosen to assist in the definition of the final design as described in section 4.5. The designs generated by this design procedure were highly unbalanced; they tended to place most points along the lower boundary of the design space. This was due to the increased uncertainty in $C_{L,max}$ along this boundary due to the low dynamic pressure. The design procedure tried to minimize the error along this boundary by placing most test points along it. Because of this behavior, these designs exposed the response surface model to bias (i.e., lack-of-fit) errors (see reference 5, pages 403-405).

It is known that D-optimal designs yield selections of test points that offer some protection against bias errors in the selection of the response surface polynomial. Thus, the second design procedure implemented a D-optimal design using $C_{L,max}$ as the response variable, and a complete cubic polynomial in M and Re .¹³ Using a D-optimal design with $C_{L,max}$ as the response variable is not statistically rigorous since, as was discussed earlier, the uncertainty in $C_{L,max}$ is not constant through the test design space. However, it was felt that the insight derived from generating a D-optimal test design would assist in the selection of a final test design.

For the cubic polynomial used in the D-optimal test design the matrix $\bar{\mathbf{X}}$ becomes:

$$\bar{\mathbf{X}} = \begin{bmatrix} 1 & M_1 & Re_1 & M_1 Re_1 & M_1^2 & Re_1^2 & M_1^2 Re_1 & M_1 Re_1^2 & M_1^3 & Re_1^3 \\ \vdots & \vdots \\ 1 & M_{n_{obs}} & Re_{n_{obs}} & M_{n_{obs}} Re_{n_{obs}} & M_{n_{obs}}^2 & Re_{n_{obs}}^2 & M_{n_{obs}}^2 Re_{n_{obs}} & M_{n_{obs}} Re_{n_{obs}}^2 & M_{n_{obs}}^3 & Re_{n_{obs}}^3 \end{bmatrix} \quad (4.36)$$

and $n_e = 10$. The D-optimal design procedure attempts to maximize the discriminant:

$$|\bar{\mathbf{X}}^T \bar{\mathbf{X}}| \quad (4.37)$$

As can be seen from equation 4.34, this quantity plays an important role in the determination of precision uncertainties. The calculations for the D-optimal design were performed using JMP[®] as described in reference 91. This software iterates in an attempt to minimize the determinant in equation 4.37, subject to the constraints specified earlier. Although there is no guarantee that the final design generated by JMP[®] is actually the D-optimal design (within the specified constraints), the design will be close to the D-optimal if the program is allowed to perform a large enough number of iterations. JMP[®] also reports the D-efficiency, which is defined by:

¹³ In fitting the pre-test analytical values of $C_{L,max}$ it was found that a cubic polynomial was appropriate for a response surface in $C_{L,max}$.

$$\text{D - efficiency} = 100 \left(\frac{1}{n_{obs}} \left| \bar{\mathbf{X}}^T \bar{\mathbf{X}} \right|^{1/n_e} \right) \quad (4.38)$$

Of the various D-optimal designs (all of them similar), one was chosen to assist in the definition of the final design as described in the next section.

4.5 Test Design and Planned Testing Sequence

The minimum precision error and D-optimal design procedures produced very different designs. Table 4.6 lists the test points selected by the minimum precision error design procedure; these points are shown graphically in figure 4.5. This test design had 10 unique test points and 8 replicates. The predicted maximum precision error in C_{Lmax} at the 95% confidence level was 0.0098; its D-efficiency was 2.7%. This test design was highly unbalanced. Other than the pre-selected test points, the design procedure placed most of the remaining test points along the lower (i.e., minimum q) boundary. Large areas of the design space were left with no test points, exposing the response surface model to bias errors. In this region the values of C_{Lmax} would need to be interpolated by the response surface. The over-emphasis of the lower boundary at the expense of large areas of the test space made this test design unsuitable without modification. Table 4.7 lists the test points selected by the D-optimal design procedure; these points are shown graphically in figure 4.6. This test design had 13 unique test points and 5 replicates. The predicted maximum precision error in C_{Lmax} at the 95% confidence level was 0.0154; its D-efficiency was 10.4%. Although the D-efficiency of this design is significantly higher than for the minimum precision error design, the maximum precision error in C_{Lmax} has increased by 57% (from 0.0098 to 0.0154). As expected from a D-optimal design the boundaries were emphasized. At the same time the D-optimal design placed points in the middle of the design space, thus avoiding large regions where C_{Lmax} needed to be interpolated by the response surface; this reduced the possibility of bias errors in the response surface model. Although the D-optimal design seemed suitable, a re-allocation of test points guided by the minimum precision uncertainty test design, was able to significantly reduce the maximum precision uncertainty with only a slight reduction in the D-efficiency. Some of the test points, and replicates, placed by the D-optimal design at the higher dynamic pressures could be moved to areas of lower dynamic pressure to reduce the maximum precision error with only a models loss of D-efficiency.

The test points chosen for the final design, generated by examining the minimum precision error and D-optimal designs, are shown in table 4.8. These points are shown graphically in figure 4.7. This compromise test design had 11 unique test points and 7 replicates. With this number of test points, complete polynomial response functions up to cubic could be generated to fit the experimental data (lower order polynomials could also be used). The replicate test points also allowed the undertaking of lack-of-fit tests to

assess the appropriateness of the chosen response function if so desired.¹⁴ The predicted maximum precision error in C_{Lmax} , at the 95% confidence level, was 0.0116, with a D-efficiency of 8.2%. This design placed sufficient points along the design space boundary, emphasized the region of low dynamic pressure with replicates to reduce the maximum precision error, and placed two points within the design space to avoid large areas of interpolation. It was this test design that was used during the initial portion of testing.

At this point a valid question to ask is whether the test design procedures used (i.e., minimum precision error and D-optimal) were really necessary to generate the test design given in table 4.8 and shown in figure 4.7. The answer is no. Given the two-dimensional nature of the test design space, and knowledge of the uncertainty structure as discussed in section 4.3, designs equally suitable to that derived above could have been generated by educated guessing. However in a more complex test design, one involving three or more independent variables for example, arriving at a suitable educated guess would be significantly more difficult. From the experience gained in designing the test for the present experiment, a test design approach incorporating the minimum precision error combined with consideration of bias in the response surface function (i.e., lack-of-fit) would be recommended (see reference 5, pages 402-420 for a discussion of such designs). Lack of time before the scheduled wind tunnel test did not allow the pursuit of this recommended approach. However, as already mentioned, the test design arrived at using the procedures discussed in this section yielded an adequate test design.

In an optimal setting, the sequence of test points would be set to confound precision errors by either blocking or randomizing them. Because of the complexities involved in operating a large wind tunnel such as the TDT, and the requirement for efficient operations, an optimal testing sequence was not possible. A complete description of the issues involved in operating the TDT at the conditions required of this test, and their effect on the testing sequence, are given in chapter 5. The pre-test planned test conditions and run schedule are shown in table 4.9. Note that the third testing day was allocated to conducting additional runs in the test design space where discrepancies between the aerodynamic analyses and experimental results were identified from the data acquired during testing days 1 and 2. The fourth testing day was allocated to testing for surface pressure measurements (see chapter 5 for further details on this aspect of the test). In chapter 5 the test conditions and sequence actually used during testing are discussed.

¹⁴ For reasons related to the error structure of the actual experiment, as discussed in chapter 6, response surface models were not created and lack-of-fit tests were not conducted to evaluate the uncertainty in the experimental results. An alternate method of evaluating uncertainty was implemented.

4.6 A Note on the Bias Uncertainty

The experimental design described in this chapter was based on the precision uncertainty of the response, without regards to the bias uncertainty in the experiment.¹⁵ Precision uncertainty can be altered by placement of the experimental test points within the test domain, and by the appropriate selection of replicate test points, allowing for optimization of the experiment. Although the bias uncertainty of the response can vary with test conditions (M and Re in the present experiment), its value cannot be altered by the placement of experimental test points within the test domain or by the selection of replicate test points. Bias uncertainty arises from invariant (i.e., non-random) errors in the wind tunnel instrumentation (e.g., pressures, temperatures, forces, angles of attack), and in other relevant quantities (e.g., fluid constants, wing area).

The approach commonly used to deal with bias uncertainty is to use the most accurate instrumentation available, and eliminate all known bias errors. This was done to the greatest extent possible during the present investigation. However, there always remains some level of bias uncertainty that can only be estimated.

Pre-test bias uncertainty analyses were performed to assess the magnitude of the bias uncertainty. Combined with the pre-test precision uncertainty analyses, an assessment was made of the total expected uncertainty in the experimental results. This assessment indicated that the expected total experimental uncertainty was small enough to achieve the investigation's objectives. A final bias uncertainty analysis of the experimental data is presented in chapter 6.

¹⁵ This bias should not be confused with the bias of the response surface (i.e., lack-of-fit) discussed earlier.

Table 4.1 – Values of constants used for fluid properties

Quantity	Value	References Used in Deriving Value
R	287.05 J/kg K	84, 85, and 86
γ	1.399	84, 87, and 88
μ_{ref}	1.846×10^{-5} N s/m ²	87 and 89
T_{ref}	300 K	
n	0.798803	

Notes:

- 1) Values from the various references were used to derive the desired quantities.
- 2) The viscosity coefficient is approximated by the relationship:

$$\mu = \mu_{ref} \left(\frac{T}{T_{ref}} \right)^n$$

as suggested in reference 90. The value of T_{ref} was chosen to be 300 K since it was close to the value at which the wind tunnel was operated. The values of μ_{ref} and n were derived using the relationship shown above, and the data from the cited references.

Table 4.2 – Pre-test precision uncertainty estimates for NF , AF , α , p_0 , p , and T_0 at the one-sigma level

Quantity	Estimate
P_{NF}	0.18 N (0.040 lb)
P_{AF}	0.065 N (0.015 lb)
P_{α}	0.00045 rad (0.052°)
P_{p_0}	2.4 Pa (0.05 psf)
P_p	2.4 Pa (0.05 psf)
P_{T_0}	0.03 K (0.054 R)

Table 4.3 – Pre-test aerodynamic analyses results

		Values at C_{Lmax}					
M	Re	L_{norm} N (lb)	C_L	C_D	α deg.	C_N	C_A
0.300	250,000	106.1 (2.216)	1.030	0.0940	11.59	1.028	-0.1148
0.300	205,000	86.5 (1.808)	1.024	0.0945	11.64	1.022	-0.1141
0.300	160,000	67.1 (1.402)	1.018	0.0968	11.78	1.016	-0.1130
0.300	115,000	47.2 (0.986)	0.996	0.0948	11.58	0.995	-0.1070
0.300	59,140	23.4 (0.488)	0.959	0.0967	11.51	0.959	-0.0966
0.350	227,500	110.9 (2.317)	1.022	0.0929	11.40	1.020	-0.1110
0.350	182,500	88.4 (1.847)	1.016	0.0944	11.48	1.014	-0.1097
0.350	137,500	65.5 (1.367)	0.998	0.0935	11.36	0.997	-0.1050
0.350	92,500	43.3 (0.904)	0.981	0.0949	11.26	0.981	-0.0985
0.400	205,000	112.4 (2.347)	1.015	0.0927	11.24	1.014	-0.1070
0.400	160,000	86.3 (1.803)	0.999	0.0919	11.12	0.998	-0.1025
0.400	115,000	60.9 (1.272)	0.981	0.0917	11.07	0.980	-0.0983
0.400	70,000	36.2 (0.755)	0.957	0.0936	11.05	0.957	-0.0915
0.400	45,070	22.6 (0.472)	0.928	0.0962	11.19	0.929	-0.0858
0.407	250,000	140.0 (2.924)	1.021	0.0919	11.13	1.019	-0.1069
0.450	227,500	137.8 (2.877)	1.008	0.0903	10.84	1.007	-0.1008
0.450	182,500	109.3 (2.282)	0.996	0.0901	10.81	0.996	-0.0984
0.450	137,500	81.2 (1.696)	0.983	0.0900	10.80	0.982	-0.0957
0.450	92,500	53.5 (1.118)	0.963	0.0906	10.82	0.963	-0.0918
0.450	47,500	26.2 (0.547)	0.918	0.0929	10.90	0.919	-0.0824
0.500	207,520	135.8 (2.835)	0.991	0.0881	10.43	0.991	-0.0928
0.500	160,000	103.6 (2.163)	0.981	0.0884	10.47	0.981	-0.0913
0.500	115,000	73.3 (1.530)	0.966	0.0885	10.48	0.965	-0.0886
0.500	70,000	43.2 (0.903)	0.936	0.0892	10.52	0.936	-0.0831
0.500	36,790	21.5 (0.488)	0.884	0.0924	10.62	0.886	-0.0721
0.550	182,500	128.8 (2.689)	0.985	0.0879	10.18	0.985	-0.0875
0.550	137,500	95.4 (1.993)	0.969	0.0872	10.13	0.969	-0.0845
0.550	92,500	62.9 (1.313)	0.948	0.0876	10.20	0.949	-0.0817
0.550	47,500	30.6 (0.639)	0.898	0.0899	10.32	0.900	-0.0725
0.600	177,160	138.1 (2.884)	1.011	0.0920	10.15	1.011	-0.0876
0.600	160,000	123.1 (2.572)	0.998	0.0902	10.03	0.999	-0.0851
0.600	115,000	86.0 (1.795)	0.970	0.0882	9.93	0.970	-0.0803
0.600	70,000	50.1 (1.047)	0.929	0.0876	9.96	0.930	-0.0744
0.600	31,410	20.5 (0.428)	0.846	0.0888	9.78	0.848	-0.0561
0.650	137,500	115.0 (2.403)	1.017	0.0921	9.67	1.018	-0.0800
0.650	92,500	73.9 (1.544)	0.971	0.0884	9.48	0.972	-0.0728
0.650	47,500	34.7 (0.724)	0.887	0.0864	9.44	0.889	-0.0602
0.700	156,160	133.6 (2.791)	0.982	0.0826	8.19	0.983	-0.0581
0.700	115,000	95.7 (1.999)	0.955	0.0917	8.96	0.957	-0.0581
0.700	70,000	54.4 (1.136)	0.891	0.0806	8.38	0.893	-0.0501
0.700	27,680	19.6 (0.409)	0.812	0.1312	12.20	0.821	-0.0433
0.750	137,500	116.7 (2.437)	0.924	0.1360	11.90	0.932	-0.0575
0.750	92,500	75.8 (1.582)	0.892	0.1328	11.70	0.900	-0.0508
0.750	47,500	36.7 (0.767)	0.842	0.1523	13.50	0.854	-0.0485
0.800	141,000	125.2 (2.614)	0.923	0.1881	14.90	0.940	-0.0554
0.800	115,000	100.5 (2.100)	0.908	0.1858	14.90	0.926	-0.0540
0.800	70,000	58.7 (1.227)	0.872	0.1701	14.10	0.887	-0.0475
0.800	25,000	19.5 (0.407)	0.810	0.1653	14.30	0.825	-0.0398

Note:

The value of C_{Lmax} and the corresponding values of C_D , α , C_N , and C_A were determined by applying the “engineering” C_{Lmax} criterion for C_L vs α curves with no mathematically defined value of C_{Lmax} within the range of α considered as described in chapter 3.

Table 4.4 – Evaluation of $P_{L,max}$ as a function of M and Re

M	Re	$P_{L,max}$ N (lb)
0.300	250,000	0.22 (0.049)
0.300	205,000	0.22 (0.049)
0.300	160,000	0.22 (0.049)
0.300	115,000	0.22 (0.049)
0.300	59,140	0.21 (0.047)
0.350	227,500	0.22 (0.049)
0.350	182,500	0.22 (0.049)
0.350	137,500	0.21 (0.047)
0.350	92,500	0.21 (0.047)
0.400	205,000	0.21 (0.047)
0.400	160,000	0.21 (0.047)
0.400	115,000	0.21 (0.047)
0.400	70,000	0.21 (0.047)
0.400	45,070	0.21 (0.047)
0.407	250,000	0.22 (0.049)
0.450	227,500	0.21 (0.047)
0.450	182,500	0.21 (0.047)
0.450	137,500	0.21 (0.047)
0.450	92,500	0.21 (0.047)
0.450	47,500	0.21 (0.047)
0.500	207,520	0.21 (0.047)
0.500	160,000	0.21 (0.047)
0.500	115,000	0.21 (0.047)
0.500	70,000	0.21 (0.047)
0.500	36,790	0.20 (0.045)
0.550	182,500	0.21 (0.047)
0.550	137,500	0.21 (0.047)
0.550	92,500	0.21 (0.047)
0.550	47,500	0.20 (0.045)
0.600	177,160	0.21 (0.047)
0.600	160,000	0.21 (0.047)
0.600	115,000	0.21 (0.047)
0.600	70,000	0.20 (0.045)
0.600	31,410	0.20 (0.045)
0.650	137,500	0.21 (0.047)
0.650	92,500	0.20 (0.045)
0.650	47,500	0.20 (0.045)
0.700	156,160	0.20 (0.045)
0.700	115,000	0.20 (0.045)
0.700	70,000	0.20 (0.045)
0.700	27,680	0.19 (0.043)
0.750	137,500	0.20 (0.045)
0.750	92,500	0.20 (0.045)
0.750	47,500	0.19 (0.043)
0.800	141,000	0.20 (0.045)
0.800	115,000	0.19 (0.043)
0.800	70,000	0.19 (0.043)
0.800	25,000	0.19 (0.043)

Table 4.5 – Pre-selected test points

<i>M</i>	<i>Re</i>
0.300	250,000
0.407	250,000
0.800	141,000
0.700	27,680

Table 4.6 – Minimum precision error test design

<i>M</i>	<i>Re</i>	No. of Tests
0.300	250,000	1
0.300	59,140	4
0.400	45,070	2
0.407	250,000	1
0.500	36,790	3
0.650	92,500	1
0.650	47,500	1
0.700	27,680	3
0.800	141,000	1
0.800	70,000	1

Unique Test Points 10
 Replicates 8
 Total Number of Test Points 18

Table 4.7 – D-optimal test design

M	Re	No. of Tests
0.300	250,000	1
0.300	205,000	1
0.300	115,000	1
0.300	59,140	2
0.407	250,000	2
0.450	182,500	1
0.450	92,500	1
0.500	36,790	1
0.600	177,160	1
0.650	92,500	1
0.700	27,680	2
0.800	141,000	2
0.800	70,000	2

Unique Test Points 13
 Replicates 5
 Total Number of Test Points 18

Table 4.8 – Final test design

M	Re	No. of Tests
0.300	250,000	1
0.300	160,000	1
0.300	59,140	4
0.407	250,000	1
0.450	137,500	1
0.500	36,790	3
0.600	177,160	1
0.650	92,500	1
0.700	27,680	3
0.800	141,000	1
0.800	70,000	1

Unique Test Points 11
 Replicates 7
 Total Number of Test Points 18

Table 4.9 – Planned test conditions and run schedule

	M	Re	Comments
Test Day 1 (9 Runs)	0.700	27,680	
	0.700	27,680	Replicate
	0.500	36,790	
	0.800	70,000	
	0.300	59,140	
	0.300	59,140	Replicate
	0.800	141,000	
	0.407	250,000	
	0.300	250,000	
Test Day 2 (9 Runs)	0.700	27,680	Replicate
	0.500	36,790	Replicate
	0.500	36,790	Replicate
	0.650	92,500	
	0.300	59,140	Replicate
	0.300	59,140	Replicate
	0.450	137,500	
	0.600	177,160	
	0.300	160,000	
Test Day 3	Up to 9 forces/moment runs depending on the results of test days 1 and 2.		
Test Day 4 (11 Runs)	0.700	27,680	
	0.500	36,790	
	0.800	70,000	
	0.650	92,500	
	0.300	59,140	
	0.800	141,000	
	0.450	137,500	
	0.600	177,160	
	0.300	160,000	
	0.407	250,000	
	0.300	250,000	

Note: Forces/moment testing on Test Days 1-3, pressure testing on Test Day 4

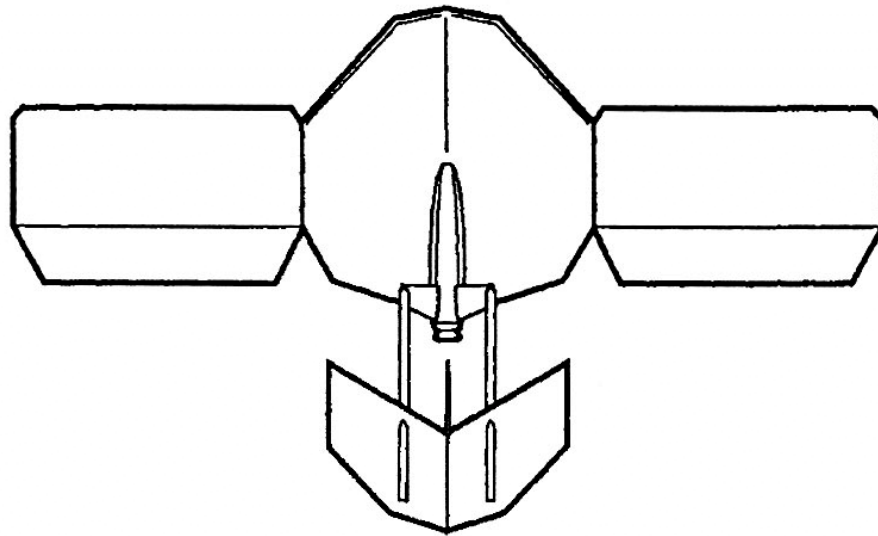


Figure 4.1 – Mars airplane design (top view) showing wing planform. Adapted from figure 2 of reference 7.

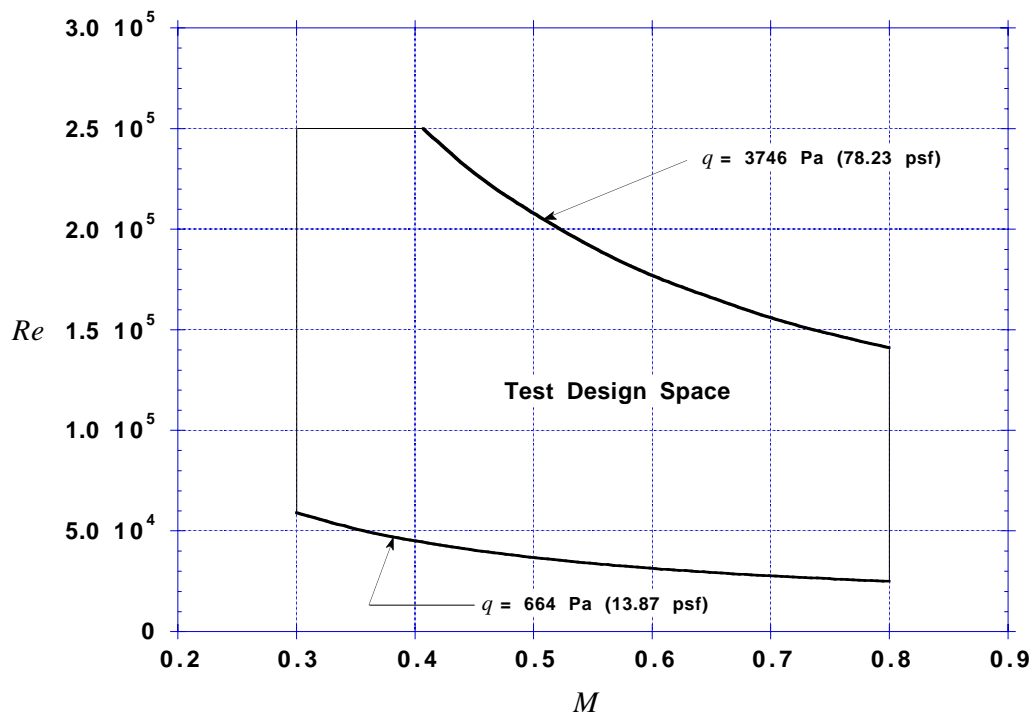


Figure 4.2 – Test design space

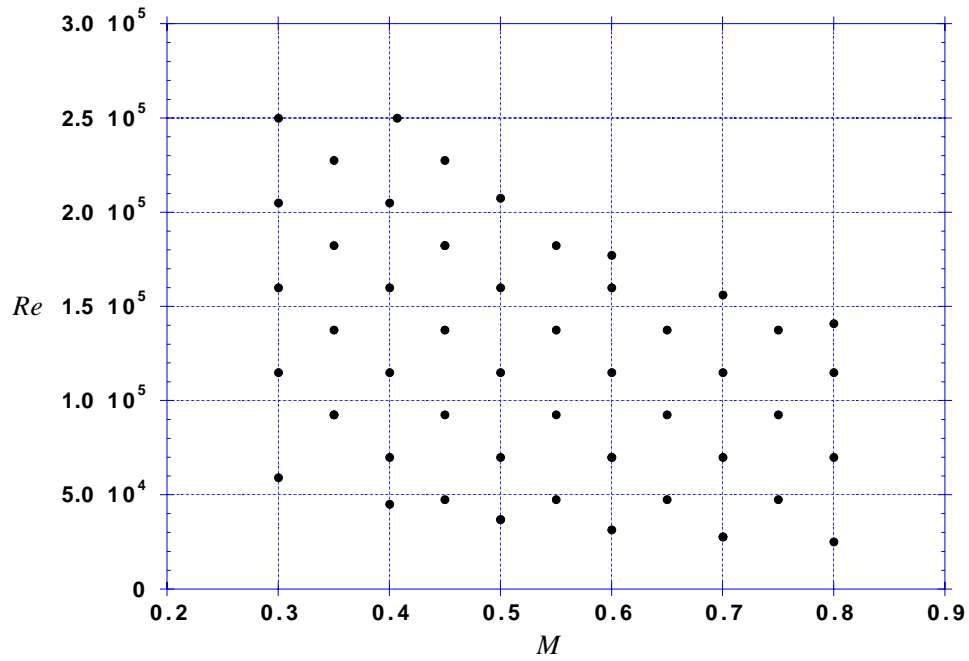


Figure 4.3 – Conditions used for pre-test aerodynamic analyses

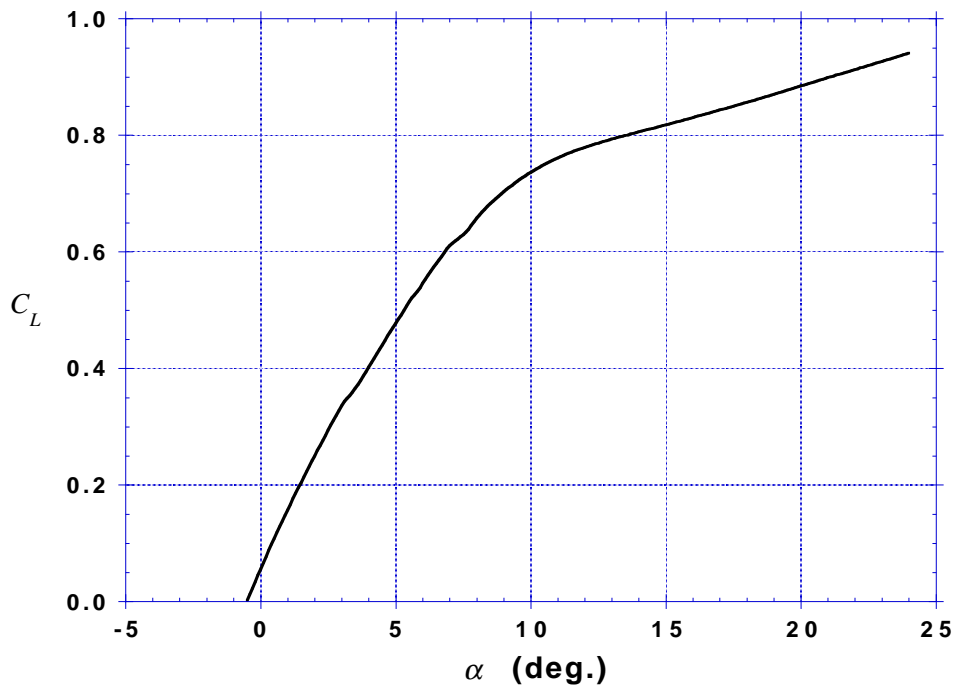


Figure 4.4 – Aerodynamic analysis C_L vs α for $M = 0.800$, $Re = 25,000$

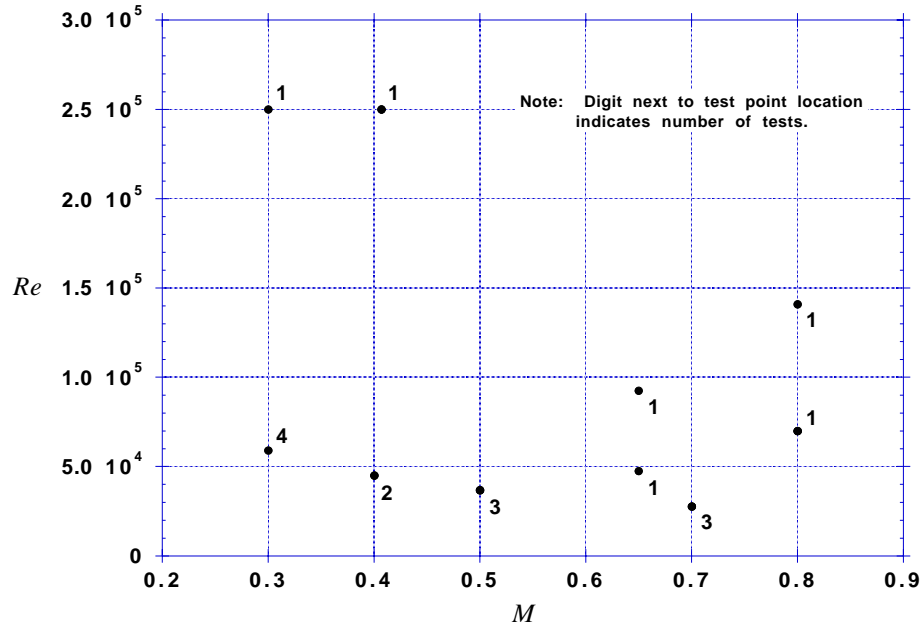


Figure 4.5 – Minimum precision error test design. Predicted maximum precision error in C_{Lmax} at the 95% confidence level = 0.0098. D-efficiency = 2.7%.

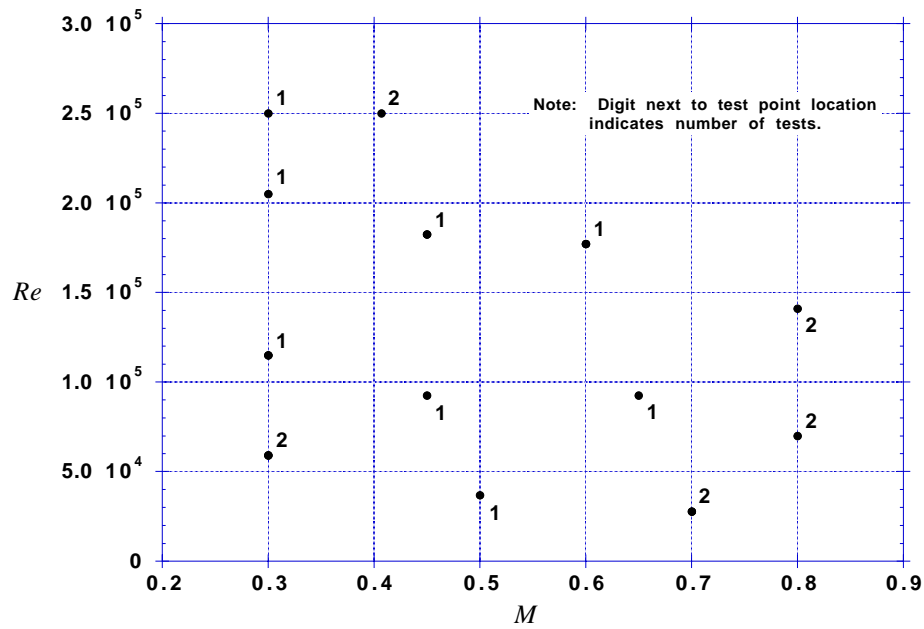


Figure 4.6 – D-optimal test design. Predicted maximum precision error in C_{Lmax} at the 95% confidence level = 0.0154. D-efficiency = 10.4%.

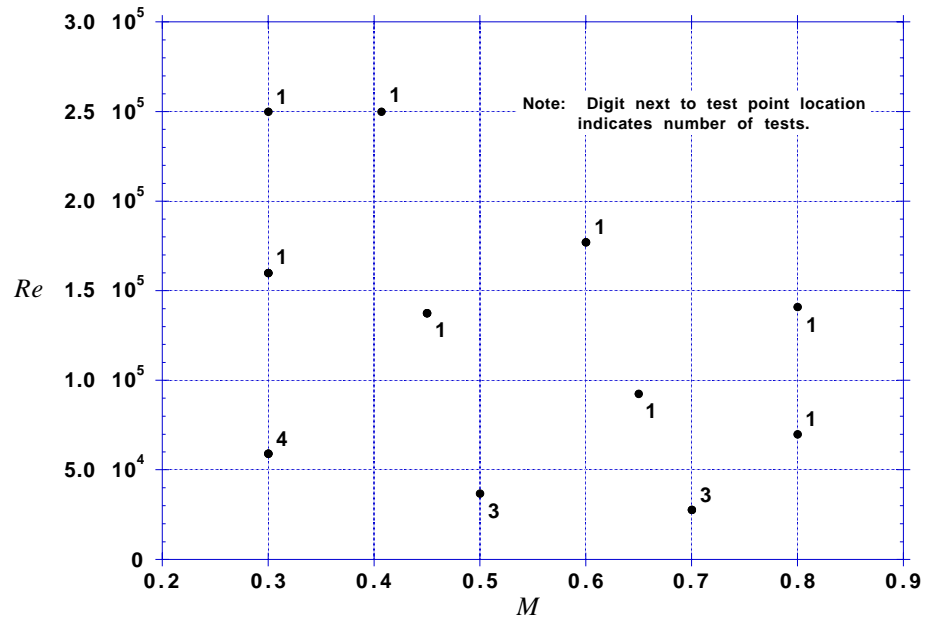


Figure 4.7 – Final test design. Predicted maximum precision error in $C_{L_{max}}$ at the 95% confidence level = 0.0116. D-efficiency = 8.2%.

Chapter 5: Test Setup and Operations

In this chapter the details of the test setup and operations are discussed. A complete description of the wind tunnel model design and fabrication is presented followed by a discussion of the wind tunnel balance and its performance, limitations, and selection rationale. Testing was conducted in the NASA Langley Research Center's Transonic Dynamics Tunnel (TDT). A description of this wind tunnel is presented giving particular attention to the effects of its operation on the execution of the test. Next, the installation of the wind tunnel model in the wind tunnel test section is described, emphasizing the calibration procedure for the angle of attack. Test operations are discussed, including the actual test sequence used, and problems encountered during testing. Finally, the raw data collected during testing is listed.

5.1 Wind Tunnel Model

The wind tunnel model consists of a rectangular wing of nominal wingspan, b , of 0.43180 m (17.000 in); chord, c , of 0.08750 m (3.445 in); wing area, S , of 0.037784 m² (58.565 in²); and aspect ratio, AR , of 4.934. The wing has no twist. This wind tunnel model is a simplified quarter-scale representation of the wing of the Mars airplane discussed in reference 7. The model's scale was selected on the basis of previous experience of Mars airplanes tested in the TDT. A model of this scale and size provides a good compromise between wind tunnel productivity (a larger model decreases wind tunnel productivity as discussed in section 5.3) and the capability of manufacturing an accurate model (it is difficult to accurately manufacture very small models). In table 5.1 a comparison is given between key parameters of the designed (i.e., nominal) and as-built wind tunnel model. The airfoil used is the MASC1 (Mars Airplane Super Critical #1) designed by Dr. Richard L. Campbell of NASA LaRC for small Mars airplane applications. This airfoil was design to operate at a Mach number of 0.63, Reynolds number of 35,000, and a section lift coefficient, c_l , of 0.653 with a chordwise loading similar to that of modern supercritical airfoils. Constraints imposed on the airfoil design were a minimum thickness to chord ratio, t/c_{max} , of 0.072, and a maximum section pitching moment coefficient about the quarter-chord, $c_{m\ c/4}$, of -0.12 . To machine the model from an aluminum block, the airfoil must have a finite trailing edge thickness of approximately 0.0005 m (0.020 in) for a model with a chord of 0.087503 m (3.445 in). The original airfoil coordinates, having a zero trailing edge thickness, were modified to accommodate the finite trailing edge thickness requirement. Nondimensional airfoil

coordinates and other information for both the original and modified MASC1 airfoil are given in appendix B, and shown graphically in figure 5.1.¹ A detailed drawing of the wing is given in figure C.2 of appendix C. The model was fabricated on a numerically controlled milling machine with hand working to obtain the final shape and finish.²

In addition to the wing, the wind tunnel model includes a balance block. The purpose of the balance block is to attach the wing to either the wind tunnel balance or the sting adapter. Figure 5.2 shows the wing and balance block assembly, while figure 5.3 shows photographs of the wing and balance block assembly from various angles, both assembled and disassembled. A detailed drawing of the balance block is given in figure C.3 of appendix C. Since the main purpose of the experiment was to determine the maximum lift coefficient of the wing, the balance block is attached to the lower surface of the wing so as to minimize aerodynamic interference with the critical flow on the wing's upper surface. Because the flow around the leading edge stagnation point also affects the maximum lift coefficient, the balance block starts aft of the leading edge (at approximately the 5 percent chord location) and has a highly swept front edge. The balance block is designed to be as small as possible, while allowing for the attachment of the wind tunnel balance or sting adapter and satisfying the wind tunnel model structural design requirements specified in the Langley Wind Tunnel Model Systems Criteria [92]. The balance block is 0.0254 m (1.00 in) wide, or about 5.9 percent of the wing span.

The wind tunnel model was designed to be used in one of two modes. In the forces/moments mode, the wind tunnel balance was attached to the balance block, and only forces and moments can be measured. Details of the wind tunnel balance are given in section 5.2. In the pressures measuring mode, the sting adapter was attached to the balance block in lieu of the wind tunnel balance. A detailed drawing of the sting adapter is given in figure C.4 of appendix C. In this mode pressure could be measured at 28 locations on the wing and at three locations on the sting adapter near the aft surface of the balance block. The wing pressure measuring locations can be clearly seen on the left wing in figure 5.3, and the tubing connections near the centerline of the wing in figure 5.3b. These wing pressures are of limited interest to the present research, and are not discussed further. Of more interest to the present investigation are the three pressures measured near the base of the balance block. These pressures were used to calculate corrections to the axial force. The three base pressures were measured at 120 degree intervals around the sting adapter (one of these locations is at the 12 o'clock position). Details of the calculation of these corrections to the axial force are discussed in the experimental data analyses (section 6.2). Although it is possible to design a model in which forces/moments and pressures can be measured at the same time, doing so requires that the balance block be significantly larger to accommodate both the wind tunnel

¹ All aerodynamic analyses were conducted with the finite trailing edge thickness coordinates.

² A partial set of as-built contour measurements were taken, but these measurements were not used in the present investigation. A more complete set of measurements would be needed in the course of an investigation to determine the reasons for the differences between the analysis and the experiment.

balance and the pressure tubing. The testing inconvenience of having two test setups was accepted in order to minimize the aerodynamic interference of a larger balance block.

Because the metric part of the wind tunnel balance is not fully within the model, a windshield was installed around it to keep undesired aerodynamic forces from being measured. This windshield is shown in figure 5.2; it can also be seen in figure 5.3c next to the wind tunnel balance, and in its correct relationship to the model in figure 5.4. The interior diameter of this windshield is 0.0267 m (1.05 in) which is large enough to allow for the wind tunnel balance to flex without touching it. The external diameter of the windshield is 0.0292 m (1.15 in). The balance block base diameter is 0.0318 m (1.25 in) which is 0.0254 m (0.1 in) greater than the external diameter of the windshield. The greater base diameter of the balance block allowed the wind tunnel balance, and thus the model, to move relative to the windshield without exposing the front edge of the windshield to the airflow. To avoid interference between the balance block and windshield, a 0.0015 m (0.060 in) gap was present between the base of the balance block and the windshield. A balsa wood fairing was installed at the appropriate location on the windshield to form an approximately continuous aerodynamic contour from the balance block and wing to the windshield. The windshield was attached to the sting downstream of the wind tunnel balance as shown in figure 5.4. In order to maintain the same aerodynamic configuration during forces/moment and pressure measuring tests, the windshield was always installed during testing.

In figure 5.5 all components of the wind tunnel model: wing, balance block, wind tunnel balance (discussed in section 5.2), sting adapter, and windshield are shown. The detailed wind tunnel model design was performed by Advanced Technologies Incorporated (ATI) under contract to NASA LaRC [93]. The drawings of reference 93 are reproduced in appendix C. Most components of the model were fabricated in the machine shop at NASA LaRC.

5.2 Wind Tunnel Balance

Selection of the wind tunnel balance depends on three considerations: availability, load range, and size. First, with regards to availability, for the present research the wind tunnel balance had to be selected from NASA LaRC's inventory of wind tunnel balances and available during the test period. Second, with regards to load range, the wind tunnel balance had to be capable of sustaining the expected loads, including an appropriate safety factor. Third, with regards to size, it was desirable for the wind tunnel balance diameter to be as small as possible. A smaller wind tunnel balance required a smaller balance block, which in turn generated less aerodynamic interference as discussed in section 5.1.

Taking the above considerations into account, wind tunnel balance UT-61A was selected. This wind tunnel balance measures all six load components: three forces

(normal, axial, and side) and three moments (pitch, yaw, and roll). Of interest to the present investigation are the normal, NF , and axial, AF , forces.³ These two forces were used to calculate lift, L , through equation 5.1:

$$L = NF \cos \alpha - AF \sin \alpha \quad (5.1)$$

A drawing of wind tunnel balance UT-61A is shown in figure 5.6, and a close-up photograph in figure 5.7. The installation of wind tunnel balance UT-61A on the balance block can be seen in figure 5.3c.

5.3 Wind Tunnel

All testing for the present research was performed in the NASA LaRC Transonic Dynamics Tunnel, usually known as the TDT (see figure 5.8). The TDT's main purpose is to investigate aeroelastic phenomena. However, its capability to operate at pressures from atmospheric to near-vacuum makes it extremely useful for Mars airplane aerodynamic research since it gives it a broad Mach/Reynolds number operating envelope as shown in figure 5.9.

The TDT is a closed-circuit, continuous-flow, variable pressure wind tunnel. The test section is square, 5.9 m (16 ft) per side with cropped corners.⁴ Slots on the floor, ceiling, and walls of the test section allow transonic operation. A schematic drawing of the TDT is shown in figure 5.10. Flow treatment to minimize turbulence is limited to a smoothing screen and a contraction ratio of 11:1. The test section turbulence at conditions of interest for the present research has been characterized and is discussed in chapter 3 and appendix A. All tunnel operating conditions (e.g., q , Re , M , etc.) are calculated from three quantities: stagnation pressure, p_0 , static pressure, p , and stagnation temperature, T_0 . The stagnation pressure and temperature are measured in the settling chamber, while the static pressure is measured in the test chamber surrounding the test section. The tunnel operator has control of p_0 and p by varying the density inside the tunnel and the fan speed. However, there is only limited control of T_0 . The cooling system's main purpose is to keep the tunnel from overheating. Thus, the stagnation temperature varies depending on operating conditions, how long the tunnel has been operating, insolation, and weather. This lack of temperature control is usually not a problem, and the run-to-run and day-to-day variation in temperature is not large. A sting mounted on a splitter plate downstream of the test section allows static force measurement tests to be conducted. A photograph of the sting with the Mars airplane wing mounted on it is shown in figure 5.11. The sting is operated by two worm screws within the splitter plate. Since the worm screws operate independently, the model angle of attack can be varied

³ NF is positive in the up (i.e., lift) direction. AF is positive in the streamwise (i.e., drag) direction. See figure 6.1.

⁴ Because of the small size of the model in this investigation as compared to the tunnel test section, no blockage or wall interference corrections to the test results were necessary.

while maintaining a fixed position at the center of the test section. In other words, changing the model angle of attack does not force the model closer to the floor or ceiling of the test section. The sting has a nominal 30 degrees range of motion. However, the range of motion used during the present research was 28 degrees to avoid triggering the limit switches at the end of the sting travel.

It can be shown that the tunnel static pressure, p , can be expressed as a function of the Reynolds and Mach numbers as:

$$p = \frac{Re}{Mc} \mu \sqrt{\frac{RT}{\gamma}} \quad (5.2)$$

Thus, the static pressure will vary proportionally with the Reynolds number and inversely proportionally with the Mach number and the model chord. Although the TDT can achieve the low pressures required to obtain the desired Reynolds and Mach numbers, these low pressures come at a cost in tunnel productivity. As shown in figure 5.12, the pumping time required to achieve low pressures in the TDT can be significant. For the present research it could be as long as three hours, in addition to the pumping system startup time which is fixed regardless of how much pumping needs to be performed. This is tunnel occupancy time that cannot be used to collect data. Note that for a given Reynolds and Mach number, a smaller model (i.e., one with a smaller chord), will require a higher static pressure and thus less pumping time. Thus, tunnel productivity can be increased by using a smaller model. A smaller model, however, is more difficult to manufacture accurately. Selecting a model scale is thus driven by the conflicting needs for high tunnel productivity and high model accuracy. The choice of model size in the present investigation was a compromise between these competing needs.

5.4 Wind Tunnel Test Setup

The model was mounted on the TDT sting system as shown in figure 5.11. Figures 5.4, 5.13, and 5.14 show close-up views of the model installation. As stated earlier, the useful angle of attack range of the TDT sting is 28 degrees, or ± 14 degrees. However, in the present investigation the low angle of attack range is of limited interest. Thus, a 10 degree knuckle adapter was used to yield an angle of attack range from -4 to 24 degrees. This 10 degree knuckle adapter can be seen in figure 5.11.

The sting angle of attack, α_s , is measured by an inclinometer installed near the wind tunnel splitter plate. However, α_s is not identical to the model angle of attack, α . The difference between α_s and α is due to the sting and wind tunnel balance flexibility. If the normal force, NF , and pitching moment about the moment balance center, PM_{bmc} on the balance are known, α can be calculated from the relationship:⁵

⁵ NF is positive in the up (i.e., lift) direction. PM_{bmc} is positive in the nose-up direction. See figure 6.1.

$$\alpha = \alpha_s + K_{NF}NF + K_{PM}PM_{bmc} \quad (5.3)$$

Values for K_{NF} and K_{PM} were determined prior to the start of testing in a calibration procedure that places fixed weights at two known locations with respect to the model (one location being the balance moment center) and measuring the change in α generated by these weights. Because the stiffnesses of the wind tunnel balance and the sting adapter were not identical, each test setup (forces/moment or pressures) had a different set of values for K_{NF} and K_{PM} ; these values are given in table 5.2. During forces/moment testing the TDT data acquisition system calculates and reports α based on the measured values of α_s , NF , and PM_{bmc} , and the given values of K_{NF} and K_{PM} . During pressure testing there was no direct measurement of NF and PM_{bmc} , and thus the TDT data acquisition system could not calculate α . However, using data from the forces/moment runs, a relationship between α_s and α was derived at a given test condition (i.e., Re and M) for the pressure runs and used to calculate α .

In an additional calibration procedure, the change in the forces and moments measured by the balance due to the weight of the model as the angle of attack changes was removed from the forces and moments reported by the TDT data acquisition system. This procedure is usually known as an “alpha tare.” For lightweight models being used over a limited angle of attack range around zero (as is the case in the present investigation), the effect of this calibration is minimal for the normal force; its main effect is on the pitching moment and axial force.

5.5 Test Operations

The operation of the wind tunnel during testing for the present investigation was as follows for a planned set of runs at various test conditions. Problems with the wind tunnel as noted later required some deviations from these procedures.

- 1) Pump the tunnel down to a pressure slightly lower than that required for the most challenging test condition (i.e., the test condition with the lowest p as calculated from equation 5.2) within the planned set. Once the desired pressure is reached, stop pumping and close the valves.
- 2) Rotate the model to zero model angle of attack and zero the wind tunnel balance.
- 3) Start the wind tunnel fan and bring the tunnel speed up to the required Mach number.
- 4) Bleed air into the tunnel until the desired starting Reynolds number is achieved. (By pumping the tunnel to a pressure lower than required we can bleed up to the desired Reynolds number. Doing this is significantly faster and more

controllable than pumping down to the desired Reynolds number while the tunnel is operating.)

- 5) Rotate the model to the lowest model angle of attack to be tested (-4°).
- 6) Start collecting data by stepping up in angle of attack until the maximum possible angle of attack is reached. Data were collected at discrete angles of attack, not while sweeping up in angle of attack. The angle of attack is increased monotonically to avoid hysteresis effects. During testing the tunnel operator continually adjusts the fan speed to maintain a constant Mach number.
- 7) After completing a given test condition, rotate the model to zero model angle of attack.
- 8) Reduce the tunnel speed to a low, but nonzero, Mach number.
- 9) If the next test condition is a replicate of the one just completed, pump the tunnel down to a pressure slightly lower than that required. Otherwise, bleed air into the tunnel until a pressure slightly lower than that required for the next test condition is reached. Note that this step requires that test conditions within a given set be organized such that every subsequent test condition needs the same or higher tunnel pressure than the previous one.
- 10) Increase the tunnel speed to the desired Mach number for the current test condition.
- 11) Repeat steps 5 through 10 for each subsequent test condition.
- 12) After all test conditions in a given set are completed, decrease the tunnel speed to zero.
- 13) Once the flow in the tunnel has completely stopped, rotate the model to zero model angle of attack and record the wind tunnel balance forces.
- 14) If another set of runs is to be conducted, return to step 1.

It should be evident that this test procedure was set up to minimize the amount of pumping required. Pumping consumes valuable time is not available for testing. However, accommodations were made so that similar test conditions and replicates were not conducted all at once. This distributes the precision uncertainty more evenly among the test conditions.

Note that testing was conducted at a constant Mach number. Because the TDT leaks (albeit at a low rate), testing at a constant Mach number implies that the Reynolds

number will increase with time as air bleeds into the tunnel and air density increases. At conditions with relatively high static pressures, the change in Reynolds number during a given test condition was very small. For example, when testing at a Mach number of 0.300 and Reynolds number of 250,000, the static pressure in the tunnel was approximately 44 kPa (911 psf). At this condition, during a 20 minute test run, the Reynolds number increased by approximately 268 or 0.1 percent which was within the experimental uncertainty of the Reynolds number determination. At conditions with low static pressure, however, the change in Reynolds number during a given test condition could be significant. For example, when testing at a Mach number of 0.800 and a Reynolds number of 25,000, the static pressure in the tunnel was approximately 1.29 kPa (27 psf). At this condition, during a 20 minute test run, the Reynolds number increased by approximately 2,000 or 8 percent. In such cases the run was started at a Reynolds number lower than desired so that the Reynolds number at the angle for the maximum lift coefficient had the desired value. Pumping during testing or between test points was not feasible; some drift in the Reynolds number for a given test condition had to be accepted.

Although the main purpose of the present investigation involves the maximum lift coefficient, the opportunity to collect a complete set of data could not be passed up. Thus, data were collected starting at -4° model angle of attack. The model angle of attack was increased in one degree increments up until the maximum lift coefficient was approached. Near the maximum lift coefficient, the model angle of attack increment was reduced as required; during some test conditions this increment was as small as 0.1° .

The pre-test selection of test conditions and its run schedule is discussed in chapter 4, section 4.5, and shown again in table 5.3 with the addition of the static pressure at which the tunnel needs to be operated to achieve the desired test conditions. This selection was made based on the following assumptions and decisions:

- Four testing days would be available.
- No more than nine forces/moment runs or ten pressure runs could be conducted in a given day while running the tunnel in a two-shift operation.
- Two days of testing would be used for forces/moment testing of the pre-selected test conditions (test days 1 and 2).
- One day of forces/moment testing would be used to pursue test conditions in which the analysis and experiment disagree (test day 3).
- One day of pressure testing would be used for pressure testing of the pre-selected test conditions (test day 4) with no replicates.

The actual run schedule of test conditions are shown in table 5.4, and their location in the test design space in figure 5.15. Most of the differences between the actual and planned

test sequence were due to electrical problems with the TDT. In order to work around these problems and perform the necessary testing as efficiently as possible, the planned test sequence was modified. The TDT management made available one and a half additional testing days to make up for the time lost due to TDT problems during test days 1 and 2. Comparing the planned and actual run schedule of test conditions, the following observations can be made:

- Data for all planned test conditions (including the desired number of replicates) were collected.
- The Mach and Reynolds numbers of the actual test conditions were very close to the planned test conditions.
- The actual run schedule was modified from the planned run schedule to work around wind tunnel problems.
- Once wind tunnel problems were resolved (after test days 1 and 2), more than nine forces/moment test runs (11 for test day 3, 12 for test day 4) were conducted per day.
- Although in the planning stages of the test it was decided not to test at $M = 0.800$, $Re = 25,000$ (see chapter 4, sub-section 4.4.4), during testing it was decided to reincorporate this condition into the test matrix in both the forces/moment and pressure tests.
- Forces/moment data for six additional replicates (Runs 27, 35, 39, 45, 46, 47) of planned test conditions were collected.
- Forces/moment data for five test conditions not in the planned test set (Runs 38, 40, 41, 42, 43) were collected to investigate conditions in which the analysis and experiment disagreed. These test conditions are shown with underlined italic numbers next to the symbols in figure 5.15. The selection of these conditions was based on the observation that the planned test condition near $M = 0.500$ and $Re = 36,790$ yielded the largest difference between the analysis and experiment.

An unexpected problem encountered during testing was the occurrence of stall flutter. At some test conditions, especially those at $M < 0.5$ and $Re > 100,000$, the stall was very abrupt and characterized by a sudden loss of lift. In addition, during the present test the dynamic pressure (and thus the lift force) at these test conditions was at its highest. The lift force caused the sting and wind tunnel balance to deform, increasing α . When the model stalled, and the lift force was reduced, the deflection of the sting and wind tunnel balance was reduced, in turn lowering α . This reduction in α suddenly placed the model at a lower, pre-stall, α . At this reduced α lift was restored and the sting and wind tunnel

balance deflected once again, increasing α . The cycle was then repeated, making the model vibrate violently in pitch. This vibration threatened to destroy the model, wind tunnel balance, and sting. The presence of this stall flutter behavior was sudden, clearly marking the stall, and thus the maximum lift coefficient. However, it also presented the following problems:

- No post-stall data could be obtained for cases with violent stall flutter.
- Wind tunnel balance force and moment signals at stall are noisy since the model is vibrating. This is not a significant a problem as it may appear, since a given value of force or moment obtained from wind tunnel balance was the average of 500 measurements (see section 5.6). Repeated tests at the same conditions yielded results with relatively small scatter. However this signal noise has other statistical implications, which are discussed in chapter 6.
- Force and moment data taken while the model was vibrating include the effect of undesired unsteady aerodynamic effects. However, these effects are rate dependent and tend to cancel when averaged over many samples. Thus, the effects of unsteady aerodynamics are assumed small, and were ignored in the present investigation.

5.6 Data Acquired

The raw data acquired during forces/moment and pressure runs are shown in tables 5.5 and 5.6, respectively. All other quantities (e.g., M , Re , q , C_L) were derived from these data as discussed in chapter 6. At each model angle of attack, data was acquired for five seconds. Thus, the number of data points acquired for each quantity was the sampling rate times five seconds. The TDT data acquisition system reports the mean value of all data points and the Root-Mean-Square (RMS) statistic of each quantity. Note that not all the data acquired is of interest to the present investigation. The data, and derived quantities such as M , Re , q , and C_L , were available both in real time and as data files for further analyses. In the present investigation all derived quantities were re-calculated after testing was concluded based on the raw data listed in tables 5.5 and 5.6. How the data were analyzed is discussed in chapter 6.

Table 5.1 – Key wind tunnel model parameters

Parameter	Design	As-Built
Wingspan, b	0.43180 m (17.000 in)	0.43220 ± 0.00006 m (17.016 ± 0.002 in)
Chord, c	0.087503 m (3.445 in)	0.087308 ± 0.000029 m (3.437 ± 0.001 in)
Wing Area, S	0.037784 m ² (58.565 in ²)	0.037732 ± 0.000534 m ² (58.484 ± 0.021 in ²)
Aspect Ratio, AR	4.934	4.951 ± 0.002

Note: Uncertainty in the “As-Built” numbers are given at the 95% confidence level.

Table 5.2 – Values of K_{NF} and K_{PM} for the forces/moment and pressures test setups

Test Setup	K_{NF}	K_{PM}
Forces/Moment (Wind Tunnel Balance)	0.00514°/N (0.0229°/lb)	0.0614°/N-m (0.00694°/in-lb)
Pressures (Sting Adapter)	0.00496°/N (0.0220°/lb)	0.0441°/N-m (0.00498°/in-lb)

Table 5.3 – Planned test conditions and run schedule

	M	Re	Approx. p , Pa (psf)	Comments
Test Day 1 (9 Runs)	0.700	27,680	2,070 (43.2)	
	0.700	27,680	2,070 (43.2)	Replicate
	0.500	36,790	3,851 (80.4)	
	0.800	70,000	4,580 (95.7)	
	0.300	59,140	10,318 (215.5)	
	0.300	59,140	10,318 (215.5)	Replicate
	0.800	141,000	9,225 (192.7)	
	0.407	250,000	32,150 (671.5)	
	0.300	250,000	43,617 (911.0)	
Test Day 2 (9 Runs)	0.700	27,680	2,070 (43.2)	Replicate
	0.500	36,790	3,851 (80.4)	Replicate
	0.500	36,790	3,851 (80.4)	Replicate
	0.650	92,500	7,448 (155.6)	
	0.300	59,140	10,318 (215.5)	Replicate
	0.300	59,140	10,318 (215.5)	Replicate
	0.450	137,500	15,993 (334.0)	
	0.600	177,160	15,454 (322.8)	
	0.300	160,000	27,915 (583.0)	
Test Day 3	Up to 9 forces/moment runs depending on the results of days 1 and 2			
Test Day 4 (11 Runs)	0.700	27,680	2,070 (43.2)	
	0.500	36,790	3,851 (80.4)	
	0.800	70,000	4,580 (95.7)	
	0.650	92,500	7,448 (155.6)	
	0.300	59,140	10,318 (215.5)	
	0.800	141,000	9,225 (192.7)	
	0.450	137,500	15,993 (334.0)	
	0.600	177,160	15,454 (322.8)	
	0.300	160,000	27,915 (583.0)	
	0.407	250,000	32,150 (671.5)	
	0.300	250,000	43,617 (911.0)	

Note: Forces/moment testing on test days 1-3; pressure testing on test day 4.

Table 5.4 – Actual test conditions and run schedule

Test Day	Run	M	Re	p, Pa (psf)	Test Type	Comments
Test Day 1 (3 Runs)	10	0.800	70,165	3,902 (81.5)	forces/moment	
	11	0.300	58,719	9,867 (206.1)	forces/moment	
	12	0.298	58,642	9,921 (207.2)	forces/moment	Replicate
Test Day 2 (4 Runs)	14	0.800	141,502	7,965 (166.4)	forces/moment	
	15	0.407	250,241	30,871 (644.8)	forces/moment	
	16	0.300	249,015	42,255 (882.5)	forces/moment	
	20	0.699	28,313	1,841 (38.5)	forces/moment	
Test Day 3 (11 Runs)	23	0.800	24,584	1,335 (27.9)	forces/moment	Test condition not in original test plan, added for completeness
	24	0.702	27,033	1,728 (36.1)	forces/moment	Replicate
	25	0.500	35,577	3,381 (70.6)	forces/moment	
	26	0.499	36,350	3,475 (72.6)	forces/moment	Replicate
	27	0.800	70,055	3,850 (80.4)	forces/moment	Replicate not in original test plan
	28	0.704	27,363	1,766 (36.9)	forces/moment	Replicate
	29	0.499	36,400	3,494 (73.0)	forces/moment	Replicate
	30	0.651	92,327	6,569 (137.2)	forces/moment	
	31	0.299	58,610	9,802 (204.7)	forces/moment	Replicate
	32	0.300	59,058	9,865 (206.0)	forces/moment	Replicate
	33	0.451	138,206	15,048 (314.3)	forces/moment	
Day 4 (12 Runs)	35	0.298	58,265	9,720 (203.0)	forces/moment	Replicate not in original test plan
	36	0.599	176,488	14,051 (293.5)	forces/moment	
	37	0.302	159,746	26,800 (559.7)	forces/moment	
	38	0.547	33,221	2,904 (60.7)	forces/moment	Test condition to investigate test/experiment disagreement
	39	0.498	35,842	3,471 (72.5)	forces/moment	Replicate to investigate test/experiment disagreement
	40	0.450	39,908	4,333 (90.5)	forces/moment	Test condition to investigate test/experiment disagreement
	41	0.502	69,940	6,746 (140.9)	forces/moment	Test condition to investigate test/experiment disagreement
	42	0.550	90,900	7,949 (166.0)	forces/moment	Test condition to investigate test/experiment disagreement
	43	0.450	92,055	10,092 (210.8)	forces/moment	Test condition to investigate test/experiment disagreement
	45	0.802	70,590	3,917 (81.8)	forces/moment	Replicate not in original test plan
	46	0.799	141,276	8,037 (167.9)	forces/moment	Replicate not in original test plan
	47	0.301	159,285	26,894 (561.7)	forces/moment	Replicate not in original test plan

Table continued on next page.

Table 5.4 – Actual test conditions and schedule - concluded

Day 5 (10 Runs)	51	0.800	27,854	1,525 (31.8)	pressure
	52	0.702	29,415	1,891 (39.5)	pressure
	53	0.505	36,620	3,450 (72.1)	pressure
	54	0.797	71,414	3,941 (82.3)	pressure
	55	0.652	93,171	6,636 (138.6)	pressure
	56	0.303	59,685	9,836 (205.4)	pressure
	57	0.801	142,028	7,995 (167.0)	pressure
	58	0.452	137,721	15,019 (313.7)	pressure
	59	0.600	176,884	14,176 (296.1)	pressure
	60	0.301	159,812	26,815 (560.0)	pressure
Test Day 6 (2 Runs)	62	0.408	249,207	30,315 (633.1)	pressure
	63	0.300	248,885	41,828 (873.6)	pressure

Notes:

- 1) *M*, *Re*, and *p* for forces/moment runs given at maximum lift condition.
- 2) *M*, *Re*, and *p* for pressure runs given at maximum model angle of attack tested.
- 3) Missing runs are either calibration, warmup, or aborted runs.

Table 5.5 – Data acquired during forces/moment testing

Quantity	Sampling Rate (Hz)	Total Number of Data Points
Stagnation Pressure, p_0	2.5	12
Static Pressure, p	2.5	12
Stagnation Temperature, T_0	3	15
Sting Angle of Attack, α_s	100	500
Model Angle of Attack, α	100	500
Normal Force, NF	100	500
Axial Force, AF	100	500
Pitching Moment, PM	100	500

Note: Data was acquired for 5 seconds. Total number of data points = Sampling Rate x 5 sec.

Table 5.6 – Data acquired during pressure testing

Quantity	Sampling Rate (Hz)	Total Number of Data Points
Stagnation Pressure, p_0	2.5	12
Static Pressure, p	2.5	12
Stagnation Temperature, T_0	3	15
Sting Angle of Attack, α_s	100	500
Base Differential Pressures, Δp_{base} (3 locations)	10	50
Wing Differential Pressures, Δp_{wing} (28 locations)	10	50

Note: Data was acquired for 5 seconds. Total number of data points = Sampling Rate x 5 sec.

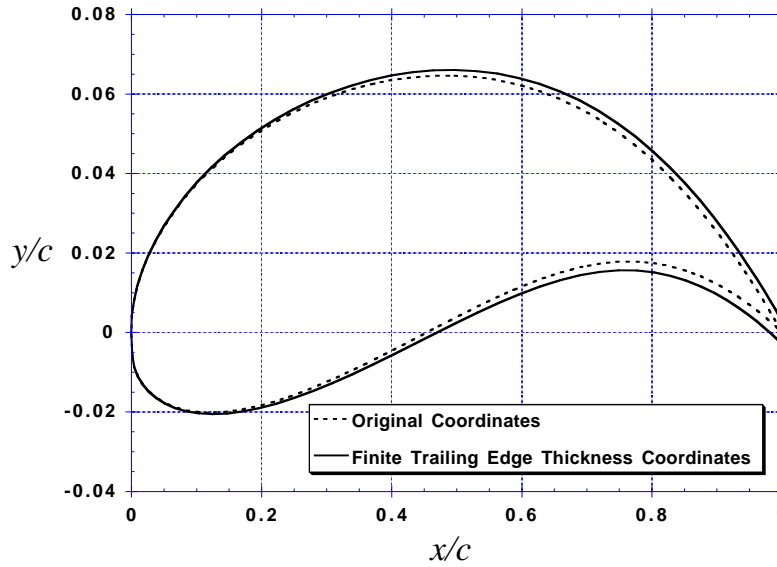


Figure 5.1 – MASC1 airfoil with zero and finite trailing edge thickness; vertical axis exaggerated for clarity

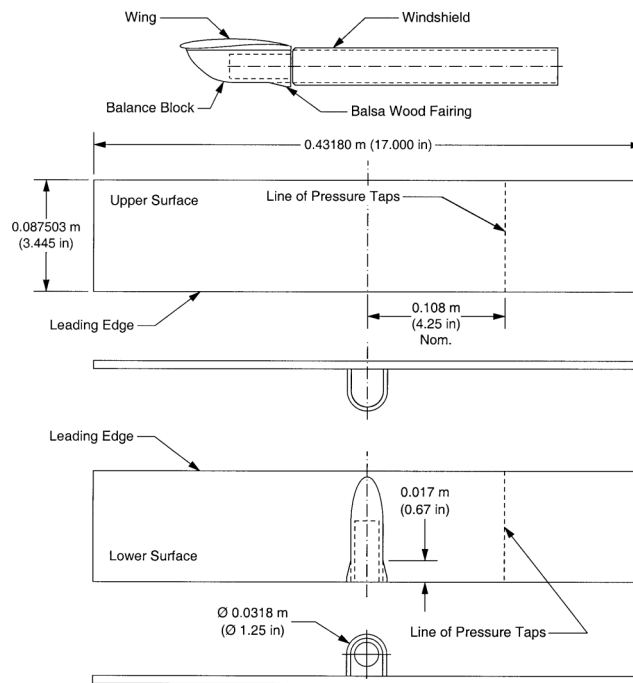
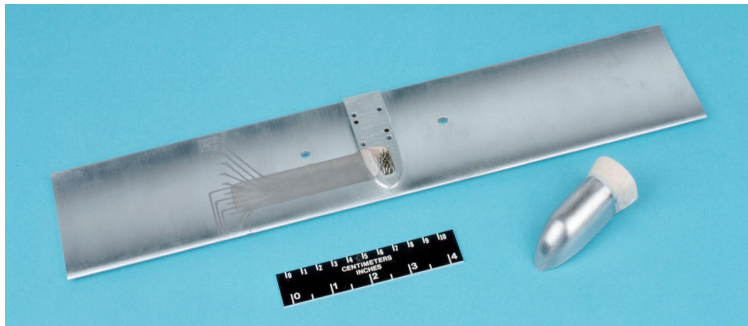


Figure 5.2 – Wing tunnel model assembly with key design dimensions noted



2001-L-00086

Figure 5.3a – Wing and balance block assembly, top view, disassembled



2001-L-00085

Figure 5.3b – Wing and balance block assembly, bottom view, disassembled



2001-L-00082

Figure 5.3c – Wing and balance block assembly, bottom view, assembled, including wind tunnel balance UT-61A and windshield

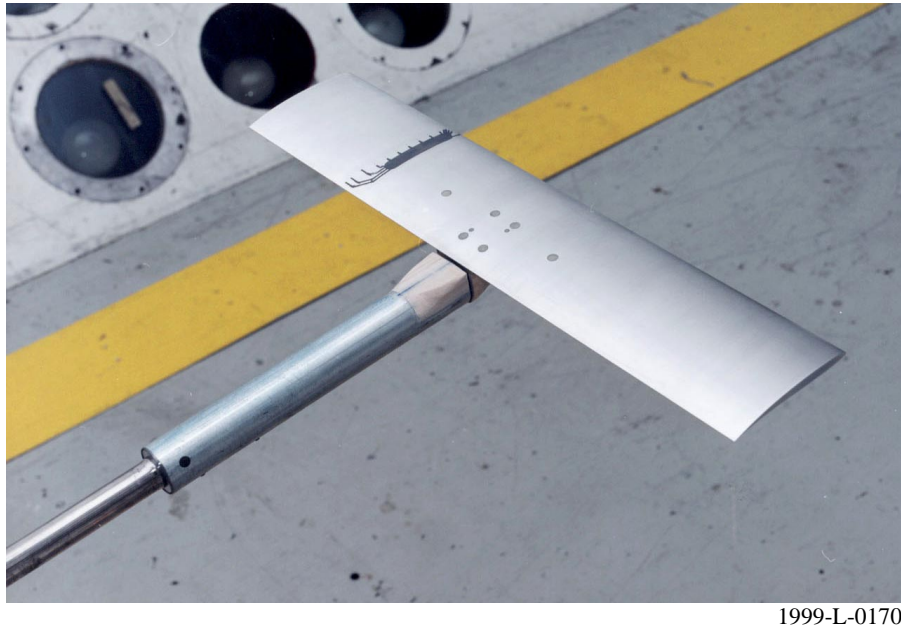


Figure 5.4 – Model in wind tunnel showing attachment of windshield to sting



Figure 5.5 – Wind tunnel model components

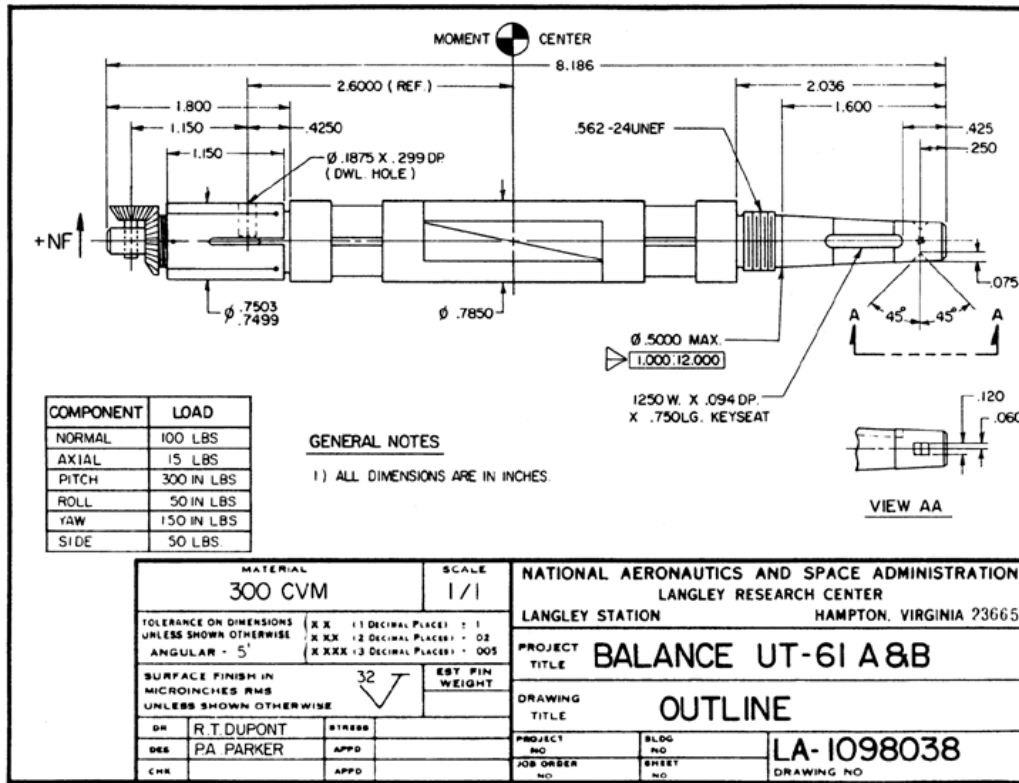


Figure 5.6 – Drawing of NASA LaRC wind tunnel balance UT-61A



2001-L-00080

Figure 5.7 – Photograph of NASA LaRC wind tunnel balance UT-61A



Figure 5.8 – NASA LaRC Transonic Dynamics Tunnel (TDT) aerial view

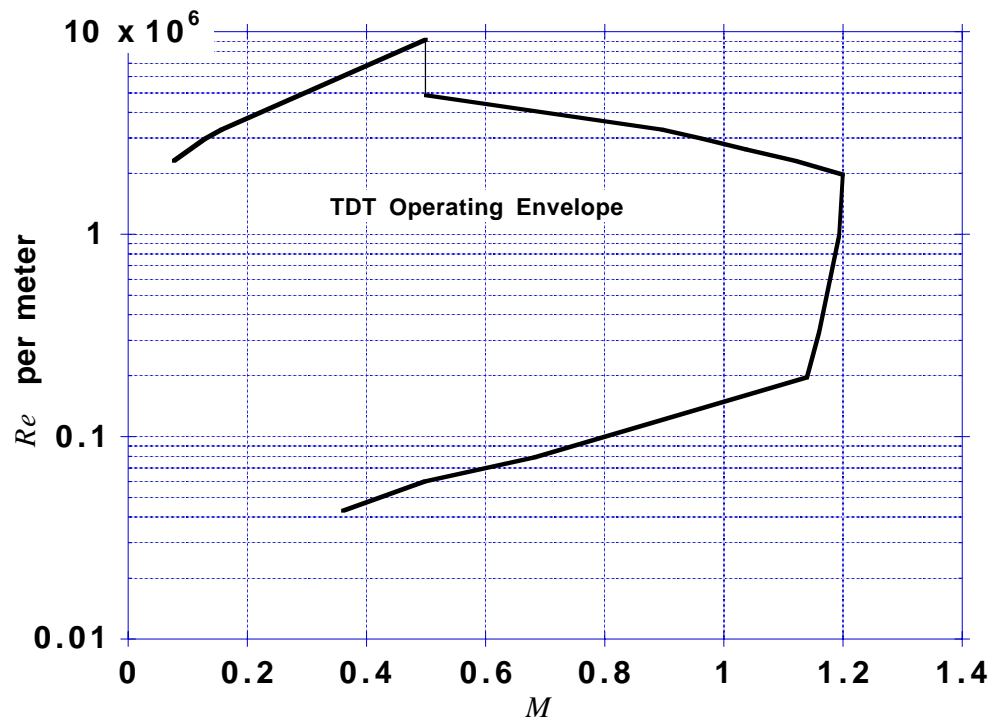


Figure 5.9 – TDT operating envelope in air; upper bound adapted from reference 94, figure 1(a)

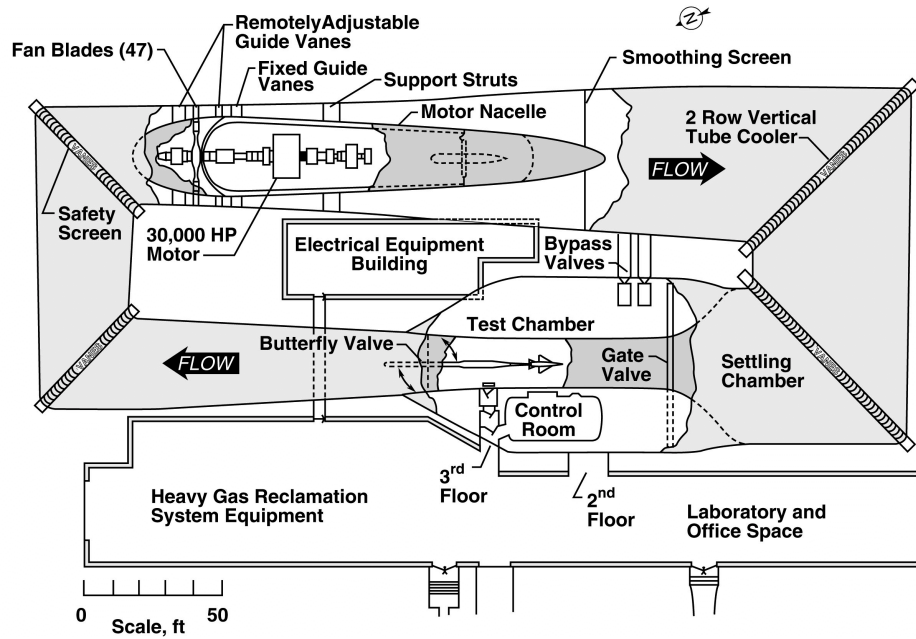


Figure 5.10 – TDT schematic drawing



1999-L-01711

Figure 5.11 – TDT sting with the Mars airplane wing

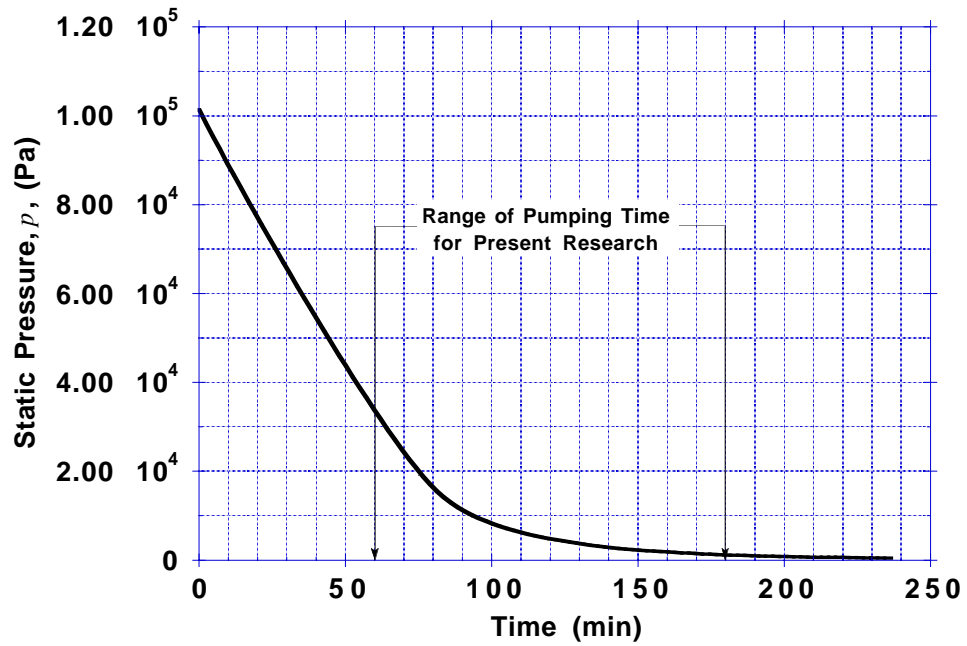
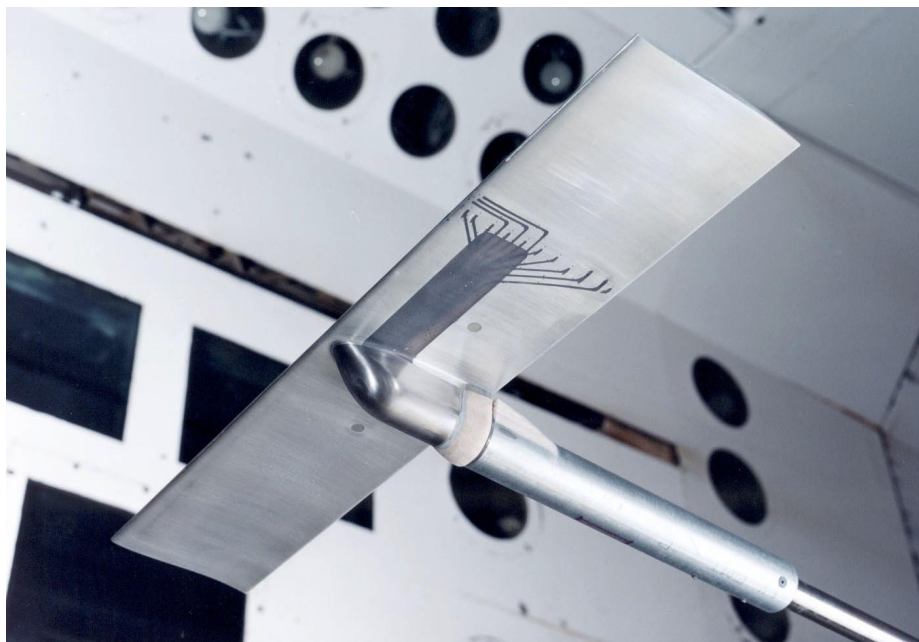


Figure 5.12 – Pumping time required to achieve low pressures in the TDT



1999-L-01701

Figure 5.13 – Model installation, view from below



1999-L-01709

Figure 5.14 – Model installation, side view

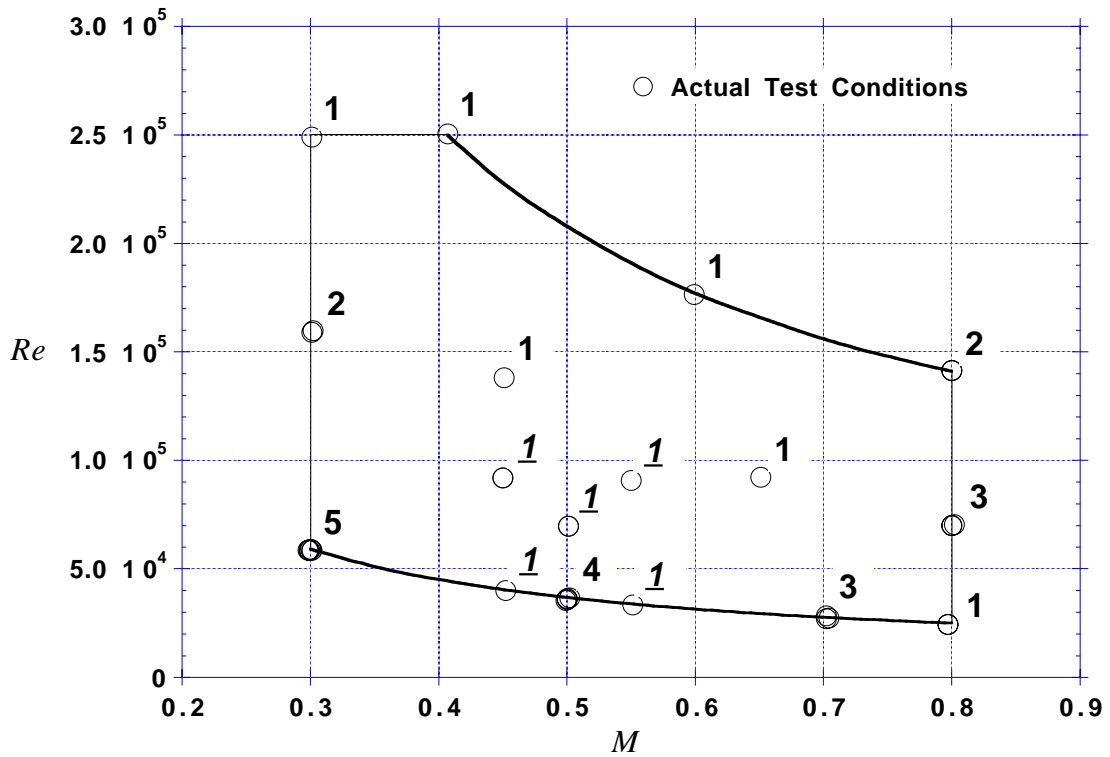


Figure 5.15 – Actual test conditions; digit next to symbol indicates number of tests

Chapter 6: Experimental Data Analyses

This chapter focuses on the derivation of the experimental test results of interest (e.g., M , Re , $C_{L\ max}$ and its uncertainty) from the raw data (e.g., p_0 , p , NF) collected during testing. This is done in the following order: wind tunnel operating parameters; forces, moments, and nondimensional aerodynamic coefficients; maximum lift coefficients and their uncertainties. The experimental test results are presented in chapter 7.

6.1 Wind Tunnel Operating Parameters

All derived wind tunnel operating parameters were determined from three wind tunnel flow measurements: p_0 , p , and T_0 . These derived parameters were calculated at every test point (known as a tab point) by the relationships shown in equations 6.1 through 6.9. Note that the factor K_q was used to generate the normalized dynamic pressure q_{norm} . As is discussed in chapter 4, this normalization is required so that every combination of M and Re has a unique dynamic pressure associated with it. This normalization had an effect on the normalized value of the lift, drag, and pitching moment as discussed in section 6.2, but had no effect on the value of the nondimensional aerodynamic coefficients since it was applied to both the dynamic pressure, forces, and moments. The pre-test assumed value of $T_{0\ ref}$ was 303.8 K. The average value of T_0 considering all forces/moment experimental runs was 296.1 K. Thus, for the analyses of the experimental data, the 296.1 K was used for $T_{0\ ref}$. The values of μ_{ref} , n , T_{ref} , γ , and R are given in table 4.1 of chapter 4 and in the Symbols section of this document. The as-built value of c was used as given in table 5.1 of chapter 5.

$$M = \sqrt{\frac{2}{\gamma - 1} \left(\left(\frac{p}{p_0} \right)^{\frac{1-\gamma}{\gamma}} - 1 \right)} \quad (6.1)$$

$$Re = \frac{\rho V c}{\mu} \quad (6.2)$$

$$q_{norm} = K_q q \quad (6.3)$$

$$q = \frac{P_0 - P}{\frac{2}{\gamma M^2} \left(\left(1 + \left(\frac{\gamma - 1}{2} \right) M^2 \right)^{\frac{\gamma}{\gamma - 1}} - 1 \right)} \quad (6.4)$$

$$V = Ma \quad (6.5)$$

$$\mu = \mu_{ref} \left(\frac{T}{T_{ref}} \right)^n \quad (6.6)$$

$$K_q = \left(\frac{T_{0\ ref}}{T_0} \right)^{n+1/2} \quad (6.7)$$

$$a = \sqrt{\gamma R T} \quad (6.8)$$

$$T = T_0 \left(\frac{P}{P_0} \right)^{\frac{\gamma - 1}{\gamma}} \quad (6.9)$$

6.2 Forces, Moments, and Nondimensional Aerodynamic Coefficients

A base pressure correction had to be applied to the axial force, AF , and the pitching moment, PM_{bmc} . For a given test condition (i.e., combination of M and Re), three differential base pressures, Δp_{base1} , Δp_{base2} , and Δp_{base3} , were measured as functions of the model angle of attack during the pressure portion of the test (i.e., Runs 51-60, 62, and 63). These differential base pressures were the difference between the static pressure and the local pressure at each one of the three locations; for example:

$$\Delta p_{base1} = p_{base1} - P \quad (6.10)$$

where p_{base1} was the static base pressure at location 1. By averaging the three differential base pressures and normalizing by the dynamic pressure, an axial force correction coefficient (as a function of M , Re , and α) was then calculated:

$$C_{base}(M, Re, \alpha) = \frac{1}{q} \left(\frac{\Delta p_{base1} + \Delta p_{base2} + \Delta p_{base3}}{3} \right) \quad (6.11)$$

Using this axial force correction coefficient, corrected axial forces, AF_{corr} , and pitching moments about the balance moment center, $PM_{bmc\ corr}$, were calculated for the corresponding forces/moment run:¹

$$AF_{corr} = AF + qC_{base}A_{base} \quad (6.12)$$

$$PM_{bmc\ corr} = PM_{bmc} + qC_{base}A_{base}y_{base} \quad (6.13)$$

A_{base} was the base area of the model, which was determined to be $8.97 \times 10^{-4} \text{ m}^2$ (1.39 in²). y_{base} was the offset between the center of pressure of the base pressure and the centerline of the wind tunnel balance, which was determined to be 0.00165 m (0.0648 in). The correction to PM_{bmc} due to base pressures was very small. Table 6.1 shows which pressure runs were used to correct AF and PM_{bmc} on forces/moment runs. Note that for most cases the values of M and Re for each pair of test runs (pressure and forces/moment) were very close – the error induced by not matching M and Re exactly is negligible. However, there were no corresponding pressure runs for forces/moment Runs 38, and 40 through 43. For these cases a nearby pressure test condition was selected to correct the AF and PM_{bmc} as shown in table 6.1. Because in all cases the base pressure axial force correction was typically between 5 to 15 percent, and the axial force was such a small contributor to the lift force (see equation 5.1), the approximations involved in the determination of the base pressure axial force correction had a very small effect on the final value of the lift force. This base pressure correction to the axial force, however, was important to the determination of the drag force. It should be noted that no other corrections were made to the axial force to account for the drag of the wind tunnel balance block. This should be kept in mind when comparing the experimental and analysis values of the drag coefficient.

The pitching moment about the quarter chord, $PM_{c/4}$ was a function of $PM_{bmc\ corr}$, NF , AF_{corr} , and the offsets between the balance moment center and the quarter chord of the airfoil (x_{bar} and y_{bar}). These offsets are shown in figure 6.1. The pitching moment about the quarter chord was calculated from:

$$PM_{c/4} = PM_{bmc\ corr} - NFx_{bar} - AF_{corr}y_{bar} \quad (6.14)$$

The values of x_{bar} and y_{bar} used were 0.1221 m (4.809 in) and 0.0157 m (0.620 in), respectively.

The normal force, axial force, and pitching moment were also normalized to the post-test value of $T_{0\ ref}$ by multiplying them by K_q :

¹ Although the pitching moment, drag force, and their nondimensional coefficients are not of principal interest to the present investigation, their calculation is described here for completeness.

$$NF_{norm} = K_q NF \quad (6.15)$$

$$AF_{norm} = K_q AF_{corr} \quad (6.16)$$

$$PM_{c/4 norm} = K_q PM_{c/4} \quad (6.17)$$

Note that the corrected axial force, AF_{corr} , was used to calculate AF_{norm} , and the pitching moment about the quarter chord, $PM_{c/4}$, was used to calculate $PM_{c/4 norm}$. Normalizing the dynamic pressure and the forces and moments was not necessary to generate the nondimensional aerodynamic coefficients. However, if further analyses of forces and moments as functions of M and Re were to be conducted (for example, by using lift results to generate a response surface of lift as a function of M and Re), normalizing the forces and moments would be important in order to use them under a consistent dynamic pressure assumption. Transformation of NF_{norm} and AF_{norm} into normalized lift, L_{norm} , and drag, D_{norm} , force components was accomplished through the relationships:

$$L_{norm} = NF_{norm} \cos \alpha - AF_{norm} \sin \alpha \quad (6.18)$$

$$D_{norm} = NF_{norm} \sin \alpha + AF_{norm} \cos \alpha \quad (6.19)$$

Finally, the nondimensional aerodynamic coefficients C_L , C_D , and C_M were calculated from:

$$C_L = \frac{L_{norm}}{q_{norm} S} \quad (6.20)$$

$$C_D = \frac{D_{norm}}{q_{norm} S} \quad (6.21)$$

$$C_M = \frac{PM_{c/4 norm}}{q_{norm} S c} \quad (6.22)$$

The as-built values for S and c (see table 5.1) were used in these calculations.

6.3 Maximum Lift Coefficients

The experimental data yielded various types of lift curves (i.e., C_L vs α), requiring different methods for extracting $C_{L max}$ from these curves. In the following discussion lift curves are categorized as one of three types: I, II, and III. Table 6.2 shows the type of C_L vs α curve for every forces/moment run. Figure 6.2 shows the same information plotted vs M and Re . Note that, in general, the type of the lift curve was isolated to a certain

region in (M, Re) space. In only one instance did replicates exhibit more than one type of lift curve, namely $M = 0.300$, $Re = 160,000$ (Runs 37 and 47).

In Type I lift curves stall were identified by a sharp onset of stall flutter. The C_L vs α data were fitted with a smoothing spline² using the *Fit Spline* utility in JMP® [91]. This utility is an implementation of the smoothing spline derived in reference 95 by Reinsch, and also discussed by Eubank in reference 96. Figure 6.3 shows an example (Run 15) of this type of lift curve. In these types of curves, the maximum lift coefficient occurred at the largest angle of attack tested as determined by the smoothing spline. At this point, two values of $C_{L,max}$ could be isolated: one from the experimental data and another from the smoothing spline. The value of $C_{L,max}$ selected for this type of lift curve was that given by the smoothing spline. The tab point and flow quantities (e.g., M , Re) associated with this value of $C_{L,max}$ were those at the maximum angle of attack. If there was more than one experimental data point at this model angle of attack, the one that minimized the difference between the experimental and splined values of $C_{L,max}$ was chosen. The data for the example in figure 6.3 are shown in table 6.3 making these choices clear.

Note that a basic *assumption* made for Type I lift curves was that stall flutter marked the stall. There is, however, an alternate explanation. It is possible that what was identified here as stall flutter (and thus stall) was actually just an angle of attack region where the flow was merely unsteady (perhaps due to shock/boundary layer interactions). Vibrations near $C_{L,max}$ were also detected for some Type I and III lift curve cases. It could be argued then that the vibrations caused by this unsteadiness did not allow the actual stall angle of attack to be reached due to the structural limitations of the wind tunnel balance and the sting. However, the following two observations give credence to the assumption that what was observed was stall flutter and that it marked the stall. First, the stall behavior predicted by the analysis (in cases where post-stall results were obtained) indicated that there was a sudden loss of lift after the stall angle of attack was exceeded for the conditions in which Type I lift curves were observed. Second, as shown later, the agreement between analysis and experimental results was excellent for cases in which Type I lift curves were observed. Given these two observations, the assumption relating stall flutter was considered to be validated.

Type II lift curves were characterized by a clearly defined $C_{L,max}$ with a measurable drop in C_L at higher angles of attack. Again, the C_L vs α data were fitted with a smoothing spline using the *Fit Spline* utility in JMP®. Figure 6.4 shows an example (Run 11) of this type of lift curves. As with the Type I lift curves, $C_{L,max}$ was determined from the smoothing spline. The tab point and flow quantities associated with this value of $C_{L,max}$ were those for the experimental point at the nearest model angle of attack. If there was more than one experimental data point at this specific model angle of attack, the one that minimized the difference between the experimental and splined values of

² A smoothing spline is not required to go through all points. All references to splines in this document imply a smoothing spline.

C_{Lmax} was chosen. The data for the example in figure 6.4 are shown in table 6.4 and the chosen tab point is identified. In this example there was only one experimental data point at the nearest experimental model angle of attack for C_{Lmax} .

Type III lift curves were characterized by the lack of a clearly defined C_{Lmax} . In these cases the engineering definition of C_{Lmax} , as discussed in chapter 4, had to be used. All but one of the test conditions for which $M \geq 0.7$ exhibited this lift curve shape. To determine the C_{Lmax} for Type III lift curves, C_L vs α was fitted with a sixth order polynomial around the estimated C_{Lmax} point using the *Fit Polynomial* utility in JMP®. The engineering C_{Lmax} was defined to occur at the α where $d^2C_L/d\alpha^2 = 0$. As with the Type I and II lift curves, C_{Lmax} was chosen from the interpolated data. Similarly, the tab point and flow quantities associated with this value of C_{Lmax} were those for the experimental point at the nearest model angle of attack. If there was more than one experimental data point at this specific model angle of attack, the one that minimized the difference between the experimental and interpolated values of C_{Lmax} was chosen. Figure 6.5 shows an example (Run 10) of this procedure. Data for the example in figure 6.5 are shown in table 6.5 and the chosen tab point is identified. In this case there was only one experimental data point at the nearest experimental model angle of attack for C_{Lmax} .

As can be seen by comparing the data in tables 5.3 and 5.4, there were small differences between the planned and actual test Mach and Reynolds numbers. For cases in which there were no replicates this difference in test conditions was of no consequence – the final aerodynamic analyses were conducted at the test values of Mach and Reynolds numbers. However, for cases in which there were replicates, it was desirable to adjust the value of C_{Lmax} to a common value of M and Re . To do this a response surface was created using the experimental values of C_{Lmax} as a function of M and Re .³ This response surface was of the form:

$$C_{Lmax RS}(M, Re) = k_0 + k_M M + k_{Re} Re + k_{M Re} M Re + k_{M^2} M^2 + k_{Re^2} Re^2 + k_{M Re^2} M Re^2 \quad (6.23)$$

The numerical values of the coefficients are given in table 6.6. The adjusted value of C_{Lmax} for a given run was then calculated from:

$$C_{Lmax adj} = C_{Lmax} + \left(C_{Lmax RS}(M, Re)_{nominal} - C_{Lmax RS}(M, Re)_{experimental} \right) \quad (6.24)$$

where, $C_{Lmax RS}(M, Re)_{nominal}$ and $C_{Lmax RS}(M, Re)_{experimental}$ are the values of C_{Lmax} predicted from the response surface equation using the nominal and experimental values of M and

³ Data for all runs except Run 23 ($M = 0.800$, $Re = 24,584$) were used in generating this response surface. This particular point created fit problems with the response surface. Since this test condition did not have a replicate, eliminating it from the response surface data set did not generate any problems. It should be noted that this response surface was only used for the purpose of adjusting C_{Lmax} to a common value of M and Re .

Re , respectively, for a particular run. The results of this adjustment were small. For all cases except Runs 20, 24, and 28 the difference was less than or equal to 0.001. For Runs 20, 24, and 28 the adjustments were -0.002 , 0.003 , and 0.004 , respectively. Finally, for a given nominal test condition, an average value of $C_{L\ max\ adj}$, denoted $\overline{C_{L\ max\ adj}}$, and calculated from all relevant runs, was determined. For test conditions with no replicates $\overline{C_{L\ max\ adj}} = C_{L\ max\ adj}$.

6.4 Uncertainties in the Maximum Lift Coefficients

This section describes the methods used to determine the precision (i.e., random), bias, and total uncertainties of the experimental maximum lift coefficients. The ultimate objective is to quantify the uncertainty of $\overline{C_{L\ max\ adj}}$.

During the design phase of the test it was expected that the precision uncertainty would be determined by methods similar to those used to design the experiment as described in chapter 4. In this approach, a response surface of the normalized lift, L_{norm} , as a function of the Mach and Reynolds number would have been created. From this response surface analysis the uncertainty in L_{norm} would have been determined, and from this uncertainty, in turn, the uncertainty in $C_{L\ max}$ would have been calculated. This approach, however, depended on the assumption that the precision standard deviation in the lift force was constant, or nearly so, over the (M, Re) test domain. Due to the occurrence of vibrations and stall flutter during testing, the assumption of constant uncertainty in the lift was shown to be invalid. In table 6.7 the normal force sample standard error of the mean, $\overline{s_{NF}}$, calculated from the 500 samples acquired at the tab points associated with $C_{L\ max}$ are listed for all test runs. As can be seen, $\overline{s_{NF}}$ was not constant throughout the test domain, and in some cases varied significantly among runs at equivalent test conditions.

Given that the response surface method for determining the precision uncertainty of the experimental values of $C_{L\ max}$ was not appropriate as discussed above, an alternate approach was selected and applied. This approach was based on the assumptions that the precision uncertainty (for a given confidence level) between runs could be approximated by a constant value. For four sets of nominal test conditions, namely (M, Re) : $(0.300, 59,140)$, $(0.500, 36,790)$, $(0.700, 27,680)$, $(0.800, 70,000)$; there were three or more replicates. Using the values of $C_{L\ max\ adj}$ for each of these nominal test conditions the values of the standard deviation of $C_{L\ max\ adj}$, $s_{C_{L\ max}}$, were calculated. These values of $s_{C_{L\ max}}$ are given in table 6.8. Based on these data, it was *assumed* that the standard deviation of $C_{L\ max\ adj}$, $\sigma_{C_{L\ max}}$, had a constant value of 0.0036 throughout the test domain. In addition, it was *assumed* that the precision uncertainty in $C_{L\ max\ adj}$ was normally distributed. Using these assumptions, the precision uncertainty of the mean, $\overline{P_{C_{L\ max}, 1-\nu}}$, at the $1 - \nu$ confidence level was calculated from:

$$\overline{P_{C_{Lmax},1-\nu}} = z(\nu/2) \frac{\sigma_{C_{Lmax}}}{\sqrt{N_{runs}}} \quad (6.25)$$

for each nominal test condition (i.e., M and Re).

Note that the assumption of constant $\sigma_{C_{Lmax}}$ would also be compatible with a response surface model of C_{Lmax} vs (M, Re). It was decided, however, not to use a response surface model for the final experimental data analysis and comparison with experimental results. Instead, a point-by-point error analysis (as discussed in this section) and comparison between the analysis and experimental results (as discussed in section 7.3) was conducted. The reason for avoiding the response surface model approach at this stage was due to the difficulty in finding an appropriate response surface model to fit the experimental data. Various polynomial functions were tried, but all of them induced unacceptable lack-of-fit errors that artificially amplified the difference between the analysis and experimental test results.

The bias uncertainty of C_{Lmax} at a $1 - \nu$ confidence level, denoted $B_{C_{Lmax},1-\nu}$, for a given tab point was calculated by the approach presented in reference 97 as shown in equation 6.26:

$$B_{C_{Lmax},1-\nu} = \left[\left(\frac{\partial C_L}{\partial NF} B_{NF,1-\nu} \right)^2 + \left(\frac{\partial C_L}{\partial AF} B_{AF,1-\nu} \right)^2 + \left(\frac{\partial C_L}{\partial \alpha} B_{\alpha,1-\nu} \right)^2 + \left(\frac{\partial C_L}{\partial p_0} B_{p_0,1-\nu} \right)^2 + \left(\frac{\partial C_L}{\partial p} B_{p,1-\nu} \right)^2 + \left(\frac{\partial C_L}{\partial c} B_{c,1-\nu} \right)^2 + \left(\frac{\partial C_L}{\partial b} B_{b,1-\nu} \right)^2 \right]^{1/2} \quad (6.26)$$

The derivatives in equation 6.26 were determined from:

$$C_L = \frac{NF \cos \alpha - AF \sin \alpha}{q(p_0, p)cb} \quad (6.27)$$

where $q(p_0, p)$ indicates that the dynamic pressure is a function of the experimentally measured total and static pressures as given by equation 6.4. $B_{NF,1-\nu}$, $B_{AF,1-\nu}$, $B_{\alpha,1-\nu}$, $B_{p_0,1-\nu}$, $B_{p,1-\nu}$, $B_{c,1-\nu}$, and $B_{b,1-\nu}$ are estimates of the bias uncertainties for NF , AF , α , p_0 , p , c , and b , respectively. The estimates for $B_{NF,1-\nu}$, $B_{AF,1-\nu}$, $B_{\alpha,1-\nu}$, $B_{p_0,1-\nu}$, $B_{p,1-\nu}$, $B_{c,1-\nu}$, and $B_{b,1-\nu}$ at the $1 - \nu = 0.95$ confidence level are given in table 6.9. They were determined from the available transducer and wind tunnel calibration data, and from discussions with TDT personnel. The values of NF , AF , α , p_0 , and p used to evaluate the derivatives and bias uncertainties were those reported by the TDT Data Acquisition System (DAS) for the specific tab point nearest to C_{Lmax} for each run, chosen as described in section 6.3.

It was assumed that the bias uncertainties for NF , AF , α , p_0 , p , c , and b were normally distributed. Consistent with these assumptions for $B_{NF,1-\nu}$, $B_{AF,1-\nu}$, $B_{\alpha,1-\nu}$, $B_{p_0,1-\nu}$, $B_{p,1-\nu}$, $B_{c,1-\nu}$, and $B_{b,1-\nu}$, the bias uncertainty in C_{Lmax} was also normally distributed. It should be emphasized that these bias quantities were *estimates*, and the bias uncertainty distribution was an *assumption*. Known bias errors were taken into account in the calculations for the various quantities. Thus, the remaining bias uncertainties were estimates by their very nature.

In cases where multiple runs were conducted at a given test condition, an average value of $B_{C_{Lmax},1-\nu}$ was calculated by:

$$\overline{B_{C_{Lmax},1-\nu}} = \frac{\sum B_{C_{Lmax},1-\nu}}{N_{runs}} \quad (6.28)$$

where N_{runs} is the number of runs at the particular test condition. If only one run occurred at a particular test condition then: $\overline{B_{C_{Lmax},1-\nu}} = B_{C_{Lmax},1-\nu}$. The values of $\overline{B_{C_{Lmax},1-\nu}}$ are thus the values of the bias uncertainty associated with $\overline{C_{Lmaxadj}}$. Note that equation 6.28 is a simple average since additional test runs do not improve our knowledge of it. Thus, equation 6.28 merely averages the results for adjacent test conditions and yields an average to be applied at the nominal values of M and Re .

Finally, the total uncertainties of the mean values of $\overline{C_{Lmaxadj}}$ at a $1 - \nu$ confidence level, denoted $\overline{U_{C_{Lmax},1-\nu}}$, were calculated from:

$$\overline{U_{C_{Lmax},1-\nu}} = \sqrt{\overline{P_{C_{Lmax},1-\nu}}^2 + \overline{B_{C_{Lmax},1-\nu}}^2} \quad (6.29)$$

$\overline{P_{C_{Lmax},1-\nu}}$ and $\overline{B_{C_{Lmax},1-\nu}}$ have to be expressed at the same confidence level, $1 - \nu$, to make equation 6.29 valid. Because of the assumptions made in the calculation of $\overline{P_{C_{Lmax},1-\nu}}$, $\overline{B_{C_{Lmax},1-\nu}}$, and $\overline{U_{C_{Lmax},1-\nu}}$, these quantities can be easily calculated for any desired value of $1 - \nu$. The ability to do so allows statistical comparisons to be made between the experimental and analysis results as discussed in section 7.3.

Table 6.1 – Pressure and forces/moment runs correspondence for base pressure corrections

Pressure Run (M, Re)	Forces/Moment Run (M, Re)
Run 51 (0.800, 27,854)	Run 23 (0.800, 24,584)
Run 52 (0.702, 29,415)	Run 20 (0.699, 28,313) Run 24 (0.702, 27,033) Run 28 (0.704, 27,363)
Run 53 (0.505, 36,620)	Run 25 (0.500, 35,577) Run 26 (0.499, 36,350) Run 29 (0.503, 36,755) Run 38 (0.547, 33,221)† Run 39 (0.498, 35,842) Run 40 (0.450, 39,908)† Run 41 (0.502, 69,940)†
Run 54 (0.797, 71,414)	Run 10 (0.800, 70,165) Run 27 (0.800, 70,055) Run 45 (0.802, 70,590)
Run 55 (0.652, 93,171)	Run 30 (0.651, 92,327) Run 42 (0.550, 90,900)†
Run 56 (0.303, 59,685)	Run 11 (0.300, 58,719) Run 12 (0.298, 58,642) Run 31 (0.299, 58,610) Run 32 (0.300, 59,058) Run 35 (0.298, 58,265)
Run 57 (0.801, 142,028)	Run 14 (0.800, 141,502) Run 46 (0.799, 141,276)
Run 58 (0.452, 137,721)	Run 33 (0.451, 138,206) Run 43 (0.450, 92,055)†
Run 59 (0.600, 176,884)	Run 36 (0.599, 176,488)
Run 60 (0.301, 159,812)	Run 37 (0.302, 159,841) Run 47 (0.301, 159,285)
Run 62 (0.408, 249,207)	Run 15 (0.407, 250,241)
Run 63 (0.300, 248,885)	Run 16 (0.300, 249,015)

Notes:

- 1) M and Re listed for pressure runs is at the maximum model angle of attack tested.
- 2) M and Re listed for forces/moment runs at the maximum lift condition.
- 3) Forces/pressure runs with † are the best match possible with a corresponding pressure run (see text).

Table 6.2 – Lift curve type for forces/moment runs

Run	M	Re	Lift Curve Type
10	0.800	70,165	III
11	0.299	58,560	II
12	0.298	58,652	II
14	0.800	141,505	I
15	0.407	250,712	I
16	0.301	249,123	I
20	0.699	28,313	III
23	0.800	24,584	III
24	0.702	27,033	III
25	0.499	35,530	II
26	0.500	36,384	II
27	0.800	70,055	III
28	0.704	27,363	III
29	0.503	36,755	II
30	0.651	92,327	II
31	0.299	58,610	II
32	0.300	59,058	II
33	0.451	138,206	I
35	0.301	58,657	II
36	0.599	176,488	I
37	0.302	159,841	II
38	0.551	33,521	II
39	0.500	35,912	II
40	0.452	40,055	II
41	0.501	69,870	II
42	0.550	90,900	I
43	0.450	92,088	II
45	0.802	70,590	III
46	0.800	141,353	I
47	0.301	159,284	I

Note: M and Re listed for forces/moment runs at the maximum lift condition

Table 6.3 – Example choice of C_{Lmax} , tab point, M , Re , and α for a Type I lift curve (Run 15)

Tab Pt.	M	Re	α (deg.)	Experimental C_L	Splined C_L	Exp. – Splined C_L
453	0.407	250,255	8.89	0.9582	0.9574	0.0008
454	0.407	250,596	9.28	0.9753	0.9761	-0.0008
455	0.407	250,532	9.79	1.0000	1.0002	-0.0002
457	0.407	250,627	9.79	1.0009	1.0002	0.0007
458	0.408	250,726	9.80	1.0004	1.0007	-0.0003
459	0.408	250,844	9.91	1.0049	1.0055	-0.0006
460	0.408	250,805	9.91	1.0048	1.0055	-0.0007
461	0.407	250,591	9.91	1.0062	1.0055	0.0007
462	0.407	250,449	10.03	1.0121	1.0104	0.0017
463	0.407	250,241	10.02	1.0130	1.0100	0.0030
464	0.407	250,707	10.02	1.0092	1.0100	-0.0008
465	0.407	250,763	10.08	1.0102	1.0123	-0.0021
466	0.407	250,712	10.08	1.0118	1.0123	-0.0005
467	0.407	250,814	10.08	1.0117	1.0123	-0.0006

Notes: Values in bold chosen as the C_{Lmax} conditionTable 6.4 – Example choice of C_{Lmax} , tab point, M , Re , and α for a Type II lift curve (Run 11)

Tab Pt.	M	Re	α (deg.)	Experimental C_L	Splined C_L	Exp. – Splined C_L
299	0.302	59,027	9.80	0.910	0.911	-0.001
300	0.301	58,789	10.31	0.938	0.939	-0.001
301	0.299	58,560	10.80	0.962	0.960	0.002
			11.00		0.962	
302	0.302	59,040	11.32	0.951	0.957	-0.006
303	0.300	58,719	11.30	0.966	0.958	0.008
304	0.299	58,676	11.42	0.963	0.954	0.009
305	0.302	59,167	11.53	0.947	0.950	-0.003
306	0.302	59,152	11.56	0.938	0.949	-0.011
307	0.302	59,228	11.64	0.942	0.948	-0.006
308	0.299	58,752	11.71	0.956	0.948	0.008
309	0.300	58,915	11.80	0.951	0.949	0.002

Note: Values in bold chosen as the C_{Lmax} condition

Table 6.5 – Example choice of C_{Lmax} , tab point, M , Re , and α for a Type III lift curve (Run 10)

Tab Pt.	M	Re	α (deg.)	Experimental C_L	Interpolated C_L	Exp. – Interpolated C_L	Interpolated $\frac{d^2 C_L}{d\alpha^2}$
262	0.801	69,776	13.30	0.848	0.848	0.000	-0.00246
263	0.802	69,897	13.80	0.853	0.854	-0.001	-0.00199
264	0.802	70,007	14.32	0.856	0.859	-0.003	-0.00153
265	0.803	70,100	14.79	0.861	0.864	-0.003	-0.00116
266	0.800	70,015	15.31	0.869	0.869	0.000	-0.00077
267	0.801	70,148	15.79	0.872	0.873	-0.001	-0.00046
			16.67		0.881		0.0
268	0.800	70,165	16.81	0.883	0.882	0.001	0.000060
269	0.800	70,294	17.80	0.892	0.891	0.001	0.000375
270	0.802	70,439	18.80	0.901	0.900	0.001	0.000491
271	0.803	70,562	19.81	0.910	0.910	0.000	0.000397

Note: Values in bold chosen as the C_{Lmax} condition

Table 6.6 – Coefficient values for the C_{Lmax} response surface in equation 6.23

k_0	8.58100×10^{-1}
k_M	7.78148×10^{-1}
k_{Re}	-2.84637×10^{-6}
k_{MRe}	7.99550×10^{-6}
k_{M^2}	-1.23404
k_{Re^2}	1.32519×10^{-11}
k_{MRe^2}	-3.51323×10^{-11}

Table 6.7 – $\overline{s_{NF}}$ for all tab points identified with C_{Lmax}

Run	Tab Point	M (Experimental)	Re (Experimental)	$\overline{s_{NF}}, N$ (lb)
16	519	0.301	249,123	21.5 (0.45)
37	1309	0.302	159,841	1.2 (0.02)
47	1683	0.301	159,284	22.6 (0.47)
11	301	0.299	58,560	0.9 (0.02)
12	340	0.298	58,652	2.5 (0.05)
31	1107	0.299	58,610	12.5 (0.26)
32	1146	0.300	59,058	8.6 (0.18)
35	1228	0.301	58,657	2.6 (0.05)
15	466	0.407	250,712	4.7 (0.10)
33	1177	0.451	138,206	1.6 (0.03)
43	1545	0.450	92,088	0.6 (0.01)
40	1443	0.452	40,055	3.1 (0.07)
41	1485	0.501	69,870	0.9 (0.02)
25	732	0.499	35,530	3.2 (0.07)
26	824	0.500	36,384	5.1 (0.11)
29	999	0.503	36,755	5.2 (0.11)
39	1401	0.500	35,912	1.5 (0.03)
42	1513	0.550	90,900	3.4 (0.07)
38	1358	0.551	33,521	1.7 (0.04)
36	1254	0.599	176,488	16.5 (0.34)
30	1061	0.651	92,327	2.2 (0.05)
20	610	0.699	28,313	0.7 (0.01)
24	702	0.702	27,033	0.9 (0.02)
28	954	0.704	27,363	0.7 (0.01)
14	421	0.800	141,505	18.3 (0.38)
46	1645	0.800	141,353	26.5 (0.55)
10	268	0.800	70,165	2.6 (0.05)
27	906	0.800	70,055	2.6 (0.06)
45	1607	0.802	70,590	2.1 (0.04)
23	666	0.800	24,584	1.2 (0.02)

Table 6.8 – Sample standard deviation of $C_{Lmax\ adj}$, $s_{C_{Lmax}}$, for nominal conditions with three or more runs

M (Nom.)	Re (Nom.)	N_{runs}	$s_{C_{Lmax}}$
0.300	59,140	5	0.0036
0.500	36,790	4	0.0033
0.700	27,680	3	0.0012
0.800	70,000	3	0.0036

Table 6.9 – Estimates of the bias uncertainty for NF , AF , α , p_0 , p , c , and b at the $1 - \nu = 0.95$ (i.e., two-sigma) confidence level

$B_{NF,1-\nu}$	0.34 N (0.08 lb)
$B_{AF,1-\nu}$	0.126 N (0.028 lb)
$B_{\alpha,1-\nu}$	0.2°
$B_{p_0,1-\nu}$	$\sqrt{(0.00016p_0 + 8.4 \text{ Pa})^2 + 369 \text{ Pa}^2}$ Pa, with p_0 in Pa $\sqrt{(0.00016p_0 + 0.175 \text{ psf})^2 + 0.16 \text{ psf}^2}$ psf, with p_0 in psf
$B_{p,1-\nu}$	$\sqrt{(0.00016p + 8.4 \text{ Pa})^2 + 369 \text{ Pa}^2}$ Pa, with p in Pa $\sqrt{(0.00016p + 0.175 \text{ psf})^2 + 0.08 \text{ psf}^2}$ psf, with p in psf
$B_{c,1-\nu}$	2.8×10^{-5} m (0.0012 in)
$B_{b,1-\nu}$	5.6×10^{-5} m (0.0022 in)

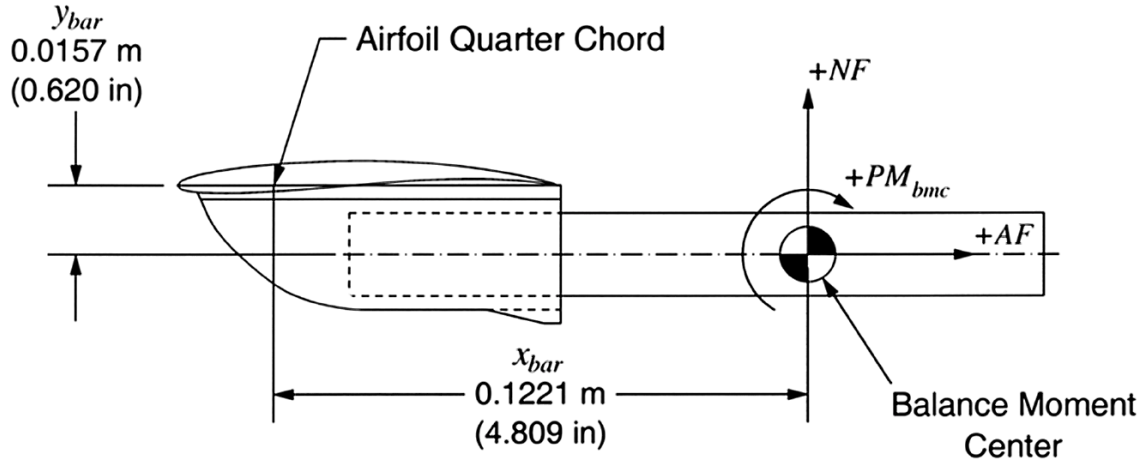


Figure 6.1 – Definition of x_{bar} and y_{bar} and sign convention for NF , AF , and PM_{bmc}

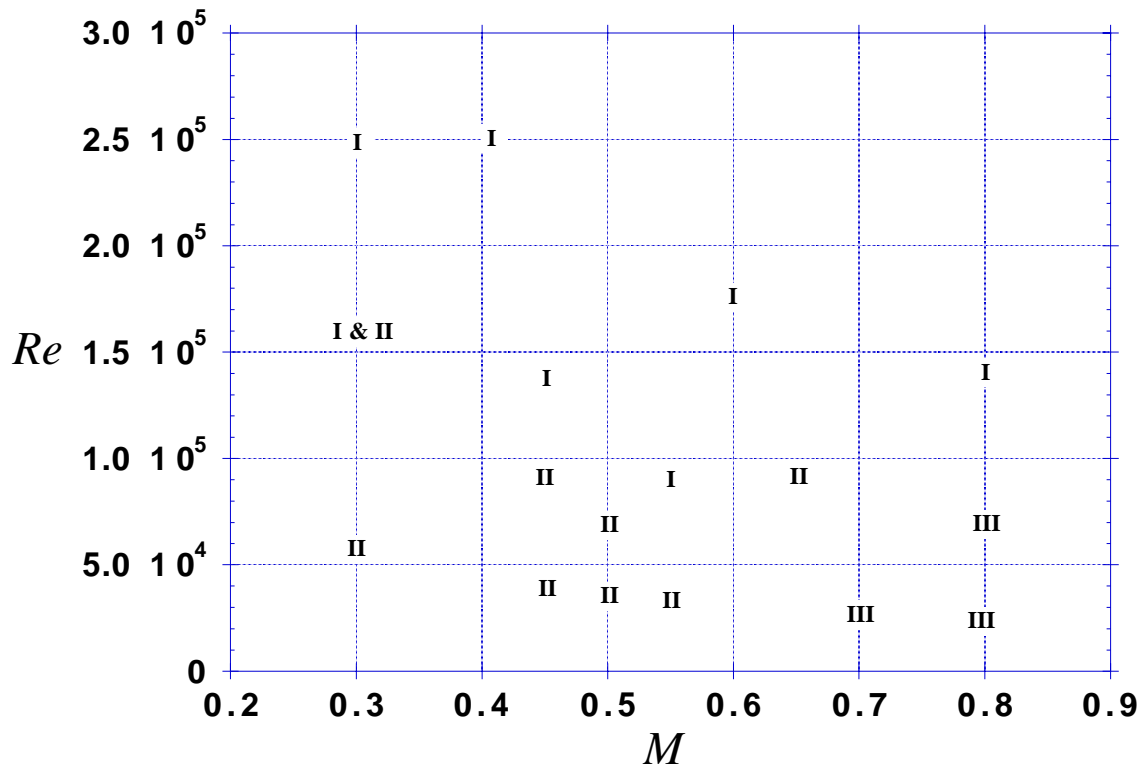


Figure 6.2 – Lift curve Type (I, II, or III) as a function of M and Re

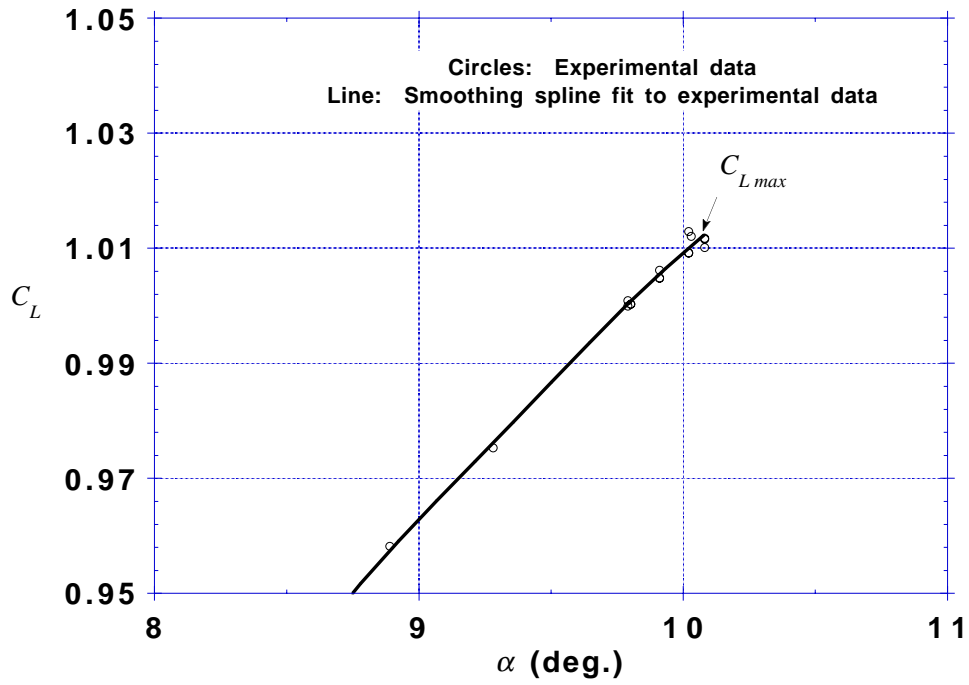


Figure 6.3 – Example of a Type I lift curve (Run 15)

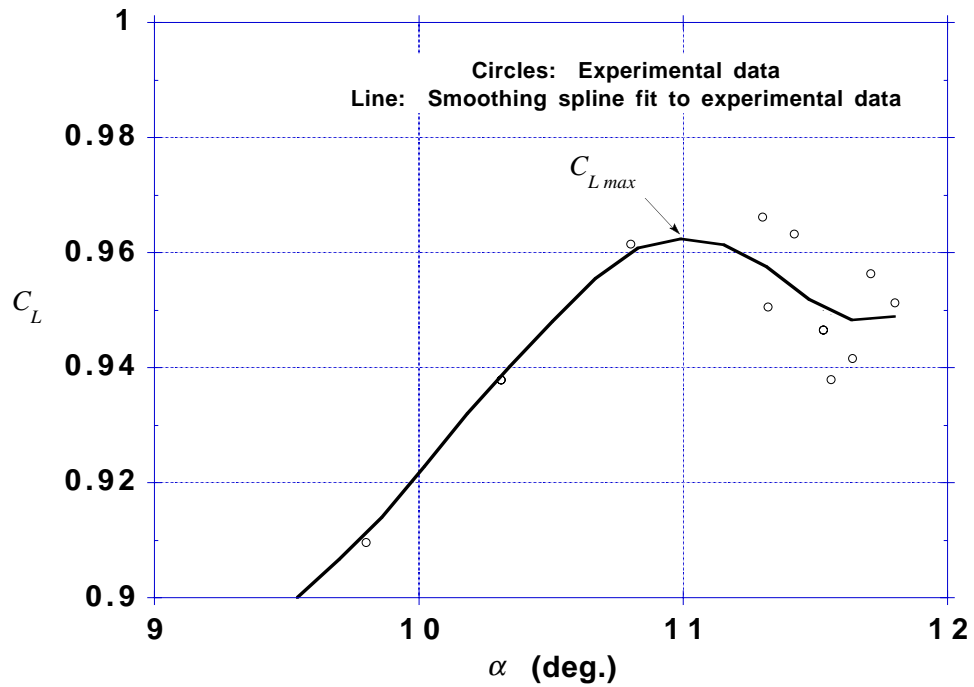


Figure 6.4 – Example of a Type II Lift curve (Run 11)

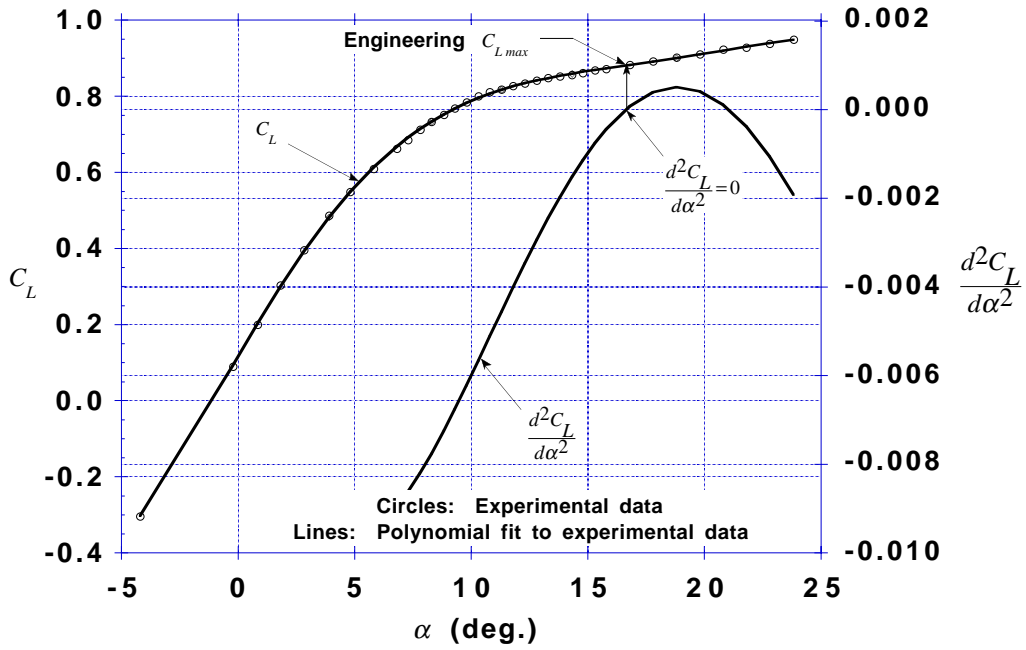


Figure 6.5 – Example of a Type III lift curve (Run 10)

Chapter 7: Experimental Test Results, Analyses Results, and Comparisons Between the Two Sets

This chapter focuses on the experimental test results, the aerodynamic analysis results, and their comparison. First, the experimental test results are presented, together with their uncertainties. Next, the aerodynamic analyses results and their uncertainties are given. Finally, the experimentally determined values of $C_{L\ max}$ are compared with those obtained from the aerodynamic analyses, and regions of discrepancies between them are identified.

7.1 Experimental Test Results

Detailed experimental test results data in both tabular and graphical form are presented in appendix D. The maximum lift coefficient data, listed by test condition, are shown in table 7.1. In this table $C_{L\ max}$, $\alpha_{C_{L\ max}}$ (i.e., the angle of attack at $C_{L\ max}$), $\overline{C_{L\ max\ adj}}$, $\overline{\alpha_{C_{L\ max}}}$ (i.e., the mean value of the angle of attack at $C_{L\ max}$) are given vs test condition. From the data on this table several observations can be made:

- The actual test conditions at $C_{L\ max}$ (i.e., M and Re) were very close to the desired test conditions.
- The adjustments made to $C_{L\ max}$ to obtain $\overline{C_{L\ max\ adj}}$ are very small, typically less than 0.001, and never greater than 0.004.
- For test conditions where replicates are available, the run-to-run range in $\overline{C_{L\ max\ adj}}$ is small, not exceeding 0.012. Given that some of these tests were conducted in separate days, these results indicate good experimental repeatability.

The uncertainty data, listed in the same order as the maximum lift coefficient data in table 7.1, are presented in table 7.2. In this table $\overline{P_{C_{L\ max}, 1-\nu}}$, $\overline{B_{C_{L\ max}, 1-\nu}}$, and $\overline{U_{C_{L\ max}, 1-\nu}}$ are given vs test condition for a confidence level of $1 - \nu = 0.95$. Note that the bias uncertainty in the experimental results is greater than or equal to the precision uncertainty in all but one case. This is not surprising, since the wind tunnel instrumentation and the

wind tunnel balance were used near the extremes of their operating range, stressing their capabilities. In retrospect, more emphasis should have been placed in reducing the bias uncertainty during the planning stages of the experiment. Reductions in the bias uncertainty could have been achieved in various ways, for example:

- Using a differential pressure transducer with an appropriate range could have reduced the bias uncertainty in the dynamic pressure. Although the absolute total and static pressure transducers would still have been required to determine the dynamic pressure, the bias uncertainty could have been reduced.
- Re-calibrating the wind tunnel balance for a smaller range of normal forces could have reduced the bias uncertainty of this key measurement.
- Performing a limited number of runs with the model inverted could have reduced the bias uncertainty in the angle of attack.

7.2 Analyses Results

Complete aerodynamic analysis results are given graphically in appendix D. In this appendix C_L vs α , C_M vs α , and C_L vs C_D are plotted for all nominal conditions (i.e., M and Re), together with the appropriate experimental data. Table 7.3 summarizes the maximum lift coefficient results from the aerodynamic analyses: $C_{Lmax}^{Analysis}$, $\alpha_{C_{Lmax}}^{Analysis}$, and $U_{C_{Lmax}, 1-\nu}^{Analysis}$ (at the $1 - \nu = 0.95$ confidence level). These aerodynamic analyses were conducted at the nominal conditions (i.e., M and Re) shown in table 7.3, and with other analyses settings (i.e., N_{panels} , $N_{vortices}$, N_{crit}) as discussed in chapter 3 and appendix A. The uncertainty in the analysis results was calculated as described in section 3.5.

The following observations can be made with regards to the aerodynamic analyses results presented graphically in appendix D (comparisons between the aerodynamic analyses and the experimental data are presented in the next section):

- As discussed in section 3.2, the lifting line analysis is not always capable of converging past C_{Lmax} . This behavior can be seen in figures D.1, D.7, D.15, and D.17.
- In numerous cases as seen in figures D.3, D.5, D.9, D.11, D.13, D.22, D.23, and D.25 the stall is sharp, with a significant reduction in C_L once the stall angle of attack is exceeded. It is interesting to note that stall flutter was observed in five out of these eight cases.¹ In retrospect, the possibility of stall flutter could have been foreseen based on the pre-test aerodynamic analyses. In cases where the

¹ A sharp stall is not sufficient to induce stall flutter; a sufficiently high dynamic pressure and sting/wind tunnel balance flexibility are also required.

predicted stall behavior was not sharp, as seen in figures D.27, D.29, D.31, and D.33, stall flutter was not a problem during testing.

- In some cases, the lifting line analysis was able to calculate results well into the post-stall region. Examples of such cases are shown in figures D.3, D.5, D.9, D.11, D.13, D.21, D.23, and D.25. These post-stall results should be considered qualitative; the lifting line analysis is not well suited for calculations of post-stall behavior involving significant regions of separated flow. In addition, the lifting line code extrapolates the two-dimensional lift data in an attempt to obtain post-stall results.

7.3 Comparison of the Experimental Test Results Against the Analyses Results

In table 7.4 the experimental and analysis results for $C_{L\ max}$ are compared at the nominal conditions. Besides repeating the $C_{L\ max}$ results presented in tables 7.2 and 7.3 for the experimental and analysis results, several additional quantities are calculated and presented in table 7.4. The quantity E is defined as the difference between the experimental and analysis values of $C_{L\ max}$:²

$$E = C_{L\ max}^{Experiment} - C_{L\ max}^{Analysis} \quad (7.1)$$

The quantity E_p is defined as the percent difference between the experimental and analysis values of $C_{L\ max}$:

$$E_p = 100 \bullet \frac{C_{L\ max}^{Experiment} - C_{L\ max}^{Analysis}}{C_{L\ max}^{Analysis}} \quad (7.2)$$

$U_{E,0.95}$ is the uncertainty of E at the 95 percent confidence level. It is calculated from:

$$U_{E,0.95} = \sqrt{\left(\overline{U_{C_{L\ max},1-\nu}}\right)^2 + \left(U_{C_{L\ max},1-\nu}^{Analysis}\right)^2} \quad (7.3)$$

using the values of $\overline{U_{C_{L\ max},1-\nu}}$ and $U_{C_{L\ max},1-\nu}^{Analysis}$ given in tables 7.2 and 7.3, respectively for $1 - \nu = 0.95$.³ The 95 percent confidence interval of E are defined by:

$$E_L = E - U_{E,0.95} \quad (7.4)$$

² $C_{L\ max}^{Experiment}$ is the same as $\overline{C_{L\ max\ adj}}$ reported in table 7.1.

³ The approach used here in defining E and $U_{E,0.95}$ is an adaptation of that suggested by Coleman and Stern in reference 66. Note that once $U_{E,0.95}$ is a total uncertainty and by itself does not distinguish between the experimental and analysis uncertainty.

$$E_U = E + U_{E,0.95} \quad (7.5)$$

With these data, the experimental and analysis results can be compared and evaluated in various ways.

Examining the columns of values for E and E_p , it can be observed that there are six conditions for which $|E| \geq 0.05$ and $|E_p| \geq 5$ percent.⁴ These conditions are: $M = 0.452$, $Re = 40,055$ ($E = -0.085$); $M = 0.501$, $Re = 69,870$ ($E = -0.051$); $M = 0.500$, $Re = 36,790$ ($E = -0.106$); $M = 0.550$, $Re = 90,900$ ($E = -0.054$); $M = 0.551$, $Re = 33,521$ ($E = -0.118$); and $M = 0.800$, $Re = 24,584$ ($E = -0.113$). The contour plot of E given in figure 7.1 clearly shows these results. Considering the subset of these cases for $0.452 \leq M \leq 0.551$, it is noted that only one of these conditions, namely $M = 0.500$, $Re = 36,790$, was a pre-selected test condition. Initial evaluation of the test data and preliminary analysis results indicated that a discrepancy between the experiment and analysis existed near this condition. Additional test conditions around this point were then selected and tests conducted. As shown by the data, these additional tests confirmed the discrepancy and allowed an assessment of its extent. This was, in essence, the successful application of anti-optimization in the present investigation: based on the results of the planned portion of the experiment, additional test points confirmed and outlined an area of discrepancy between experiments and analyses. Comparing the analysis C_L vs α curves and the experimental data for these conditions, as shown in figures D.13, D.15, D.17, D.19, and D.21 of appendix D, confirms the disagreement. This disagreement is made more evident when a comparison is made with the C_L vs α curve for a case in which the agreement between the analysis and experiment was excellent; for example, the condition at $M = 0.300$, $Re = 59,140$ shown in figure D.5 of appendix D. For this condition $E = -0.001$. As can be seen from the contour plot in figure 7.1, the area of discrepancy is centered at $M = 0.551$ on the lower Reynolds number boundary of the test domain. The value of absolute value of E is reduced to less than 0.05 along the lower Reynolds number boundary of the test domain (around $M = 0.551$) for $M \leq 0.39$ and $M \geq 0.68$. The upper Reynolds number reach of the $|E| = 0.05$ contour is 95,000.

Comparing the differences between the analysis and experimental values of $C_{L,max}$ without considering the uncertainties in both sets of data, is not sufficient. Thus, an evaluation of the effect of uncertainty on E is warranted. In table 7.4, the 95 percent confidence interval of E , (E_L , E_U) calculated as shown in equations 7.4 and 7.5, are shown for all test conditions. One way of interpreting these confidence intervals is by examining their maximum absolute values, $|E_L|$ and $|E_U|$. These maximum values indicate how large $|E|$ could be given the assumed analysis and experimental uncertainties at the 95 percent confidence level. Using this consideration for $|E_L|$ or $|E_U| \geq 0.05$ (whichever is largest) isolates all the conditions mentioned previously, in addition to $M = 0.700$,

⁴ The author's experience with the preliminary design of airplanes for the exploration of Mars indicates that analysis results validated to this level are sufficient for preliminary design purposes.

$Re = 27,680$ ($|E_L| = 0.075$) and $M = 0.800$, $Re = 141,000$ ($|E_U| = 0.051$). For both of these conditions reducing the uncertainties in the experimental and analysis results would help in refining the probability that discrepancies in C_{Lmax} at this level (i.e., 0.05 or greater) exist between the analysis and experimental results. Examining the experimental uncertainties table 7.2 indicates that a good approach would be to reduce the experimental bias uncertainty for the condition at $M = 0.700$, and reducing the analysis uncertainty for the condition at $M = 0.800$.

Examination of the analysis and experimental C_L vs α data indicates that the discrepancy observed at $M = 0.800$, $Re = 24,584$ is an artifact of the engineering definition of C_{Lmax} . The C_L vs α plot for this condition is shown in figure 7.2. For comparison the C_L vs α plot for $M = 0.551$, $Re = 33,521$ shown in figure 7.3.^{5,6} Although both of these cases have similar values of E ,⁷ it is clear from comparing these figures that the analysis does a better job of predicting C_L vs α at high values of C_L for the condition at $M = 0.800$ than for the condition at $M = 0.551$. Performing a different comparison between the analysis and experimental C_L data can quantify this. An alternate comparison variable, $|E_{alt}|$ defined as:

$$|E_{alt}| = \text{Maximum} \left| C_{Lmax}^{Experiment} - C_{Lmax}^{Analysis} \right|_{\alpha=10^\circ \text{ to } 20^\circ} \quad (7.6)$$

was applied to the three conditions for which the engineering definition of C_{Lmax} had been used (namely and $M = 0.800$, $Re = 24,584$; $M = 0.800$, $Re = 70,000$; and $M = 0.700$, $Re = 27,680$). The angle of attack range was selected to be from 10 to 20 degrees to include the higher values of C_L and provide a broad base of comparison. The corresponding values of $|E_{alt}|$ are given in the last column of table 7.4. None of the values of $|E_{alt}|$ exceed 0.05, the previously determined threshold for acceptable agreement between the experiments and the analyses. The same conclusion can be reached by examining the plots of C_L vs α (which include both the experimental and analysis data) for each of these three conditions as shown in figures 7.2, 7.4, and 7.5. Another contour plot using $|E|$ for all conditions with Type I and II C_L vs α curves and $|E_{alt}|$ for all conditions with Type III C_L vs α curves is shown in figure 7.6. This contour plot shows that the disagreement around $M = 0.8$, $Re = 25,000$ is not as large as indicated by E alone (as shown in figure 7.1) using the engineering definition of C_{Lmax} . The problem with the engineering definition of C_{Lmax} is that it is sensitive to small changes in the shape (and thus curvature) of the C_L vs α curve. During the planning stages of the experiment it was determined that it was important to define how the data was to be analyzed prior to testing to avoid having pre-conceived notions of what the results should look like affect the conclusions. Although this goal was achieved, the data shows that the engineering definition of C_{Lmax} is not reliable for comparison purposes. Figure 7.6 also shows that the

⁵ These figures are also given in appendix D as figures D.31 and D.21, respectively.

⁶ Comments regarding the C_M vs α curve are given at the end of this section.

⁷ $E = -0.118$ for the condition at $M = 0.551$, $Re = 33,521$; $E = -0.113$ for the condition at $M = 0.800$, $Re = 24,584$.

region where there disagreement in $C_{L,max}$ is greater than 0.05 is somewhat narrower than that determined using $|E|$ alone; the 0.05 contour boundary on this figure encompasses $0.39 \leq M \leq 0.61$ along the lower Reynolds number boundary.

It is interesting to note that an informal survey of aerodynamicists performed before the test was conducted indicated unanimously that the worst correlation in $C_{L,max}$ between analysis and experiments was expected at the highest Mach number and lowest Reynolds numbers. The results presented here partially contradicted this opinion. The worst correlation in $C_{L,max}$ was found at intermediate Mach numbers – an unforeseen result.

Although discrepancies between the analysis and experiment have been isolated, additional work remains to be done to understand their nature. Although the experiment is a fair test of the analysis, certain issues regarding the experiment need to be looked at in more detail. Examples of these include the effect of the wind tunnel balance block and the accuracy of the model. Additional data already collected, in particular the wing surface pressures, can shed light on the reasons for the discrepancies. All this is interesting work but beyond the scope of the present investigation.

In summary, the following key conclusions can be re-stated:

- The aerodynamic analysis was validated in its ability to predict $C_{L,max}$ within 0.05 in a significant portion of the test domain.
- Careful planning of the experiment and application of anti-optimization isolated differences between the analysis and experimental values of $C_{L,max}$ greater than 0.05 at intermediate Mach numbers and moderate to low Reynolds numbers. The concept of anti-optimization proved itself useful in isolating discrepancies and validating the analysis.
- Application of the engineering definition of $C_{L,max}$ does not yield reliable values of $C_{L,max}$ for use in comparisons of analysis and experimental results. The problem with the engineering definition of $C_{L,max}$ is that it is sensitive to small changes in the shape (and thus curvature) of the C_L vs α curve.
- Comparing the analysis and experimental results for $C_{L,max}$ while taking into account their uncertainties yielded additional insight into the differences between these two sets of results. Taking uncertainties into consideration identified the same conditions yielding differences in $C_{L,max} \geq 0.05$ as were identified without consideration of the uncertainties (i.e., by only considering E). However, two additional conditions ($M = 0.700$, $Re = 27,680$ and $M = 0.8$, $Re = 141,000$) were identified as possible areas of discrepancies by the comparison taking uncertainty into account. This demonstrated the need for taking uncertainty into account when comparing analysis and experimental results.

From the graphs in appendix D, comparisons of a more general nature can be made between the analysis and experimental results. Although much of the data presented in these graphs is not of primary interest to the present research, a few observations are noted here:

- In general, the aerodynamic analysis predicts $C_{L\ max}$ occurring at the same or higher angles of attack than shown by the experimental data.
- In most cases the experimentally determined C_L vs α curve lies to the left of the calculated curve (i.e., a given value of C_L is observed at a lower angle of attack in the experimental data).
- The difference in stall behavior between the analysis results and experimental data (as shown by the C_L vs α curves) is most markedly different at the lower Reynolds numbers investigated ($33,521 \leq Re \leq 40,055$) and Mach numbers from 0.452 to 0.551.
- In most cases the analyses tends to underpredict the drag coefficient. This is probably due to the fact that the drag of the wind tunnel balance block was not taken into account in the analyses.
- The accuracy of the calculated pitching moment decreases with increasing Mach number and decreasing Reynolds number. Although the pitching moment is usually not predicted as accurately as the lift, the observed trend points towards a problem in either the analysis or the experiment. Examination airfoil surface pressure data obtained during testing (but not discussed here) may help explain this discrepancy between the experimental and analysis pitching moment curves.

Table 7.1 – Summary of experimental data

Run	Tab Point	M (Exp.)	Re (Exp.)	C_{Lmax}	$\alpha_{C_{Lmax}}$ (deg.)	M (Nom.)	Re (Nom.)	$C_{Lmax\ adj}$	$\overline{C_{Lmax\ adj}}$	$\overline{\alpha_{C_{Lmax}}}$ (deg.)
16	519	0.301	249,123	1.023	10.67	0.301	249,123	1.023	1.023	10.67
37	1309	0.302	159,841	0.992	10.54	0.300	160,000	0.991		
47	1683	0.301	159,284	1.003	10.80	"	"	1.003	0.997	10.67
11	301	0.299	58,560	0.962	10.80	0.300	59,140	0.962		
12	340	0.298	58,652	0.954	11.04	"	"	0.955		
31	1107	0.299	58,610	0.962	11.31	"	"	0.962		
32	1146	0.300	59,058	0.956	11.04	"	"	0.956		
35	1228	0.301	58,657	0.962	11.10	"	"	0.962	0.959	11.06
15	466	0.407	250,712	1.012	10.08	0.407	250,712	1.012	1.012	10.08
33	1177	0.451	138,206	0.991	10.12	0.451	138,206	0.991	0.991	10.12
43	1545	0.450	92,088	0.980	10.05	0.45	92,088	0.980	0.980	10.05
40	1443	0.452	40,055	0.985	10.50	0.452	40,055	0.985	0.985	10.50
41	1485	0.501	69,870	0.986	9.78	0.501	69,870	0.986	0.986	9.78
25	732	0.499	35,530	0.986	9.80	0.500	36,790	0.987		
26	824	0.500	36,384	0.985	10.05	"	"	0.985		
29	999	0.503	36,755	0.991	10.05	"	"	0.992		
39	1401	0.500	35,912	0.984	10.07	"	"	0.985	0.987	9.99
42	1513	0.550	90,900	0.998	9.54	0.550	90,900	0.998	0.998	9.54
38	1358	0.551	33,521	0.978	9.26	0.551	33,521	0.978	0.978	9.26
36	1254	0.599	176,488	0.998	8.81	0.599	176,488	0.998	0.998	8.81
30	1061	0.651	92,327	0.978	7.81	0.651	92,327	0.978	0.978	7.81
20	610	0.699	28,313	0.853	15.86	0.700	27,680	0.851		
24	702	0.702	27,033	0.846	16.86	"	"	0.849		
28	954	0.704	27,363	0.847	16.80	"	"	0.851	0.850	16.51
14	421	0.800	141,505	0.888	10.75	0.800	141,000	0.888		
46	1645	0.800	141,353	0.888	10.81	"	"	0.888	0.888	10.78
10	268	0.800	70,165	0.881	16.81	0.800	70,000	0.881		
27	906	0.800	70,055	0.879	15.79	"	"	0.879		
45	1607	0.802	70,590	0.873	16.10	"	"	0.874	0.878	16.23
23	666	0.800	24,584	0.921	19.79	0.800	24,584	0.921	0.921	19.79

Table 7.2 – Summary of the uncertainty in the experimental data

Run	M (Nom.)	Re (Nom.)	$\overline{P_{C_{L,max},1-\nu}}$	$\overline{B_{C_{L,max},1-\nu}}$	$\overline{U_{C_{L,max},1-\nu}}$
16	0.301	249,123	0.007	0.011	0.013
37	0.300	160,000	0.005	0.016	0.017
47	"	"			
11	0.300	59,140	0.003	0.039	0.039
12	"	"			
31	"	"			
32	"	"			
35	"	"			
15	0.407	250,712	0.007	0.008	0.010
33	0.451	138,206	0.007	0.011	0.013
43	0.450	92,088	0.007	0.016	0.018
40	0.452	40,055	0.007	0.037	0.038
41	0.501	69,870	0.007	0.019	0.020
25	0.500	36,790	0.004	0.037	0.037
26	"	"			
29	"	"			
39	"	"			
42	0.550	90,900	0.007	0.013	0.015
38	0.551	33,521	0.007	0.035	0.036
36	0.599	176,488	0.007	0.006	0.010
30	0.651	92,327	0.007	0.011	0.013
20	0.700	27,680	0.004	0.029	0.029
24	"	"			
28	"	"			
14	0.800	141,000	0.005	0.005	0.007
46	"	"			
10	0.800	70,000	0.004	0.010	0.011
27	"	"			
45	"	"			
23	0.800	24,584	0.007	0.030	0.031

Note: All uncertainties in this table given for $1 - \nu = 0.95$

Table 7.3 – Summary of aerodynamic analysis results

M (Nom.)	Re (Nom.)	$C_{L\max}^{Analysis}$	$\alpha_{C_{L\max}}^{Analysis}$
0.301	249,123	1.036	11.89
0.300	160,000	1.012	11.74
0.300	59,140	0.958	11.70
0.407	250,712	1.021	10.99
0.451	138,206	0.978	11.14
0.450	92,088	0.960	10.75
0.452	40,055	0.900	11.04
0.501	69,870	0.935	10.56
0.500	36,790	0.881	10.79
0.550	90,900	0.944	10.41
0.551	33,521	0.860	10.45
0.599	176,488	1.011	9.16
0.651	92,327	0.969	9.61
0.700	27,680	0.810	11.68
0.800	141,000	0.918	15.40
0.800	70,000	0.872	14.51
0.800	24,584	0.808	14.22

Notes:

- 1) $U_{C_{L\max}, 1-\nu}^{Analysis} = 0.020$ for $1 - \nu = 0.95$; see chapter 3.
- 2) The engineering definition of $C_{L\max}$ was used for the conditions $M = 0.800$, $Re = 70,000$ and $M = 0.800$, $Re = 24,584$; see chapter 3.

Table 7.4 – Comparison of experimental and analysis results for C_{Lmax}

M (Nom.)	Re (Nom.)	C_{Lmax} Experiment	C_{Lmax} Analysis	E	E_p	$U_{E,0.95}$	95% Confidence Interval of E (E_L, E_U)	$ E_{atl} $
0.301	249,123	1.036	1.023	0.013	1.3	0.024	(-0.011, 0.037)	
0.300	160,000	1.012	0.997	0.015	1.5	0.026	(-0.011, 0.041)	
0.300	59,140	0.958	0.959	-0.001	-0.1	0.044	(-0.045, 0.043)	
0.407	250,712	1.021	1.012	0.009	0.9	0.022	(-0.013, 0.031)	
0.451	138,206	0.978	0.991	-0.013	-1.3	0.024	(-0.037, 0.011)	
0.450	92,088	0.960	0.980	-0.020	-2.1	0.027	(-0.047, 0.007)	
0.452	40,055	0.900	0.985	-0.085	-9.4	0.043	(-0.128, -0.042)	
0.501	69,870	0.935	0.986	-0.051	-5.5	0.028	(-0.079, -0.023)	
0.500	36,790	0.881	0.987	-0.106	-12.0	0.042	(-0.148, -0.064)	
0.550	90,900	0.944	0.998	-0.054	-5.7	0.025	(-0.079, -0.029)	
0.551	33,521	0.860	0.978	-0.118	-13.7	0.041	(-0.159, -0.077)	
0.599	176,488	1.011	0.998	0.013	1.3	0.022	(-0.009, 0.035)	
0.651	92,327	0.969	0.978	-0.009	-0.9	0.024	(-0.033, 0.015)	
0.700	27,680	0.810	0.850	-0.040	-4.9	0.035	(-0.075, -0.005)	0.048
0.800	141,000	0.918	0.888	0.030	3.3	0.021	(0.009, 0.051)	
0.800	70,000	0.872	0.878	-0.006	-0.7	0.023	(-0.029, 0.017)	0.023
0.800	24,584	0.808	0.921	-0.113	-14.0	0.037	(-0.150, -0.076)	0.046

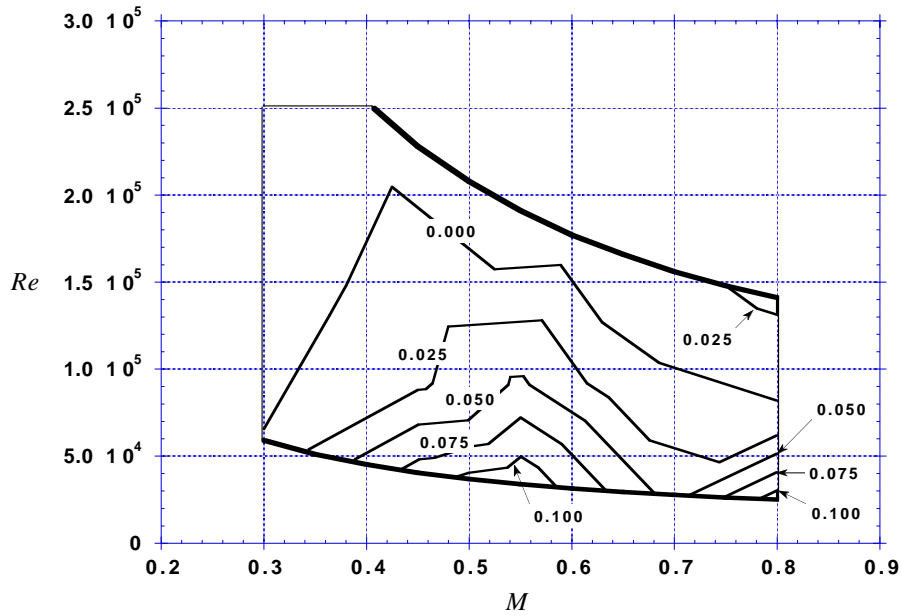


Figure 7.1 – Contour plot of $|E|$, a measure of the difference between the analysis and experimental values of C_{Lmax} over the test domain

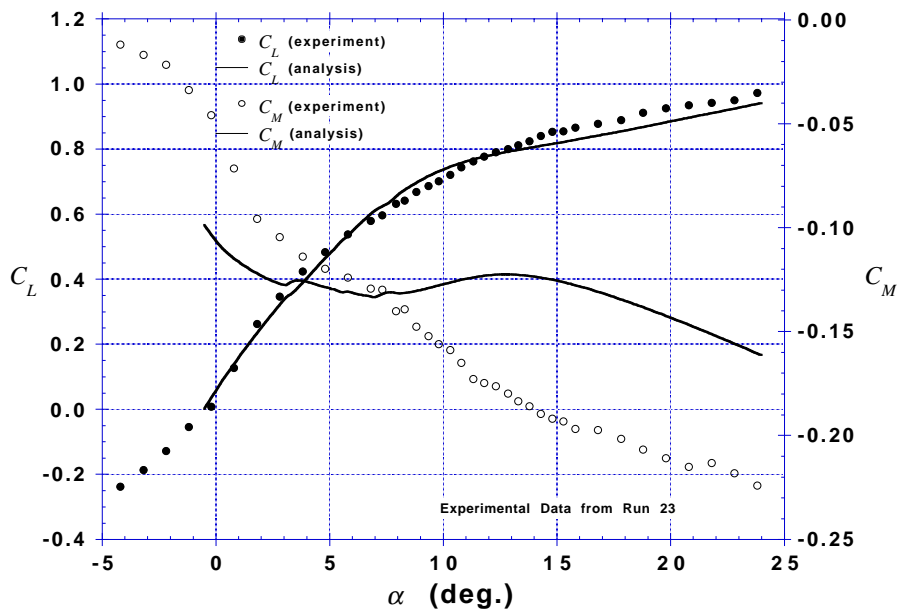


Figure 7.2 – C_L and C_M vs α ; nominal conditions $M = 0.800$, $Re = 24,584$

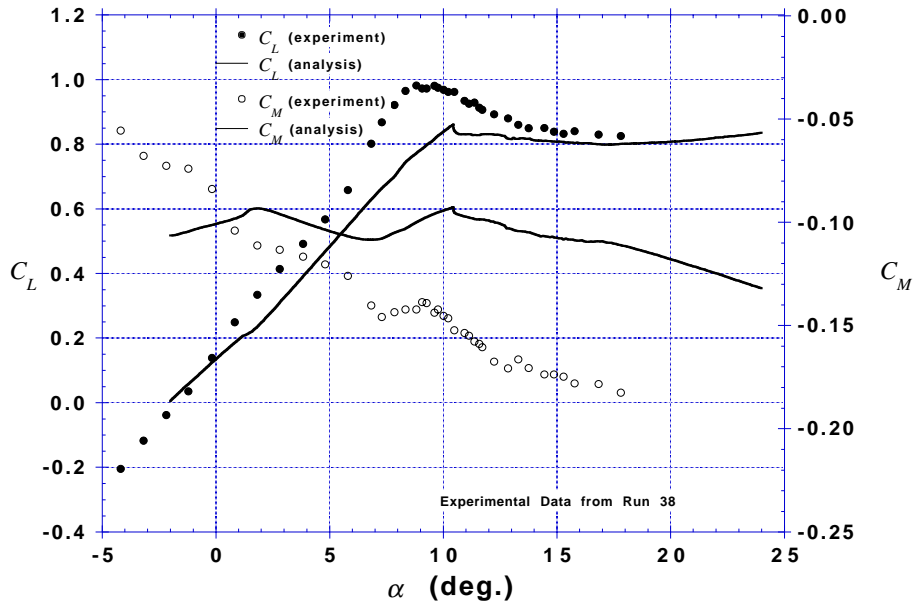


Figure 7.3 – C_L and C_M vs α ; nominal conditions $M = 0.551$, $Re = 33,521$

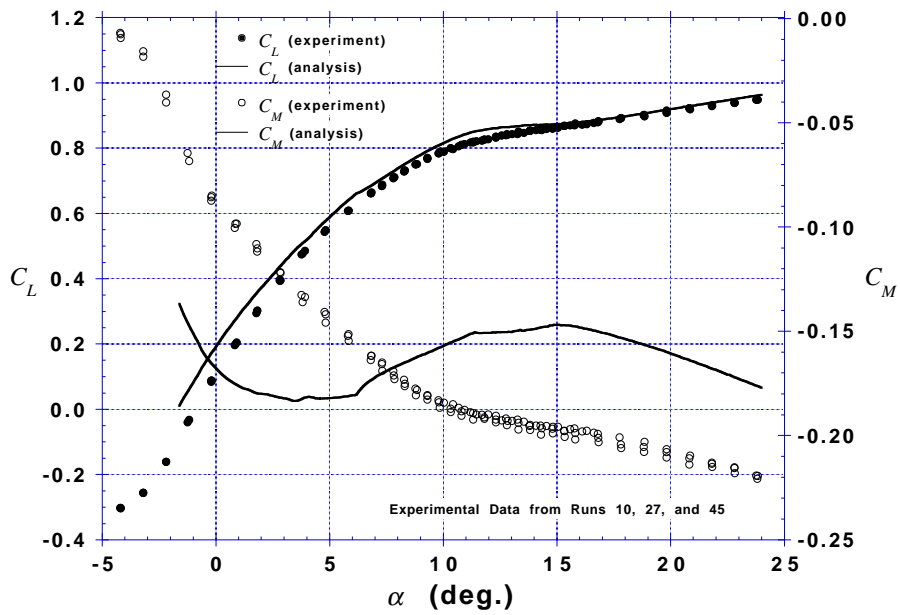


Figure 7.4 – C_L and C_M vs α ; nominal conditions $M = 0.800$, $Re = 70,000$

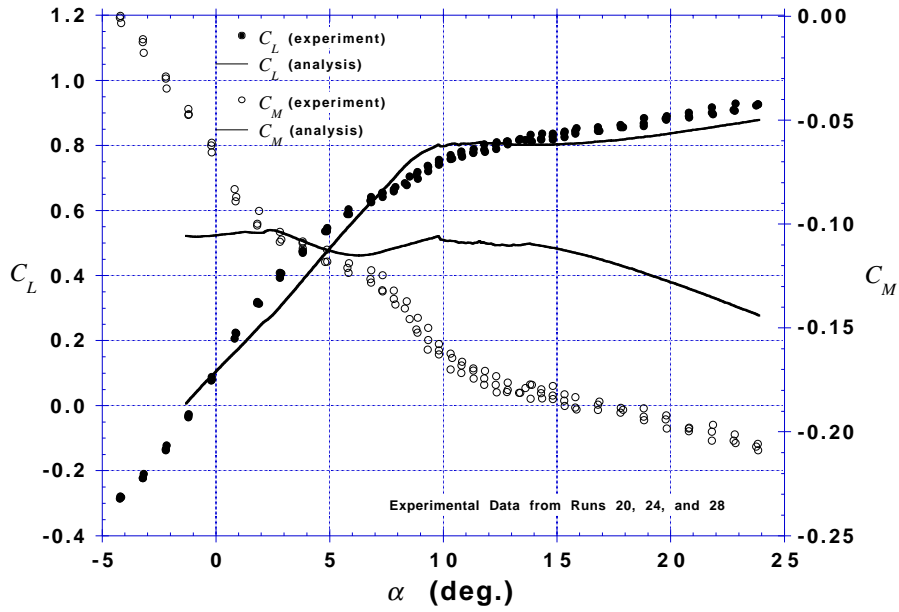


Figure 7.5 – C_L and C_M vs α ; nominal conditions $M = 0.700$, $Re = 27,680$

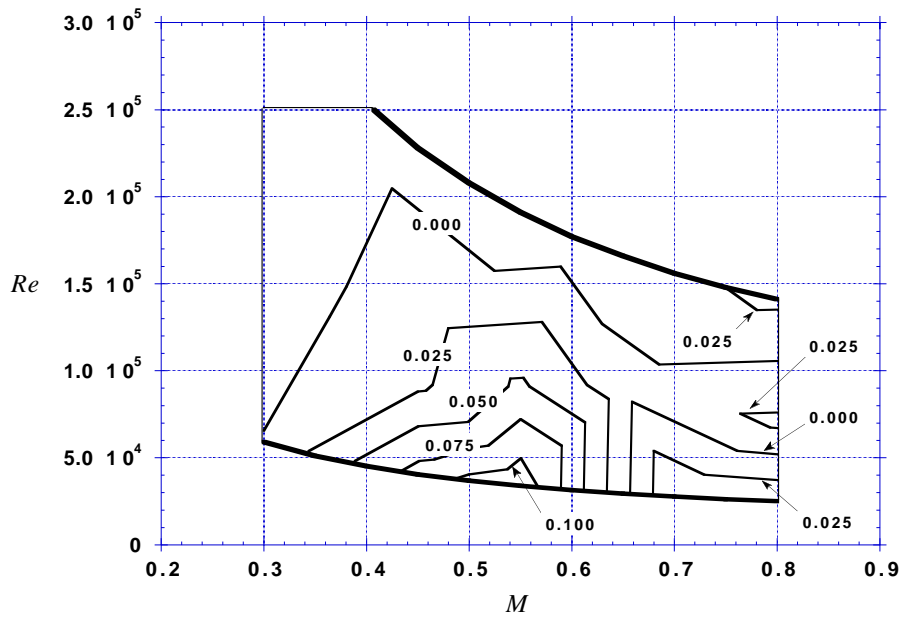


Figure 7.6 – Contour plot using $|E|$ for all conditions with Type I and II C_L vs α curves and $|E_{alt}|$ for all conditions with Type III C_L vs α curves: measures of the difference between the experimental and analysis values of $C_{L,max}$ over the test domain

Chapter 8: Conclusions and Observations

The primary objectives of the present investigation were to develop an approach for the validation of codes and/or analyses¹ through experiments that applied the concept of anti-optimization, and to demonstrate and evaluate the effectiveness of this approach. The key step in the proposed approach was planning the experiment in two phases. In the first phase tests were conducted at pre-selected conditions (i.e., Mach and Reynolds numbers in the present investigation) to obtain a global picture of the differences between the analyses and experiments, and support a second round of testing. The second phase involved using the results obtained in the first phase to select test conditions that would maximize the differences between the analyses and experiments – in other words, applying anti-optimization. The present investigation succeeded in demonstrating the usefulness of the anti-optimization approach in the process of validating aerodynamic analyses. This is the principal contribution of the work reported herein.

The analysis used as an example for the proposed approach was a combination of codes used to predict the maximum lift coefficient, $C_{L\max}$, of a three-dimensional wing. Discrepancies between the analysis and experiment results were discovered in an unexpected region of the test domain, while in another region where significant discrepancies were expected the analysis and experimental results showed good agreement. In particular, the aerodynamic analysis' ability to predict $C_{L\max}$ within 0.05 (an acceptable level of accuracy for design purposes) was shown for a significant portion of the test domain. Careful planning of the experiment and the application of anti-optimization isolated differences between the analysis and experimental values of $C_{L\max}$ greater than 0.05 in a region ($0.39 \leq M \leq 0.61$; $Re \leq 95,000$) centered at $M = 0.551$ and $Re = 33,521$ along the lower Reynolds number boundary of the test domain.² Prior to the start of testing it was expected that the area of greatest difference would be centered around $M = 0.8$, $Re = 25,000$. The analysis and experimental results showed this expectation to be incorrect, and the anti-optimization approach led to an unexpected area of discrepancy.

¹ In this work a code is considered to be a single computer program. An analysis is defined here as a single code or combination of codes used to yield the output parameter being investigated (e.g., maximum lift coefficient). In general the term code is used here to refer to specific computer programs.

² A more complete discussion of the comparison between analyses and experiments can be found in chapter 7.

An additional contribution of the present investigation is in the generation of an aerodynamic database (i.e., C_L , C_D , and C_M vs α) at low Reynolds numbers and transonic Mach numbers for a documented and carefully conducted experiment. These data will be useful in validating aerodynamic codes in this unusual flight regime and in the design of robotic airplanes for the exploration of Mars.

Additional conclusions, observations, and lessons learned from the present investigation are listed below, in the same order as they appear in the dissertation, with reference to the chapter in which they appear.

- 1) A convergence study was performed for the two-dimensional airfoil code, MSES. This convergence study was conducted by varying the number of grid points on the surface of the airfoil, N_{grid} . For the airfoil used in the present investigation, within the Mach and Reynolds numbers range considered, MSES yields converged results for $N_{grid} \geq 155$ up to a Mach number of 0.6. It was not possible to formally establish convergence for a Mach number of 0.8 because it became very difficult to obtain solutions with $N_{grid} > 155$. However, given the trend for $0.3 \leq M \leq 0.6$, the results generated at a Mach number of 0.8 with $N_{grid} = 155$ were assumed to be converged. All final MSES calculations were performed with $N_{grid} = 155$. (Chapter 3)
- 2) At a Mach number of 0.8, MSES was unable to converge to a solution for angles of attack around $c_{l\ max}$. It is possible that steady state solutions at these conditions do not exist. Such behavior at transonic Mach numbers has been observed and reported by other researchers. In order to proceed with the calculations of the three-dimensional wing aerodynamic coefficients, the two-dimensional airfoil aerodynamic coefficients were interpolated with a polynomial over the range of angles of attack where MSES was unable to converge. (Chapter 3)
- 3) At a Mach number of 0.8 there was not a mathematically identifiable value of $C_{L\ max}$ in the range of angles of attack considered (up to 24°). An engineering value of $C_{L\ max}$ was defined as the value of C_L where $d^2C_L/d\alpha^2 = 0$. This definition of $C_{L\ max}$ was used for all conditions where a mathematically identifiable value of $C_{L\ max}$ could not be obtained. (Chapter 3)
- 4) The numerical noise associated with the calculations (as shown by the MSES convergence study) varied throughout the Mach and Reynolds numbers range considered. The general trend was a reduction in the numerical noise at lower Reynolds numbers. (Chapter 3)
- 5) A convergence study was performed for the lifting line code over the range of Mach and Reynolds numbers being considered. This convergence study was conducted by varying the number of vortices on the wing, $N_{vortices}$. The results indicated that for $N_{vortices} = 300$, $C_{L\ max}$ was within 0.001 of its extrapolated value for $N_{vortices} = \infty$. All final calculations were performed with $N_{vortices} = 300$. (Chapter 3)

- 6) A sensitivity study was conducted to determine the effect of the wind tunnel turbulence on the value of C_{Lmax} . The wind tunnel turbulence effect was captured by the parameter N_{crit} . Since the wind tunnel turbulence was experimentally measured, N_{crit} had an uncertainty associated with it. Calculations were performed for the mean value of N_{crit} , and at the extremes of the 95 percent confidence interval of the mean. The results indicated that C_{Lmax} was insensitive to N_{crit} . This observation was consistent with the expected behavior of the boundary layer at C_{Lmax} for the airfoil and low Reynolds numbers used in this investigation. (Chapter 3)
- 7) An estimated value of the uncertainty in the analysis value of C_{Lmax} , $U_{C_{Lmax},1-\nu}^{Analysis}$, was created. This value was determined by considering the MSES convergence study data and the N_{crit} sensitivity study data. Thus, $U_{C_{Lmax},1-\nu}^{Analysis}$ was set to a constant value of 0.02 over the Mach and Reynolds numbers considered in this investigation. It was assumed that this value encompassed a 95 percent confidence interval of any future calculation (i.e., $1 - \nu = 0.95$). (Chapter 3)
- 8) Given the two-dimensional nature of the test design space, and knowledge of the uncertainty structure, test designs equally suitable to that derived in chapter 4 could have been generated by examination. The use of RSM was not necessary. However in a more complex test design, one involving three or more independent variables for example, arriving at a suitable test design by examination would be significantly more difficult. From the experience gained in designing the test for the present experiment, an approach incorporating the minimum precision error combined with consideration of bias in the response surface function (i.e., lack-of-fit) is recommended. (Chapter 4)
- 9) The actual test conditions at C_{Lmax} (i.e., M and Re) were very close to the desired test conditions. (Chapter 6)
- 10) For all but one of the test conditions at $M \geq 0.7$, determination of C_{Lmax} from the experimental data had to be done by applying the engineering definition of C_{Lmax} (i.e., C_{Lmax} occurs at the angle of attack where $d^2C_L/d\alpha^2 = 0$). (Chapter 6)
- 11) During wind tunnel testing, stall flutter was observed for numerous operating conditions. The occurrence of stall flutter was more prevalent at operating conditions with higher dynamic pressures and sharp stall characteristics. (Chapter 6)
- 12) The occurrence of stall flutter invalidated the assumption that the uncertainty in the lift force was approximately constant through the test design space. As a consequence of this, the precision uncertainty of the experimental results could not be determined by the planned RSM approach. An alternate approach involving assumptions regarding the standard deviation and distribution of the precision uncertainty of the experimental results was implemented. (Chapter 6)

- 13) For test conditions where replicates were available, the run-to-run range variation in $C_{L\ max}$ was small, not exceeding 0.012. Given that some of these tests were conducted on separate days, these results indicate good experimental repeatability. (Chapter 7)
- 14) The bias uncertainty in the experimental results was greater than or equal to the precision uncertainty at all but one of the test conditions. In retrospect, more emphasis should have been placed in reducing the bias uncertainty during the planning stages of the experiment. Reductions in the bias uncertainty could have been achieved in various ways, for example:
 - Using a differential pressure transducer with an appropriate range could have reduced the bias uncertainty in the dynamic pressure. Although the absolute total and static pressure transducers would still have been required to determine the dynamic pressure, the bias uncertainty could have been reduced.
 - Re-calibrating the wind tunnel balance for a smaller range of normal forces could have reduced the bias uncertainty of this key measurement.
 - Performing a limited number of runs with the model inverted could have reduced the bias uncertainty in the angle of attack. (Chapter 7)
- 15) The lifting line analysis was not always capable of converging past $C_{L\ max}$. (Chapter 7)
- 16) The aerodynamic analysis predicted sharp stall behavior, with a significant reduction in C_L once the angle of attack was exceeded, for various conditions. Stall flutter was observed experimentally for several, but not all, of these conditions. A sharp stall is not sufficient to induce stall flutter; a sufficiently high dynamic pressure and enough sting/wind tunnel balance flexibility is also required. In retrospect, the occurrence of stall flutter could have been foreseen based on the pre-test aerodynamic analyses. For conditions in which the predicted stall behavior was not sharp, stall flutter was not a problem during testing. (Chapter 7)
- 17) In some cases, the analysis was capable of predicting results well into the post-stall region. These post-stall results should be considered qualitative; the lifting line formulation is not well suited for calculations of post-stall behavior involving significant regions of separated flow. In addition, the lifting line code extrapolates the two-dimensional lift data in an attempt to obtain post-stall results. (Chapter 7)
- 18) Application of the “engineering” definition of $C_{L\ max}$ does not yield reliable values of $C_{L\ max}$ for use in comparisons of analysis and experimental results. The problem with the engineering definition of $C_{L\ max}$ is that it is sensitive to small changes in the shape (and thus curvature) of the C_L vs α curve. This behavior was particularly evident at

the condition $M = 0.800$, $Re = 24,584$, where application of the engineering definition of $C_{L\ max}$ yielded a difference of 0.113 between the experimental and analysis values of $C_{L\ max}$. Comparison of the experimental and analysis C_L vs α curves for this condition over the angle of attack range from 10 to 20 degrees indicated a maximum absolute value difference of 0.046. (Chapter 7)

- 19) Comparing the analysis and experimental results for $C_{L\ max}$ while taking into account their uncertainties yielded additional insight into the differences between these two sets of results. Taking uncertainties into consideration identified the same conditions yielding differences in $C_{L\ max} \geq 0.05$ as were identified without consideration of the uncertainties. However, two additional conditions were identified as possible areas of discrepancies by the comparison taking uncertainty into account. This demonstrated the need for taking uncertainty into account when comparing analysis and experimental results. (Chapter 7)

References

- 1) Unger, R. E., "Integrated Aerodynamic-Structural Wing Design Optimization," Ph.D. Dissertation, Aerospace and Ocean Engineering Department, Virginia Polytechnic Institute and State University, Blacksburg, March 1992.
- 2) Haftka, R. T. and Kao, P-J., "The Use of Optimization for Sharpening Differences Between Models," paper presented at the ASME Winter Annual Meeting, November 25-30, Dallas, 1990.
- 3) Elishakoff, I., "An Idea of the Uncertainty Triangle," *The Shock and Vibration Digest*, Vol. 22, No. 10, 1990, p. 1.
- 4) Elishakoff, I., "Convex Versus Probabilistic Models of Uncertainty in Structural Dynamics," *Structural Dynamics: Recent Advances*, Elsevier Applied Science, London, 1990, pp. 3-21.
- 5) Myers, R. H. and Montgomery, D. C., *Response Surface Methodology: Process and Product Optimization Using Designed Experiments*, John Wiley & Sons, New York, 1995.
- 6) Seeman, G. R., "A Concept Study of a Remotely Piloted Vehicle for Mars Exploration," NASA CR 157942, 1978.
- 7) Murray, J. E. and Tartabini, P. V., "Development of a Mars Airplane Entry, Descent, and Flight Trajectory," AIAA Paper 2001-0839, 2001.
- 8) Haftka, R. T., Scott, E. P., and Cruz, J. R., "Optimization and Experiments: A Survey," *Applied Mechanics Reviews*, Vol. 51, No. 7, 1998, pp. 435-448.
- 9) Box, G. E. P. and Wilson, K. B., "On the Experimental Attainment of Optimum Conditions," *Journal of the Royal Statistical Society, Series B (Methodological)*, Vol. 13, No. 1, 1951, pp. 1-45.
- 10) Hill, W. J. and Hunter, W. G., "A Review of Response Surface Methodology: A Literature Survey," *Technometrics*, Vol. 8, No. 4, 1966, pp. 571-590.

- 11) Mead, R. and Pike, D. J., "A Review of Response Surface Methodology from a Biometric Viewpoint," *Biometrics*, Vol. 31, 1985, pp. 803-851.
- 12) Cornell, J. A., *How to Apply Response Surface Methodology*, 2nd edition, American Society for Quality Control, Milwaukee, 1990.
- 13) Fisher, R. A. and MacKenzie, W.A., "Studies in Crop Variations. II. The Manurial Response of Different Potato Varieties," *Journal of Agricultural Science*, Vol. 13, 1923, pp. 311-320.
- 14) Roy, R. K., *A Primer on the Taguchi Method*, Van Nostrand Reinhold, New York, 1990.
- 15) Walter, E. and Pronzato, L., "Qualitative and Quantitative Experiment Design for Phenomenological Models – A Survey," *Automatica*, Vol. 26, No. 2, 1990, pp. 195-213.
- 16) DeLoach, R., "Applications of Modern Experiment Design to Wind Tunnel Testing at NASA Langley Research Center," AIAA Paper 98-0713, 1998.
- 17) DeLoach, R., "Tailoring Wind Tunnel Data Volume Requirements Through the Formal Design of Experiments," AIAA Paper 98-2884, 1998.
- 18) DeLoach, R., "Improved Quality in Aerospace Testing Through the Modern Design of Experiments," AIAA Paper 2000-0825, 2000.
- 19) Landman, D., Simpson, J., Hall, B., and Sumner, T., "Use of Designed Experiments in Wind Tunnel Testing of Performance Automobiles," SAE Paper 2002-01-3313, 2002.
- 20) Landman, D., "Experimental Geometry Optimization Techniques for Multi-Element Airfoils," Ph.D. Dissertation, Old Dominion University, Norfolk, May 1998.
- 21) Stuckman, B. E., Care, M. C., and Stuckman, P. L., "System Optimization Using Experimental Evaluation of Design Performance," *Engineering Optimization*, Vol. 16, 1990, pp. 275-290.
- 22) Semones, G. B. and Lim, H. C., "Experimental Multivariable Adaptive Optimization of the Steady-State Cellular Productivity of a Continuous Baker's Yeast Culture," *Biotechnology and Bioengineering*, Vol. 33, No. 1, 1989, pp. 16-25.

- 23) Spendley, W., Hext, G. R., and Himsworth, F. R., "Sequential Application of Simplex Designs in Optimisation and Evolutionary Operation," *Technometrics*, Vol. 4, No. 4, 1962, pp. 441-461.
- 24) Hill, P. D. H., "A Review of Experimental Design Procedures for Regression Model Discrimination," *Technometrics*, Vol. 20, No. 1, 1978, pp. 15-21.
- 25) Hunter, W. G. and Reiner, A. M., "Designs for Discriminating Between Two Rival Models," *Technometrics*, Vol. 7, No. 3, 1965, pp. 307-323.
- 26) Froment, G. F., "Model Discrimination and Parameter Estimation in Heterogeneous Catalysis," *AIChE Journal*, Vol. 21, No. 6, 1975, pp. 1041-1057.
- 27) Box, G. E. P. and Hill, W. J., "Discrimination Among Mechanistic Models," *Technometrics*, Vol. 9, No. 1, 1967, pp. 57-71.
- 28) Schmid-Hempel, P., "Efficient Nectar-Collecting by Honeybees. I. Economic Models," *Journal of Animal Ecology*, Vol. 56, 1987, pp. 209-218.
- 29) Knopman, D. S. and Voss, C. I., "Discrimination Among One-Dimensional Models of Solute Transport in Porous Media: Implications for Sampling Design," *Water Resources Research*, Vol. 24, No. 11, 1988, pp. 1859-1876.
- 30) Eberhardt, L. L. and Thomas, J. M., "Designing Environmental Field Studies," *Ecological Monographs*, Vol. 61, No. 1, 1991, pp. 53-73.
- 31) Hunter, W. G. and Mezaki, R., "An Experimental Design Strategy for Distinguishing Among Rival Mechanistic Models. An Application to the Catalytic Hydrogenation of Propylene," *The Canadian Journal of Chemical Engineering*, Vol. 45, 1967, pp. 247-249.
- 32) Froment, G. F. and Mezaki, R., "Sequential Discrimination and Estimation Procedures for Rate Modeling in Heterogeneous Catalysis," *Chemical Engineering Science*, Vol. 25, 1970, pp. 292-301.
- 33) Pritchard, D. J. and Bacon, D. W., "Potential Pitfalls in Model Discrimination," *The Canadian Journal of Chemical Engineering*, Vol. 32, 1974, pp. 103-109.
- 34) Atkinson, A. C., "A Comparison of Two Criteria for the Design of Experiments for Discriminating Between Models," *Technometrics*, Vol. 23, No. 3, 1981, pp. 301-305.
- 35) Atkinson, A. C., "Planning Experiments to Detect Inadequate Regression Models," *Biometrika*, Vol. 52, No. 2, 1972, pp. 275-293.

- 36) Candas, B., Lalonde, J., and Normand, M., "A Model of the Distribution and Metabolism of Corticotropin-Releasing Factor," *American Journal of Physiology*, Vol. 254, No. 1, 1988, pp. E104-E112.
- 37) Wamelen, A. van, Haftka, R. T., and Johnson, E. R., "Optimal Layups for Composite Specimens to Accentuate the Differences Between Competing Failure Criteria," *Proceedings of the American Society for Composites, 8th Technical Conference*, Technomic, Lancaster, 1993, pp. 1045-1055.
- 38) "Validation of Computational Fluid Dynamics, Volume 1: Symposium Papers and Round Table Discussion," AGARD CP 437, 1988.
- 39) "Validation of Computational Fluid Dynamics, Volume 2: Poster Papers," AGARD CP 437, 1988.
- 40) Sacher, P. W., Bradley Jr., R. G., and Schmidt, W., "Technical Evaluation Report on the Fluid Dynamics Symposium on Validation of CFD," AGARD AR 257, 1989.
- 41) Bradley, R. G., "CFD Validation Philosophy," *Validation of Computational Fluid Dynamics, Volume 1: Symposium Papers and Round Table Discussion*, AGARD CP 437, 1988, pp. 1-1 – 1-6.
- 42) Marvin, J. G., "Accuracy Requirements and Benchmark Experiments for CFD Validation," *Validation of Computational Fluid Dynamics, Volume 1: Symposium Papers and Round Table Discussion*, AGARD CP 437, 1988, pp. 2-1 – 2-15.
- 43) Boerstoel, J. W., "Numerical Accuracy Assessment," *Validation of Computational Fluid Dynamics, Volume 1: Symposium Papers and Round Table Discussion*, AGARD CP 437, 1988, pp. 3-1 – 3-18.
- 44) Special Section on Computational Fluid Dynamics Simulations, *AIAA Journal*, Vol. 36, No. 5, 1998, pp. 665-764.
- 45) Roache, P. J., *Verification and Validation in Computational Science and Engineering*, Hermosa Publishers, Albuquerque, 1998.
- 46) *Guide for the Verification and Validation of Computational Fluid Dynamics Simulations*, AIAA, 1998.
- 47) Oberkampf, W. L., Trucano, T. G., and Hirsch, C., "Verification, Validation, and Predictive Capability in Computational Engineering and Physics," Sandia Report SAND2003-3769, 2003.

- 48) Oberkampf, W. L., "A Proposed Framework for Computational Fluid Dynamics Code Calibration/Validation," AIAA Paper No. 94-2540, 1994.
- 49) Blottner, F. G., "Accurate Navier-Stokes Results for the Hypersonic Flow over a Spherical Nosedip," *Journal of Spacecraft and Rockets*, Vol. 27, No. 2, 1990, pp. 113-122.
- 50) Boehm, B., *Software Engineering Economics*, Prentice-Hall, Englewood Cliffs, 1982.
- 51) Aeschliman, D. P., Oberkampf, W. L., and Blottner, F. G., "A Proposed Methodology for Computational Fluid Dynamics Code Verification, Calibration, and Validation," *Proceedings of the 16th International Congress on Instrumentation in Aerospace Simulation Facilities (ICIASF)*, 1995.
- 52) Aeschliman, D. P. and Oberkampf, W. L., "Experimental Methodology for Computational Fluid Dynamics Code Validation," *AIAA Journal*, Vol. 36, No. 5, 1998, pp. 733-741.
- 53) Roache, P. J., "Verification of Codes and Calculations," *AIAA Journal*, Vol. 36, No. 5, 1998, pp. 696-702.
- 54) McWherter Walker, M. and Oberkampf, W. L., "Joint Computational/Experimental Aerodynamics Research on a Hypersonic Vehicle, Part 2: Computational Results," *AIAA Journal*, Vol. 30, No. 8, 1992, pp. 2010-2016.
- 55) Melnik, R. E., Siclari, M. J., Barber, T., and Verhoff, A., "A Process for Industry Certification of Physical Simulation Codes," AIAA Paper 94-2235, 1994.
- 56) Fortier, M., "Validation of a User-Friendly CFD Code for Prediction of the Aerodynamic Characteristics of Flight Vehicles," *Validation of Computational Fluid Dynamics, Volume 2: Poster Papers*, AGARD CP 437, 1988, pp. 7-1 – 7-19.
- 57) "Experimental Data Base for Computer Program Assessment," AGARD AR 138, 1979.
- 58) "Experimental Data Base for Computers Program Assessment – Addendum," AGARD AR 138 Addendum, 1984.
- 59) "A Selection of Experimental Test Cases for the Validation of CFD Codes, Volume I," AGARD AR 303, 1994.
- 60) "A Selection of Experimental Test Cases for the Validation of CFD Codes, Volume II," AGARD AR 303, 1994.

- 61) Baltar, J. Y. and Tjonneland, E., "Slender Cone CFD and Experimental Data Comparisons in Hypersonic Flow," *Validation of Computational Fluid Dynamics, Volume 2: Poster Papers*, AGARD CP 437, 1988, pp. 6-1 – 6-14.
- 62) Bertin, J. J., Martelluci, A., Neumann, R. D., and Stetson, K. F., "Developing a Data Base for the Calibration and Validation of Hypersonic CFD Codes – Sharp Cones," AIAA Paper 93-3044, 1993.
- 63) Bobbitt, P. J., "The Pros and Cons of Code Validation," AIAA Paper 88-2535, 1988.
- 64) Marvin, J. G. and Holst, T. L., "CFD Validation for Aerodynamic Flows – Challenge for the '90's," AIAA Paper 90-2995, 1990.
- 65) "Quality Assessment for Wind Tunnel Testing," AGARD AR 304, 1994.
- 66) Coleman, H. W. and Stern, F., "Uncertainties and CFD Code Validation," *ASME Journal of Fluids Engineering*, Vol. 119, 1997, pp. 795-803.
- 67) Firmin, M. C. P. and McDonald, M. A., "The Design of the Garteur Low Aspect-Ratio Wing for Use in the Validation of Shear Layer and Overall Flow Prediction Methods," *Validation of Computational Fluid Dynamics, Volume 2: Poster Papers*, AGARD CP 437, 1988, pp. 5-1 – 5-17.
- 68) Cutler, A. D., Danehy, P. M., Springer, R. R., DeLoach, R., and Capriotti, D. P., "CARS Thermometry in a Supersonic Combustor for CFD Code Validation," AIAA Paper 2002-0743, 2002.
- 69) Drela, M. and Giles, M. B., "ISES: A Two-Dimensional Viscous Aerodynamic Design and Analysis Code," AIAA Paper 87-0424, 1987.
- 70) Giles, M. B. and Drela, M., "Two-Dimensional Transonic Aerodynamic Design Method," *AIAA Journal*, Vol. 25, No. 9, 1987, pp. 1199-1206.
- 71) Drela, M. and Giles, M. B., "Viscous-Inviscid Analysis of Transonic and Low Reynolds Number Airfoils," *AIAA Journal*, Vol. 25, No. 10, 1987, pp. 1347-1355.
- 72) Mack, L. M., "Transition Prediction and Linear Stability Theory," *AGARD Conference Proceedings No. 224, Laminar-Turbulence Transition*, AGARD-CP-224, NATO Advisory Group for Aerospace Research and Development, 1977, pp. 1-1 – 1-22.
- 73) Mack, L. M., "Transition and Laminar Instability," NASA CP 153203, 1977.

- 74) Drela, M., "Low-Reynolds-Number Airfoil Design for the M.I.T. Daedalus Prototype: A Case Study," *Journal of Aircraft*, Vol. 25, No. 8, 1988, pp. 724-732.
- 75) Drela, M., "Transonic Low-Reynolds Number Airfoils," *Journal of Aircraft*, Vol. 29, No. 6, 1992, pp. 1106-1113.
- 76) Greer, D., Hamory, P., Krake, K., and Drela, M., "Design and Predictions of High-Altitude (Low Reynolds Number) Aerodynamic Flight Experiment," *Journal of Aircraft*, Vol. 37, No. 4, 2000, pp. 684-689.
- 77) McDevitt, J. B., Levy, L. L., and Deiwert, G. S., "Transonic Flow About a Thick Circular-Arc Airfoil," *AIAA Journal*, Vol. 14, No. 5, 1976, pp. 606-613.
- 78) Levy, L. L., "Experimental and Computational Steady and Unsteady Transonic Flows About a Thick Airfoil," *AIAA Journal*, Vol. 16, No. 6, 1978, pp. 564-572.
- 79) Vander Kam, J. C., "Reduced-Order High-Fidelity Methodologies for the Design of Civil Transport High-Lift Systems," M.S. Thesis, University of California, Davis, 2000.
- 80) Paris, J. K., "Advancements in the Design Methodology for Multi-Element High-Lift Systems on Subsonic Civil Transport Aircraft," M.S. Thesis, University of California, Davis, 1998.
- 81) Weissinger, J., "The Lift Distribution of Swept-Back Wings," NACA TM 1120, 1947.
- 82) Anderson Jr., J. D., Corda, S., and Van Wie, D. M., "Numerical Lifting Line Theory Applied to Drooped Leading-Edge Wings Below and Above Stall," *Journal of Aircraft*, Vol. 17, No. 12, 1980, pp. 898-904.
- 83) Sears, W. R., "Some Recent Developments in Airfoil Theory," *Journal of the Aeronautical Sciences*, Vol. 23, No. 5, 1956, pp. 490-499.
- 84) Raznjevic, K., *Handbook of Thermodynamic Tables and Charts*, Hemisphere Publishing, Washington, 1976.
- 85) Jordan, D. P. and Mintz, M. D., *Air Tables*, McGraw-Hill, New York, 1965.
- 86) Sychev, V. V., Vasserman, A. A., Kozlov, A. D., Spiridonov, G. A., and Tsymarny, V. A., *Thermodynamic Properties of Air*, Hemisphere Publishing, Washington, 1987.
- 87) Division Scientifique, *Gas Encyclopaedia*, Elsevier Scientific Publishing, 1976.

- 88) Avallone, E. A. and Baumeister III, T. (Editors), *Marks' Standard Handbook for Mechanical Engineers*, Ninth Edition, McGraw-Hill, 1987.
- 89) Lide, D. R. (Editor-in-Chief), *CRC Handbook of Chemistry and Physics*, 81st Edition, CRC Press, Boca Raton, 2000.
- 90) White, F. M., *Viscous Fluid Flow*, 2nd, McGraw-Hill, New York, 1991.
- 91) *JMP[®] Statistics and Graphics Guide*, Version 3.1, SAS Institute, Cary, 1995.
- 92) "Wind-Tunnel Model Systems Criteria," NASA Langley Research Center, LAPG 1710.15, May 1992.
- 93) Shekoski, T. L., "Analysis of LaRC Mars Airplane Test Wing," Advanced Technologies Incorporated Report for NASA Model No. RBL-00-0134, September 2000.
- 94) Aeroelasticity Branch Staff, "The Langley Transonic Dynamics Tunnel," Langley Working Paper LWP-799, 1969.
- 95) Reinsch, C. H., "Smoothing by Spline Functions," *Numerische Mathematik*, Vol. 10, 1967, pp. 177-183.
- 96) Eubank, R. L., *Spline Smoothing and Nonparametric Regression*, Marcel Dekker, New York, 1988.
- 97) Coleman, H. W. and Steele, W. G., *Experimentation and Uncertainty Analysis for Engineers*, John Wiley & Sons, New York, 1989.

Appendix A: Wind Tunnel Turbulence and N_{crit}

Wind tunnel turbulence can be characterized by the turbulence intensity, TI . Turbulence intensity for the Transonic Dynamics Tunnel was measured by Catherine M. McGinley of the NASA Langley Research Center at the conditions of interest for the present investigation during the summer of 1999.¹ Figure A.1 shows the Mach and Reynolds numbers combinations for which these data are available, and an outline of the test design space for the testing conducted during the present investigation (see chapter 4, section 4.2 for details of the test design space definition). In the calculation of Reynolds number, a reference length of 0.087503 m (3.445 in) was used. This reference length is equal to the nominal chord length of the wind tunnel model (see chapter 5, section 5.1 for details on the wind tunnel model). For values of $TI > 0.001$, Mack [72, 73] shows that the boundary layer transition parameter, N_{crit} , can be related to TI by:

$$N_{crit} = -8.43 - 2.4 \ln(TI) \quad (A.1)$$

This relationship was derived for incompressible flows based on data from flat plate transition data. Although in the present investigation transonic Mach numbers are considered, equation A.1 is nonetheless used to determine N_{crit} . The use of this method to determine N_{crit} is consistent with the boundary layer transition criterion implemented in MSES [75].

The turbulence intensity data, and the values of N_{crit} calculated from it are given in Table A.1. From these data a response surface relating N_{crit} to M and Re over the test design space was generated. A response surface of the form:

$$N_{crit\ RS}(M, Re) = b_0 + b_M M + b_{Re} Re + b_{MRe} MRe + b_{Re^2} Re^2 \quad (A.2)$$

was found to yield an adequate fit to the data (the values of the coefficients are given in Table A.2). This response surface was used to generate the values of N_{crit} used in the two-dimensional airfoil analyses. A comparison between the values of N_{crit} calculated from the experimental TI data using equation A.1 and the values calculated from the response surface are given in Table A.3. This comparison includes the upper and lower

¹ These data have not been previously published.

95% confidence envelope of the mean for the value of N_{crit} calculated from the response surface. Note that this confidence envelope only includes precision (i.e., random) uncertainty. Bias (i.e., systematic) uncertainty was not available and is not included in the confidence interval. The sensitivity of C_{Lmax} results to the value of N_{crit} is discussed in chapter 3, section 3.4.

Table A.1 – Turbulence intensity data and calculated values of N_{crit}

M	Re	TI	N_{crit}
0.249	439,179	0.00312	5.419
0.298	105,480	0.00273	5.741
0.247	88,005	0.00291	5.589
0.696	225,691	0.00347	5.163
0.599	201,296	0.00338	5.229
0.499	172,860	0.00318	5.371
0.399	141,757	0.00303	5.485
0.302	38,524	0.00440	4.595
0.247	31,952	0.00437	4.608
0.703	87,110	0.00503	4.274
0.600	77,346	0.00490	4.334
0.501	66,727	0.00467	4.449
0.400	54,559	0.00416	4.729
0.294	26,453	0.00478	4.395
0.244	22,332	0.00510	4.240
0.700	62,934	0.00421	4.699
0.601	56,297	0.00420	4.705
0.498	48,217	0.00426	4.671
0.400	40,005	0.00466	4.457

Notes:

- 1) Re based on reference length of 0.08750 m (3.445 in)
- 2) N_{crit} calculated from equation A.1

Table A.2 – Values of the coefficients in the response surface for N_{crit}

b_0	4.21364
b_M	-8.44595×10^{-1}
b_{Re}	2.15901×10^{-5}
b_{MRe}	$-0.1.09410 \times 10^{-5}$
b_{Re^2}	-3.55622×10^{-11}

Table A.3 – Comparison of N_{crit} values

M	Re	N_{crit} from Experimental Data and Equation A.1	Response Surface N_{crit}	Response Surface N_{crit} Lower Mean 95% Confidence Envelope	Response Surface N_{crit} Upper Mean 95% Confidence Envelope
0.249	439,179	5.419	5.430	4.956	5.903
0.298	105,480	5.741	5.500	5.252	5.747
0.247	88,005	5.589	5.393	5.155	5.631
0.696	225,691	5.163	4.968	4.572	5.364
0.599	201,296	5.229	5.292	5.044	5.541
0.499	172,860	5.371	5.518	5.298	5.738
0.399	141,757	5.485	5.605	5.354	5.855
0.302	38,524	4.595	4.610	4.436	4.784
0.247	31,952	4.608	4.573	4.353	4.792
0.703	87,110	4.274	4.561	4.341	4.781
0.600	77,346	4.334	4.656	4.485	4.828
0.501	66,727	4.449	4.707	4.570	4.843
0.400	54,559	4.729	4.710	4.582	4.837
0.294	26,453	4.395	4.426	4.216	4.637
0.244	22,332	4.240	4.412	4.160	4.664
0.700	62,934	4.699	4.358	4.103	4.613
0.601	56,297	4.705	4.439	4.239	4.638
0.498	48,217	4.671	4.488	4.333	4.644
0.400	40,005	4.457	4.507	4.360	4.655

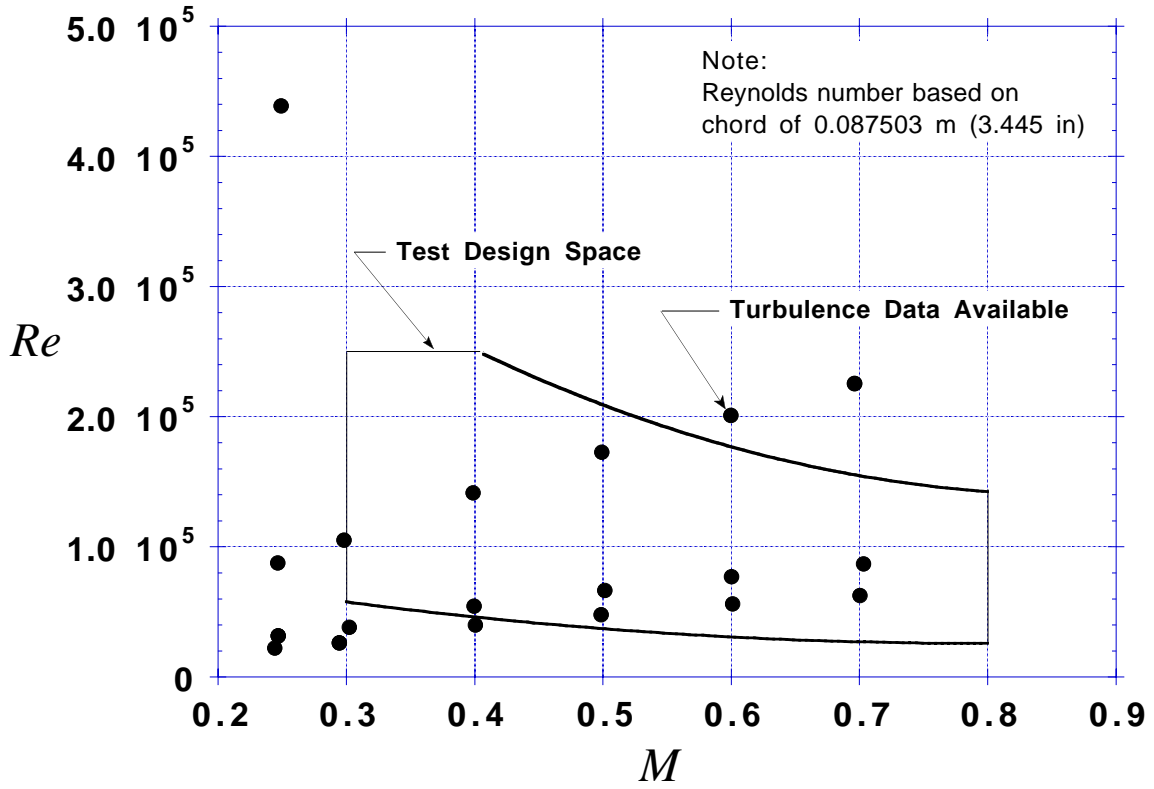


Figure A.1 – Available turbulence data and test design space

Appendix B: MASC1 Airfoil Nondimensional Coordinates

Table B.1 – MASC1 airfoil nondimensional coordinates

Original Coordinates (Zero Trailing Edge Thickness): t/c_{max} 0.071 at $x/c = 0.28$ Max Camber 3.7% at $x/c = 0.63$
 Finite Trailing Edge Thickness Coordinates: 0.073 at $x/c = 0.31$ 3.7% at $x/c = 0.63$

Original Coordinates (Zero Trailing Edge Thickness)		Finite Trailing Edge Thickness Coordinates	
x/c	y/c	x/c	y/c
1.0000000	0.0000000	1.0000000	0.0029028
0.9989160	0.0003326	0.9989159	0.0032322
0.9956651	0.0013063	0.9956651	0.0041964
0.9902691	0.0028753	0.9902691	0.0057498
0.9827499	0.0049977	0.9827499	0.0078504
0.9731494	0.0076274	0.9731494	0.0104522
0.9614891	0.0107279	0.9614891	0.0135188
0.9478421	0.0142250	0.9478421	0.0169763
0.9322513	0.0180485	0.9322513	0.0207546
0.9148004	0.0221142	0.9148004	0.0247696
0.8955730	0.0263357	0.8955730	0.0289354
0.8746324	0.0306319	0.8746324	0.0331707
0.8520823	0.0349154	0.8520824	0.0373888
0.8280262	0.0391049	0.8280262	0.0415084
0.8025672	0.0431266	0.8025672	0.0454562
0.7758179	0.0469139	0.7758179	0.0491660
0.7478808	0.0504126	0.7478808	0.0525835
0.7188879	0.0535754	0.7188879	0.0556621
0.6889706	0.0563668	0.6889706	0.0583667
0.6582499	0.0587634	0.6582499	0.0606741
0.6268563	0.0607508	0.6268563	0.0625705
0.5949302	0.0623230	0.5949302	0.0640499
0.5625915	0.0634824	0.5625915	0.0651155
0.5299998	0.0642356	0.5299998	0.0657741
0.4972847	0.0645949	0.4972847	0.0660384

0.4645855	0.0645752	0.4645855	0.0659238
0.4320416	0.0641932	0.4320416	0.0654473
0.3997822	0.0634661	0.3997822	0.0646266
0.3679665	0.0624118	0.3679665	0.0634800
0.3367139	0.0610467	0.3367139	0.0620241
0.3061636	0.0593872	0.3061636	0.0602759
0.2764451	0.0574492	0.2764451	0.0582516
0.2476776	0.0552487	0.2476776	0.0559677
0.2199903	0.0528047	0.2199903	0.0534433
0.1935123	0.0501406	0.1935123	0.0507024
0.1683427	0.0472777	0.1683426	0.0477664
0.1445910	0.0442232	0.1445910	0.0446429
0.1223571	0.0409875	0.1223571	0.0413426
0.1017400	0.0375871	0.1017400	0.0378824
0.0828389	0.0340458	0.0828389	0.0342862
0.0657126	0.0303878	0.0657126	0.0305785
0.0504398	0.0266483	0.0504398	0.0267947
0.0370987	0.0228695	0.0370987	0.0229772
0.0257278	0.0190843	0.0257278	0.0191590
0.0163955	0.0153317	0.0163955	0.0153793
0.0091222	0.0116044	0.0091222	0.0116308
0.0039483	0.0078921	0.0039482	0.0079035
0.0008966	0.0041245	0.0008966	0.0041271
0.0000000	0.0000000	0.0000000	0.0000000
0.0013023	-0.0055274	0.0013024	-0.0055311
0.0046455	-0.0086959	0.0046455	-0.0087094
0.0100751	-0.0110646	0.0100751	-0.0110938
0.0175905	-0.0130959	0.0175905	-0.0131469
0.0271559	-0.0148902	0.0271559	-0.0149690
0.0387521	-0.0164653	0.0387521	-0.0165778
0.0523084	-0.0178032	0.0523084	-0.0179550
0.0677834	-0.0188734	0.0677834	-0.0190701
0.0850958	-0.0196440	0.0850958	-0.0198910
0.1041646	-0.0200918	0.1041646	-0.0203941
0.1249292	-0.0202025	0.1249292	-0.0205652
0.1472895	-0.0199711	0.1472895	-0.0203986
0.1711455	-0.0194000	0.1711455	-0.0198968
0.1963976	-0.0184979	0.1963976	-0.0190680
0.2229364	-0.0172801	0.2229364	-0.0179272
0.2506624	-0.0157564	0.2506624	-0.0164840
0.2794462	-0.0139447	0.2794462	-0.0147558
0.3091590	-0.0118700	0.3091590	-0.0127674
0.3396821	-0.0095644	0.3396821	-0.0105505
0.3708871	-0.0070673	0.3708871	-0.0081439
0.4026360	-0.0044255	0.4026360	-0.0055943

0.4348110	-0.0016884	0.4348110	-0.0029506
0.4672543	0.0010865	0.4672543	-0.0002699
0.4998386	0.0038405	0.4998386	0.0023896
0.5324263	0.0065109	0.5324263	0.0049654
0.5648803	0.0090333	0.5648803	0.0073936
0.5970731	0.0113436	0.5970731	0.0096104
0.6288477	0.0133780	0.6288477	0.0115525
0.6600861	0.0150808	0.6600861	0.0131647
0.6906505	0.0164036	0.6906505	0.0143988
0.7204123	0.0173107	0.7204123	0.0152196
0.7492525	0.0177820	0.7492525	0.0156070
0.7770411	0.0178144	0.7770411	0.0155588
0.8036476	0.0174232	0.8036476	0.0150904
0.8289704	0.0166420	0.8289704	0.0142356
0.8528976	0.0155211	0.8528976	0.0130454
0.8753263	0.0141231	0.8753263	0.0115822
0.8961538	0.0125188	0.8961538	0.0099174
0.9152766	0.0107856	0.9152765	0.0081288
0.9326317	0.0089973	0.9326317	0.0062901
0.9481363	0.0072265	0.9481363	0.0044743
0.9617071	0.0055419	0.9617071	0.0027503
0.9733017	0.0040019	0.9733017	0.0011767
0.9828480	0.0026640	0.9828480	-0.0001890
0.9903245	0.0015579	0.9903245	-0.0013168
0.9956898	0.0007191	0.9956898	-0.0021711
0.9989222	0.0001846	0.9989222	-0.0027150
1.0000000	0.0000000	1.0000000	-0.0029028

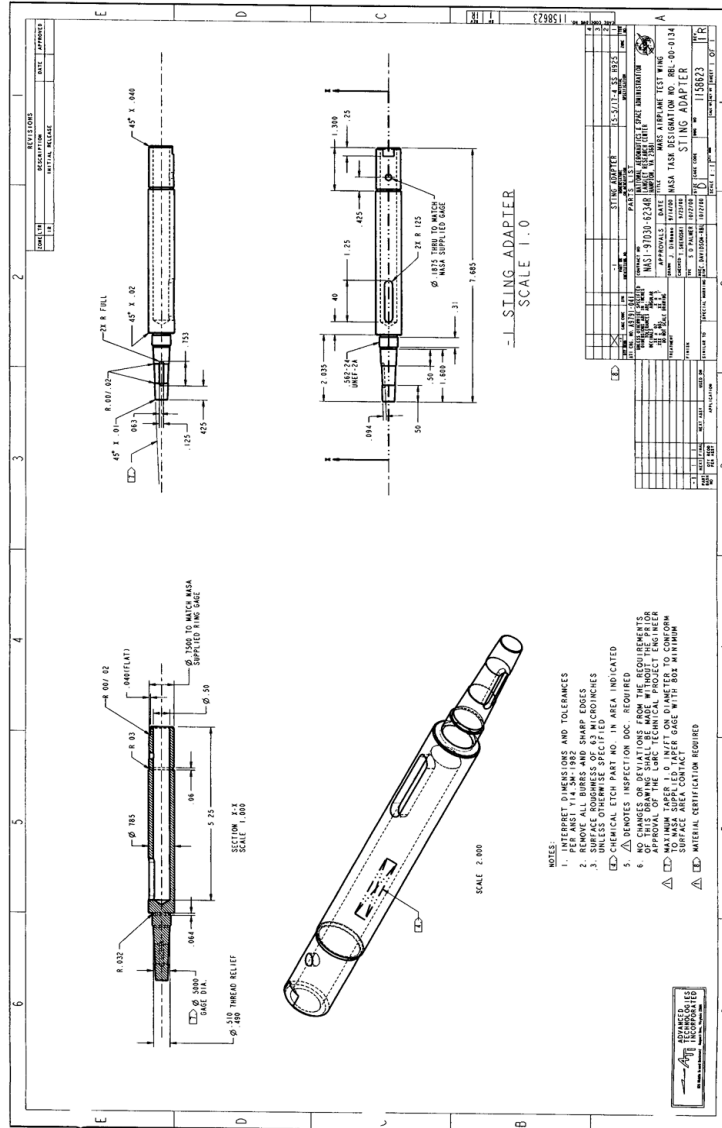


Figure C.4 - Drawing 1158623, sting adapter

Appendix D: Experimental Data and Analyses Results

Table D.1 – Data from Run 10; nominal conditions $M = 0.800$, $Re = 70,000$

Tab Pt.	M	Re	q_{norm} (Pa)	q_{norm} (psf)	α (deg.)	C_L	C_D	C_M	L/D
241	0.801	68355	1689.7	35.29	-4.20	-0.303	0.0673	-0.0079	-4.50
242	0.802	68514	1694.1	35.38	-0.21	0.089	0.0377	-0.0859	2.37
243	0.801	68507	1692.9	35.36	0.85	0.200	0.0394	-0.0986	5.07
244	0.799	68544	1691.6	35.33	1.82	0.303	0.0441	-0.1104	6.88
245	0.803	68821	1704.2	35.59	2.83	0.396	0.0517	-0.1223	7.66
246	0.802	68857	1702.9	35.57	3.91	0.486	0.0627	-0.1337	7.75
247	0.799	68801	1697.6	35.46	4.82	0.549	0.0748	-0.1420	7.34
248	0.800	68876	1700.5	35.52	5.82	0.609	0.0894	-0.1515	6.81
249	0.801	69007	1705.7	35.62	6.81	0.662	0.1060	-0.1618	6.25
250	0.801	69106	1708.4	35.68	7.29	0.685	0.1143	-0.1651	5.99
251	0.799	69062	1703.8	35.59	7.81	0.712	0.1243	-0.1712	5.73
252	0.801	69248	1711.7	35.75	8.30	0.733	0.1339	-0.1752	5.47
253	0.803	69365	1716.6	35.85	8.83	0.752	0.1436	-0.1782	5.24
254	0.803	69422	1718.4	35.89	9.30	0.768	0.1524	-0.1806	5.04
255	0.802	69411	1716.9	35.86	9.80	0.785	0.1622	-0.1841	4.84
256	0.800	69404	1714.3	35.80	10.31	0.801	0.1730	-0.1871	4.63
257	0.801	69508	1717.3	35.87	10.80	0.811	0.1820	-0.1884	4.46
258	0.801	69567	1719.5	35.91	11.30	0.818	0.1906	-0.1892	4.29
259	0.802	69701	1724.7	36.02	11.80	0.827	0.2005	-0.1913	4.13
260	0.802	69745	1725.7	36.04	12.30	0.834	0.2095	-0.1924	3.98
261	0.800	69709	1721.7	35.96	12.81	0.842	0.2192	-0.1930	3.84
262	0.801	69776	1723.9	36.00	13.30	0.848	0.2289	-0.1939	3.70
263	0.802	69897	1728.7	36.11	13.80	0.853	0.2379	-0.1950	3.59
264	0.802	70007	1732.1	36.18	14.32	0.856	0.2469	-0.1964	3.47
265	0.803	70100	1735.9	36.26	14.79	0.861	0.2564	-0.1967	3.36
266	0.800	70015	1729.1	36.11	15.31	0.869	0.2670	-0.1978	3.25
267	0.801	70148	1734.0	36.22	15.79	0.872	0.2757	-0.1988	3.16
268	0.800	70165	1732.4	36.18	16.81	0.883	0.2961	-0.2012	2.98
269	0.800	70294	1736.2	36.26	17.80	0.892	0.3152	-0.2042	2.83
270	0.802	70439	1742.1	36.38	18.80	0.901	0.3351	-0.2055	2.69
271	0.803	70562	1746.7	36.48	19.81	0.910	0.3558	-0.2080	2.56
272	0.800	70604	1743.6	36.42	20.81	0.923	0.3782	-0.2110	2.44
274	0.801	70747	1748.6	36.52	21.81	0.929	0.3988	-0.2134	2.33
275	0.800	70764	1747.6	36.50	22.80	0.939	0.4213	-0.2156	2.23
276	0.797	70709	1741.8	36.38	23.82	0.949	0.4456	-0.2193	2.13

Table D.2 – Data from Run 11; nominal conditions $M = 0.300$, $Re = 59,140$

Tab Pt.	M	Re	q_{norm} (Pa)	q_{norm} (psf)	α (deg.)	C_L	C_D	C_M	L/D
280	0.302	58230	619.7	12.94	-4.20	-0.069	0.0288	-0.0925	-2.38
281	0.302	58360	621.6	12.98	-0.20	0.182	0.0261	-0.0865	6.99
282	0.302	58394	622.1	12.99	0.80	0.265	0.0282	-0.0974	9.40
283	0.299	57870	610.7	12.75	1.80	0.345	0.0337	-0.1054	10.26
284	0.302	58402	621.7	12.98	2.80	0.411	0.0389	-0.1060	10.57
285	0.302	58443	622.2	12.99	3.81	0.482	0.0439	-0.1078	10.99
286	0.302	58442	621.8	12.99	4.80	0.575	0.0515	-0.1133	11.18
287	0.300	58054	613.1	12.81	5.81	0.691	0.0612	-0.1230	11.29
288	0.302	58474	621.8	12.99	6.80	0.768	0.0693	-0.1245	11.09
289	0.302	58574	623.7	13.03	7.29	0.793	0.0733	-0.1222	10.81
290	0.302	58567	623.2	13.02	7.80	0.817	0.0800	-0.1208	10.22
291	0.299	58132	613.6	12.82	7.81	0.830	0.0814	-0.1204	10.20
292	0.299	58035	611.4	12.77	7.81	0.835	0.0820	-0.1236	10.19
293	0.301	58547	622.0	12.99	7.81	0.821	0.0806	-0.1198	10.19
294	0.302	58640	623.7	13.03	7.81	0.820	0.0806	-0.1221	10.18
295	0.299	58250	614.6	12.84	7.81	0.831	0.0816	-0.1218	10.19
296	0.300	58512	618.0	12.91	8.31	0.854	0.0867	-0.1190	9.85
297	0.302	58991	628.0	13.12	8.79	0.866	0.0925	-0.1166	9.36
298	0.302	58906	626.1	13.08	9.30	0.891	0.0985	-0.1141	9.05
299	0.302	59027	628.4	13.12	9.80	0.910	0.1076	-0.1131	8.45
300	0.301	58789	622.9	13.01	10.31	0.938	0.1164	-0.1122	8.06
301	0.299	58560	617.9	12.90	10.80	0.962	0.1282	-0.1160	7.50
302	0.302	59040	627.9	13.11	11.32	0.951	0.1352	-0.1192	7.03
303	0.300	58719	620.2	12.95	11.30	0.966	0.1373	-0.1199	7.04
304	0.299	58676	619.1	12.93	11.42	0.963	0.1405	-0.1212	6.86
305	0.302	59167	629.2	13.14	11.53	0.947	0.1358	-0.1235	6.97
306	0.302	59152	628.7	13.13	11.56	0.938	0.1345	-0.1219	6.98
307	0.302	59228	630.1	13.16	11.64	0.942	0.1346	-0.1232	6.99
308	0.299	58752	619.6	12.94	11.71	0.956	0.1339	-0.1297	7.14
309	0.300	58915	622.8	13.01	11.80	0.951	0.1346	-0.1317	7.07

Table D.3 – Data from Run 12; nominal conditions $M = 0.300$, $Re = 59,140$

Tab Pt.	M	Re	q_{norm} (Pa)	q_{norm} (psf)	α (deg.)	C_L	C_D	C_M	L/D
317	0.301	58683	622.4	13.00	-4.20	-0.076	0.0292	-0.0874	-2.59
318	0.298	58249	612.8	12.80	-3.21	-0.004	0.0261	-0.0918	-0.17
319	0.301	58792	624.2	13.04	-2.21	0.056	0.0249	-0.0870	2.24
320	0.301	58796	624.1	13.03	-1.21	0.116	0.0262	-0.0856	4.41
321	0.302	58891	626.0	13.07	-0.20	0.179	0.0258	-0.0869	6.93
322	0.301	58770	623.2	13.02	0.80	0.261	0.0281	-0.0951	9.29
323	0.299	58404	615.0	12.84	1.79	0.340	0.0332	-0.1034	10.25
324	0.298	58340	613.5	12.81	2.81	0.410	0.0391	-0.1058	10.46
325	0.301	58941	626.3	13.08	3.80	0.476	0.0432	-0.1064	11.01
326	0.301	58933	625.8	13.07	4.81	0.570	0.0511	-0.1123	11.16
327	0.301	58916	625.4	13.06	5.82	0.676	0.0599	-0.1202	11.28
328	0.301	58992	626.7	13.09	6.81	0.758	0.0684	-0.1216	11.08
329	0.299	58492	615.8	12.86	7.82	0.827	0.0813	-0.1218	10.17
330	0.301	58898	624.3	13.04	8.29	0.838	0.0845	-0.1167	9.92
331	0.301	58995	626.2	13.08	8.80	0.859	0.0916	-0.1132	9.38
332	0.301	58956	625.2	13.06	9.33	0.887	0.0982	-0.1125	9.03
333	0.301	59033	626.6	13.09	9.80	0.907	0.1070	-0.1150	8.47
334	0.298	58594	616.6	12.88	10.31	0.940	0.1163	-0.1129	8.08
335	0.301	59139	628.0	13.12	10.79	0.940	0.1250	-0.1113	7.53
336	0.301	59075	626.6	13.09	10.79	0.942	0.1252	-0.1127	7.52
337	0.301	59172	628.5	13.13	10.79	0.940	0.1249	-0.1123	7.53
338	0.301	59110	627.0	13.09	11.04	0.947	0.1300	-0.1133	7.28
339	0.298	58642	616.9	12.88	11.04	0.962	0.1322	-0.1163	7.28
340	0.298	58652	616.9	12.88	11.04	0.960	0.1318	-0.1142	7.28
341	0.300	58915	622.4	13.00	11.37	0.955	0.1346	-0.1208	7.10
342	0.301	59117	626.5	13.09	11.37	0.949	0.1337	-0.1194	7.10
343	0.301	59118	626.5	13.09	11.37	0.943	0.1344	-0.1168	7.02
344	0.300	59085	625.6	13.07	11.40	0.952	0.1366	-0.1215	6.97
345	0.301	59132	626.5	13.09	11.40	0.952	0.1367	-0.1201	6.96
346	0.301	59249	628.8	13.13	11.40	0.946	0.1377	-0.1174	6.87
347	0.301	59168	627.0	13.09	11.48	0.941	0.1337	-0.1192	7.03
348	0.299	58838	619.7	12.94	11.48	0.955	0.1361	-0.1226	7.02
349	0.298	58776	618.3	12.91	11.48	0.947	0.1226	-0.1238	7.72
350	0.301	59361	630.5	13.17	11.60	0.943	0.1307	-0.1268	7.22
351	0.301	59267	628.3	13.12	11.60	0.933	0.1245	-0.1220	7.49

Table D.4 – Data from Run 14; nominal conditions $M = 0.800$, $Re = 141,000$

Tab Pt.	M	Re	q_{norm} (Pa)	q_{norm} (psf)	α (deg.)	C_L	C_D	C_M	L/D
399	0.797	139808	3443.0	71.91	-4.25	-0.297	0.0625	-0.0219	-4.76
400	0.801	140343	3469.1	72.45	-3.24	-0.216	0.0507	-0.0438	-4.26
401	0.802	140431	3472.2	72.52	-2.23	-0.080	0.0404	-0.0793	-1.97
402	0.801	140432	3470.0	72.47	-1.24	0.073	0.0362	-0.1146	2.02
403	0.801	140531	3473.5	72.55	-0.23	0.206	0.0378	-0.1340	5.44
404	0.803	140768	3484.7	72.78	0.79	0.307	0.0422	-0.1411	7.27
405	0.802	140752	3481.9	72.72	1.80	0.395	0.0483	-0.1451	8.17
406	0.802	140730	3479.6	72.67	2.78	0.464	0.0547	-0.1452	8.48
407	0.801	140711	3477.0	72.62	3.82	0.552	0.0653	-0.1546	8.46
408	0.802	140863	3483.2	72.75	4.80	0.643	0.0769	-0.1645	8.36
409	0.802	140881	3483.3	72.75	5.81	0.722	0.0916	-0.1724	7.89
410	0.802	141030	3488.3	72.85	6.78	0.783	0.1081	-0.1783	7.25
411	0.800	140928	3480.8	72.70	7.26	0.810	0.1170	-0.1812	6.92
412	0.801	141066	3486.8	72.82	7.76	0.829	0.1259	-0.1826	6.59
413	0.801	141082	3486.5	72.82	8.25	0.845	0.1345	-0.1828	6.28
414	0.801	141155	3488.3	72.85	8.87	0.861	0.1460	-0.1839	5.89
415	0.800	141138	3485.4	72.79	9.26	0.871	0.1539	-0.1859	5.66
416	0.801	141282	3491.5	72.92	9.72	0.878	0.1623	-0.1864	5.41
417	0.800	141337	3490.4	72.90	10.26	0.885	0.1720	-0.1884	5.15
418	0.801	141404	3493.8	72.97	10.26	0.885	0.1726	-0.1888	5.13
419	0.799	141272	3486.0	72.81	10.26	0.887	0.1727	-0.1892	5.14
420	0.801	141523	3496.5	73.03	10.75	0.887	0.1788	-0.1891	4.96
421	0.800	141505	3495.3	73.00	10.75	0.887	0.1802	-0.1893	4.92
422	0.800	141502	3494.6	72.99	10.75	0.889	0.1810	-0.1897	4.91

Table D.5 – Data from Run 15; nominal conditions $M = 0.407$, $Re = 250,712$

Tab Pt.	M	Re	q_{norm} (Pa)	q_{norm} (psf)	α (deg.)	C_L	C_D	C_M	L/D
438	0.407	250202	3523.9	73.60	-4.22	-0.021	0.0201	-0.1134	-1.06
439	0.407	250194	3523.5	73.59	-3.25	0.065	0.0188	-0.1201	3.48
440	0.407	250258	3525.2	73.63	-2.24	0.156	0.0185	-0.1269	8.45
441	0.407	250120	3520.7	73.53	-1.21	0.241	0.0205	-0.1320	11.72
442	0.407	250260	3524.8	73.62	-0.20	0.319	0.0236	-0.1347	13.53
443	0.408	250582	3533.5	73.80	0.80	0.395	0.0277	-0.1378	14.23
444	0.408	250617	3534.4	73.82	1.81	0.475	0.0328	-0.1401	14.48
445	0.408	250430	3529.2	73.71	2.80	0.569	0.0382	-0.1453	14.88
446	0.407	250406	3528.0	73.68	3.79	0.663	0.0441	-0.1505	15.05
447	0.407	250129	3519.6	73.51	4.82	0.742	0.0514	-0.1481	14.44
448	0.407	250368	3526.3	73.65	5.79	0.792	0.0587	-0.1410	13.49
449	0.407	250420	3528.1	73.69	6.82	0.844	0.0679	-0.1343	12.43
450	0.408	250580	3532.0	73.77	7.27	0.868	0.0723	-0.1317	12.01
451	0.407	250405	3526.8	73.66	7.80	0.898	0.0783	-0.1298	11.46
452	0.407	250520	3529.5	73.71	8.31	0.925	0.0843	-0.1275	10.97
453	0.407	250255	3521.7	73.55	8.89	0.958	0.0927	-0.1256	10.34
454	0.407	250596	3530.4	73.73	9.28	0.975	0.0984	-0.1246	9.91
455	0.407	250532	3528.7	73.70	9.79	1.000	0.1076	-0.1237	9.29
457	0.407	250627	3530.8	73.74	9.79	1.001	0.1078	-0.1241	9.28
458	0.408	250726	3533.6	73.80	9.80	1.000	0.1080	-0.1241	9.27
459	0.408	250844	3536.2	73.86	9.91	1.005	0.1100	-0.1242	9.13
460	0.408	250805	3535.1	73.83	9.91	1.005	0.1100	-0.1238	9.13
461	0.407	250591	3529.0	73.70	9.91	1.006	0.1102	-0.1244	9.14
462	0.407	250449	3524.2	73.61	10.03	1.012	0.1132	-0.1246	8.94
463	0.407	250241	3518.6	73.49	10.02	1.013	0.1131	-0.1248	8.96
464	0.407	250707	3531.6	73.76	10.02	1.009	0.1127	-0.1245	8.96
465	0.407	250763	3532.5	73.78	10.08	1.010	0.1139	-0.1247	8.87
466	0.407	250712	3531.7	73.76	10.08	1.012	0.1142	-0.1251	8.86
467	0.407	250814	3534.3	73.82	10.08	1.012	0.1142	-0.1251	8.86

Table D.6 – Data from Run 16; nominal conditions $M = 0.301$, $Re = 249,123$

Tab Pt.	M	Re	q_{norm} (Pa)	q_{norm} (psf)	α (deg.)	C_L	C_D	C_M	L/D
469	0.301	248996	2643.5	55.21	-4.21	-0.009	0.0187	-0.1124	-0.47
470	0.301	249080	2644.9	55.24	-3.18	0.079	0.0176	-0.1186	4.51
471	0.301	248798	2638.5	55.11	-2.20	0.165	0.0181	-0.1255	9.12
472	0.301	249249	2648.0	55.31	-1.18	0.249	0.0197	-0.1295	12.59
473	0.302	249586	2654.8	55.45	-0.13	0.332	0.0229	-0.1335	14.51
474	0.301	249212	2646.7	55.28	0.81	0.405	0.0266	-0.1372	15.26
475	0.301	249258	2647.5	55.29	1.86	0.489	0.0319	-0.1409	15.32
476	0.301	248731	2635.8	55.05	2.84	0.578	0.0371	-0.1453	15.56
477	0.301	249223	2646.2	55.27	3.80	0.653	0.0425	-0.1453	15.37
478	0.302	249456	2651.3	55.37	4.81	0.724	0.0484	-0.1428	14.95
479	0.301	249388	2649.7	55.34	5.81	0.777	0.0562	-0.1370	13.82
480	0.301	249422	2650.2	55.35	6.81	0.829	0.0649	-0.1316	12.78
481	0.301	248937	2639.3	55.12	7.31	0.859	0.0706	-0.1303	12.18
482	0.302	249558	2652.4	55.40	7.82	0.884	0.0755	-0.1279	11.70
483	0.301	249370	2648.6	55.32	8.29	0.910	0.0813	-0.1265	11.20
484	0.302	249598	2653.2	55.41	8.81	0.937	0.0880	-0.1249	10.65
485	0.301	249480	2650.5	55.36	9.30	0.963	0.0952	-0.1239	10.11
486	0.301	248955	2639.5	55.13	9.81	0.992	0.1046	-0.1232	9.49
491	0.301	249147	2642.4	55.19	9.91	0.996	0.1065	-0.1237	9.35
492	0.301	249403	2647.9	55.30	9.91	0.995	0.1065	-0.1242	9.34
493	0.301	249454	2648.8	55.32	9.91	0.995	0.1066	-0.1239	9.34
494	0.301	249442	2648.3	55.31	10.02	0.999	0.1084	-0.1232	9.22
495	0.301	249426	2647.9	55.30	10.02	1.000	0.1088	-0.1239	9.19
496	0.301	249423	2648.0	55.30	10.02	1.000	0.1089	-0.1236	9.18
497	0.301	249370	2646.9	55.28	10.13	1.004	0.1111	-0.1237	9.04
498	0.301	249010	2639.1	55.12	10.13	1.008	0.1115	-0.1241	9.04
499	0.301	248976	2638.2	55.10	10.13	1.008	0.1116	-0.1241	9.03
500	0.301	249384	2646.8	55.28	10.22	1.009	0.1135	-0.1238	8.89
501	0.301	249481	2648.6	55.32	10.22	1.008	0.1130	-0.1234	8.93
502	0.301	249373	2646.4	55.27	10.22	1.009	0.1131	-0.1234	8.93
503	0.301	249643	2651.8	55.38	10.34	1.012	0.1158	-0.1234	8.74
504	0.301	249544	2649.5	55.34	10.34	1.012	0.1158	-0.1238	8.74
505	0.301	249593	2650.4	55.36	10.34	1.013	0.1160	-0.1244	8.74
506	0.301	249568	2650.1	55.35	10.44	1.017	0.1184	-0.1244	8.59
507	0.301	249071	2639.5	55.13	10.44	1.021	0.1189	-0.1250	8.59
508	0.301	249187	2641.7	55.17	10.44	1.021	0.1190	-0.1251	8.58
509	0.301	249039	2638.5	55.11	10.54	1.024	0.1217	-0.1255	8.42
510	0.302	249783	2654.3	55.44	10.54	1.018	0.1209	-0.1249	8.42
511	0.301	249681	2652.1	55.39	10.54	1.019	0.1211	-0.1251	8.42
512	0.301	249671	2651.6	55.38	10.58	1.021	0.1226	-0.1249	8.33
513	0.301	249568	2649.4	55.33	10.57	1.021	0.1219	-0.1253	8.38
514	0.301	249677	2651.6	55.38	10.58	1.022	0.1222	-0.1248	8.36
515	0.301	249480	2647.1	55.29	10.62	1.024	0.1237	-0.1257	8.28
516	0.301	249692	2651.8	55.38	10.62	1.023	0.1232	-0.1255	8.30

Continued

Table D.6 – Data from Run 16, continued

Tab Pt.	M	Re	q_{norm} (Pa)	q_{norm} (psf)	α (deg.)	C_L	C_D	C_M	L/D
517	0.300	249015	2637.5	55.08	10.61	1.026	0.1238	-0.1255	8.29
518	0.300	249075	2638.4	55.10	10.66	1.021	0.1236	-0.1296	8.26
519	0.301	249123	2639.3	55.12	10.67	1.023	0.1242	-0.1290	8.24
520	0.301	249523	2647.9	55.30	10.67	1.020	0.1239	-0.1279	8.23

Table D.7 – Data from Run 20; nominal conditions $M = 0.700$, $Re = 27,680$

Tab Pt.	M	Re	q_{norm} (Pa)	q_{norm} (psf)	α (deg.)	C_L	C_D	C_M	L/D
581	0.696	25702	572.3	11.95	-4.17	-0.281	0.0660	-0.0037	-4.26
582	0.699	25892	578.6	12.08	-3.23	-0.222	0.0560	-0.0127	-3.97
583	0.706	26189	589.6	12.31	-2.22	-0.133	0.0440	-0.0303	-3.02
584	0.701	26194	586.5	12.25	-1.22	-0.031	0.0397	-0.0477	-0.79
585	0.704	26326	591.4	12.35	-0.22	0.078	0.0361	-0.0623	2.17
586	0.705	26455	595.1	12.43	0.88	0.222	0.0411	-0.0871	5.41
587	0.701	26477	593.0	12.38	1.81	0.320	0.0455	-0.1001	7.04
588	0.699	26513	592.8	12.38	2.81	0.409	0.0528	-0.1087	7.75
589	0.703	26714	599.4	12.52	3.80	0.475	0.0613	-0.1094	7.75
590	0.703	26779	601.1	12.55	4.89	0.547	0.0738	-0.1182	7.41
591	0.700	26827	600.1	12.53	5.82	0.604	0.0842	-0.1236	7.18
592	0.702	26938	604.3	12.62	6.81	0.642	0.0984	-0.1282	6.52
593	0.704	27079	608.3	12.70	7.32	0.654	0.1054	-0.1326	6.21
594	0.703	27127	609.2	12.72	7.89	0.673	0.1163	-0.1389	5.79
595	0.699	27082	605.4	12.64	8.51	0.705	0.1304	-0.1458	5.40
596	0.702	27229	610.8	12.76	8.85	0.719	0.1365	-0.1524	5.27
597	0.703	27359	614.4	12.83	9.31	0.738	0.1471	-0.1605	5.02
598	0.701	27418	614.4	12.83	9.80	0.756	0.1565	-0.1628	4.83
599	0.702	27537	617.7	12.90	10.31	0.771	0.1679	-0.1700	4.59
600	0.703	27554	618.5	12.92	10.78	0.782	0.1764	-0.1718	4.43
601	0.703	27734	622.7	13.01	11.33	0.789	0.1873	-0.1745	4.21
602	0.700	27723	620.1	12.95	11.79	0.804	0.1971	-0.1773	4.08
603	0.702	27832	624.2	13.04	12.34	0.811	0.2084	-0.1811	3.89
604	0.704	27994	629.1	13.14	12.83	0.813	0.2157	-0.1798	3.77
605	0.703	28024	629.3	13.14	13.37	0.821	0.2258	-0.1813	3.64
606	0.699	27985	625.5	13.06	13.83	0.834	0.2361	-0.1841	3.53
607	0.701	28107	629.4	13.14	14.33	0.837	0.2446	-0.1839	3.42
608	0.704	28263	634.8	13.26	14.81	0.837	0.2535	-0.1843	3.30
609	0.703	28300	635.0	13.26	15.33	0.843	0.2635	-0.1876	3.20
610	0.699	28313	632.8	13.22	15.86	0.853	0.2748	-0.1893	3.10
611	0.702	28473	638.2	13.33	16.80	0.857	0.2911	-0.1895	2.94
612	0.704	28681	644.5	13.46	17.78	0.863	0.3089	-0.1908	2.79
613	0.699	28682	641.3	13.39	18.81	0.885	0.3321	-0.1944	2.66
614	0.704	28873	648.5	13.54	19.82	0.891	0.3518	-0.1984	2.53
615	0.704	28970	651.0	13.60	20.79	0.901	0.3726	-0.1997	2.42
616	0.699	28897	646.1	13.49	21.81	0.918	0.3967	-0.2042	2.31
617	0.698	28936	645.6	13.48	22.85	0.929	0.4208	-0.2054	2.21
618	0.701	29111	652.1	13.62	23.82	0.927	0.4387	-0.2057	2.11

Table D.8 – Data from Run 23; nominal conditions $M = 0.800$, $Re = 24,584$

Tab Pt.	M	Re	q_{norm} (Pa)	q_{norm} (psf)	α (deg.)	C_L	C_D	C_M	L/D
633	0.808	22677	564.0	11.78	-4.21	-0.237	0.0717	-0.0122	-3.31
634	0.802	22817	564.6	11.79	-3.20	-0.186	0.0608	-0.0172	-3.05
635	0.800	22818	563.6	11.77	-2.21	-0.128	0.0517	-0.0219	-2.47
636	0.804	23041	570.8	11.92	-1.20	-0.054	0.0435	-0.0340	-1.23
637	0.799	23040	568.4	11.87	-0.21	0.009	0.0408	-0.0462	0.21
638	0.805	23189	575.3	12.01	0.79	0.128	0.0420	-0.0716	3.05
639	0.807	23331	579.5	12.10	1.80	0.263	0.0480	-0.0959	5.47
640	0.801	23298	575.5	12.02	2.79	0.347	0.0566	-0.1046	6.12
641	0.800	23342	576.2	12.03	3.81	0.424	0.0653	-0.1141	6.49
642	0.805	23476	582.1	12.16	4.80	0.484	0.0767	-0.1199	6.32
643	0.805	23559	584.5	12.21	5.80	0.538	0.0878	-0.1241	6.13
644	0.804	23593	584.5	12.21	6.80	0.579	0.1016	-0.1294	5.70
645	0.803	23621	584.7	12.21	7.31	0.597	0.1087	-0.1300	5.49
646	0.800	23624	583.3	12.18	7.92	0.632	0.1198	-0.1403	5.27
647	0.805	23803	590.1	12.32	8.29	0.642	0.1247	-0.1394	5.14
648	0.803	23808	589.6	12.31	8.81	0.669	0.1367	-0.1477	4.89
649	0.805	23872	591.8	12.36	9.34	0.687	0.1457	-0.1523	4.71
650	0.805	23929	593.4	12.39	9.79	0.702	0.1536	-0.1561	4.57
651	0.801	23931	591.6	12.36	10.30	0.722	0.1637	-0.1590	4.41
652	0.799	23922	590.1	12.33	10.78	0.745	0.1743	-0.1652	4.27
653	0.801	23992	592.7	12.38	11.31	0.763	0.1869	-0.1729	4.08
654	0.804	24064	596.2	12.45	11.79	0.777	0.1962	-0.1749	3.96
655	0.804	24118	597.8	12.48	12.30	0.791	0.2063	-0.1763	3.83
656	0.806	24201	600.7	12.55	12.84	0.801	0.2162	-0.1798	3.70
657	0.806	24230	601.2	12.56	13.28	0.812	0.2253	-0.1835	3.60
658	0.803	24227	600.0	12.53	13.79	0.825	0.2364	-0.1859	3.49
659	0.800	24220	598.0	12.49	14.28	0.841	0.2502	-0.1896	3.36
660	0.800	24237	598.4	12.50	14.79	0.853	0.2617	-0.1920	3.26
661	0.804	24355	603.6	12.61	15.27	0.855	0.2696	-0.1932	3.17
662	0.805	24417	605.5	12.65	15.80	0.867	0.2815	-0.1968	3.08
663	0.805	24488	607.6	12.69	16.79	0.878	0.3013	-0.1974	2.92
664	0.804	24519	607.7	12.69	17.81	0.890	0.3204	-0.2017	2.78
665	0.797	24477	602.9	12.59	18.78	0.912	0.3453	-0.2068	2.64
666	0.800	24584	607.2	12.68	19.79	0.926	0.3663	-0.2109	2.53
667	0.802	24667	610.1	12.74	20.79	0.935	0.3883	-0.2150	2.41
668	0.803	24749	612.7	12.80	21.79	0.943	0.4084	-0.2132	2.31
669	0.803	24834	614.8	12.84	22.80	0.951	0.4311	-0.2182	2.21
670	0.801	24897	615.3	12.85	23.80	0.973	0.4607	-0.2241	2.11

Table D.9 – Data from Run 24; nominal conditions $M = 0.700$, $Re = 27,680$

Tab Pt.	M	Re	q_{norm} (Pa)	q_{norm} (psf)	α (deg.)	C_L	C_D	C_M	L/D
672	0.696	25268	562.5	11.75	-4.23	-0.285	0.0680	-0.0011	-4.20
673	0.700	25427	569.0	11.88	-3.22	-0.223	0.0531	-0.0113	-4.19
674	0.703	25568	574.1	11.99	-2.22	-0.136	0.0437	-0.0292	-3.12
675	0.704	25655	576.2	12.03	-1.22	-0.035	0.0369	-0.0449	-0.94
676	0.700	25637	573.5	11.98	-0.19	0.080	0.0358	-0.0611	2.22
677	0.704	25787	579.5	12.10	0.81	0.206	0.0381	-0.0834	5.41
678	0.705	25876	582.1	12.16	1.89	0.314	0.0428	-0.0939	7.34
679	0.705	25941	583.4	12.18	2.81	0.394	0.0511	-0.1039	7.71
680	0.701	25903	579.9	12.11	3.81	0.470	0.0586	-0.1086	8.03
681	0.703	26015	583.9	12.20	4.87	0.536	0.0700	-0.1125	7.66
682	0.704	26120	586.8	12.26	5.85	0.589	0.0819	-0.1190	7.19
683	0.704	26189	588.8	12.30	6.82	0.626	0.0938	-0.1224	6.68
684	0.700	26133	584.6	12.21	7.32	0.642	0.1034	-0.1247	6.21
685	0.700	26188	585.8	12.24	7.82	0.660	0.1112	-0.1322	5.93
686	0.704	26334	591.9	12.36	8.38	0.678	0.1220	-0.1373	5.56
687	0.705	26404	593.9	12.40	8.87	0.698	0.1329	-0.1452	5.26
688	0.702	26352	591.0	12.34	9.32	0.721	0.1422	-0.1501	5.07
689	0.700	26360	589.7	12.32	9.81	0.741	0.1540	-0.1579	4.81
690	0.698	26400	589.3	12.31	10.38	0.760	0.1649	-0.1646	4.61
691	0.701	26472	592.6	12.38	10.82	0.766	0.1739	-0.1663	4.40
692	0.701	26503	593.4	12.39	11.32	0.777	0.1830	-0.1705	4.25
693	0.703	26634	598.1	12.49	11.82	0.781	0.1925	-0.1706	4.06
694	0.703	26675	598.9	12.51	12.32	0.790	0.2015	-0.1732	3.92
695	0.700	26627	595.7	12.44	12.82	0.804	0.2122	-0.1763	3.79
696	0.698	26617	594.0	12.41	13.61	0.817	0.2272	-0.1790	3.60
697	0.701	26729	598.9	12.51	13.89	0.813	0.2301	-0.1773	3.53
698	0.702	26774	600.1	12.53	14.31	0.819	0.2400	-0.1796	3.41
699	0.703	26854	602.9	12.59	14.82	0.819	0.2476	-0.1779	3.31
700	0.702	26885	603.0	12.59	15.32	0.826	0.2573	-0.1819	3.21
701	0.698	26832	599.1	12.51	15.80	0.837	0.2682	-0.1833	3.12
702	0.702	27033	606.4	12.67	16.86	0.845	0.2870	-0.1855	2.94
703	0.702	27054	606.9	12.67	17.90	0.857	0.3081	-0.1894	2.78
704	0.705	27215	612.0	12.78	18.80	0.860	0.3239	-0.1887	2.66
705	0.699	27168	607.5	12.69	19.80	0.880	0.3463	-0.1921	2.54
706	0.704	27318	613.5	12.81	20.80	0.887	0.3663	-0.1980	2.42
707	0.701	27343	612.4	12.79	21.85	0.897	0.3874	-0.1966	2.32
708	0.701	27398	613.6	12.82	22.81	0.907	0.4091	-0.2013	2.22
709	0.696	27347	609.4	12.73	23.83	0.927	0.4378	-0.2089	2.12

Table D.10 – Data from Run 25; nominal conditions $M = 0.500$, $Re = 36,790$

Tab Pt.	M	Re	q_{norm} (Pa)	q_{norm} (psf)	α (deg.)	C_L	C_D	C_M	L/D
710	0.501	34920	592.6	12.38	-4.21	-0.174	0.0469	-0.0668	-3.70
711	0.503	35047	596.2	12.45	-3.21	-0.089	0.0389	-0.0740	-2.28
712	0.506	35298	604.3	12.62	-2.20	-0.019	0.0339	-0.0708	-0.55
713	0.505	35270	602.7	12.59	-1.21	0.053	0.0299	-0.0718	1.75
714	0.504	35259	601.4	12.56	-0.15	0.146	0.0303	-0.0778	4.81
715	0.501	35093	595.1	12.43	0.81	0.246	0.0342	-0.0924	7.20
716	0.500	35083	594.2	12.41	1.82	0.337	0.0390	-0.1006	8.64
717	0.504	35399	604.1	12.62	2.80	0.410	0.0434	-0.1053	9.45
718	0.503	35355	601.6	12.57	3.79	0.483	0.0491	-0.1070	9.84
719	0.500	35233	596.6	12.46	4.80	0.565	0.0595	-0.1102	9.50
720	0.500	35257	596.6	12.46	5.81	0.663	0.0689	-0.1198	9.63
721	0.503	35444	602.9	12.59	6.83	0.793	0.0814	-0.1296	9.75
722	0.503	35468	603.4	12.60	7.30	0.852	0.0877	-0.1335	9.72
723	0.503	35539	605.1	12.64	7.87	0.899	0.0947	-0.1295	9.49
724	0.500	35422	599.6	12.52	8.30	0.937	0.1025	-0.1276	9.14
725	0.500	35448	600.1	12.53	8.80	0.966	0.1107	-0.1256	8.72
726	0.502	35544	603.5	12.60	8.80	0.958	0.1098	-0.1233	8.73
727	0.503	35682	607.8	12.69	8.80	0.956	0.1096	-0.1262	8.72
728	0.503	35670	607.0	12.68	9.34	0.974	0.1190	-0.1238	8.19
729	0.504	35738	609.1	12.72	9.35	0.974	0.1193	-0.1248	8.16
730	0.503	35683	606.9	12.68	9.35	0.978	0.1198	-0.1241	8.16
731	0.503	35756	609.1	12.72	9.80	0.979	0.1292	-0.1253	7.58
732	0.499	35530	600.9	12.55	9.80	0.990	0.1306	-0.1248	7.58
733	0.500	35577	602.3	12.58	9.80	0.990	0.1287	-0.1252	7.69
734	0.501	35661	604.4	12.62	10.06	0.987	0.1365	-0.1276	7.23
735	0.503	35816	609.6	12.73	10.06	0.981	0.1357	-0.1276	7.23
736	0.503	35806	609.2	12.72	10.06	0.984	0.1342	-0.1295	7.33
737	0.503	35849	610.1	12.74	10.32	0.977	0.1412	-0.1296	6.92
738	0.503	35854	610.1	12.74	10.32	0.978	0.1392	-0.1286	7.02
739	0.503	35899	611.4	12.77	10.32	0.974	0.1386	-0.1268	7.03
740	0.502	35878	610.1	12.74	10.55	0.975	0.1443	-0.1307	6.76
741	0.500	35792	606.3	12.66	10.55	0.979	0.1468	-0.1332	6.67
742	0.500	35811	606.8	12.67	10.55	0.982	0.1455	-0.1348	6.75
743	0.504	36058	614.9	12.84	10.84	0.968	0.1517	-0.1382	6.38
744	0.505	36120	616.6	12.88	10.84	0.967	0.1516	-0.1394	6.38
745	0.503	36054	614.1	12.83	10.84	0.961	0.1505	-0.1354	6.39
746	0.503	36109	615.0	12.84	11.05	0.957	0.1549	-0.1430	6.18
747	0.505	36219	618.4	12.92	11.04	0.948	0.1550	-0.1382	6.11
748	0.502	36046	612.4	12.79	11.05	0.965	0.1583	-0.1414	6.09
749	0.500	35973	609.0	12.72	11.30	0.956	0.1603	-0.1429	5.96
750	0.500	35993	609.5	12.73	11.30	0.954	0.1579	-0.1420	6.04
751	0.503	36183	615.8	12.86	11.30	0.947	0.1607	-0.1427	5.89
752	0.503	36263	617.8	12.90	11.56	0.941	0.1656	-0.1455	5.68
753	0.504	36299	618.9	12.93	11.56	0.931	0.1656	-0.1454	5.62

Continued

Table D.10 – Data from Run 25, continued

Tab Pt.	M	Re	q_{norm} (Pa)	q_{norm} (psf)	α (deg.)	C_L	C_D	C_M	L/D
754	0.504	36316	619.3	12.94	11.56	0.934	0.1682	-0.1460	5.55
755	0.503	36285	617.7	12.90	11.81	0.932	0.1716	-0.1488	5.43
756	0.500	36145	612.1	12.79	11.81	0.932	0.1735	-0.1492	5.37
757	0.500	36152	612.2	12.79	11.81	0.941	0.1774	-0.1531	5.30
758	0.500	36183	612.6	12.80	12.06	0.923	0.1755	-0.1507	5.26
759	0.503	36357	618.6	12.92	12.06	0.924	0.1818	-0.1541	5.08
760	0.504	36430	620.8	12.97	12.06	0.919	0.1827	-0.1535	5.03
761	0.503	36398	619.4	12.94	12.30	0.912	0.1850	-0.1553	4.93
762	0.504	36483	622.0	12.99	12.29	0.903	0.1847	-0.1519	4.89
763	0.503	36417	619.4	12.94	12.30	0.912	0.1869	-0.1539	4.88
764	0.500	36336	615.6	12.86	12.55	0.903	0.1908	-0.1565	4.73
765	0.500	36365	616.1	12.87	12.55	0.904	0.1929	-0.1555	4.68
766	0.500	36333	614.8	12.84	12.55	0.911	0.1946	-0.1584	4.68
767	0.502	36512	620.8	12.97	12.79	0.898	0.1954	-0.1576	4.60
768	0.502	36536	621.3	12.98	12.79	0.893	0.1963	-0.1563	4.55
769	0.502	36527	620.8	12.96	12.79	0.896	0.1968	-0.1586	4.55
770	0.503	36605	622.9	13.01	13.29	0.875	0.2038	-0.1584	4.29
771	0.504	36704	625.9	13.07	13.29	0.868	0.2042	-0.1553	4.25
772	0.503	36646	623.8	13.03	13.30	0.877	0.2064	-0.1594	4.25
773	0.498	36407	614.4	12.83	13.79	0.872	0.2173	-0.1617	4.01
774	0.500	36520	617.9	12.90	13.79	0.871	0.2169	-0.1634	4.02
775	0.502	36670	623.0	13.01	13.79	0.866	0.2155	-0.1608	4.02
776	0.502	36732	624.4	13.04	14.30	0.854	0.2246	-0.1650	3.80
777	0.503	36793	626.1	13.08	14.30	0.850	0.2235	-0.1624	3.80
778	0.503	36810	626.5	13.09	14.30	0.851	0.2238	-0.1633	3.80
779	0.500	36708	621.9	12.99	14.79	0.850	0.2357	-0.1660	3.61
780	0.500	36748	622.8	13.01	14.79	0.850	0.2335	-0.1665	3.64
781	0.500	36741	622.4	13.00	14.79	0.848	0.2350	-0.1654	3.61
782	0.504	37014	631.4	13.19	15.30	0.835	0.2413	-0.1660	3.46
783	0.503	36960	629.3	13.14	15.30	0.838	0.2422	-0.1677	3.46
784	0.503	36948	628.4	13.12	15.30	0.837	0.2420	-0.1664	3.46
785	0.504	37062	631.5	13.19	15.79	0.832	0.2520	-0.1694	3.30
786	0.499	36876	623.9	13.03	16.81	0.838	0.2742	-0.1749	3.06
787	0.502	37058	629.5	13.15	17.80	0.826	0.2920	-0.1759	2.83
788	0.503	37189	632.9	13.22	18.79	0.817	0.3027	-0.1729	2.70

Table D.11 – Data from Run 26; nominal conditions $M = 0.500$, $Re = 36,790$

Tab Pt.	M	Re	q_{norm} (Pa)	q_{norm} (psf)	α (deg.)	C_L	C_D	C_M	L/D
789	0.501	35233	597.8	12.49	-4.24	-0.169	0.0463	-0.0688	-3.66
790	0.502	35350	600.8	12.55	-3.19	-0.082	0.0381	-0.0763	-2.15
791	0.500	35270	597.4	12.48	-2.21	-0.017	0.0342	-0.0748	-0.49
792	0.499	35219	594.9	12.42	-1.20	0.055	0.0302	-0.0730	1.82
793	0.503	35532	605.1	12.64	-0.21	0.145	0.0299	-0.0805	4.84
794	0.502	35505	603.5	12.60	0.80	0.250	0.0336	-0.0968	7.43
795	0.503	35574	605.2	12.64	1.79	0.334	0.0380	-0.1040	8.77
796	0.500	35445	599.7	12.53	2.81	0.418	0.0440	-0.1066	9.50
797	0.503	35747	608.8	12.71	3.82	0.488	0.0513	-0.1097	9.51
798	0.504	35847	611.0	12.76	4.79	0.564	0.0588	-0.1145	9.59
799	0.501	35707	605.5	12.65	5.79	0.669	0.0692	-0.1241	9.68
800	0.503	35871	610.5	12.75	6.78	0.791	0.0825	-0.1308	9.59
801	0.503	35935	611.9	12.78	7.29	0.853	0.0880	-0.1343	9.70
802	0.503	35977	612.4	12.79	7.82	0.898	0.0941	-0.1303	9.54
803	0.501	35875	608.2	12.70	8.30	0.937	0.1030	-0.1297	9.09
804	0.501	35894	608.6	12.71	8.30	0.936	0.1029	-0.1296	9.09
805	0.500	35912	608.6	12.71	8.30	0.936	0.1029	-0.1285	9.09
806	0.504	36161	616.7	12.88	8.56	0.941	0.1062	-0.1271	8.86
807	0.503	36125	615.5	12.85	8.56	0.945	0.1067	-0.1295	8.85
808	0.504	36168	616.3	12.87	8.56	0.943	0.1065	-0.1288	8.85
809	0.505	36279	619.4	12.94	8.79	0.948	0.1091	-0.1255	8.69
810	0.502	36113	613.4	12.81	8.79	0.957	0.1102	-0.1279	8.69
811	0.500	36028	610.0	12.74	8.79	0.965	0.1111	-0.1302	8.68
812	0.499	36023	609.2	12.72	9.05	0.977	0.1152	-0.1282	8.48
813	0.502	36197	614.8	12.84	9.05	0.968	0.1141	-0.1270	8.49
814	0.503	36294	617.8	12.90	9.05	0.968	0.1142	-0.1284	8.48
815	0.504	36422	621.3	12.98	9.29	0.969	0.1185	-0.1272	8.18
816	0.503	36341	618.3	12.91	9.29	0.972	0.1187	-0.1268	8.19
817	0.501	36237	614.5	12.83	9.29	0.976	0.1192	-0.1254	8.19
818	0.499	36232	612.9	12.80	9.55	0.988	0.1251	-0.1286	7.89
819	0.502	36408	618.9	12.93	9.55	0.977	0.1236	-0.1235	7.90
820	0.503	36451	620.1	12.95	9.55	0.975	0.1233	-0.1238	7.90
821	0.503	36484	620.6	12.96	9.80	0.981	0.1284	-0.1288	7.64
822	0.503	36517	621.5	12.98	9.80	0.980	0.1282	-0.1281	7.64
823	0.502	36498	620.6	12.96	9.80	0.981	0.1284	-0.1283	7.64
824	0.500	36384	615.6	12.86	10.05	0.986	0.1349	-0.1286	7.31
825	0.500	36434	616.9	12.88	10.05	0.990	0.1356	-0.1325	7.30
826	0.499	36350	613.9	12.82	10.05	0.995	0.1363	-0.1314	7.30
827	0.502	36626	622.9	13.01	10.30	0.983	0.1407	-0.1352	6.99
828	0.501	36553	620.4	12.96	10.30	0.982	0.1403	-0.1333	7.00
829	0.502	36660	623.4	13.02	10.30	0.975	0.1373	-0.1307	7.10
830	0.503	36731	625.1	13.06	10.55	0.973	0.1448	-0.1358	6.72
831	0.500	36574	619.2	12.93	10.55	0.984	0.1466	-0.1387	6.71
832	0.499	36550	618.0	12.91	10.55	0.988	0.1473	-0.1400	6.71

Continued

Table D.11 – Data from Run 26, continued

Tab Pt.	M	Re	q_{norm} (Pa)	q_{norm} (psf)	α (deg.)	C_L	C_D	C_M	L/D
833	0.504	36892	628.7	13.13	10.80	0.966	0.1515	-0.1390	6.38
834	0.503	36847	627.0	13.09	10.80	0.967	0.1516	-0.1384	6.38
835	0.504	36913	629.1	13.14	10.80	0.960	0.1503	-0.1365	6.39
836	0.502	36861	626.6	13.09	11.15	0.962	0.1600	-0.1471	6.01
837	0.503	36935	628.8	13.13	11.15	0.956	0.1568	-0.1431	6.09
838	0.500	36754	622.0	12.99	11.15	0.962	0.1616	-0.1445	5.95
839	0.503	37027	630.2	13.16	11.29	0.955	0.1608	-0.1474	5.94
840	0.504	37103	632.3	13.21	11.29	0.944	0.1606	-0.1471	5.88
841	0.503	37063	630.6	13.17	11.29	0.944	0.1625	-0.1419	5.81
842	0.500	36952	625.6	13.07	11.79	0.934	0.1721	-0.1522	5.43
843	0.500	36992	626.5	13.08	11.80	0.936	0.1765	-0.1508	5.30
844	0.500	36997	626.5	13.08	11.80	0.939	0.1792	-0.1537	5.24
845	0.503	37246	634.2	13.25	12.30	0.905	0.1855	-0.1561	4.88
846	0.504	37291	635.5	13.27	12.30	0.905	0.1873	-0.1555	4.83
847	0.503	37284	635.1	13.26	12.30	0.906	0.1856	-0.1569	4.88
848	0.500	37189	629.7	13.15	12.81	0.899	0.1980	-0.1610	4.54
849	0.503	37405	637.0	13.30	12.81	0.887	0.1970	-0.1574	4.50
850	0.504	37455	638.3	13.33	12.81	0.889	0.1956	-0.1603	4.55
851	0.503	37512	638.8	13.34	13.30	0.873	0.2052	-0.1641	4.25
852	0.501	37386	634.1	13.24	13.30	0.879	0.2087	-0.1629	4.21
853	0.501	37415	634.6	13.25	13.30	0.876	0.2081	-0.1623	4.21
854	0.503	37558	638.9	13.34	13.80	0.863	0.2146	-0.1629	4.02
855	0.503	37582	639.5	13.36	13.80	0.858	0.2153	-0.1612	3.98
856	0.502	37530	637.7	13.32	13.80	0.866	0.2155	-0.1637	4.02
857	0.499	37436	632.6	13.21	14.31	0.859	0.2277	-0.1672	3.77
858	0.500	37524	635.2	13.27	14.31	0.857	0.2272	-0.1659	3.77
860	0.503	37781	643.0	13.43	14.80	0.839	0.2321	-0.1640	3.61
861	0.502	37768	642.1	13.41	14.80	0.840	0.2324	-0.1653	3.61
862	0.502	37775	642.2	13.41	14.80	0.842	0.2328	-0.1652	3.61
863	0.499	37647	636.3	13.29	15.30	0.846	0.2461	-0.1707	3.44
864	0.500	37721	638.4	13.33	15.30	0.843	0.2453	-0.1690	3.44
865	0.499	37692	637.2	13.31	15.30	0.847	0.2463	-0.1703	3.44
866	0.502	37906	644.0	13.45	15.80	0.835	0.2525	-0.1726	3.31
867	0.502	37920	644.1	13.45	15.80	0.833	0.2520	-0.1695	3.31
868	0.502	37965	645.4	13.48	15.80	0.834	0.2520	-0.1685	3.31
869	0.499	37856	639.9	13.37	16.80	0.837	0.2728	-0.1743	3.07
870	0.499	37846	639.5	13.36	16.80	0.837	0.2730	-0.1739	3.07
871	0.499	37865	639.9	13.37	16.80	0.839	0.2716	-0.1755	3.09
872	0.502	38132	648.1	13.54	17.80	0.823	0.2918	-0.1753	2.82

Table D.12 – Data from Run 27; nominal conditions $M = 0.800$, $Re = 70,000$

Tab Pt.	M	Re	q_{norm} (Pa)	q_{norm} (psf)	α (deg.)	C_L	C_D	C_M	L/D
877	0.801	68671	1697.4	35.45	-4.20	-0.302	0.0669	-0.0096	-4.51
878	0.803	68827	1704.3	35.59	-3.21	-0.256	0.0563	-0.0185	-4.54
879	0.802	68852	1702.8	35.56	-2.21	-0.161	0.0478	-0.0405	-3.37
880	0.804	68977	1708.8	35.69	-1.19	-0.032	0.0411	-0.0686	-0.79
881	0.806	69111	1715.3	35.82	-0.21	0.084	0.0384	-0.0875	2.20
882	0.802	68985	1706.9	35.65	0.82	0.197	0.0395	-0.1006	5.00
883	0.799	68884	1699.9	35.50	1.80	0.301	0.0435	-0.1120	6.91
884	0.801	69018	1705.4	35.62	2.79	0.395	0.0519	-0.1253	7.61
885	0.804	69277	1717.1	35.86	3.80	0.477	0.0621	-0.1362	7.68
886	0.804	69294	1716.9	35.86	4.82	0.549	0.0755	-0.1460	7.27
887	0.803	69309	1716.2	35.84	5.83	0.609	0.0903	-0.1547	6.74
888	0.803	69361	1716.9	35.86	6.80	0.662	0.1067	-0.1638	6.20
889	0.801	69350	1714.2	35.80	7.31	0.688	0.1159	-0.1690	5.93
890	0.802	69392	1716.8	35.86	7.84	0.712	0.1256	-0.1730	5.67
891	0.802	69428	1717.4	35.87	8.29	0.731	0.1332	-0.1763	5.49
892	0.803	69525	1721.2	35.95	8.79	0.751	0.1433	-0.1807	5.24
893	0.802	69548	1720.9	35.94	9.30	0.769	0.1530	-0.1828	5.03
894	0.800	69509	1716.5	35.85	9.83	0.789	0.1637	-0.1866	4.82
895	0.800	69539	1717.1	35.86	10.32	0.801	0.1729	-0.1887	4.63
896	0.802	69640	1722.1	35.97	10.79	0.811	0.1821	-0.1905	4.45
897	0.803	69802	1728.4	36.10	11.30	0.820	0.1913	-0.1924	4.29
898	0.803	69801	1727.3	36.08	11.80	0.827	0.2003	-0.1920	4.13
899	0.803	69886	1730.5	36.14	12.31	0.836	0.2105	-0.1936	3.97
900	0.800	69806	1724.2	36.01	12.79	0.844	0.2198	-0.1951	3.84
901	0.800	69813	1723.4	35.99	13.30	0.852	0.2296	-0.1971	3.71
902	0.803	70019	1733.5	36.21	13.80	0.855	0.2386	-0.1973	3.58
903	0.802	70016	1732.3	36.18	14.30	0.861	0.2482	-0.1995	3.47
904	0.803	70089	1734.9	36.23	14.81	0.863	0.2564	-0.1989	3.37
905	0.801	70093	1732.9	36.19	15.33	0.869	0.2672	-0.2006	3.25
906	0.800	70055	1729.2	36.11	15.79	0.876	0.2768	-0.2019	3.16
907	0.802	70194	1736.0	36.26	16.82	0.882	0.2957	-0.2032	2.98
908	0.801	70210	1735.5	36.25	17.81	0.893	0.3157	-0.2060	2.83
909	0.802	70332	1739.8	36.34	18.81	0.903	0.3358	-0.2078	2.69
910	0.800	70266	1735.1	36.24	19.81	0.916	0.3579	-0.2106	2.56
911	0.800	70345	1737.4	36.29	20.81	0.924	0.3786	-0.2139	2.44
912	0.800	70392	1738.1	36.30	21.82	0.931	0.3997	-0.2150	2.33
913	0.799	70405	1737.5	36.29	22.81	0.939	0.4217	-0.2180	2.23
914	0.798	70378	1734.7	36.23	23.80	0.950	0.4446	-0.2207	2.14

Table D.13 – Data from Run 28; nominal conditions $M = 0.700$, $Re = 27,680$

Tab Pt.	M	Re	q_{norm} (Pa)	q_{norm} (psf)	α (deg.)	C_L	C_D	C_M	L/D
924	0.704	25822	580.3	12.12	-4.21	-0.278	0.0694	-0.0002	-4.00
925	0.703	25935	581.9	12.15	-3.18	-0.209	0.0549	-0.0179	-3.81
926	0.696	25824	575.3	12.01	-2.18	-0.122	0.0445	-0.0351	-2.74
927	0.702	26038	584.1	12.20	-1.21	-0.026	0.0397	-0.0475	-0.64
928	0.703	26083	585.2	12.22	-0.19	0.089	0.0385	-0.0657	2.31
929	0.704	26166	587.9	12.28	0.86	0.225	0.0416	-0.0893	5.41
930	0.706	26250	590.9	12.34	1.80	0.315	0.0454	-0.1008	6.95
931	0.702	26210	587.4	12.27	2.87	0.407	0.0534	-0.1076	7.61
932	0.701	26226	587.4	12.27	3.81	0.476	0.0622	-0.1120	7.66
933	0.705	26369	593.3	12.39	4.80	0.536	0.0725	-0.1183	7.40
934	0.706	26436	595.5	12.44	5.77	0.590	0.0844	-0.1212	6.99
935	0.706	26517	597.3	12.47	6.79	0.631	0.0972	-0.1266	6.49
936	0.699	26366	589.1	12.30	7.31	0.655	0.1063	-0.1321	6.16
937	0.703	26555	596.0	12.45	7.82	0.666	0.1151	-0.1361	5.78
938	0.705	26652	599.4	12.52	8.30	0.684	0.1251	-0.1407	5.47
939	0.703	26664	598.8	12.51	8.80	0.709	0.1349	-0.1508	5.25
940	0.699	26626	595.4	12.43	9.33	0.735	0.1480	-0.1559	4.97
941	0.700	26685	597.0	12.47	9.80	0.749	0.1564	-0.1608	4.79
942	0.702	26762	600.1	12.53	10.31	0.759	0.1669	-0.1624	4.55
943	0.703	26827	602.1	12.57	10.80	0.773	0.1759	-0.1682	4.39
944	0.704	26908	604.5	12.63	11.31	0.779	0.1862	-0.1695	4.19
945	0.705	26992	607.3	12.68	11.79	0.788	0.1945	-0.1742	4.05
946	0.700	26899	601.6	12.56	12.29	0.803	0.2073	-0.1774	3.87
947	0.699	26924	601.5	12.56	12.79	0.813	0.2169	-0.1808	3.75
948	0.701	27016	605.2	12.64	13.32	0.817	0.2256	-0.1813	3.62
949	0.703	27103	608.3	12.70	13.80	0.817	0.2326	-0.1772	3.51
950	0.704	27193	611.4	12.77	14.30	0.820	0.2408	-0.1814	3.41
951	0.704	27213	611.2	12.77	14.80	0.828	0.2505	-0.1826	3.30
952	0.699	27153	607.1	12.68	15.31	0.838	0.2637	-0.1850	3.18
953	0.700	27205	608.6	12.71	15.79	0.845	0.2732	-0.1884	3.09
954	0.704	27363	614.7	12.84	16.80	0.845	0.2890	-0.1869	2.92
955	0.704	27424	616.1	12.87	17.80	0.857	0.3072	-0.1885	2.79
956	0.704	27468	617.0	12.89	18.80	0.868	0.3278	-0.1927	2.65
957	0.701	27501	616.2	12.87	19.78	0.883	0.3503	-0.1940	2.52
958	0.704	27607	620.1	12.95	20.79	0.891	0.3710	-0.1984	2.40
959	0.703	27673	621.4	12.98	21.81	0.901	0.3914	-0.1999	2.30
960	0.703	27714	622.0	12.99	22.76	0.910	0.4126	-0.2043	2.20
961	0.698	27647	617.1	12.89	23.76	0.924	0.4363	-0.2070	2.12

Table D.14 – Data from Run 29; nominal conditions $M = 0.500$, $Re = 36,790$

Tab Pt.	M	Re	q_{norm} (Pa)	q_{norm} (psf)	α (deg.)	C_L	C_D	C_M	L/D
962	0.500	35492	601.4	12.56	-4.20	-0.163	0.0493	-0.0667	-3.31
963	0.502	35595	604.4	12.62	-3.21	-0.081	0.0396	-0.0723	-2.04
964	0.505	35850	612.6	12.79	-2.22	-0.008	0.0347	-0.0719	-0.24
965	0.505	35885	613.1	12.80	-1.20	0.061	0.0328	-0.0707	1.86
966	0.502	35768	608.1	12.70	-0.21	0.155	0.0315	-0.0805	4.92
967	0.500	35683	604.3	12.62	0.83	0.260	0.0356	-0.0946	7.30
968	0.504	35925	612.1	12.78	1.82	0.342	0.0399	-0.0996	8.57
969	0.504	35991	613.9	12.82	2.80	0.421	0.0452	-0.1070	9.32
970	0.502	35912	610.5	12.75	3.81	0.495	0.0535	-0.1096	9.27
971	0.503	36014	613.5	12.81	4.83	0.574	0.0619	-0.1083	9.27
972	0.500	35875	607.8	12.69	5.81	0.677	0.0741	-0.1235	9.14
973	0.501	35951	609.5	12.73	6.80	0.809	0.0850	-0.1331	9.52
974	0.503	36110	614.8	12.84	7.35	0.864	0.0924	-0.1334	9.35
975	0.502	36101	614.0	12.82	7.81	0.906	0.0973	-0.1305	9.31
976	0.503	36165	615.7	12.86	8.32	0.934	0.1054	-0.1265	8.86
977	0.503	36151	614.9	12.84	8.32	0.937	0.1058	-0.1277	8.85
978	0.504	36238	617.4	12.90	8.32	0.933	0.1035	-0.1274	9.02
979	0.500	36066	610.7	12.75	8.55	0.957	0.1083	-0.1271	8.84
980	0.499	36051	609.9	12.74	8.55	0.958	0.1104	-0.1270	8.68
981	0.502	36196	615.0	12.84	8.55	0.952	0.1078	-0.1261	8.83
982	0.503	36295	617.5	12.90	8.83	0.963	0.1121	-0.1237	8.59
983	0.503	36309	617.6	12.90	8.83	0.963	0.1121	-0.1243	8.59
984	0.503	36338	618.4	12.92	8.83	0.964	0.1123	-0.1240	8.59
985	0.501	36290	615.9	12.86	9.11	0.981	0.1192	-0.1265	8.22
986	0.499	36154	611.0	12.76	9.11	0.989	0.1203	-0.1281	8.22
987	0.499	36218	612.7	12.80	9.11	0.986	0.1199	-0.1261	8.22
988	0.500	36257	613.6	12.82	9.33	0.992	0.1225	-0.1256	8.10
989	0.503	36476	620.9	12.97	9.33	0.980	0.1230	-0.1256	7.97
990	0.502	36418	618.7	12.92	9.33	0.984	0.1215	-0.1235	8.10
991	0.503	36554	622.2	13.00	9.55	0.984	0.1252	-0.1241	7.86
992	0.503	36573	622.7	13.00	9.56	0.987	0.1259	-0.1266	7.84
993	0.501	36465	618.0	12.91	9.56	0.994	0.1268	-0.1269	7.84
994	0.499	36400	615.1	12.85	9.80	0.998	0.1331	-0.1278	7.50
995	0.502	36604	622.1	12.99	9.80	0.989	0.1320	-0.1263	7.49
996	0.502	36649	623.2	13.02	9.80	0.989	0.1320	-0.1276	7.49
997	0.502	36667	623.4	13.02	10.05	0.992	0.1385	-0.1288	7.16
998	0.502	36708	624.3	13.04	10.05	0.987	0.1376	-0.1288	7.17
999	0.503	36755	625.6	13.07	10.05	0.990	0.1383	-0.1310	7.16
1000	0.500	36633	620.5	12.96	10.26	0.994	0.1420	-0.1306	7.00
1001	0.500	36664	621.3	12.98	10.26	0.989	0.1412	-0.1311	7.01
1002	0.499	36615	619.3	12.93	10.26	0.994	0.1401	-0.1317	7.10
1003	0.503	36859	627.0	13.09	10.55	0.982	0.1487	-0.1353	6.61
1004	0.503	36932	629.1	13.14	10.55	0.980	0.1445	-0.1359	6.78
1005	0.503	36899	627.9	13.11	10.55	0.982	0.1448	-0.1350	6.78

Continued

Table D.14 – Data from Run 29, continued

Tab Pt.	M	Re	q_{norm} (Pa)	q_{norm} (psf)	α (deg.)	C_L	C_D	C_M	L/D
1006	0.501	36930	626.5	13.08	10.80	0.979	0.1520	-0.1395	6.44
1007	0.503	37049	630.6	13.17	10.80	0.971	0.1488	-0.1383	6.53
1008	0.503	37069	631.0	13.18	10.80	0.975	0.1475	-0.1393	6.61
1009	0.503	37126	632.1	13.20	11.04	0.962	0.1547	-0.1423	6.22
1010	0.504	37173	633.4	13.23	11.05	0.962	0.1549	-0.1391	6.21
1011	0.504	37239	635.1	13.26	11.05	0.961	0.1567	-0.1390	6.13
1012	0.500	37060	627.9	13.11	11.31	0.958	0.1599	-0.1440	5.99
1013	0.500	37038	627.1	13.10	11.31	0.959	0.1638	-0.1438	5.85
1014	0.503	37265	634.7	13.26	11.32	0.953	0.1612	-0.1436	5.91
1015	0.504	37362	636.9	13.30	11.81	0.934	0.1745	-0.1519	5.35
1016	0.503	37364	636.5	13.29	11.81	0.927	0.1749	-0.1467	5.30
1017	0.504	37381	637.0	13.30	11.81	0.935	0.1785	-0.1497	5.24
1018	0.500	37232	630.7	13.17	12.32	0.922	0.1915	-0.1563	4.82
1019	0.501	37310	632.8	13.22	12.32	0.925	0.1921	-0.1565	4.82
1020	0.503	37419	636.7	13.30	12.32	0.917	0.1905	-0.1541	4.82
1021	0.503	37452	637.1	13.31	12.82	0.901	0.2004	-0.1611	4.50
1022	0.503	37511	638.9	13.34	12.82	0.897	0.2013	-0.1578	4.45
1023	0.503	37506	638.4	13.33	12.82	0.896	0.1992	-0.1588	4.50
1024	0.500	37430	634.3	13.25	13.30	0.891	0.2116	-0.1629	4.21
1025	0.500	37407	633.2	13.22	13.30	0.891	0.2134	-0.1620	4.17
1026	0.502	37561	638.3	13.33	13.30	0.882	0.2094	-0.1594	4.21
1027	0.502	37646	640.1	13.37	13.80	0.870	0.2164	-0.1640	4.02
1028	0.504	37761	643.5	13.44	13.80	0.863	0.2184	-0.1628	3.95
1029	0.503	37733	642.2	13.41	13.80	0.867	0.2174	-0.1638	3.99
1030	0.499	37534	634.3	13.25	14.29	0.872	0.2287	-0.1686	3.81
1031	0.501	37714	640.2	13.37	14.29	0.863	0.2283	-0.1668	3.78
1032	0.502	37783	642.4	13.42	14.29	0.853	0.2257	-0.1618	3.78
1033	0.502	37792	642.0	13.41	14.84	0.849	0.2372	-0.1664	3.58
1034	0.503	37935	646.3	13.50	14.84	0.849	0.2352	-0.1679	3.61
1035	0.502	37841	642.9	13.43	14.84	0.846	0.2346	-0.1660	3.61
1036	0.500	37802	640.0	13.37	15.31	0.850	0.2491	-0.1703	3.41
1037	0.499	37781	639.2	13.35	15.31	0.848	0.2484	-0.1674	3.41
1038	0.502	37952	644.8	13.47	15.31	0.844	0.2472	-0.1679	3.41
1039	0.504	38164	650.4	13.58	15.80	0.835	0.2560	-0.1707	3.26
1040	0.504	38163	650.4	13.58	15.80	0.835	0.2560	-0.1691	3.26
1041	0.501	38013	644.5	13.46	15.80	0.847	0.2577	-0.1723	3.29
1042	0.503	38289	652.3	13.62	16.80	0.833	0.2730	-0.1729	3.05
1043	0.504	38350	654.1	13.66	16.80	0.829	0.2717	-0.1710	3.05
1044	0.503	38317	652.4	13.63	16.80	0.830	0.2719	-0.1710	3.05

Table D.15 – Data from Run 30; nominal conditions $M = 0.651$, $Re = 92,327$

Tab Pt.	M	Re	q_{norm} (Pa)	q_{norm} (psf)	α (deg.)	C_L	C_D	C_M	L/D
1045	0.653	91644	1940.7	40.53	-4.19	-0.172	0.0443	-0.0769	-3.89
1046	0.652	91670	1940.4	40.53	-3.15	-0.034	0.0331	-0.1068	-1.03
1047	0.652	91699	1939.5	40.51	-2.20	0.065	0.0289	-0.1177	2.25
1048	0.653	91922	1948.3	40.69	-1.19	0.151	0.0296	-0.1179	5.08
1049	0.653	91838	1944.9	40.62	-1.19	0.151	0.0297	-0.1184	5.08
1050	0.653	91913	1946.6	40.65	-0.17	0.217	0.0312	-0.1146	6.97
1051	0.652	91839	1942.5	40.57	0.81	0.290	0.0345	-0.1148	8.41
1052	0.653	92085	1952.1	40.77	1.81	0.368	0.0380	-0.1161	9.67
1053	0.653	92066	1950.6	40.74	2.87	0.468	0.0455	-0.1248	10.29
1054	0.652	92000	1946.5	40.65	3.80	0.548	0.0531	-0.1296	10.32
1055	0.651	91951	1942.5	40.57	4.81	0.640	0.0623	-0.1355	10.27
1056	0.652	92173	1950.7	40.74	5.80	0.802	0.0750	-0.1520	10.70
1057	0.652	92157	1949.9	40.72	5.80	0.802	0.0750	-0.1511	10.70
1058	0.652	92179	1950.3	40.73	6.31	0.879	0.0820	-0.1533	10.71
1059	0.651	92147	1946.7	40.66	6.81	0.932	0.0892	-0.1509	10.45
1060	0.651	92266	1951.3	40.75	7.31	0.963	0.0960	-0.1478	10.03
1061	0.651	92327	1952.6	40.78	7.81	0.979	0.1034	-0.1438	9.46
1062	0.652	92391	1954.2	40.81	8.30	0.974	0.1091	-0.1448	8.92
1063	0.651	92357	1951.3	40.75	8.54	0.975	0.1086	-0.1483	8.98
1064	0.651	92487	1955.6	40.84	8.79	0.967	0.1038	-0.1502	9.31
1065	0.651	92532	1956.9	40.87	8.57	0.972	0.1130	-0.1448	8.60

Table D.16 – Data from Run 31; nominal conditions $M = 0.300$, $Re = 59,140$

Tab Pt.	M	Re	q_{norm} (Pa)	q_{norm} (psf)	α (deg.)	C_L	C_D	C_M	L/D
1084	0.301	58622	622.8	13.01	-4.20	-0.067	0.0306	-0.0912	-2.17
1085	0.299	58286	615.2	12.85	-3.20	0.007	0.0275	-0.0958	0.27
1086	0.302	58812	626.2	13.08	-2.21	0.066	0.0265	-0.0890	2.47
1087	0.302	58717	624.0	13.03	-1.20	0.124	0.0264	-0.0849	4.72
1088	0.301	58715	623.6	13.02	-0.20	0.189	0.0281	-0.0869	6.72
1089	0.299	58415	616.7	12.88	0.81	0.275	0.0308	-0.0973	8.94
1090	0.302	58808	625.0	13.05	1.81	0.345	0.0352	-0.1020	9.82
1091	0.302	58904	626.9	13.09	2.83	0.414	0.0411	-0.1032	10.06
1092	0.302	58871	626.0	13.07	3.80	0.486	0.0460	-0.1075	10.57
1093	0.302	58884	626.0	13.07	4.81	0.579	0.0538	-0.1112	10.76
1094	0.300	58528	618.1	12.91	5.80	0.695	0.0634	-0.1239	10.96
1095	0.302	58968	627.4	13.10	6.85	0.776	0.0728	-0.1251	10.66
1096	0.302	58908	626.0	13.07	7.30	0.802	0.0765	-0.1236	10.48
1097	0.302	59091	629.7	13.15	7.80	0.824	0.0810	-0.1187	10.17
1098	0.303	59163	631.1	13.18	8.30	0.846	0.0877	-0.1164	9.64
1099	0.302	59019	627.8	13.11	8.80	0.873	0.0934	-0.1130	9.35
1100	0.302	58982	626.9	13.09	9.31	0.900	0.1017	-0.1132	8.85
1101	0.299	58562	617.7	12.90	9.80	0.932	0.1103	-0.1142	8.45
1102	0.301	58898	624.6	13.05	10.03	0.931	0.1143	-0.1119	8.14
1103	0.301	58900	624.6	13.05	10.30	0.940	0.1183	-0.1121	7.95
1104	0.301	58999	626.5	13.08	10.55	0.945	0.1214	-0.1098	7.78
1105	0.301	58949	625.2	13.06	10.82	0.954	0.1272	-0.1107	7.49
1106	0.301	59026	626.6	13.09	11.05	0.958	0.1338	-0.1131	7.16
1107	0.299	58610	617.4	12.89	11.31	0.972	0.1381	-0.1200	7.04
1108	0.301	58936	624.3	13.04	11.55	0.959	0.1398	-0.1237	6.86
1109	0.301	59011	625.7	13.07	11.79	0.959	0.1397	-0.1303	6.86
1110	0.301	59048	626.2	13.08	12.06	0.935	0.1136	-0.1284	8.24

Table D.17 – Data from Run 32; nominal conditions $M = 0.300$, $Re = 59,140$

Tab Pt.	M	Re	q_{norm} (Pa)	q_{norm} (psf)	α (deg.)	C_L	C_D	C_M	L/D
1124	0.299	58362	614.5	12.83	-4.20	-0.073	0.0315	-0.0877	-2.33
1125	0.303	59111	630.1	13.16	-3.20	0.002	0.0271	-0.0889	0.06
1126	0.302	59124	630.1	13.16	-2.17	0.063	0.0265	-0.0885	2.39
1127	0.302	59077	629.1	13.14	-1.19	0.120	0.0262	-0.0827	4.56
1128	0.299	58564	617.6	12.90	-0.20	0.187	0.0284	-0.0862	6.58
1129	0.302	59085	628.6	13.13	0.79	0.266	0.0300	-0.0950	8.88
1130	0.302	59235	631.4	13.19	1.80	0.336	0.0345	-0.0968	9.73
1131	0.302	59068	627.7	13.11	2.81	0.409	0.0407	-0.1026	10.06
1132	0.298	58520	615.7	12.86	3.87	0.499	0.0478	-0.1100	10.45
1133	0.301	59059	627.1	13.10	4.82	0.581	0.0521	-0.1109	11.14
1134	0.302	59139	628.5	13.13	5.81	0.683	0.0624	-0.1195	10.94
1135	0.302	59233	630.4	13.17	6.81	0.769	0.0716	-0.1212	10.75
1136	0.301	59133	628.1	13.12	7.86	0.825	0.0820	-0.1161	10.06
1137	0.300	58880	622.1	12.99	8.31	0.857	0.0891	-0.1151	9.62
1138	0.302	59338	631.7	13.19	8.80	0.868	0.0930	-0.1115	9.34
1139	0.302	59337	631.7	13.19	9.38	0.898	0.1028	-0.1124	8.73
1140	0.302	59271	630.2	13.16	9.80	0.918	0.1089	-0.1120	8.43
1141	0.303	59479	634.4	13.25	10.05	0.919	0.1115	-0.1083	8.25
1142	0.300	58954	622.9	13.01	10.30	0.947	0.1195	-0.1108	7.92
1143	0.299	58900	621.5	12.98	10.55	0.956	0.1232	-0.1113	7.76
1144	0.302	59362	631.2	13.18	10.81	0.950	0.1271	-0.1096	7.48
1145	0.302	59424	632.1	13.20	10.90	0.951	0.1286	-0.1121	7.39
1146	0.300	59058	623.8	13.03	11.04	0.965	0.1329	-0.1145	7.26
1147	0.302	59462	632.1	13.20	11.15	0.954	0.1313	-0.1147	7.27
1148	0.302	59519	633.0	13.22	11.25	0.951	0.1323	-0.1174	7.19
1149	0.302	59550	633.5	13.23	11.35	0.945	0.1308	-0.1194	7.22
1150	0.302	59582	634.0	13.24	11.45	0.955	0.1363	-0.1234	7.01
1151	0.298	58929	619.7	12.94	11.54	0.963	0.1382	-0.1208	6.97
1152	0.301	59456	630.8	13.17	11.65	0.958	0.1359	-0.1261	7.05
1153	0.302	59637	634.3	13.25	11.74	0.934	0.1250	-0.1246	7.47
1154	0.301	59533	632.0	13.20	11.85	0.940	0.1219	-0.1283	7.71

Table D.18 – Data from Run 33; nominal conditions $M = 0.451$, $Re = 138,206$

Tab Pt.	M	Re	q_{norm} (Pa)	q_{norm} (psf)	α (deg.)	C_L	C_D	C_M	L/D
1155	0.451	137555	2124.8	44.38	-4.21	-0.069	0.0264	-0.1002	-2.62
1156	0.450	137401	2119.2	44.26	-3.19	0.019	0.0228	-0.1070	0.81
1157	0.450	137487	2121.4	44.31	-2.21	0.100	0.0219	-0.1130	4.58
1158	0.452	137819	2131.9	44.53	-1.19	0.176	0.0229	-0.1152	7.69
1159	0.452	137862	2133.4	44.56	-0.20	0.247	0.0256	-0.1155	9.66
1160	0.452	137910	2134.3	44.57	0.79	0.318	0.0293	-0.1168	10.87
1161	0.452	137927	2134.3	44.58	1.80	0.392	0.0337	-0.1181	11.63
1162	0.452	138050	2137.7	44.65	2.84	0.477	0.0417	-0.1225	11.44
1163	0.451	137698	2126.1	44.41	3.84	0.576	0.0478	-0.1296	12.04
1164	0.450	137651	2124.5	44.37	4.82	0.697	0.0556	-0.1412	12.54
1165	0.452	138078	2137.7	44.65	5.78	0.776	0.0630	-0.1400	12.32
1166	0.452	138083	2137.3	44.64	6.81	0.830	0.0717	-0.1326	11.58
1167	0.452	138052	2136.1	44.61	7.31	0.856	0.0765	-0.1284	11.18
1168	0.451	137969	2133.1	44.55	7.79	0.880	0.0819	-0.1254	10.74
1169	0.450	137580	2120.2	44.28	8.33	0.912	0.0891	-0.1239	10.24
1170	0.450	137663	2122.4	44.33	8.80	0.937	0.0953	-0.1217	9.83
1171	0.451	137976	2132.3	44.53	9.04	0.944	0.0989	-0.1198	9.55
1172	0.451	138018	2133.1	44.55	9.30	0.956	0.1029	-0.1198	9.29
1173	0.451	138057	2133.6	44.56	9.55	0.969	0.1070	-0.1196	9.06
1174	0.451	138001	2131.3	44.51	9.79	0.979	0.1110	-0.1186	8.82
1175	0.450	137796	2124.5	44.37	9.92	0.987	0.1139	-0.1201	8.67
1176	0.451	138077	2133.1	44.55	10.02	0.987	0.1153	-0.1193	8.56
1177	0.451	138206	2136.2	44.62	10.12	0.990	0.1176	-0.1195	8.42

Table D.19 – Data from Run 35; nominal conditions $M = 0.300$, $Re = 59,140$

Tab Pt.	M	Re	q_{norm} (Pa)	q_{norm} (psf)	α (deg.)	C_L	C_D	C_M	L/D
1204	0.299	58057	612.8	12.80	-4.20	-0.070	0.0296	-0.0919	-2.37
1205	0.300	58151	614.7	12.84	-3.19	0.005	0.0239	-0.0953	0.22
1206	0.302	58554	623.0	13.01	-2.18	0.064	0.0251	-0.0914	2.57
1207	0.302	58628	624.4	13.04	-1.22	0.121	0.0246	-0.0879	4.92
1208	0.302	58684	625.3	13.06	-0.23	0.184	0.0243	-0.0900	7.56
1209	0.299	58176	614.2	12.83	0.78	0.272	0.0290	-0.1010	9.40
1210	0.299	58115	612.8	12.80	1.79	0.350	0.0320	-0.1064	10.93
1211	0.302	58627	623.5	13.02	2.78	0.411	0.0370	-0.1069	11.10
1212	0.302	58658	624.0	13.03	3.79	0.485	0.0440	-0.1106	11.01
1213	0.301	58577	622.1	12.99	4.80	0.580	0.0500	-0.1149	11.60
1214	0.301	58566	621.7	12.98	5.84	0.692	0.0597	-0.1273	11.58
1215	0.300	58324	616.1	12.87	6.79	0.779	0.0700	-0.1275	11.14
1216	0.299	58161	612.5	12.79	7.30	0.813	0.0752	-0.1261	10.80
1217	0.301	58651	622.7	13.01	7.81	0.824	0.0788	-0.1211	10.47
1218	0.301	58620	622.2	12.99	8.28	0.850	0.0853	-0.1179	9.95
1219	0.302	58736	624.5	13.04	8.87	0.873	0.0921	-0.1133	9.48
1220	0.300	58506	619.4	12.94	9.28	0.901	0.0986	-0.1157	9.13
1221	0.302	58817	625.9	13.07	9.78	0.916	0.1056	-0.1157	8.67
1222	0.299	58251	613.5	12.81	10.05	0.942	0.1115	-0.1150	8.45
1223	0.299	58307	614.4	12.83	10.36	0.953	0.1186	-0.1163	8.04
1224	0.298	58060	609.2	12.72	10.67	0.969	0.1241	-0.1147	7.81
1225	0.301	58669	621.9	12.99	10.77	0.953	0.1257	-0.1142	7.58
1226	0.301	58638	621.2	12.97	10.88	0.955	0.1279	-0.1136	7.47
1227	0.301	58678	621.8	12.99	10.99	0.958	0.1302	-0.1166	7.36
1228	0.301	58657	621.4	12.98	11.10	0.958	0.1320	-0.1145	7.26
1229	0.298	58279	612.9	12.80	11.20	0.972	0.1316	-0.1204	7.39
1230	0.298	58265	612.4	12.79	11.30	0.972	0.1332	-0.1228	7.30
1231	0.298	58289	612.9	12.80	11.38	0.962	0.1325	-0.1232	7.26
1232	0.300	58708	621.7	12.99	11.50	0.951	0.1350	-0.1243	7.05
1233	0.300	58711	621.7	12.99	11.62	0.954	0.1334	-0.1269	7.15
1234	0.300	58739	622.2	12.99	11.73	0.941	0.1266	-0.1259	7.43
1235	0.301	58780	622.8	13.01	11.82	0.957	0.1313	-0.1326	7.29
1236	0.301	58900	625.1	13.06	11.95	0.938	0.1236	-0.1309	7.59

Table D.20 – Data from Run 36; nominal conditions $M = 0.599$, $Re = 176,488$

Tab Pt.	M	Re	q_{norm} (Pa)	q_{norm} (psf)	α (deg.)	C_L	C_D	C_M	L/D
1237	0.599	175865	3471.8	72.51	-4.20	-0.095	0.0299	-0.1047	-3.19
1238	0.599	176157	3481.9	72.72	-3.19	0.011	0.0245	-0.1175	0.44
1239	0.601	176542	3497.9	73.06	-2.22	0.101	0.0226	-0.1235	4.46
1240	0.601	176616	3500.9	73.12	-1.25	0.184	0.0237	-0.1282	7.79
1241	0.602	176746	3504.7	73.20	-0.03	0.279	0.0279	-0.1297	10.01
1242	0.602	176817	3507.4	73.25	0.83	0.344	0.0313	-0.1294	10.98
1243	0.601	176656	3499.7	73.09	1.78	0.415	0.0362	-0.1304	11.48
1244	0.602	176799	3505.7	73.22	2.78	0.479	0.0407	-0.1290	11.78
1245	0.601	176748	3503.4	73.17	3.92	0.634	0.0495	-0.1461	12.81
1246	0.601	176807	3504.6	73.19	4.81	0.761	0.0599	-0.1585	12.72
1247	0.600	176550	3493.4	72.96	5.77	0.851	0.0690	-0.1553	12.35
1248	0.600	176572	3493.2	72.96	6.79	0.907	0.0794	-0.1438	11.43
1249	0.601	176756	3501.2	73.12	7.28	0.932	0.0854	-0.1392	10.91
1250	0.601	176688	3499.0	73.08	7.81	0.961	0.0929	-0.1356	10.34
1251	0.600	176657	3496.7	73.03	8.08	0.975	0.0972	-0.1344	10.03
1252	0.601	176792	3501.6	73.13	8.51	0.991	0.1039	-0.1319	9.53
1253	0.601	176713	3498.4	73.06	8.55	0.993	0.1049	-0.1316	9.47
1254	0.599	176488	3487.6	72.84	8.81	0.997	0.1089	-0.1332	9.15

Table D.21 – Data from Run 37; nominal conditions $M = 0.300$, $Re = 160,000$

Tab Pt.	M	Re	q_{norm} (Pa)	q_{norm} (psf)	α (deg.)	C_L	C_D	C_M	L/D
1283	0.300	158526	1676.0	35.00	-4.20	-0.043	0.0222	-0.1006	-1.92
1284	0.301	158888	1683.3	35.16	-3.19	0.039	0.0194	-0.1046	2.00
1285	0.301	159013	1686.0	35.21	-2.24	0.116	0.0191	-0.1103	6.06
1286	0.301	159217	1690.1	35.30	-1.22	0.190	0.0204	-0.1123	9.28
1287	0.301	159314	1692.0	35.34	-0.24	0.264	0.0229	-0.1164	11.51
1288	0.300	158750	1679.7	35.08	0.79	0.344	0.0274	-0.1195	12.57
1289	0.302	159497	1695.1	35.40	1.79	0.421	0.0319	-0.1230	13.18
1290	0.301	159454	1694.2	35.38	2.85	0.507	0.0370	-0.1269	13.69
1291	0.301	159315	1691.0	35.32	3.79	0.602	0.0433	-0.1349	13.91
1292	0.300	159025	1684.2	35.18	4.85	0.702	0.0513	-0.1399	13.69
1293	0.302	159602	1696.7	35.44	5.83	0.762	0.0583	-0.1343	13.07
1294	0.302	159603	1696.6	35.43	6.78	0.808	0.0659	-0.1281	12.26
1295	0.301	159539	1695.1	35.40	7.30	0.835	0.0711	-0.1257	11.75
1296	0.302	159591	1696.2	35.43	7.82	0.862	0.0766	-0.1232	11.24
1297	0.301	159118	1685.7	35.21	8.32	0.892	0.0826	-0.1224	10.79
1298	0.302	159609	1696.2	35.43	8.80	0.912	0.0886	-0.1201	10.30
1299	0.301	159617	1696.1	35.42	9.34	0.940	0.0960	-0.1193	9.79
1300	0.302	159693	1697.8	35.46	9.84	0.964	0.1042	-0.1186	9.25
1301	0.302	159700	1697.8	35.46	10.16	0.977	0.1105	-0.1188	8.84
1302	0.302	159721	1698.0	35.46	10.17	0.978	0.1108	-0.1181	8.82
1303	0.302	159680	1697.1	35.44	10.16	0.978	0.1106	-0.1182	8.84
1304	0.301	159227	1687.1	35.24	10.33	0.990	0.1147	-0.1188	8.64
1305	0.300	159125	1684.8	35.19	10.33	0.991	0.1148	-0.1200	8.63
1306	0.301	159261	1687.6	35.25	10.33	0.991	0.1149	-0.1195	8.63
1307	0.302	159840	1699.8	35.50	10.54	0.991	0.1189	-0.1200	8.33
1308	0.302	159796	1698.9	35.48	10.54	0.992	0.1190	-0.1201	8.33
1309	0.302	159841	1699.9	35.50	10.54	0.992	0.1191	-0.1198	8.33
1310	0.302	159746	1697.6	35.45	10.77	0.998	0.1248	-0.1228	8.00
1311	0.301	159732	1697.1	35.45	10.76	0.993	0.1215	-0.1256	8.17
1312	0.302	159819	1698.9	35.48	10.76	0.991	0.1213	-0.1240	8.17
1313	0.301	159371	1689.4	35.28	10.79	0.995	0.1223	-0.1260	8.14
1314	0.301	159379	1689.5	35.29	10.78	0.989	0.1159	-0.1290	8.53
1315	0.302	159878	1699.8	35.50	10.77	0.978	0.1105	-0.1303	8.85

Table D.22 – Data from Run 38; nominal conditions $M = 0.551$, $Re = 33,521$

Tab Pt.	M	Re	q_{norm} (Pa)	q_{norm} (psf)	α (deg.)	C_L	C_D	C_M	L/D
1341	0.551	32716	602.7	12.59	-4.20	-0.204	0.0518	-0.0558	-3.94
1342	0.551	32775	604.0	12.61	-3.19	-0.117	0.0412	-0.0680	-2.84
1343	0.550	32806	603.3	12.60	-2.19	-0.038	0.0340	-0.0729	-1.11
1344	0.551	32871	605.4	12.64	-1.22	0.036	0.0314	-0.0742	1.14
1345	0.550	32894	604.6	12.63	-0.18	0.139	0.0295	-0.0841	4.70
1346	0.547	32803	600.2	12.53	0.82	0.249	0.0333	-0.1042	7.48
1347	0.551	33066	608.5	12.71	1.81	0.334	0.0394	-0.1113	8.48
1348	0.552	33150	611.1	12.76	2.79	0.414	0.0446	-0.1135	9.27
1349	0.550	33093	608.3	12.70	3.82	0.492	0.0532	-0.1168	9.26
1350	0.549	33111	607.6	12.69	4.80	0.568	0.0611	-0.1205	9.30
1351	0.550	33204	610.6	12.75	5.80	0.659	0.0720	-0.1261	9.15
1352	0.550	33250	611.8	12.78	6.82	0.802	0.0865	-0.1404	9.27
1353	0.551	33323	613.6	12.81	7.28	0.868	0.0940	-0.1460	9.24
1354	0.551	33366	614.4	12.83	7.84	0.922	0.1022	-0.1436	9.02
1355	0.547	33203	607.6	12.69	8.32	0.966	0.1100	-0.1423	8.78
1356	0.547	33221	607.6	12.69	8.80	0.982	0.1202	-0.1423	8.17
1357	0.551	33472	616.6	12.88	9.06	0.973	0.1234	-0.1388	7.88
1358	0.551	33521	617.5	12.90	9.26	0.973	0.1285	-0.1393	7.57
1359	0.548	33423	612.7	12.80	9.60	0.981	0.1370	-0.1439	7.16
1360	0.549	33520	615.3	12.85	9.76	0.975	0.1386	-0.1423	7.03
1361	0.551	33675	620.6	12.96	10.00	0.969	0.1435	-0.1455	6.75
1362	0.552	33743	622.4	13.00	10.20	0.963	0.1436	-0.1466	6.70
1363	0.549	33691	618.5	12.92	10.48	0.962	0.1515	-0.1524	6.35
1364	0.552	33906	625.5	13.06	10.92	0.935	0.1571	-0.1537	5.95
1365	0.552	33984	627.0	13.10	11.13	0.926	0.1606	-0.1550	5.77
1366	0.548	33854	620.6	12.96	11.37	0.930	0.1707	-0.1578	5.45
1367	0.552	34058	628.0	13.12	11.57	0.914	0.1745	-0.1590	5.24
1368	0.553	34154	630.9	13.18	11.71	0.907	0.1789	-0.1606	5.07
1369	0.553	34217	632.2	13.20	12.23	0.893	0.1914	-0.1675	4.67
1370	0.550	34122	627.1	13.10	12.84	0.881	0.2039	-0.1708	4.32
1371	0.552	34255	631.7	13.19	13.28	0.861	0.2099	-0.1664	4.10
1372	0.553	34394	635.4	13.27	13.75	0.850	0.2182	-0.1706	3.89
1373	0.548	34232	627.9	13.11	14.43	0.851	0.2334	-0.1737	3.65
1374	0.552	34439	635.3	13.27	14.86	0.839	0.2388	-0.1737	3.51
1375	0.554	34567	639.5	13.36	15.28	0.833	0.2456	-0.1749	3.39
1376	0.550	34485	634.3	13.25	15.77	0.841	0.2575	-0.1781	3.26
1377	0.552	34655	639.7	13.36	16.82	0.830	0.2727	-0.1784	3.04
1378	0.552	34734	641.1	13.39	17.80	0.826	0.2967	-0.1826	2.78

Table D.23 – Data from Run 39; nominal conditions $M = 0.500$, $Re = 36,790$

Tab Pt.	M	Re	q_{norm} (Pa)	q_{norm} (psf)	α (deg.)	C_L	C_D	C_M	L/D
1379	0.503	35368	602.0	12.57	-4.19	-0.162	0.0468	-0.0704	-3.46
1380	0.504	35450	604.2	12.62	-3.21	-0.080	0.0373	-0.0777	-2.15
1381	0.501	35371	600.4	12.54	-2.22	-0.011	0.0333	-0.0777	-0.32
1382	0.504	35600	607.2	12.68	-1.20	0.059	0.0309	-0.0751	1.91
1383	0.501	35455	601.0	12.55	-0.20	0.150	0.0297	-0.0819	5.04
1384	0.500	35450	600.2	12.54	0.83	0.258	0.0336	-0.1006	7.68
1385	0.503	35652	607.0	12.68	1.79	0.336	0.0376	-0.1047	8.94
1386	0.504	35704	608.4	12.71	2.80	0.414	0.0430	-0.1083	9.64
1387	0.503	35728	608.4	12.71	3.80	0.488	0.0508	-0.1114	9.60
1388	0.502	35708	607.2	12.68	4.78	0.568	0.0589	-0.1172	9.64
1389	0.499	35543	600.9	12.55	5.84	0.673	0.0702	-0.1247	9.59
1390	0.499	35562	601.0	12.55	6.82	0.806	0.0849	-0.1384	9.50
1391	0.503	35832	609.6	12.73	7.30	0.853	0.0883	-0.1349	9.66
1392	0.503	35859	610.0	12.74	7.83	0.897	0.0945	-0.1332	9.50
1393	0.502	35853	609.5	12.73	8.05	0.913	0.0981	-0.1349	9.30
1394	0.500	35776	605.9	12.65	8.30	0.934	0.1029	-0.1311	9.08
1395	0.499	35716	603.4	12.60	8.56	0.955	0.1080	-0.1348	8.84
1396	0.502	35901	609.7	12.73	8.82	0.959	0.1091	-0.1285	8.79
1397	0.502	35981	611.9	12.78	9.07	0.966	0.1144	-0.1268	8.45
1398	0.502	35969	611.1	12.76	9.31	0.975	0.1195	-0.1287	8.16
1399	0.503	36052	613.6	12.81	9.55	0.974	0.1234	-0.1268	7.90
1400	0.502	36007	611.9	12.78	9.81	0.978	0.1299	-0.1273	7.53
1401	0.500	35912	607.8	12.69	10.07	0.988	0.1356	-0.1313	7.29
1402	0.498	35842	605.2	12.64	10.22	0.993	0.1407	-0.1349	7.06
1403	0.502	36101	613.7	12.82	10.47	0.981	0.1429	-0.1368	6.86
1404	0.502	36115	613.7	12.82	10.62	0.969	0.1431	-0.1385	6.77
1405	0.502	36152	614.6	12.84	10.79	0.971	0.1500	-0.1409	6.47
1406	0.503	36213	616.3	12.87	11.06	0.954	0.1510	-0.1423	6.32
1407	0.502	36171	614.6	12.84	11.30	0.960	0.1577	-0.1473	6.08
1408	0.499	36036	609.2	12.72	11.53	0.953	0.1676	-0.1507	5.68
1409	0.503	36277	617.1	12.89	12.01	0.921	0.1765	-0.1515	5.22
1410	0.502	36312	617.6	12.90	12.66	0.902	0.1943	-0.1630	4.64
1411	0.504	36403	620.5	12.96	13.34	0.875	0.2067	-0.1640	4.24
1412	0.502	36354	618.1	12.91	13.81	0.867	0.2161	-0.1681	4.01
1413	0.500	36242	613.5	12.81	14.17	0.862	0.2246	-0.1695	3.84
1414	0.498	36180	611.0	12.76	14.87	0.856	0.2385	-0.1746	3.59
1415	0.502	36395	618.2	12.91	15.32	0.841	0.2455	-0.1717	3.43
1416	0.503	36476	620.4	12.96	15.84	0.838	0.2544	-0.1752	3.29
1417	0.503	36554	622.2	12.99	16.83	0.830	0.2697	-0.1762	3.08
1418	0.500	36431	617.2	12.89	17.81	0.833	0.2887	-0.1806	2.89

Table D.24 – Data from Run 40; nominal conditions $M = 0.452$, $Re = 40,055$

Tab Pt.	M	Re	q_{norm} (Pa)	q_{norm} (psf)	α (deg.)	C_L	C_D	C_M	L/D
1419	0.453	39525	613.7	12.82	-4.14	-0.123	0.0412	-0.0846	-2.97
1420	0.453	39551	614.1	12.83	-3.22	-0.052	0.0352	-0.0862	-1.48
1421	0.454	39592	615.0	12.84	-2.23	0.013	0.0316	-0.0819	0.40
1422	0.451	39449	609.9	12.74	-1.20	0.078	0.0304	-0.0800	2.57
1423	0.451	39420	608.6	12.71	-0.21	0.160	0.0292	-0.0865	5.46
1424	0.454	39677	616.4	12.87	0.79	0.255	0.0325	-0.0956	7.84
1425	0.454	39772	618.2	12.91	1.77	0.334	0.0369	-0.1038	9.06
1426	0.451	39538	610.4	12.75	2.84	0.423	0.0436	-0.1125	9.70
1427	0.451	39569	610.9	12.76	3.84	0.498	0.0498	-0.1145	9.99
1428	0.454	39857	619.5	12.94	4.81	0.568	0.0571	-0.1162	9.95
1429	0.453	39797	617.4	12.89	5.86	0.669	0.0680	-0.1248	9.84
1430	0.453	39798	617.0	12.89	6.83	0.788	0.0793	-0.1324	9.94
1431	0.449	39532	608.3	12.71	7.33	0.854	0.0868	-0.1356	9.83
1432	0.448	39520	607.5	12.69	7.80	0.890	0.0929	-0.1333	9.58
1433	0.452	39811	616.3	12.87	8.05	0.892	0.0936	-0.1265	9.54
1434	0.452	39825	616.3	12.87	8.29	0.911	0.0980	-0.1273	9.30
1435	0.452	39894	618.1	12.91	8.57	0.926	0.1007	-0.1269	9.19
1436	0.452	39889	617.7	12.90	8.83	0.940	0.1048	-0.1281	8.96
1437	0.453	39972	619.8	12.95	9.11	0.949	0.1089	-0.1248	8.72
1438	0.449	39670	609.9	12.74	9.30	0.972	0.1149	-0.1241	8.46
1439	0.451	39920	617.3	12.89	9.56	0.972	0.1175	-0.1244	8.27
1440	0.453	40026	620.3	12.96	9.80	0.972	0.1215	-0.1228	8.00
1441	0.452	40047	620.4	12.96	10.09	0.979	0.1272	-0.1229	7.69
1442	0.452	40067	620.8	12.97	10.29	0.981	0.1328	-0.1262	7.39
1443	0.452	40055	620.0	12.95	10.50	0.986	0.1369	-0.1278	7.20
1444	0.450	39908	614.8	12.84	10.81	0.991	0.1463	-0.1329	6.77
1445	0.452	40150	621.8	12.99	11.12	0.976	0.1487	-0.1360	6.56
1446	0.453	40203	623.1	13.01	11.34	0.969	0.1510	-0.1425	6.42
1447	0.453	40256	624.4	13.04	11.61	0.960	0.1574	-0.1414	6.10
1448	0.450	40065	617.5	12.90	11.83	0.956	0.1674	-0.1451	5.71
1449	0.450	40137	619.3	12.93	12.07	0.948	0.1716	-0.1507	5.53
1450	0.453	40342	625.3	13.06	12.32	0.933	0.1803	-0.1541	5.18
1451	0.453	40371	626.2	13.08	12.57	0.919	0.1851	-0.1546	4.97
1452	0.454	40458	628.3	13.12	12.81	0.917	0.1885	-0.1589	4.87
1453	0.452	40381	625.3	13.06	13.07	0.905	0.1955	-0.1598	4.63
1454	0.449	40201	619.3	12.93	13.31	0.906	0.2055	-0.1616	4.41
1455	0.452	40448	626.7	13.09	13.57	0.885	0.2047	-0.1597	4.32
1456	0.454	40576	630.2	13.16	13.82	0.877	0.2069	-0.1627	4.24
1457	0.453	40595	630.2	13.16	14.31	0.864	0.2212	-0.1665	3.91
1458	0.451	40458	625.4	13.06	14.81	0.853	0.2322	-0.1664	3.67
1459	0.451	40450	624.6	13.04	15.31	0.849	0.2432	-0.1718	3.49
1460	0.453	40647	630.6	13.17	15.80	0.836	0.2491	-0.1711	3.36
1461	0.453	40691	631.2	13.18	16.78	0.828	0.2661	-0.1739	3.11

Table D.25 – Data from Run 41; nominal conditions $M = 0.501$, $Re = 69,870$

Tab Pt.	M	Re	q_{norm} (Pa)	q_{norm} (psf)	α (deg.)	C_L	C_D	C_M	L/D
1462	0.501	69111	1171.8	24.47	-4.21	-0.099	0.0352	-0.0942	-2.83
1463	0.501	69219	1175.1	24.54	-3.21	-0.010	0.0293	-0.1017	-0.36
1464	0.500	69125	1171.0	24.46	-2.20	0.071	0.0280	-0.1058	2.53
1466	0.502	69362	1178.2	24.61	-2.20	0.070	0.0278	-0.1049	2.53
1467	0.502	69416	1179.1	24.63	-1.22	0.127	0.0285	-0.0997	4.45
1468	0.499	69129	1168.6	24.41	-0.20	0.198	0.0294	-0.1017	6.74
1469	0.499	69162	1169.1	24.42	0.85	0.277	0.0307	-0.1040	9.02
1470	0.502	69476	1179.6	24.64	1.80	0.360	0.0353	-0.1101	10.22
1471	0.502	69589	1183.0	24.71	2.78	0.436	0.0406	-0.1145	10.74
1472	0.502	69540	1180.9	24.66	3.87	0.528	0.0477	-0.1208	11.05
1473	0.502	69640	1183.9	24.73	4.80	0.617	0.0557	-0.1270	11.09
1474	0.500	69469	1177.2	24.59	5.83	0.747	0.0666	-0.1380	11.22
1475	0.499	69363	1173.3	24.50	6.81	0.841	0.0765	-0.1358	10.99
1476	0.502	69644	1182.9	24.70	7.30	0.867	0.0825	-0.1328	10.51
1477	0.502	69668	1183.3	24.71	7.77	0.895	0.0874	-0.1278	10.24
1478	0.502	69693	1183.8	24.72	8.11	0.911	0.0919	-0.1257	9.91
1479	0.500	69538	1177.3	24.59	8.29	0.929	0.0951	-0.1261	9.77
1480	0.502	69840	1187.0	24.79	8.55	0.934	0.0982	-0.1225	9.51
1481	0.502	69796	1185.3	24.76	8.77	0.945	0.1022	-0.1225	9.24
1482	0.502	69837	1186.3	24.78	9.05	0.958	0.1067	-0.1226	8.98
1483	0.502	69881	1187.2	24.80	9.29	0.963	0.1103	-0.1210	8.73
1484	0.500	69668	1178.9	24.62	9.54	0.982	0.1159	-0.1233	8.47
1485	0.501	69870	1185.6	24.76	9.78	0.984	0.1193	-0.1222	8.24
1486	0.502	69940	1187.7	24.81	10.05	0.989	0.1246	-0.1226	7.94
1487	0.502	70061	1190.7	24.87	10.30	0.964	0.1111	-0.1305	8.68

Table D.26 – Data from Run 42; nominal conditions $M = 0.550$, $Re = 90,900$

Tab Pt.	M	Re	q_{norm} (Pa)	q_{norm} (psf)	α (deg.)	C_L	C_D	C_M	L/D
1493	0.549	89879	1649.7	34.46	-4.20	-0.097	0.0326	-0.0991	-2.99
1494	0.551	90205	1660.8	34.69	-3.19	-0.003	0.0271	-0.1065	-0.13
1495	0.551	90372	1665.4	34.78	-2.20	0.079	0.0248	-0.1116	3.19
1496	0.550	90286	1661.4	34.70	-1.21	0.152	0.0258	-0.1113	5.91
1497	0.549	90152	1655.6	34.58	-0.22	0.218	0.0280	-0.1110	7.80
1498	0.552	90625	1672.5	34.93	0.82	0.290	0.0302	-0.1104	9.61
1499	0.552	90617	1671.5	34.91	1.83	0.369	0.0341	-0.1131	10.82
1500	0.550	90478	1665.0	34.77	2.81	0.457	0.0411	-0.1193	11.13
1501	0.553	90800	1676.4	35.01	3.79	0.540	0.0480	-0.1233	11.25
1502	0.552	90770	1674.5	34.97	4.83	0.652	0.0570	-0.1339	11.44
1503	0.550	90573	1666.1	34.80	5.80	0.783	0.0668	-0.1442	11.72
1504	0.552	90786	1673.8	34.96	6.79	0.866	0.0773	-0.1382	11.20
1505	0.552	90850	1675.1	34.98	7.31	0.896	0.0829	-0.1340	10.81
1506	0.552	90901	1676.7	35.02	7.81	0.924	0.0889	-0.1307	10.39
1507	0.550	90710	1668.7	34.85	8.04	0.940	0.0923	-0.1291	10.19
1508	0.550	90721	1668.1	34.84	8.29	0.953	0.0964	-0.1287	9.88
1509	0.551	90922	1675.3	34.99	8.55	0.960	0.0993	-0.1273	9.67
1510	0.552	91048	1679.4	35.08	8.92	0.974	0.1049	-0.1249	9.29
1511	0.552	91068	1679.6	35.08	9.04	0.980	0.1069	-0.1256	9.17
1512	0.550	90910	1672.7	34.93	9.29	0.990	0.1113	-0.1253	8.89
1513	0.550	90900	1671.9	34.92	9.54	0.998	0.1163	-0.1260	8.58

Table D.27 – Data from Run 43; nominal conditions $M = 0.450$, $Re = 92,088$

Tab Pt.	M	Re	q_{norm} (Pa)	q_{norm} (psf)	α (deg.)	C_L	C_D	C_M	L/D
1523	0.450	91344	1407.7	29.40	-4.19	-0.076	0.0281	-0.0986	-2.72
1524	0.451	91630	1416.3	29.58	-3.20	0.007	0.0241	-0.1029	0.30
1525	0.452	91810	1421.4	29.69	-2.21	0.086	0.0224	-0.1066	3.83
1526	0.452	91857	1422.3	29.71	-1.19	0.155	0.0240	-0.1067	6.48
1527	0.450	91569	1412.5	29.50	-0.22	0.220	0.0257	-0.1062	8.56
1528	0.451	91861	1420.7	29.67	0.79	0.287	0.0288	-0.1067	9.97
1529	0.452	91911	1422.0	29.70	1.79	0.364	0.0333	-0.1097	10.96
1530	0.450	91666	1413.0	29.51	2.83	0.452	0.0427	-0.1173	10.59
1531	0.450	91789	1416.5	29.58	3.80	0.543	0.0480	-0.1231	11.32
1532	0.452	92119	1426.8	29.80	4.82	0.642	0.0551	-0.1291	11.65
1533	0.452	92123	1426.4	29.79	5.82	0.758	0.0639	-0.1381	11.85
1534	0.452	92080	1424.8	29.76	6.79	0.822	0.0718	-0.1322	11.44
1535	0.450	91824	1415.8	29.57	7.31	0.854	0.0774	-0.1283	11.04
1536	0.452	92209	1427.4	29.81	7.80	0.875	0.0827	-0.1245	10.57
1537	0.451	92154	1425.3	29.77	8.05	0.886	0.0855	-0.1223	10.36
1538	0.451	92155	1424.9	29.76	8.33	0.899	0.0892	-0.1218	10.07
1539	0.450	91924	1417.2	29.60	8.56	0.916	0.0927	-0.1216	9.88
1540	0.450	91914	1416.4	29.58	8.79	0.928	0.0956	-0.1210	9.70
1541	0.451	92214	1425.4	29.77	9.06	0.935	0.0997	-0.1199	9.38
1542	0.451	92264	1426.7	29.80	9.31	0.946	0.1032	-0.1192	9.17
1543	0.451	92266	1426.3	29.79	9.57	0.958	0.1077	-0.1173	8.90
1544	0.451	92311	1427.2	29.81	9.79	0.966	0.1119	-0.1175	8.63
1545	0.450	92088	1419.5	29.65	10.05	0.980	0.1177	-0.1181	8.33
1546	0.450	92055	1418.4	29.62	10.29	0.989	0.1225	-0.1193	8.07
1552	0.451	92518	1430.1	29.87	10.34	0.982	0.1233	-0.1190	7.96
1553	0.451	92588	1431.9	29.91	10.41	0.948	0.1017	-0.1267	9.32

Table D.28 – Data from Run 45; nominal conditions $M = 0.800$, $Re = 70,000$

Tab Pt.	M	Re	q_{norm} (Pa)	q_{norm} (psf)	α (deg.)	C_L	C_D	C_M	L/D
1566	0.802	68810	1701.3	35.53	-4.22	-0.301	0.0661	-0.0072	-4.56
1567	0.801	68844	1701.0	35.53	-3.21	-0.256	0.0564	-0.0160	-4.54
1568	0.804	69067	1711.1	35.74	-2.21	-0.161	0.0476	-0.0368	-3.38
1569	0.804	69087	1712.1	35.76	-1.26	-0.039	0.0412	-0.0647	-0.94
1570	0.804	69128	1713.0	35.78	-0.19	0.089	0.0378	-0.0851	2.35
1571	0.802	69074	1707.9	35.67	0.90	0.205	0.0392	-0.0985	5.22
1572	0.803	69203	1713.0	35.78	1.77	0.295	0.0430	-0.1082	6.86
1573	0.804	69274	1715.8	35.84	2.82	0.395	0.0505	-0.1217	7.81
1574	0.803	69275	1714.7	35.81	3.76	0.475	0.0611	-0.1327	7.77
1575	0.803	69321	1716.4	35.85	4.77	0.544	0.0734	-0.1408	7.41
1576	0.801	69270	1711.8	35.75	5.80	0.608	0.0888	-0.1523	6.85
1577	0.800	69269	1710.7	35.73	6.84	0.665	0.1064	-0.1618	6.25
1578	0.803	69439	1718.7	35.90	7.28	0.684	0.1144	-0.1658	5.98
1579	0.802	69436	1717.3	35.87	7.79	0.708	0.1231	-0.1691	5.75
1580	0.802	69512	1720.1	35.93	8.27	0.729	0.1320	-0.1733	5.52
1581	0.801	69455	1715.9	35.84	8.77	0.751	0.1419	-0.1775	5.29
1582	0.800	69452	1714.5	35.81	9.30	0.771	0.1523	-0.1810	5.06
1583	0.799	69482	1714.5	35.81	9.78	0.785	0.1613	-0.1831	4.87
1584	0.801	69605	1720.6	35.93	10.01	0.790	0.1659	-0.1843	4.76
1585	0.802	69686	1724.0	36.01	10.42	0.798	0.1732	-0.1850	4.61
1586	0.802	69711	1723.9	36.00	10.67	0.806	0.1781	-0.1867	4.52
1587	0.800	69694	1720.9	35.94	10.92	0.813	0.1839	-0.1878	4.42
1588	0.800	69699	1720.4	35.93	11.19	0.818	0.1889	-0.1889	4.33
1589	0.802	69832	1726.8	36.06	11.44	0.822	0.1932	-0.1899	4.25
1590	0.802	69902	1729.0	36.11	11.69	0.824	0.1974	-0.1900	4.18
1591	0.802	69971	1730.9	36.15	11.96	0.828	0.2022	-0.1899	4.09
1592	0.800	69937	1726.7	36.06	12.31	0.833	0.2087	-0.1905	3.99
1593	0.799	69947	1726.0	36.05	12.56	0.839	0.2146	-0.1927	3.91
1594	0.802	70118	1734.6	36.23	12.75	0.840	0.2174	-0.1918	3.86
1595	0.802	70162	1735.8	36.25	13.02	0.843	0.2223	-0.1930	3.79
1596	0.802	70230	1737.8	36.29	13.26	0.844	0.2263	-0.1924	3.73
1597	0.803	70290	1740.0	36.34	13.54	0.848	0.2315	-0.1934	3.66
1598	0.800	70209	1733.9	36.21	13.79	0.854	0.2371	-0.1954	3.60
1599	0.800	70256	1734.5	36.23	14.07	0.856	0.2421	-0.1953	3.54
1600	0.802	70393	1741.7	36.38	14.27	0.857	0.2462	-0.1953	3.48
1601	0.803	70408	1742.4	36.39	14.53	0.859	0.2507	-0.1954	3.43
1602	0.802	70436	1742.3	36.39	14.82	0.861	0.2560	-0.1958	3.36
1603	0.803	70514	1745.2	36.45	15.03	0.863	0.2597	-0.1958	3.32
1604	0.800	70424	1739.4	36.33	15.31	0.869	0.2663	-0.1979	3.27
1605	0.800	70431	1738.6	36.31	15.56	0.871	0.2709	-0.1969	3.22
1606	0.799	70434	1738.1	36.30	15.75	0.871	0.2739	-0.1966	3.18
1607	0.802	70590	1745.7	36.46	16.10	0.872	0.2806	-0.1981	3.11
1608	0.801	70587	1744.6	36.44	16.30	0.874	0.2840	-0.1978	3.08
1609	0.802	70658	1747.7	36.50	16.60	0.878	0.2908	-0.1987	3.02

Continued

Table D.28 – Data from Run 45, continued

1610	0.802	70705	1749.2	36.53	16.78	0.880	0.2936	-0.1992	3.00
1611	0.799	70609	1742.3	36.39	17.75	0.890	0.3128	-0.2009	2.84
1612	0.801	70774	1749.6	36.54	18.84	0.898	0.3339	-0.2030	2.69
1613	0.800	70744	1747.4	36.50	19.81	0.910	0.3549	-0.2065	2.56
1614	0.800	70767	1747.1	36.49	20.85	0.919	0.3767	-0.2096	2.44
1615	0.798	70756	1744.4	36.43	21.80	0.932	0.3990	-0.2129	2.33
1616	0.801	70974	1753.7	36.63	22.80	0.940	0.4219	-0.2152	2.23
1617	0.801	71001	1753.9	36.63	23.76	0.949	0.4435	-0.2192	2.14

Table D.29 – Data from Run 46; nominal conditions $M = 0.800$, $Re = 141,000$

Tab Pt.	M	Re	q_{norm} (Pa)	q_{norm} (psf)	α (deg.)	C_L	C_D	C_M	L/D
1618	0.801	140571	3474.2	72.56	-4.16	-0.293	0.0614	-0.0221	-4.77
1619	0.803	140862	3488.3	72.86	-3.19	-0.210	0.0501	-0.0442	-4.18
1620	0.804	140977	3493.9	72.97	-2.19	-0.076	0.0405	-0.0791	-1.89
1621	0.804	140977	3493.3	72.96	-1.12	0.089	0.0363	-0.1167	2.45
1622	0.803	140954	3490.8	72.91	-0.21	0.207	0.0382	-0.1339	5.41
1623	0.801	140745	3479.6	72.67	0.82	0.312	0.0424	-0.1417	7.36
1624	0.803	140953	3490.3	72.90	1.79	0.395	0.0484	-0.1447	8.16
1625	0.804	141031	3493.6	72.97	2.80	0.466	0.0554	-0.1457	8.41
1626	0.803	140976	3489.4	72.88	3.78	0.550	0.0646	-0.1542	8.51
1627	0.803	141033	3490.6	72.90	4.80	0.645	0.0770	-0.1650	8.38
1628	0.801	140868	3480.8	72.70	5.85	0.728	0.0928	-0.1735	7.85
1629	0.801	140960	3484.5	72.78	6.79	0.787	0.1087	-0.1785	7.23
1630	0.802	140984	3486.3	72.81	7.30	0.812	0.1179	-0.1813	6.89
1631	0.801	140978	3484.6	72.78	7.87	0.835	0.1277	-0.1823	6.54
1632	0.801	141024	3485.3	72.79	8.05	0.840	0.1310	-0.1824	6.41
1633	0.801	141028	3484.7	72.78	8.30	0.848	0.1354	-0.1829	6.26
1634	0.800	141014	3482.9	72.74	8.58	0.857	0.1412	-0.1840	6.07
1635	0.801	141157	3489.5	72.88	8.79	0.860	0.1448	-0.1840	5.94
1636	0.801	141195	3490.6	72.90	9.04	0.866	0.1495	-0.1846	5.79
1637	0.801	141189	3489.7	72.88	9.29	0.871	0.1545	-0.1854	5.64
1638	0.801	141199	3489.5	72.88	9.55	0.877	0.1593	-0.1862	5.50
1639	0.800	141121	3484.0	72.76	9.82	0.881	0.1645	-0.1869	5.35
1640	0.799	141150	3483.3	72.75	10.05	0.886	0.1690	-0.1881	5.24
1641	0.801	141321	3493.2	72.96	10.29	0.886	0.1730	-0.1889	5.12
1642	0.801	141306	3491.1	72.91	10.56	0.887	0.1767	-0.1891	5.02
1643	0.801	141378	3494.4	72.98	10.56	0.887	0.1756	-0.1886	5.05
1644	0.801	141348	3491.7	72.93	10.57	0.888	0.1771	-0.1891	5.01
1645	0.800	141353	3491.1	72.91	10.81	0.887	0.1791	-0.1887	4.96
1646	0.800	141353	3491.5	72.92	10.80	0.887	0.1752	-0.1888	5.06
1647	0.799	141276	3485.9	72.80	10.81	0.890	0.1806	-0.1897	4.93

Table D.30 – Data from Run 47; nominal conditions $M = 0.300$, $Re = 160,000$

Tab Pt.	M	Re	q_{norm} (Pa)	q_{norm} (psf)	α (deg.)	C_L	C_D	C_M	L/D
1654	0.301	158938	1688.5	35.26	-4.22	-0.041	0.0218	-0.1002	-1.87
1655	0.301	158532	1679.4	35.08	-3.21	0.040	0.0193	-0.1063	2.08
1656	0.300	158473	1678.0	35.05	-2.20	0.121	0.0190	-0.1108	6.34
1657	0.302	159157	1692.6	35.35	-1.20	0.194	0.0202	-0.1138	9.63
1658	0.302	159189	1693.0	35.36	-0.20	0.269	0.0230	-0.1159	11.73
1659	0.301	159046	1689.3	35.28	0.80	0.346	0.0272	-0.1189	12.75
1660	0.301	158628	1680.5	35.10	1.80	0.428	0.0323	-0.1237	13.25
1661	0.302	159235	1693.2	35.36	2.81	0.506	0.0366	-0.1254	13.85
1662	0.302	159275	1693.9	35.38	3.80	0.602	0.0434	-0.1337	13.88
1663	0.302	159345	1695.3	35.41	4.80	0.697	0.0503	-0.1393	13.85
1664	0.301	158926	1685.8	35.21	5.80	0.768	0.0578	-0.1351	13.29
1665	0.302	159398	1695.8	35.42	6.79	0.811	0.0658	-0.1276	12.32
1666	0.302	159327	1694.0	35.38	7.31	0.836	0.0707	-0.1240	11.82
1667	0.302	159442	1696.2	35.43	7.80	0.862	0.0758	-0.1223	11.36
1668	0.301	159032	1687.2	35.24	8.31	0.894	0.0823	-0.1220	10.86
1669	0.302	159457	1696.4	35.43	8.81	0.915	0.0881	-0.1204	10.39
1670	0.302	159573	1698.6	35.48	9.05	0.928	0.0919	-0.1199	10.10
1671	0.302	159536	1697.7	35.46	9.31	0.940	0.0952	-0.1188	9.87
1672	0.302	159519	1697.2	35.45	9.56	0.952	0.0991	-0.1176	9.60
1673	0.301	159004	1685.9	35.21	9.80	0.969	0.1044	-0.1185	9.29
1674	0.302	159562	1697.7	35.46	9.90	0.967	0.1054	-0.1174	9.18
1675	0.302	159604	1698.6	35.48	10.03	0.973	0.1080	-0.1177	9.01
1676	0.302	159543	1697.2	35.45	10.10	0.977	0.1091	-0.1179	8.96
1677	0.302	159567	1697.4	35.45	10.20	0.980	0.1113	-0.1173	8.80
1678	0.301	159091	1686.8	35.23	10.30	0.992	0.1140	-0.1190	8.70
1679	0.302	159513	1695.8	35.42	10.40	0.990	0.1157	-0.1182	8.55
1680	0.302	159562	1696.7	35.44	10.50	0.992	0.1180	-0.1183	8.41
1681	0.302	159693	1699.0	35.48	10.60	0.997	0.1207	-0.1196	8.27
1682	0.302	159785	1700.8	35.52	10.71	0.999	0.1229	-0.1191	8.13
1683	0.301	159285	1689.9	35.29	10.80	1.004	0.1244	-0.1275	8.07

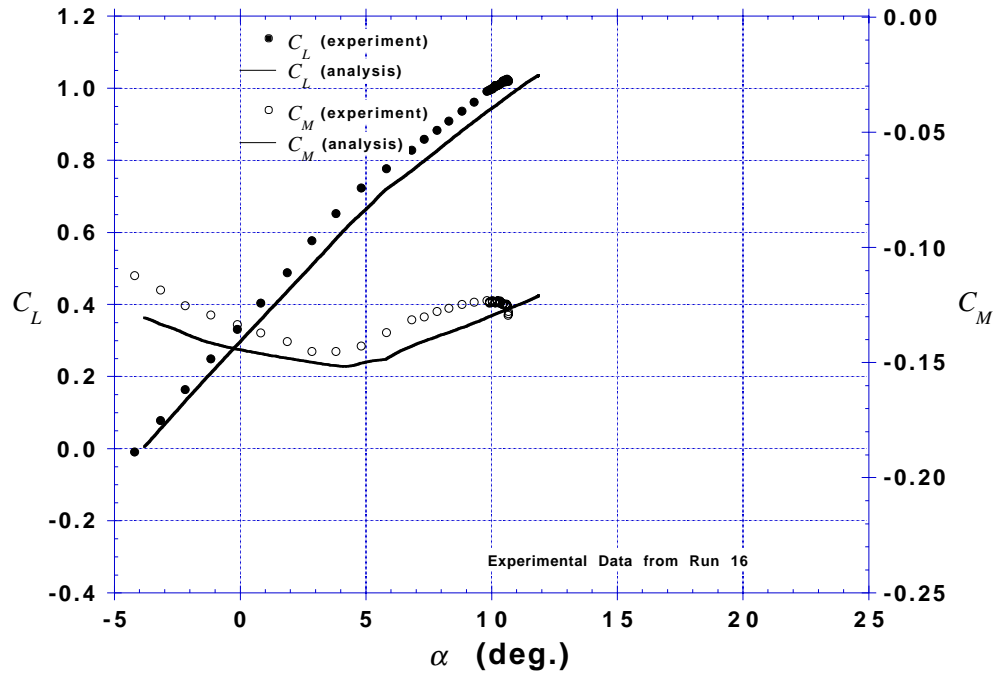


Figure D.1 – C_L and C_M vs α ; nominal conditions $M = 0.301$, $Re = 249,123$

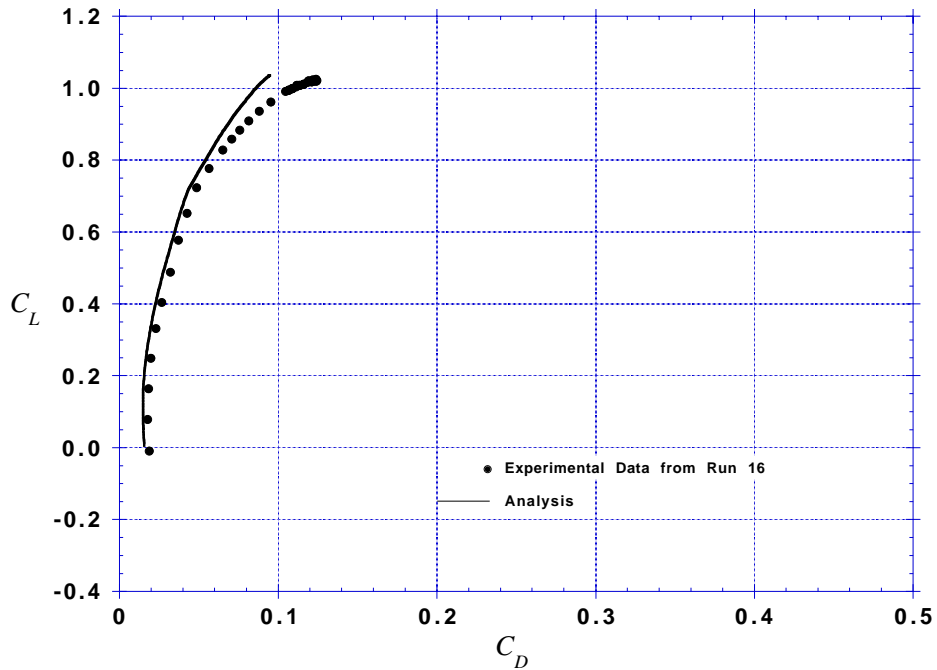


Figure D.2 – C_L vs C_D ; nominal conditions $M = 0.301$, $Re = 249,123$

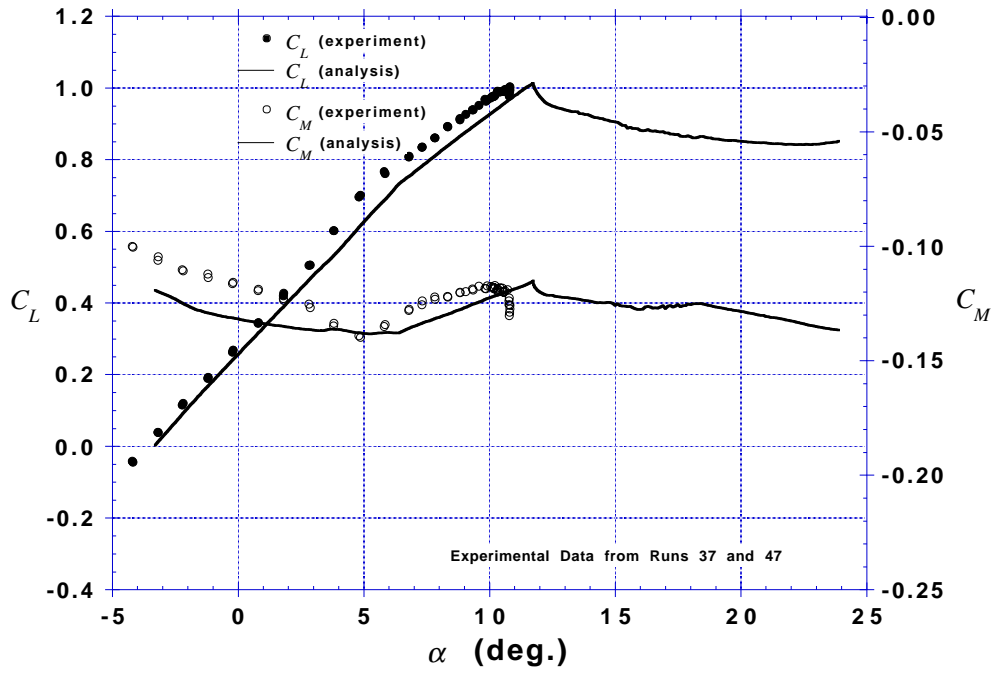


Figure D.3 – C_L and C_M vs α ; nominal conditions $M = 0.300$, $Re = 160,000$

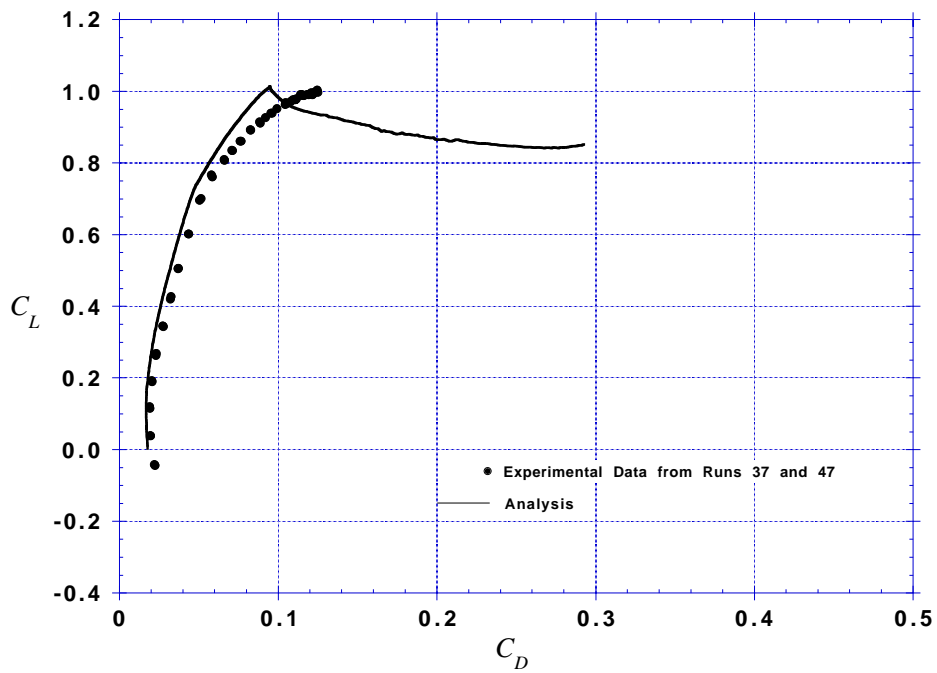


Figure D.4 – C_L vs C_D ; nominal conditions $M = 0.300$, $Re = 160,000$

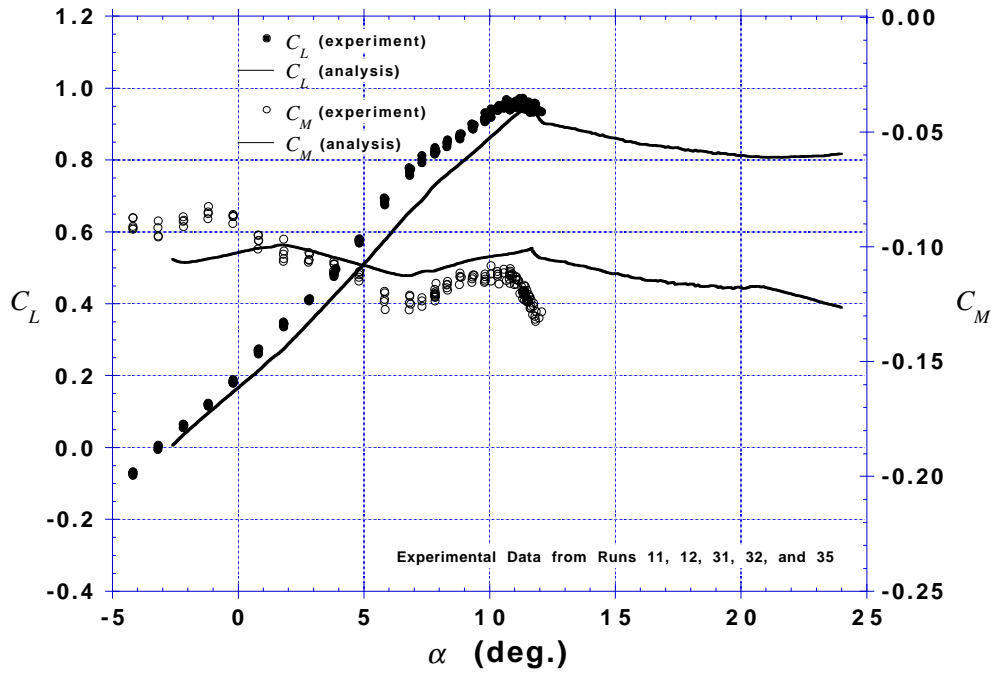


Figure D.5 – C_L and C_M vs α ; nominal conditions $M = 0.300$, $Re = 59,140$

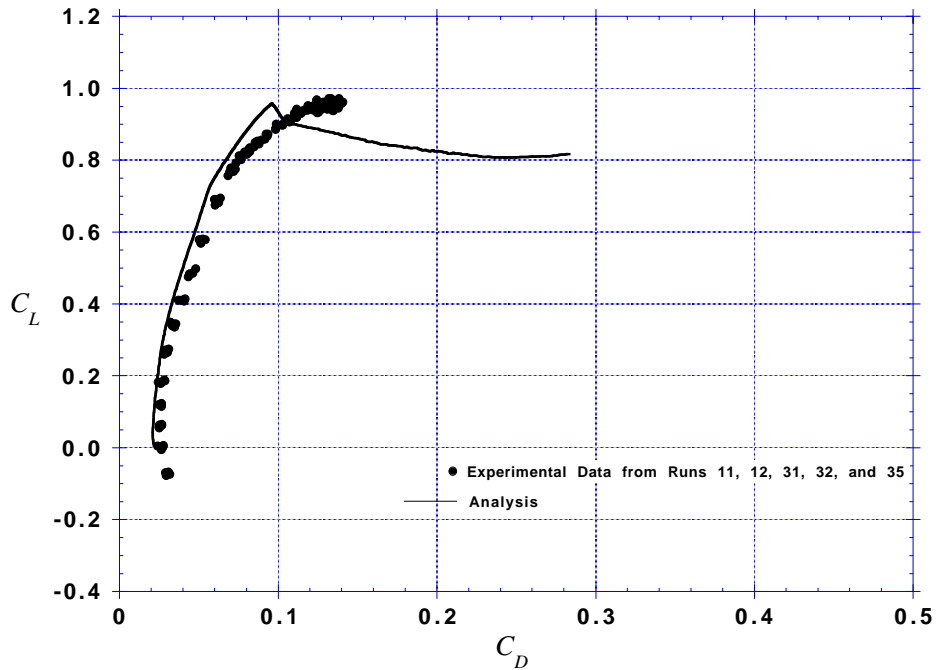


Figure D.6 – C_L vs C_D ; nominal conditions $M = 0.300$, $Re = 59,140$

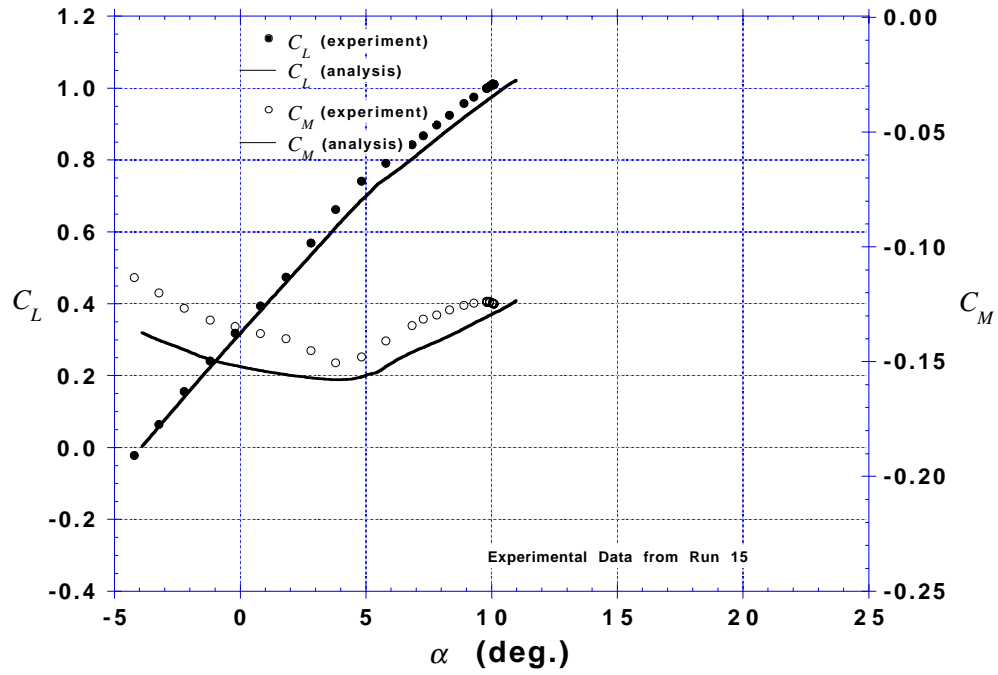


Figure D.7 – C_L and C_M vs α ; nominal conditions $M = 0.407$, $Re = 250,712$

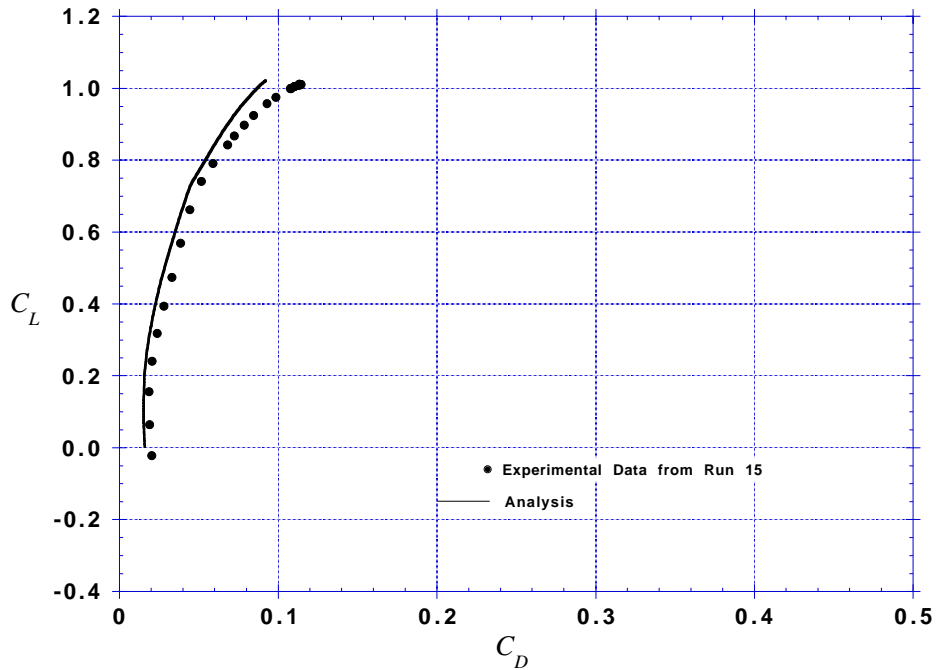


Figure D.8 – C_L vs C_D ; nominal conditions $M = 0.407$, $Re = 250,712$

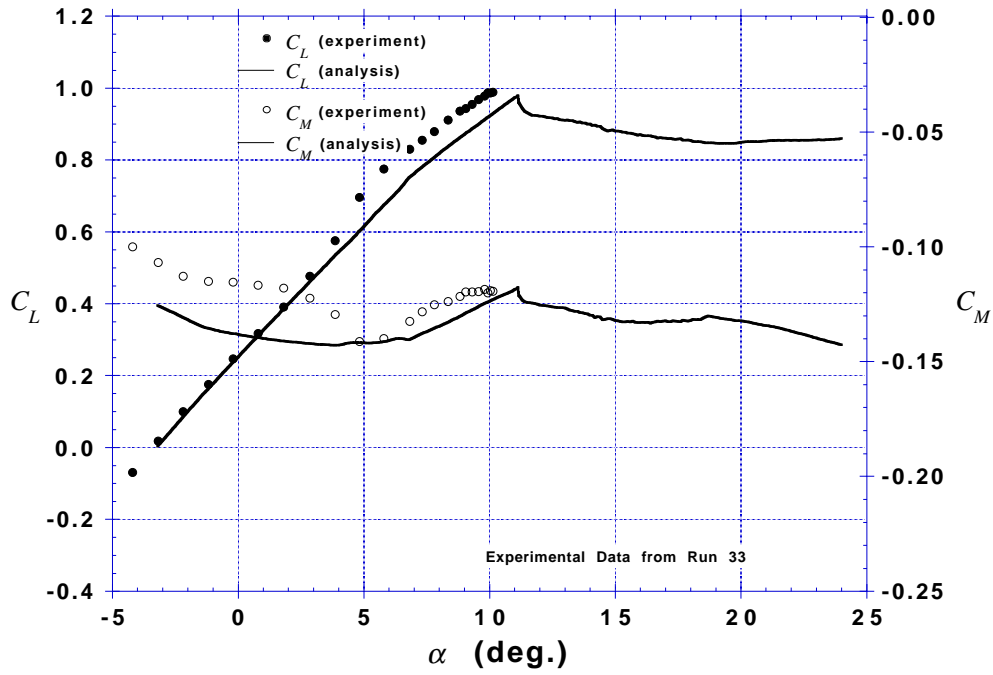


Figure D.9 – C_L and C_M vs α ; nominal conditions $M = 0.451$, $Re = 138,206$

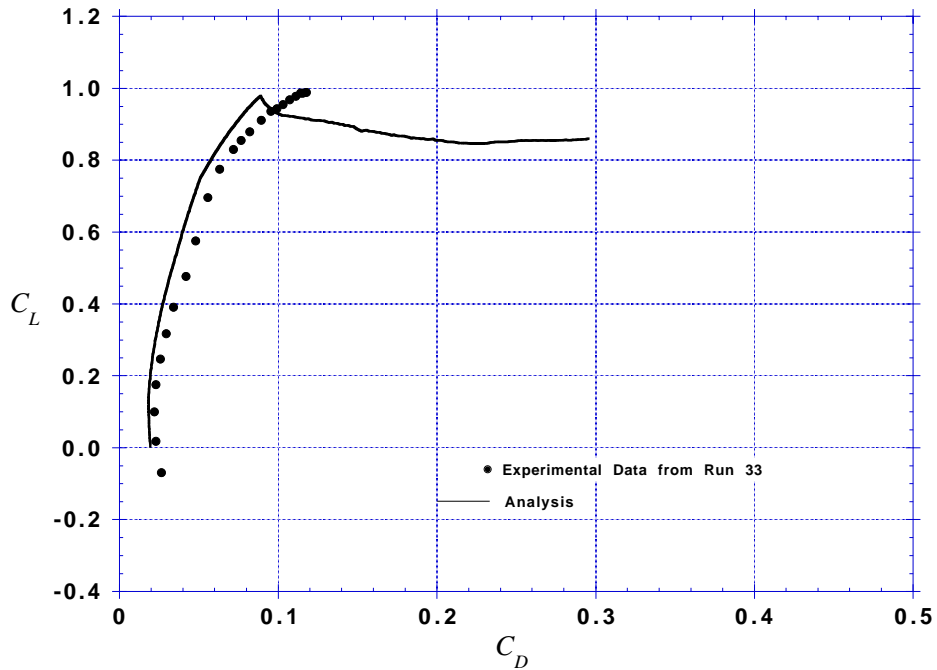


Figure D.10 – C_L vs C_D ; nominal conditions $M = 0.451$, $Re = 138,206$

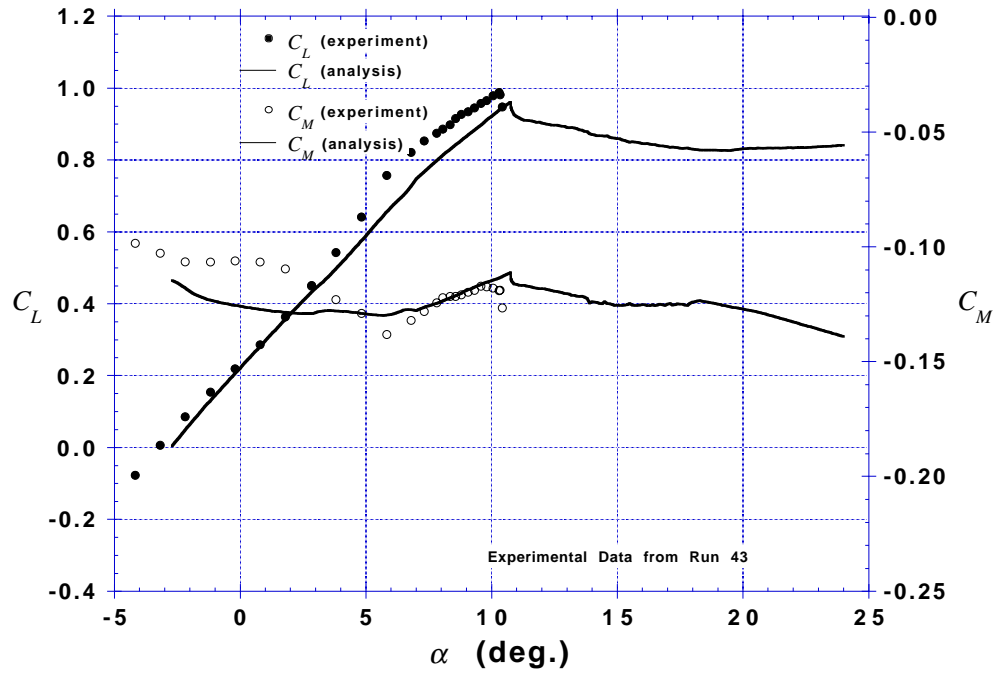


Figure D.11 – C_L and C_M vs α ; nominal conditions $M = 0.450$, $Re = 92,088$

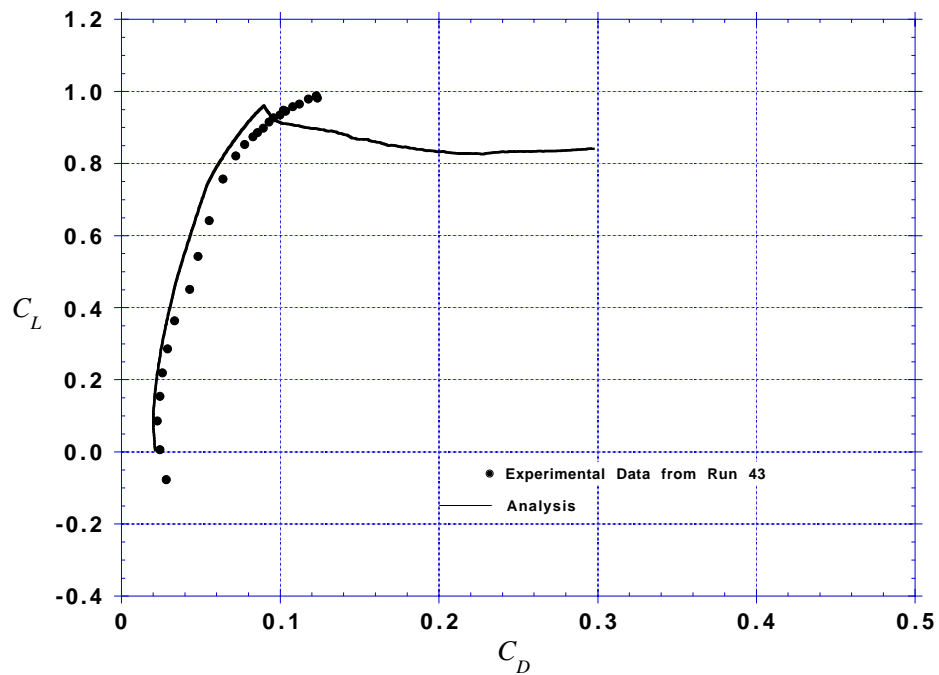


Figure D.12 – C_L vs C_D ; nominal conditions $M = 0.450$, $Re = 92,088$

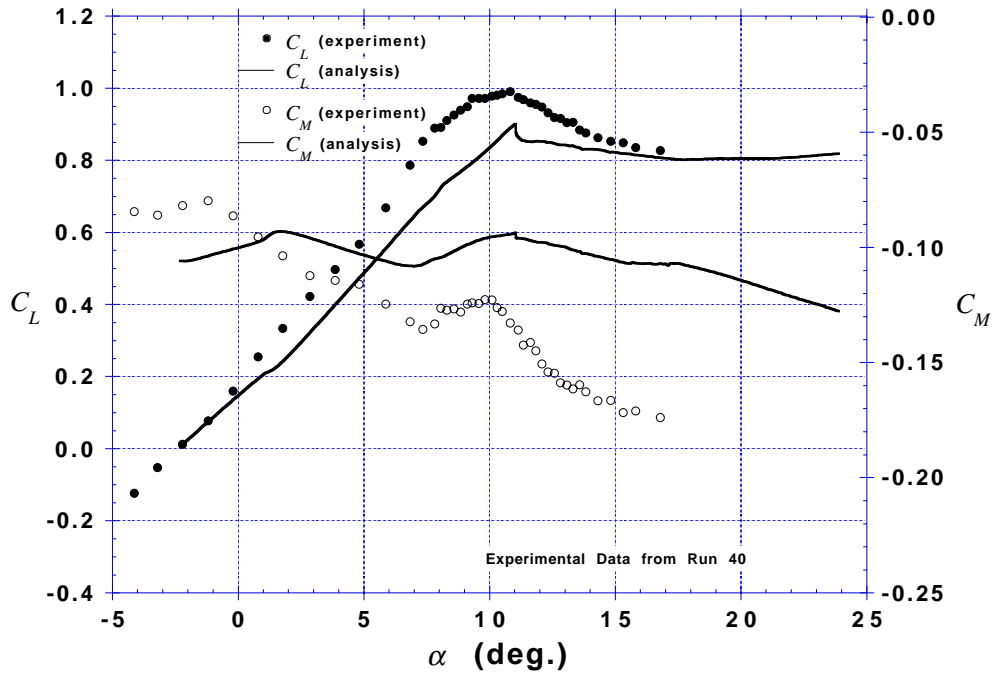


Figure D.13 – C_L and C_M vs α ; nominal conditions $M = 0.452$, $Re = 40,055$

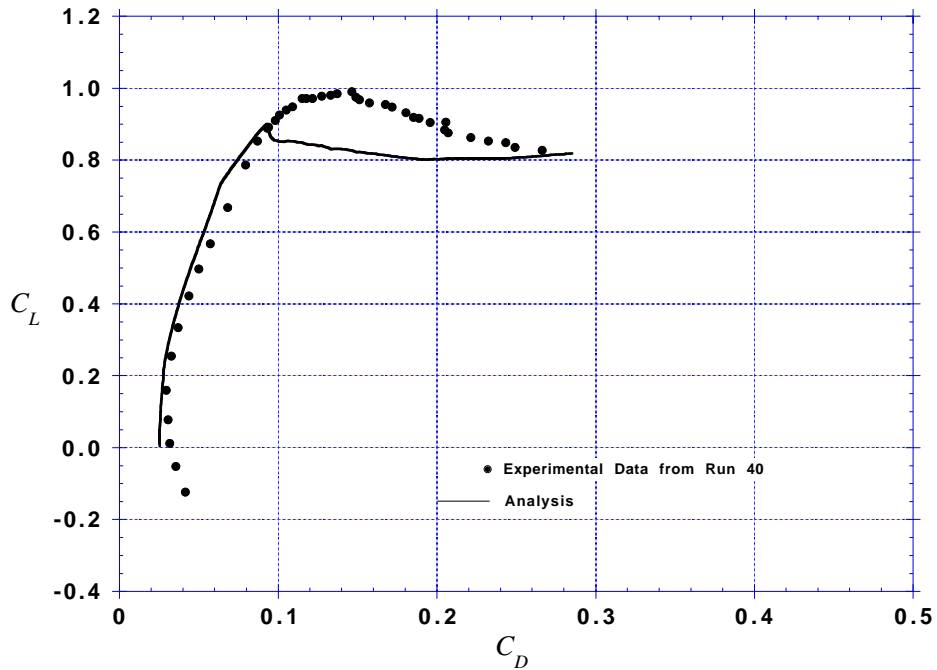


Figure D.14 – C_L vs C_D ; nominal conditions $M = 0.452$, $Re = 40,055$

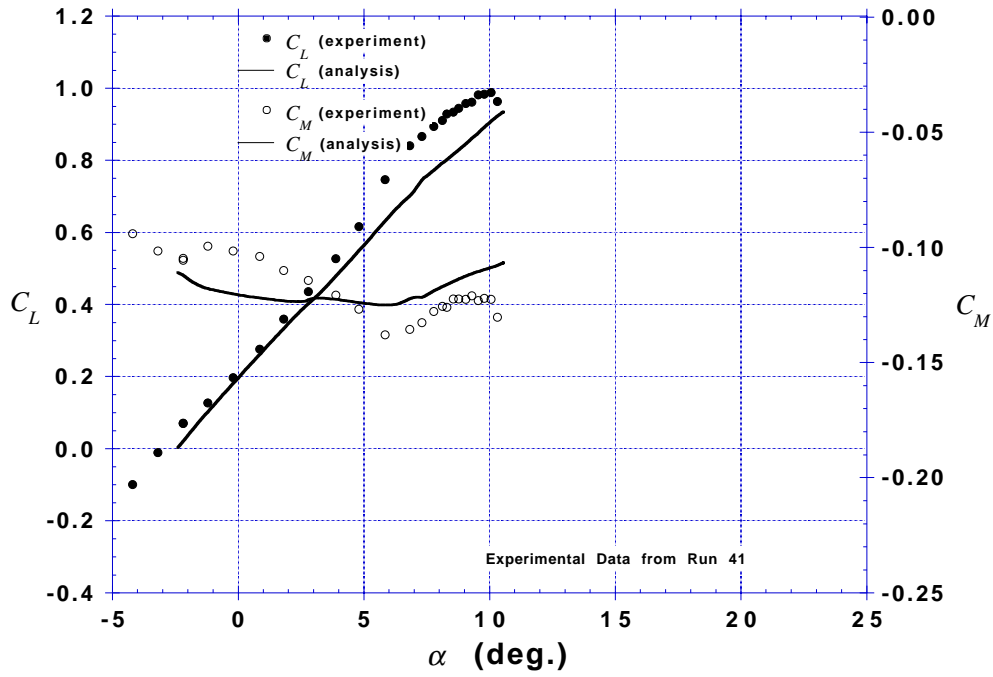


Figure D.15 – C_L and C_M vs α ; nominal conditions $M = 0.501$, $Re = 69,870$

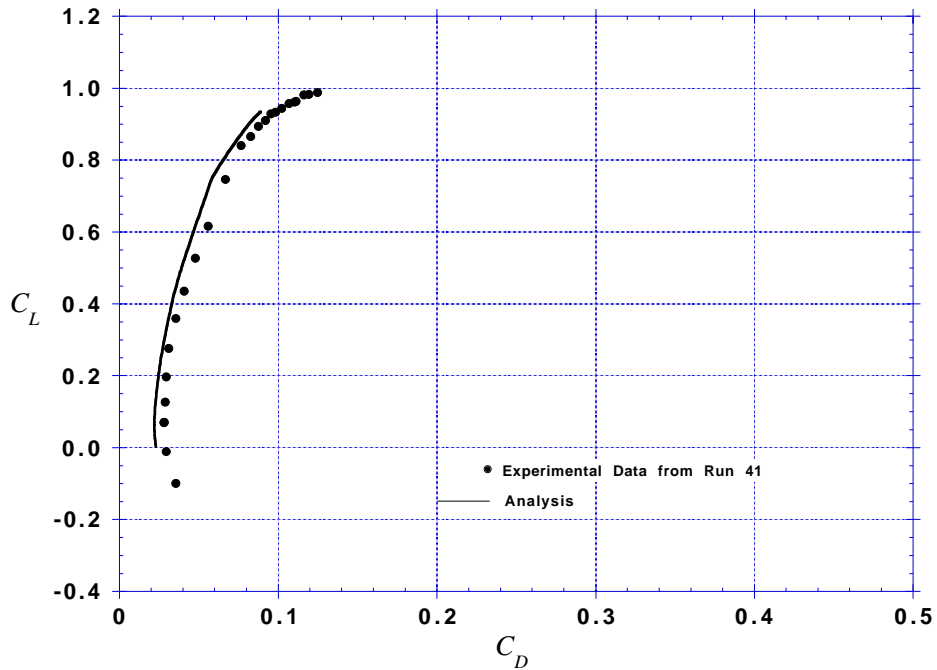


Figure D.16 – C_L vs C_D ; nominal conditions $M = 0.501$, $Re = 69,870$

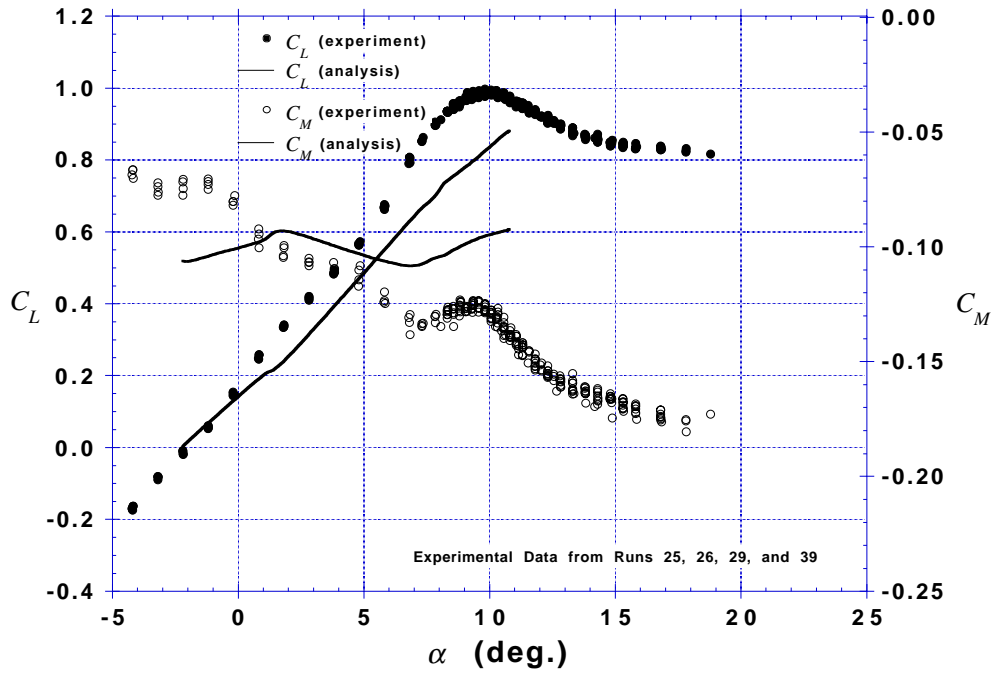


Figure D.17 – C_L and C_M vs α ; nominal conditions $M = 0.500$, $Re = 36,790$

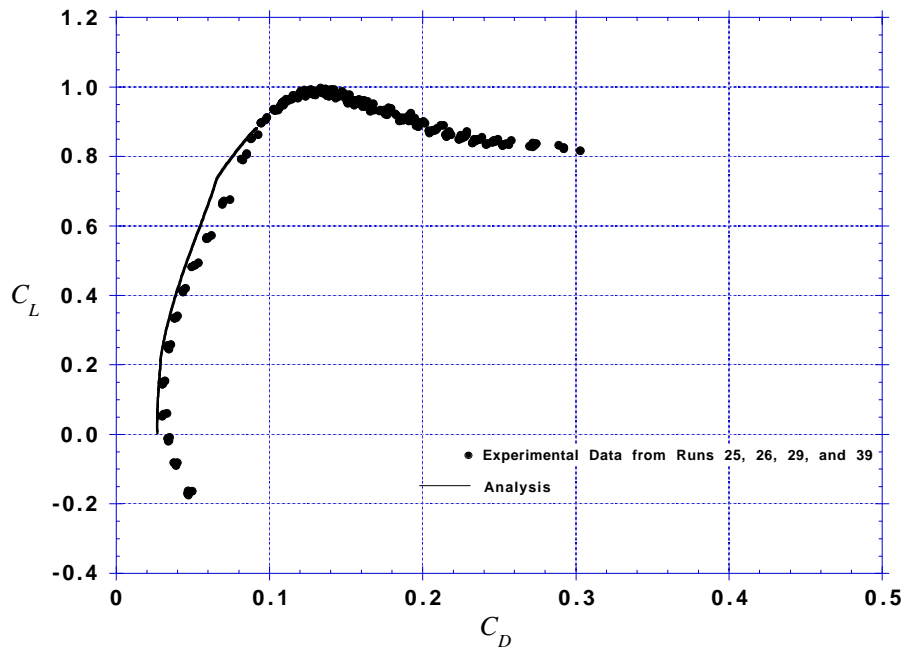


Figure D.18 – C_L vs C_D ; nominal conditions $M = 0.500$, $Re = 36,790$

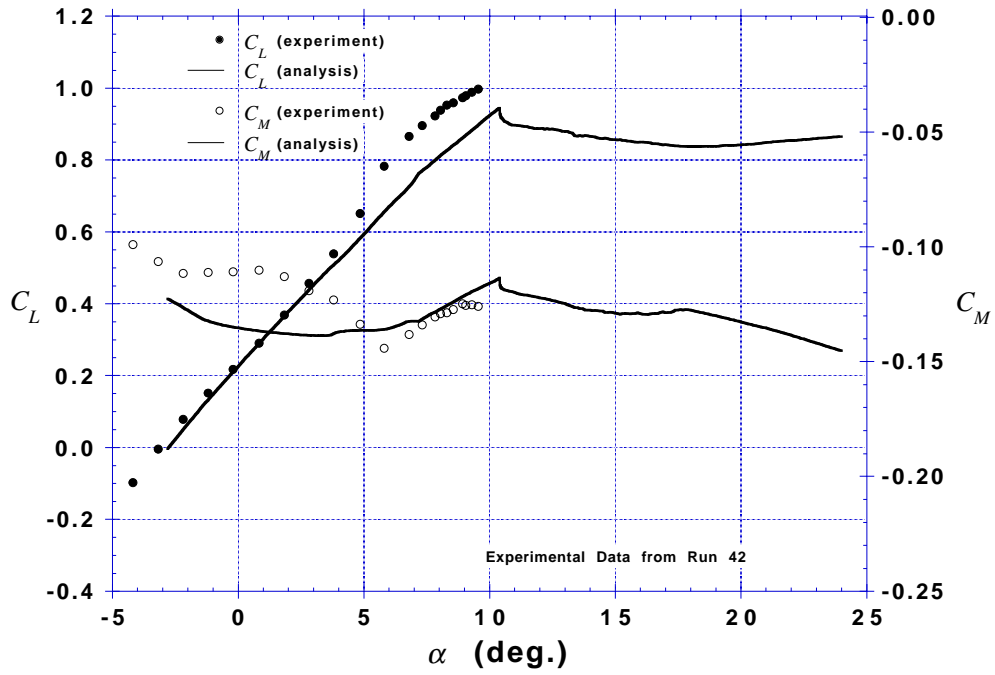


Figure D.19 – C_L and C_M vs α ; nominal conditions $M = 0.550$, $Re = 90,900$

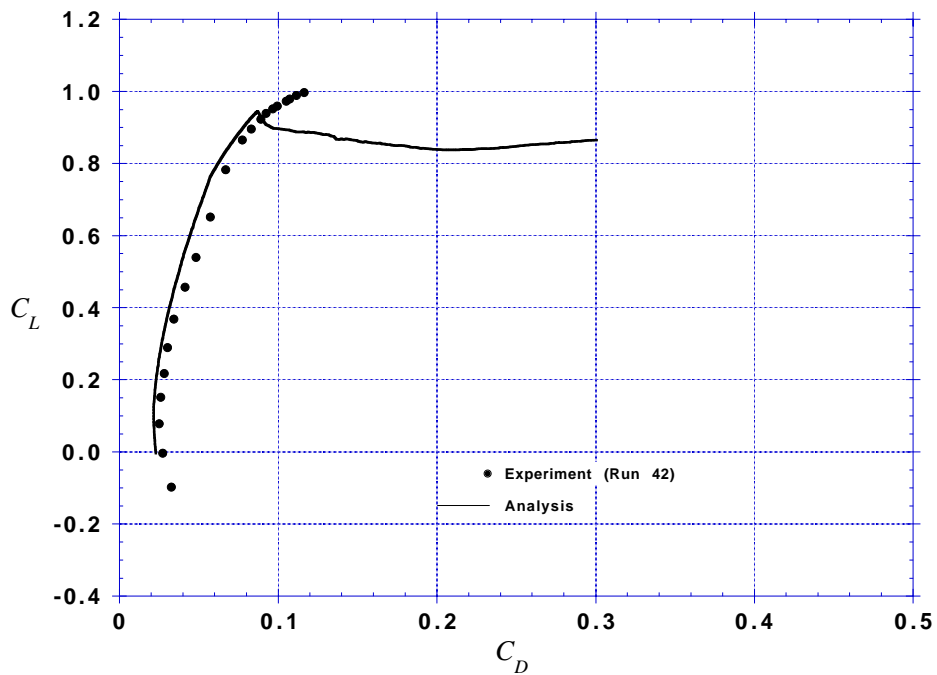


Figure D.20 – C_L vs C_D ; nominal conditions $M = 0.550$, $Re = 90,900$

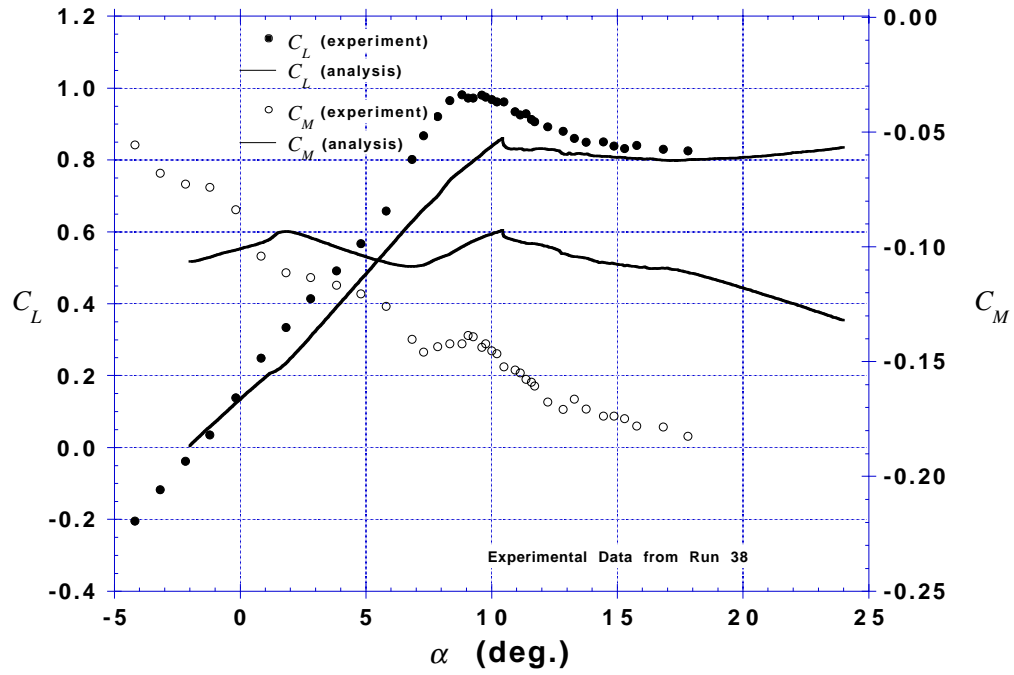


Figure D.21 – C_L and C_M vs α ; nominal conditions $M = 0.551$, $Re = 33,521$

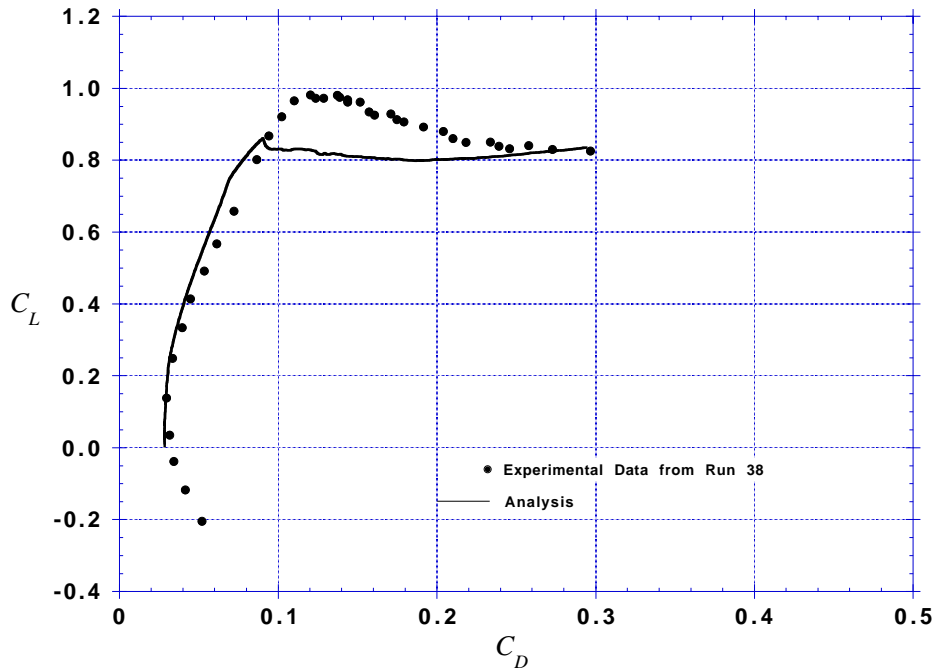


Figure D.22 – C_L vs C_D ; nominal conditions $M = 0.551$, $Re = 33,521$

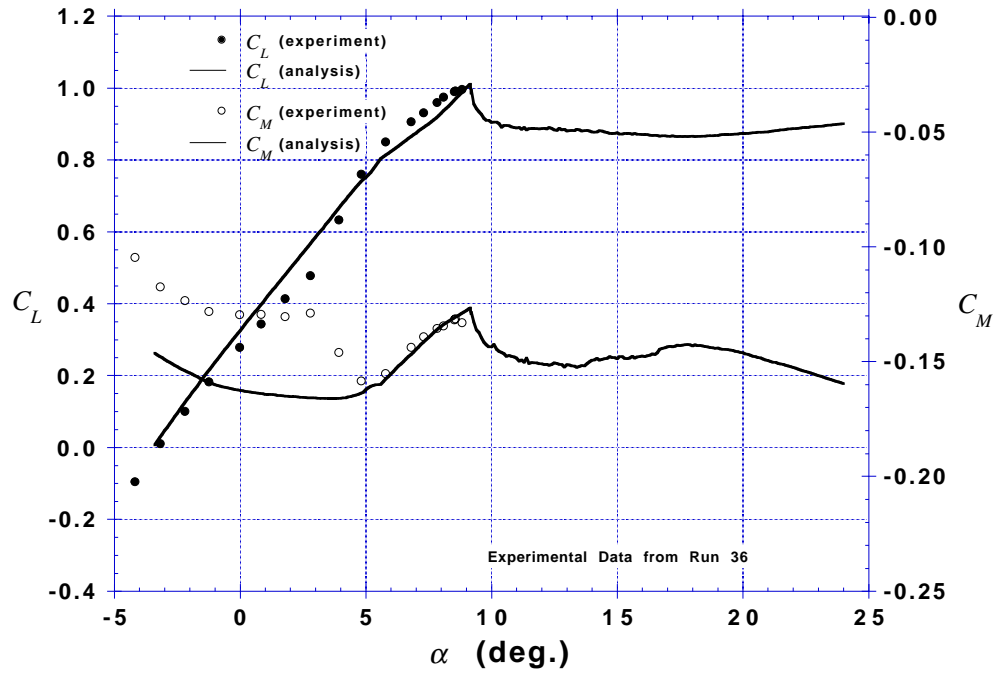


Figure D.23 – C_L and C_M vs α ; nominal conditions $M = 0.599$, $Re = 176,488$

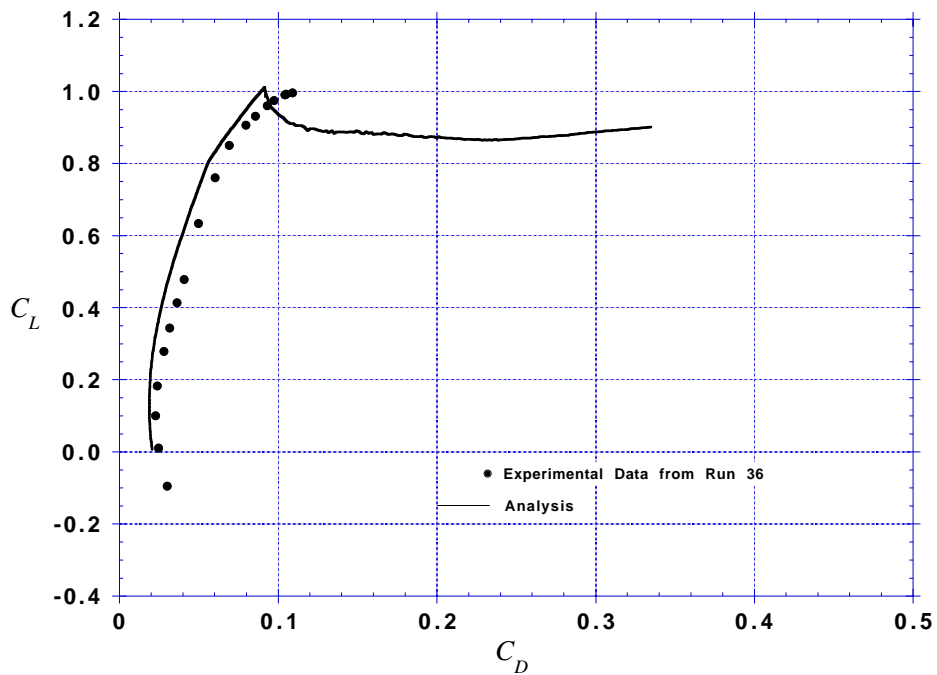


Figure D.24 – C_L vs C_D ; nominal conditions $M = 0.599$, $Re = 176,488$

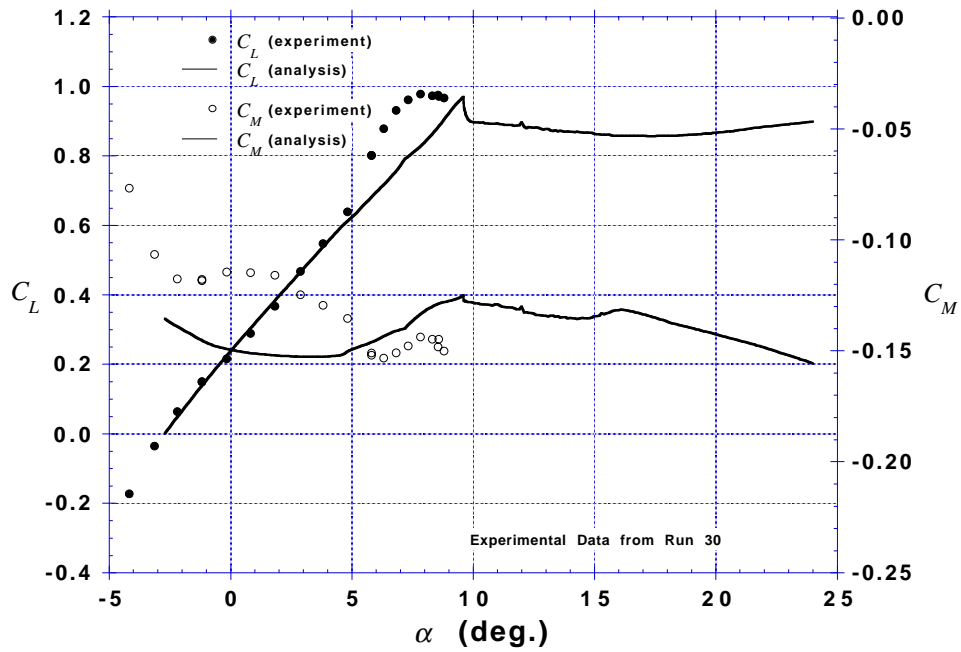


Figure D.25 – C_L and C_M vs α ; nominal conditions $M = 0.651$, $Re = 92,327$

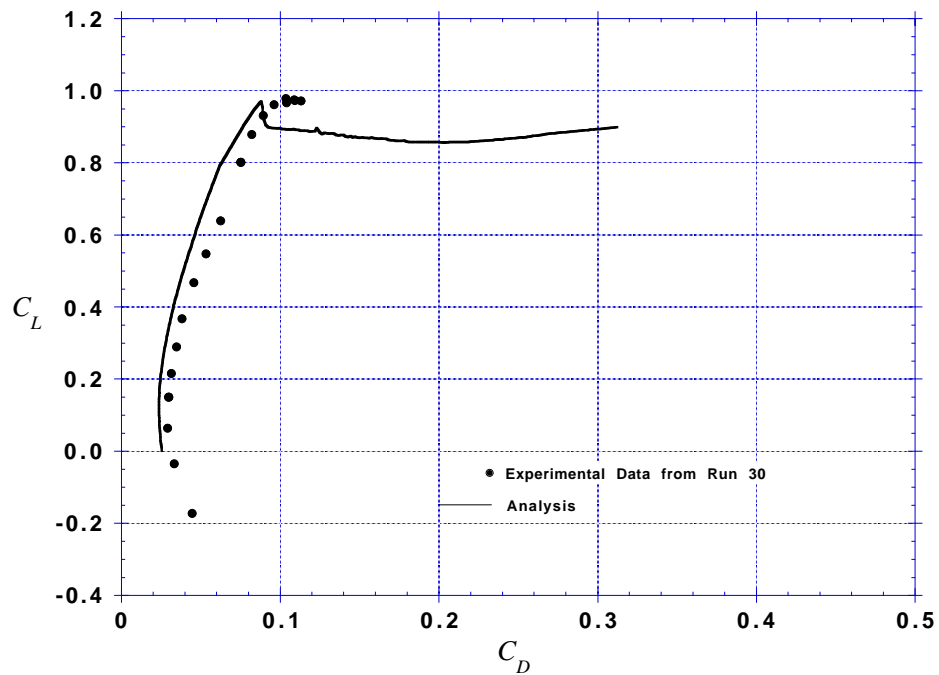


Figure D.26 – C_L vs C_D ; nominal conditions $M = 0.651$, $Re = 92,327$

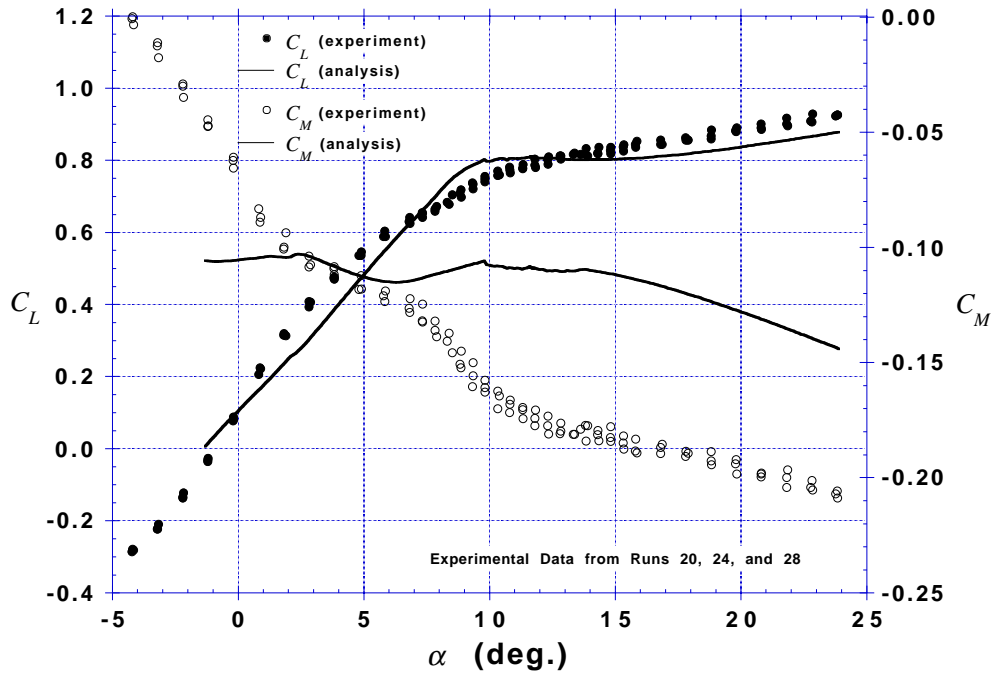


Figure D.27 – C_L and C_M vs α ; nominal conditions $M = 0.700$, $Re = 27,680$

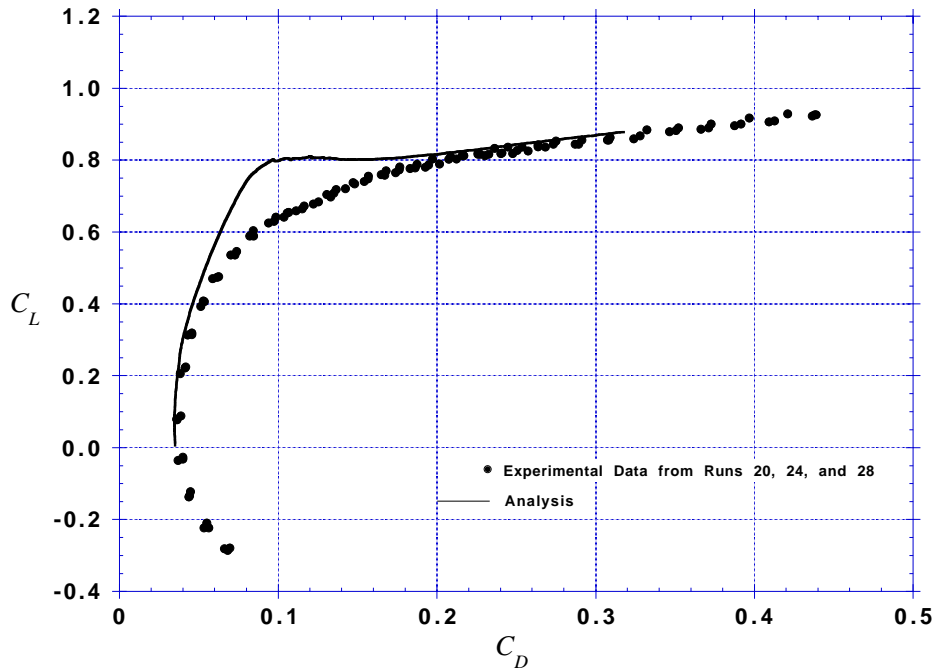


Figure D.28 – C_L vs C_D ; nominal conditions $M = 0.700$, $Re = 27,680$

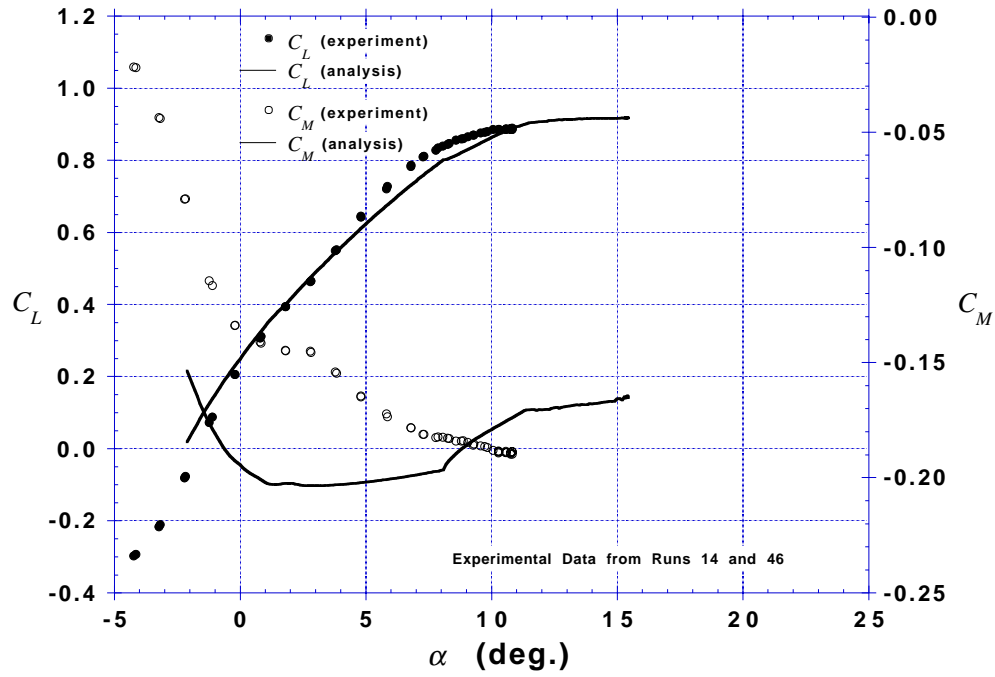


Figure D.29 – C_L and C_M vs α ; nominal conditions $M = 0.800$, $Re = 141,000$

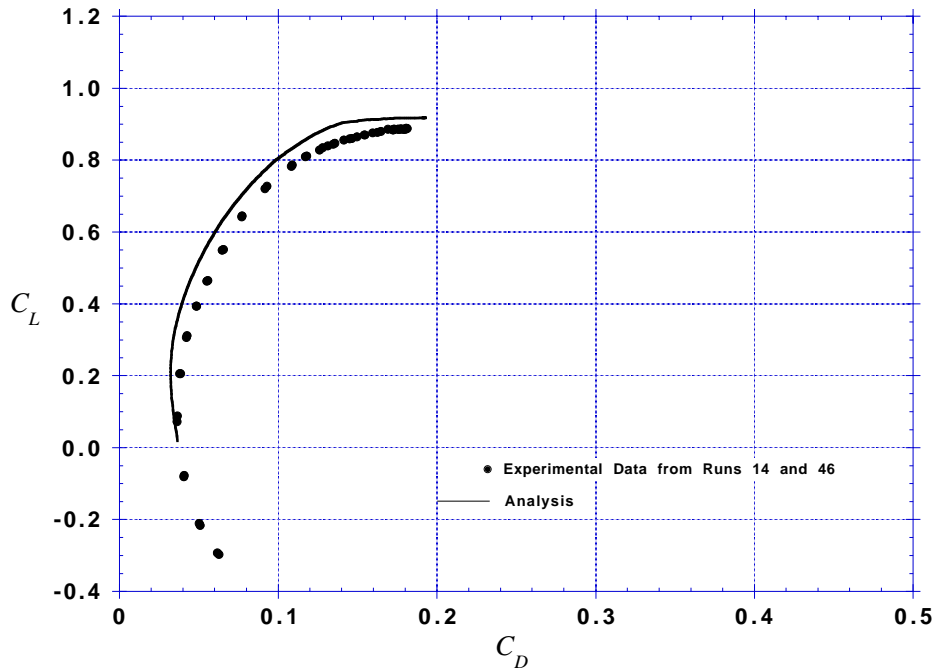


Figure D.30 – C_L vs C_D ; nominal conditions $M = 0.800$, $Re = 141,000$

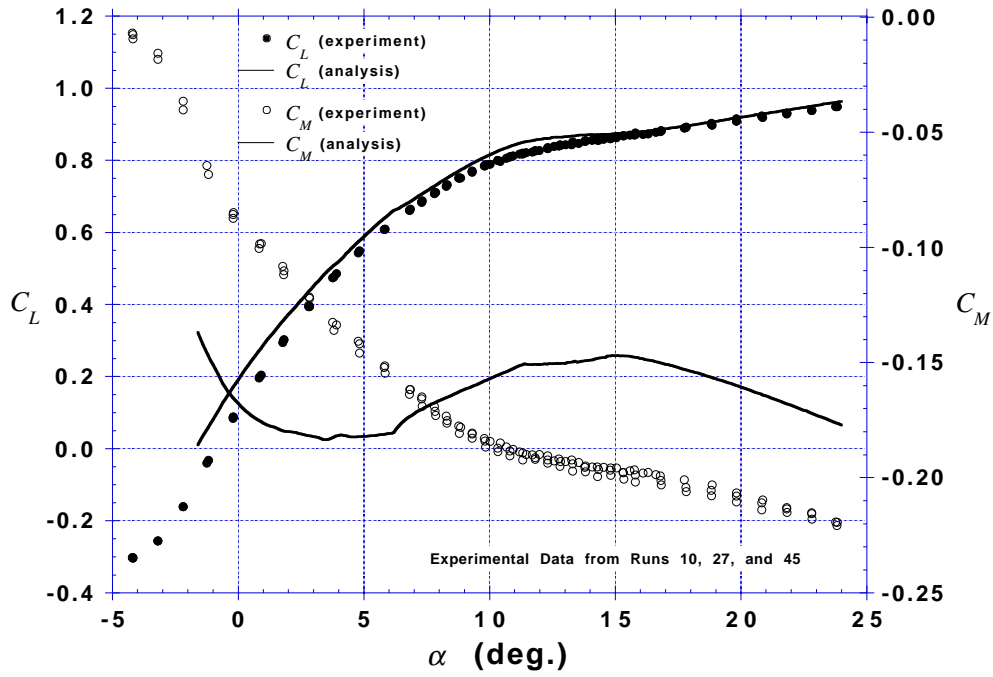


Figure D.31 – C_L and C_M vs α ; nominal conditions $M = 0.800$, $Re = 70,000$

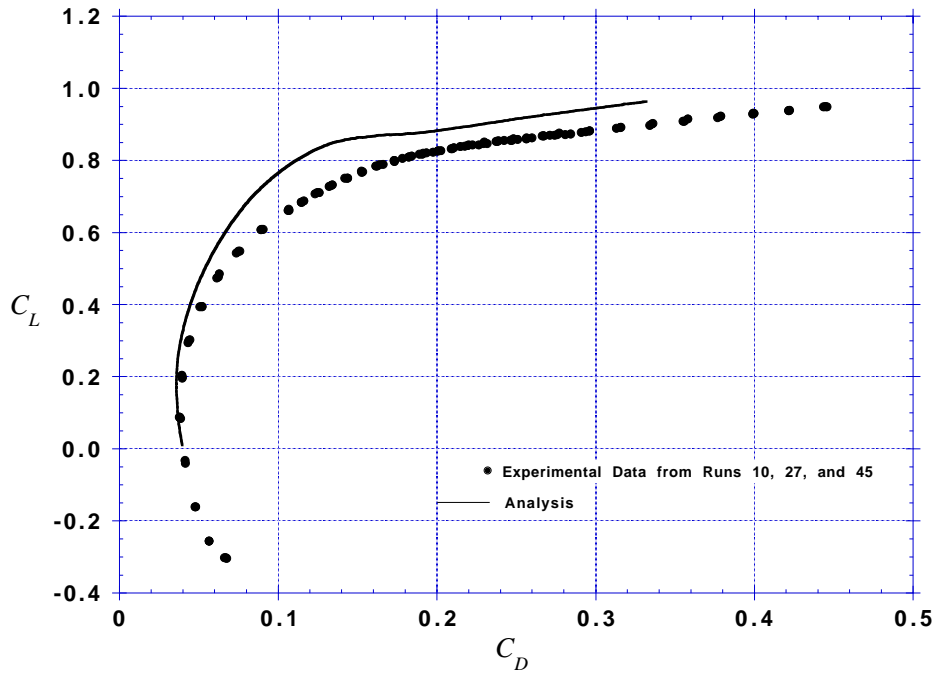


Figure D.32 – C_L vs C_D ; nominal conditions $M = 0.800$, $Re = 70,000$

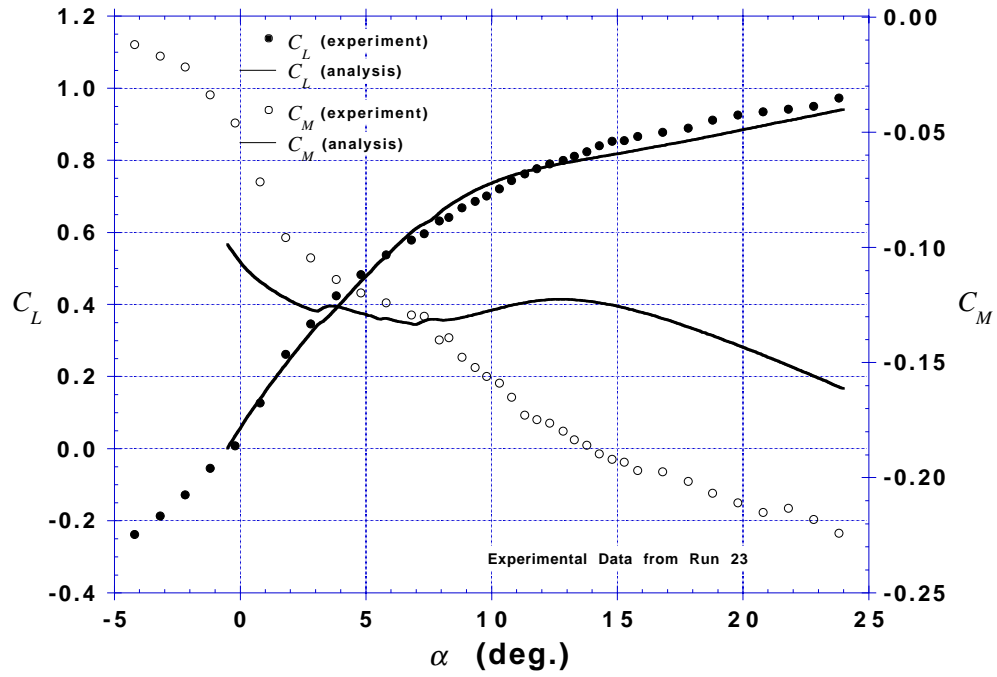


Figure D.33 – C_L and C_M vs α ; nominal conditions $M = 0.800$, $Re = 24,584$

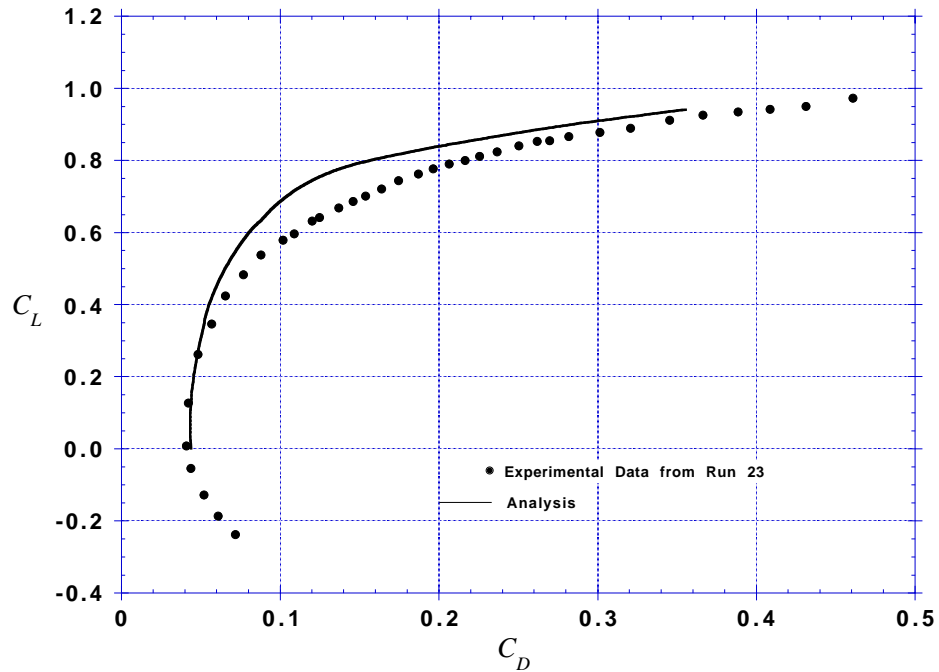


Figure D.34 – C_L vs C_D ; nominal conditions $M = 0.800$, $Re = 24,584$

Vita

Juan R. Cruz was born and raised in Puerto Rico where he completed his education through high school. He attended the Massachusetts Institute of Technology as an undergraduate, receiving a Bachelors of Science degree in Aerospace Engineering in 1986. He completed a Masters in Science degree in Aerospace Engineering from the George Washington University in 1992. That same year he initiated his studies for the Doctor of Philosophy degree in Aerospace Engineering at the Virginia Polytechnic Institute and State University. Mr. Cruz's professional career started as a structural engineer for the Beech Aircraft Corporation. He was involved in the design and construction of the Monarch and Daedalus human powered aircraft at the Massachusetts Institute of Technology, both as a student and as a member of the research staff. Since 1988 Mr. Cruz has been a research engineer at the NASA Langley Research Center. While employed at NASA he has had the opportunity to work on high-altitude unmanned aircraft and on flight systems for the robotic exploration of Mars. His current professional goal is to be involved with the first flight of an aircraft on Mars. Personal interests related to his professional career include various types of motorless flight, including sailplanes and hang gliders.